The Performance of Road Ironwork Installations

by C.J. Brown, MEng

Thesis submitted to the University of Nottingham
for the Degree of Doctor of Philosophy, February 1997

Contents

Abstract

Road ironwork units are installed at the top of a manhole chamber using a bedding material which often fails prematurely resulting in a severe impairment to riding quality for vehicles and can be hazardous in extreme cases. Failure of the surrounding bituminous road surfacing is also very common. The repair of failed installations is a source of considerable expenditure to highway authorities. The aim of this research was to identify the causes of failure of road ironwork installations and to develop ideas for providing improved service life.

A major laboratory test facility was constructed to allow an investigation of the behaviour of road ironwork installations at full scale under realistic loading. Tensile strains were recorded in the bedding material during these experiments and were used to identify possible failure mechanisms. These data and other measurements were later used to verify three-dimensional finite element analyses of the configurations tested in the laboratory. These calculations revealed that a region of tensile stress developed in the bedding material which was in excess of the fatigue strength. Cracks developed at this position in the laboratory experiments and were also noted in field observations. Other laboratory experiments revealed that bedding materials with high shrinkage characteristics can result in the development of cracks in the bedding layer without the application of any load.

This information was used to develop a specification for an improved bedding material and refine the design of a standard ironwork frame. Samples of these components were produced and used in subsequent experiments. The use of these products is considered to increase the longevity of a reinstatement but may not be able to withstand the worst loading condition, so further work is necessary.

Field experiments provided information on the in-situ stiffness of pavements in the proximity of a manhole. It was found that they are considerably stiffer in the region above the manhole chamber wall. This was considered to influence the strain magnitudes induced by an applied load in the bituminous layer thus inducing premature fatigue cracking.

Declaration

The work described in this thesis was carried out at the Department of Civil Engineering, University of Nottingham between September, 1993 and October, 1996. This work has not been submitted in this or in any other form in support of an application for a degree or other qualification at this or any other University.

Acknowledgements

I would like to thank the following for their help and assistance over the duration of this research:

Professor S.F. Brown and Dr. M.G. Coutie for their supervision.

Barry Brodrick for his help in the development of experimental apparatus and testing.

Andy Leyko for the fabrication of numerous pieces of apparatus and maintenance of the laboratory test facility.

All the other members of the Pavement and Geotechnics research group, past and present, especially Gordon Airey, Dr. Mike Gibb, Walt Hislop, Hamdy Ibrahim, Dr. John Read, Ian Richardson, Paul Sanders, Dr. Todd Scholz and M.A. Shahid for their help in laying the bituminous materials used in the laboratory test facility.

Mike Bettison and Geoff Mitchell for the use of apparatus in the concrete and structures laboratories.

Rachel Ramsden and Carolyn Parkinson for typing this thesis and other reports relating to this research.

All of the staff at the Cripps Computing Centre who have assisted with my problems relating to computers.

Dr. Richard Edwards, Andrew Scott, Alan Pendleton, John Pickavance, Jason Smith and Gareth Cook of Stanton plc for their invaluable assistance.

Chris Jennison, Jamie Denton and John Dobriski of SWK Pavement Engineering Ltd for arranging the use of the Falling Weight Deflectometer and additional support.

John Smith, Andy Patel and Luigi Cordani of Strucom Ltd for their advice and assistance in the use the ANSYS finite element analysis program.

Pippa Wong for her help and support over the last three years.

I would also like to thank the numerous highway engineers I have contacted over the duration of this research for the benefit of their experience and allowing me to carry out tests in their locality.

Finally, I would like to thank anyone else who has contributed to this research who has not been mentioned above.

List of Figures

List of Tables

1. Introduction

The term 'road ironwork' is used to refer to covers that are placed over manholes, drainage gullies, water valves and the like. Such ironwork can be found in virtually all highways, especially in urban areas. Highway engineers from local authorities and utility companies have revealed that there is a high incidence of premature failure in these installations providing access to manholes. These failures are generally characterised by a severe deterioration of the bedding material immediately beneath the ironwork and in the surrounding bituminous surfacing. These characteristics have also been observed during the course of this research and a description is given in Section 1.2. Rocking of the ironwork in failed installations can occur under traffic causing severe noise pollution but the ironwork itself remains intact in virtually all cases. In some instances highway engineers have found that failed installations have been the cause of road traffic accidents.

Since most road ironwork installations are in urban areas, the repairs can cause considerable traffic congestion. Local authorities are aware of this consequence and often carry out reinstatements as quickly as possible and at times when it is least likely to cause disruption to traffic. Materials that are claimed to have a high rate of strength development are nearly always used to avoid long curing periods and to minimise traffic disruption. Nevertheless, these repairs often deteriorate soon afterwards and require replacement.

Attempts have been made by authorities responsible for the maintenance of road ironwork to reduce the incidence of failure. It was considered from experience and judgement that unsuitable methods and materials were being used so specifications were developed which described preferred procedures and material properties. Proprietary component materials were selected by measuring physical properties in laboratory conditions and comparing their performance to the specified values. These experiments usually involved measuring the rate of compressive strength development of the material used as bedding for the ironwork. However, not all of these approaches have been successful.

Stanton plc are the largest manufacturer of ironwork units in the U.K. and were approached by several highway engineers to discuss the matter. It became apparent that the failure of road ironwork installations was a common problem. The cost to local authorities and utilities of repairing faulty installations in the U.K. was estimated by Stanton plc to be £207m in 1993. This figure was determined from sales of ironwork and their market share. Stanton plc have a reputation for innovative product development and it was considered that research in this field would maintain their technical lead over other manufacturers. The research described in this thesis resulted from this initiative and was funded under the DoT LINK programme with industrial sponsorship from Stanton plc and SWK Pavement Engineering Ltd. The principal objective was to investigate the reasons for the high incidence of failure and to develop a suitable remedy.

A literature review and discussions with highway engineers during the initial stages of this research did not reveal any previous fundamental studies to investigate the in-situ behaviour of road ironwork and identify the causes of failure. Correspondence with other research institutions world-wide also indicated that no relevant work has been carried out.

This study employed three techniques to examine the problem. These were laboratory experiments, field experiments and site observations, and finite element analysis. A description of the purpose of each aspect of the research is described in Section 1.3.

Local authorities and utilities have been dealing with this problem for a number of years. During this time they have amassed a considerable amount of experience and are familiar with the characteristics of failed installations. This research involved working closely with these bodies to benefit from their accumulated knowledge.

1.1 Notation and Sign Convention

Ironwork is commonly bedded on the top of a manhole chamber using a layer of a proprietary product, which is usually a cementitious or polymer resin based mortar. This layer will be referred to as the "bedding layer" or "bedding" and sometimes includes another material such as a quarry tile as an inert spacer. Each component used to form this layer will be referred to as a "bedding material". The thickness of the bedding layer depends on the height the underside of the ironwork has to be raised from the chamber surface so that the topside is level with the surrounding road surface. A reinstatement is completed by placing and compacting hot or cold bituminous road surfacing between the outside of the ironwork and the existing pavement. This layer will be referred to as the bituminous material. A typical section through a manhole is shown in Figure 1.1 and the notation will be referred to throughout this thesis.

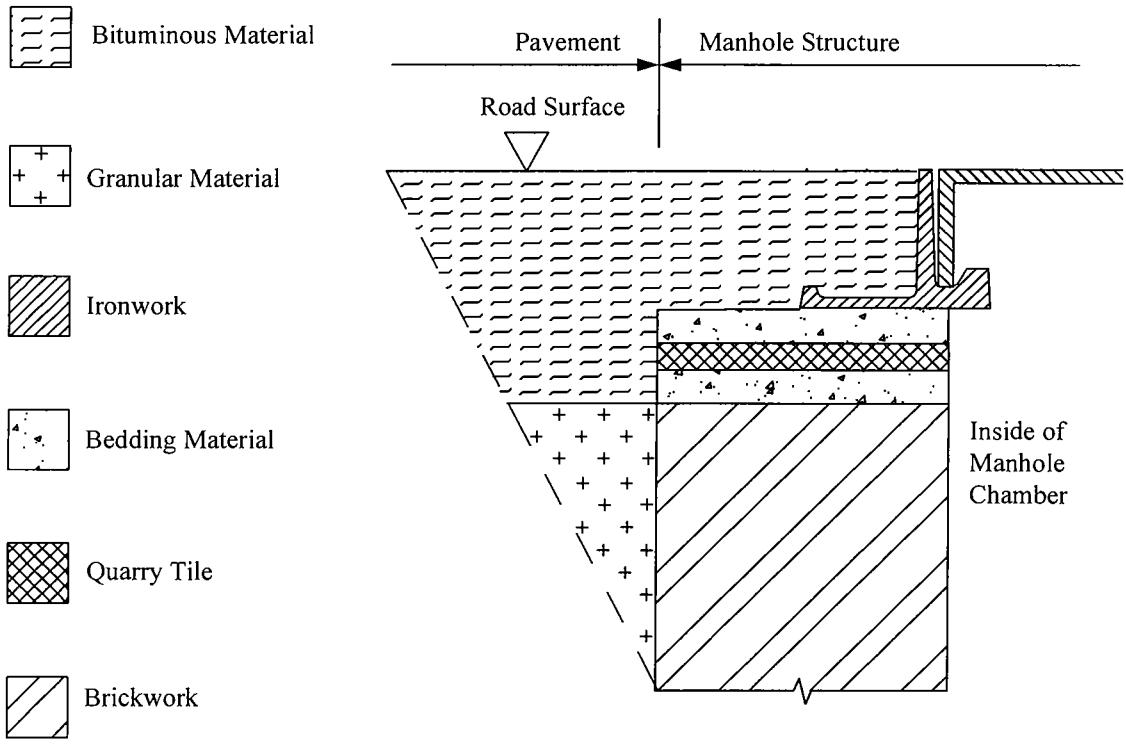

Figure 1.1: Typical cross section through a manhole

Reference will be made to measured and calculated values of stress and strain. The units of stress and strain are quoted in MPa and microstrain respectively. Positive values will denote tension in all cases. Values of the static modulus of cementitious

materials and the Young's modulus of other materials, such as ductile iron, will be quoted in GPa. The use of these terms will be described in Chapter 2.

1.2 Characteristics of a Failed Installation

Several road ironwork installations were viewed to determine the characteristics of failure. A photograph of a typical failed installation is shown in Figure 1.2.

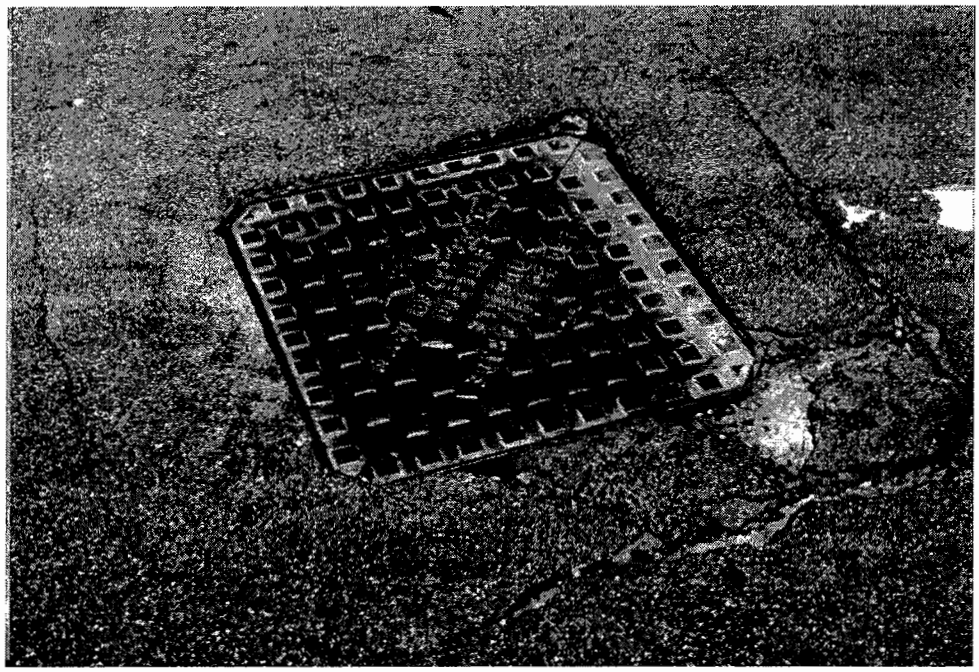

Figure 1.2: Photograph of a typical failed installation

The typical characteristics on the surface are that the surrounding bituminous material is usually cracked. In some cases it may be in a very poor condition with areas that have completely disintegrated. The level of the ironwork is sometimes below the surrounding carriageway surface although some remain at the same height. Almost invariably, the ironwork cover remains firmly seated within the frame and the whole unit rocks on its support. This produces a distinctive noise as vehicles pass. Inspections of such ironwork have found no indication of deterioration in the iron.

Routine reinstatements allowed an inspection of the bedding layer of failed installations. This consisted of a cementitious material in most cases. It usually contained several vertical cracks at a distance between 150mm and 250mm from the corners. These generally ran approximately perpendicular across the full width of the

chamber wall. Additionally, a concentration of several vertical cracks were located under the corners of the ironwork. These normally reduced the bedding material to small fragments in this region. The fragments had occasionally broken free and dropped into the manhole.

The bedding material was sometimes heavily crazed in the area directly beneath the frame web. In these instances there did not appear to be a greater concentration around the corners. These cracks were also aligned vertically. In all cases it was noticed that the cracks all had clean fractures. There was no evidence of crushing or attrition of the bedding material. Illustrations of these points are shown in Figures 1.3 and 1.4

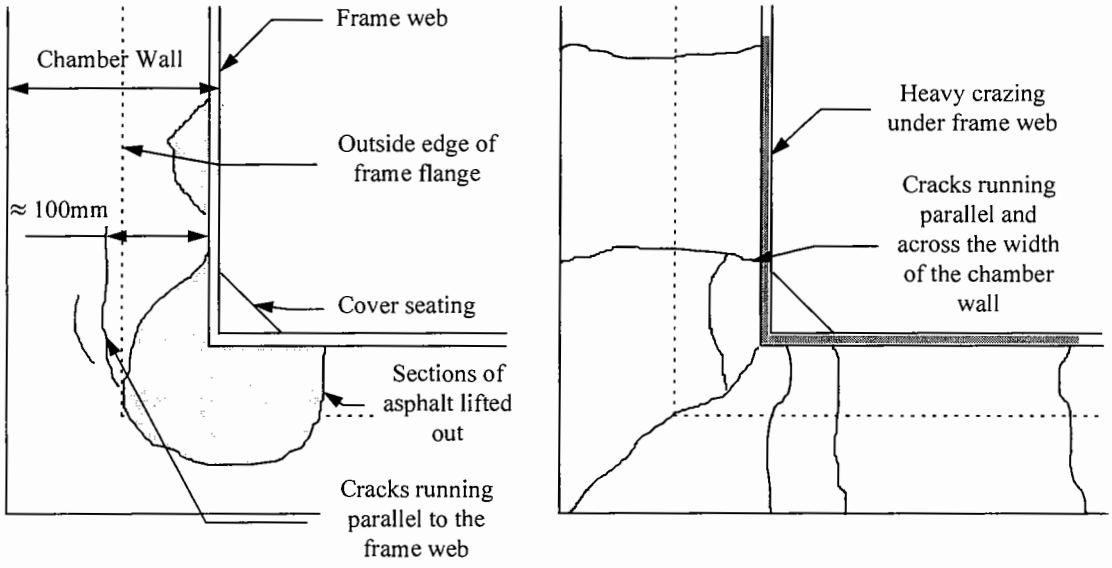

(a) Deterioration in surrounding asphalt

(b) Deterioration in bedding material

Figure 1.3: Plan view of the characteristics of failed installations

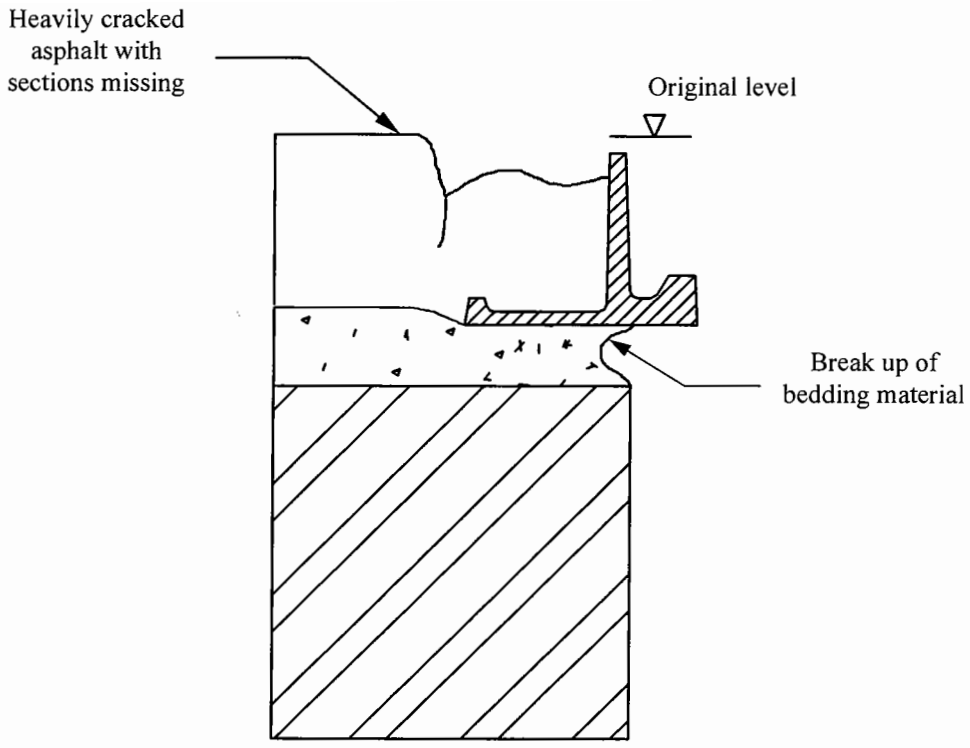

Figure 1.4: Section through a typical failed installation

During a review of the various specifications, it became apparent that a failure criterion was not clearly defined. Some did not specify any failure threshold whilst others only classified failure to have occurred when the level of the cover was greater than a specified limit beneath the surrounding carriageway [1,2]. This does not account for severe cracking of the bituminous surfacing or movement of the ironwork unit which are also failure characteristics. It was considered that this research should also provide a realistic failure criterion.

1.3 Organisation of Thesis

This research was carried out to investigate the causes of failure of road ironwork installations and to develop materials and techniques that will result in a longer service life for a reinstatement.

Chapter 2 contains a description of the various components used in road ironwork installations and a presentation of the mechanical properties of various proprietary

bedding materials determined during initial laboratory experiments. This information was later used in the finite element analyses and compared to the values of stress and strain determined through further laboratory and theoretical research. This chapter also includes a description of the relevant codes of practice relating to the performance of other component materials in road ironwork installations and a discussion of reinstatement specifications.

Field observations and experiments were carried out to study the in-situ behaviour of road ironwork installations which are described in Chapter 3. This involved closely monitoring three installations after reinstatement on the A1 trunk road at Sandy, Bedfordshire throughout the course of this research. The deterioration characteristics of the bedding and bituminous materials during this period are later used as evidence to support likely failure mechanisms identified during further laboratory experiments and theoretical calculations. Other field experiments involved studying the behaviour of a manhole and the surrounding pavement under an applied load. This information was also used to identify the possible mechanisms that cause deterioration in the surrounding bituminous materials.

A major laboratory test facility was constructed to study the behaviour of road ironwork installations under closely controlled conditions. The results from the field experiments were applied to the design of this apparatus to ensure it was simulative of field conditions. A sensitivity analysis was also carried out to determine the most influential variables within road ironwork installations. This information was used to develop an experimental programme. This development is described in Chapter 4.

The results from experiments using the laboratory test facility are described in Chapter 5. Resilient strain and displacement measurements at discreet points from a variety of road ironwork configurations are presented which provide an understanding of how such installations behave under an applied load. This provides an indication of likely failure mechanisms. Comparisons are also drawn between the field evidence and the deterioration of the laboratory specimens.

Three-dimensional finite element analyses were carried out using the geometry of some of the configurations tested in the laboratory. This part of the research provided calculated values of strain at all points within the structure which was a useful supplement to the laboratory experiments. The analyses were verified by comparing the calculated and measured values of strain and were subsequently used to provide calculated values of stress. These values were compared to the strengths of the bedding material to further study the failure mechanisms identified during the laboratory experiments. The direction of the calculated stress was compared to the crack patterns seen in the field and laboratory as further evidence. The finite element analyses also provided an indication of the behaviour of the ironwork under an applied load and the effect this may have on the surrounding backfill material. This is presented in Chapter 6.

The field, laboratory and theoretical research indicated several shortcomings to the properties of the component materials. These findings are discussed in Chapter 7 and the properties of an improved bedding material are specified. Additionally, the design of the ironwork frame was refined. Samples of these components were manufactured and tested in the laboratory and in field trials which allowed an assessment of their performance. Additionally, the failure criteria and methods of reinstatement are also discussed.

Chapter 8 contains the conclusions from this research and recommendations for future work.

2. Component Materials of a Manhole and Ironwork Reinstatement Specifications

2.1 Introduction

A manhole consists of several component materials, each of significantly different composition. Investigations have been made to study the behaviour of each material and measure relevant material properties. It is considered that these properties may influence the behaviour of a road ironwork installation. The elastic properties were later used in finite element analyses and the strengths of these materials were compared to the magnitudes of stress and strain determined through later research. This information was used to identify failure mechanisms.

Attempts have been made to increase the longevity of an installation by recommending methods of installation. A brief description of these methods and their assumptions is presented.

2.2 Bedding Materials

A proprietary product is nearly always used to form the bedding layer in reinstatements. These are produced by several manufacturers and traded under many different brand names. The products can be classified into five groups by their material type. These are cementitious mortars, polymer resins, high density polyethylene spacers, quarry tiles and fibrous boards. Each material is either used exclusively to provide the bedding layer, or a combination of two types is used. This is common practice with the high density polyethylene spacer, quarry tiles and fibrous board. These materials are normally bedded with a cementitious mortar. Materials that have to be prepared before use are claimed to develop high strengths very quickly. This allows reinstatements to be re-opened to traffic after a few hours without sustaining any immediate damage. The other products that do not have to be prepared on site are claimed to possess adequate strength. Each material will be described separately.

2.2.1 Cementitious Bedding Mortars

Discussions with highway engineers and manufacturers have revealed that cementitious mortars are the most common type of bedding material. These products are normally prepared in 25kg bags containing a dry blend of Ordinary Portland Cement (OPC), aggregate and an accelerator to allow rapid strength development. Only water is required to be added on site. A proprietary mortar with these components was chosen for use in this research. This will be referred to as mortar A. This material is commonly used in practice and is typical of this generic variety of bedding material.

A sample of mortar A was sieved to study the aggregate sizes. This was carried out in accordance with BS1377: Part 2: 1990 [3]. A graph illustrating the grading is shown in Figure 2.1.

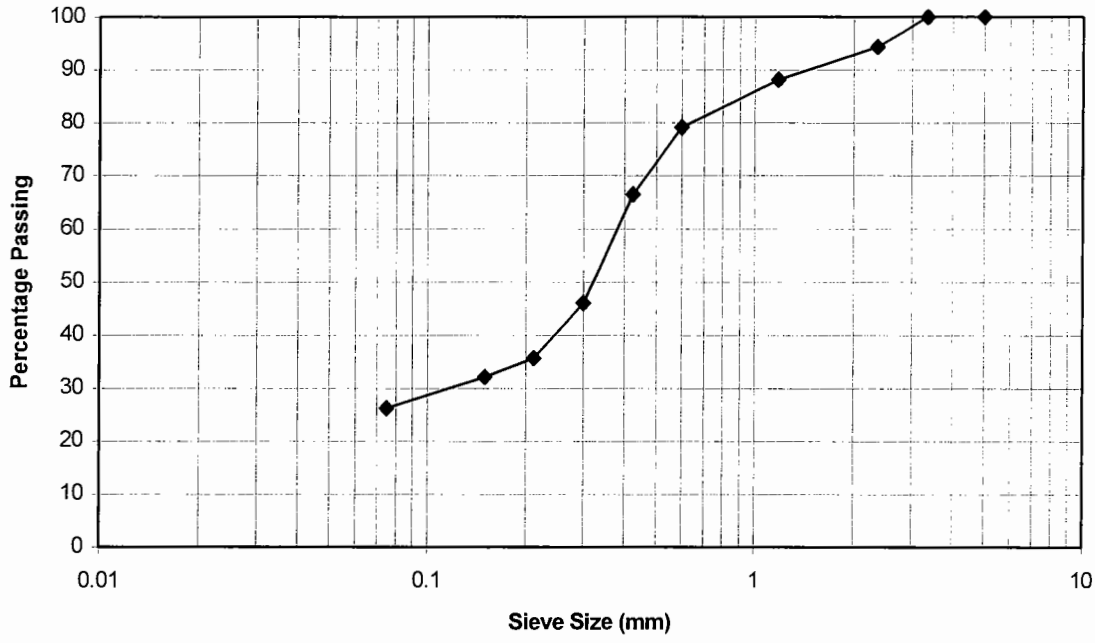

Figure 2.1: Grading of proprietary bedding mortar

It was found that 95% of the dry mixture passed through a 2.36mm sieve. Even proportions were retained by the smaller sieves indicating a 'continuously graded' mixture [4].

The high rate of gain of strength is achieved by various methods which result in an acceleration of the hydration reaction. A common method is to add calcium chloride to the cement paste. However, this can cause corrosion of ferrous metals, so it is not suitable for the bedding of road ironwork [5]. Acceleration without the risk of corrosion can be achieved by the addition of calcium formate which is a preferred accelerator when ferrous metals are present. Hydration starts at the surface of the cement particles so acceleration can be achieved by grinding the cement clinker to a very fine powder. This increases the surface area of the cement particles allowing hydration to occur at a faster rate. Discussions with the manufacturer revealed that mortar A has both of these acceleration mechanisms. An OPC consists mainly of four compounds. The names, abbreviation and proportions of a typical OPC are shown in Table 2.1 [6].

Table 2.1: Proportions of compounds found in OPC

Name of compound	Abbreviation	Compound Composition (%)
Tricalcium Silicate	C_3S	54.1
Dicalcium Silicate	C_2S	16.6
Tricalcium Aluminate	C_3A	10.8
Tetracalcium Aluminoferrite	C_4AF	9.1
Other	-	9.4

The two types of calcium silicate produce the main strength bearing components after reacting with water. These products are called calcium - silicate - hydrates (C-S-H) or tobermorite, and the rate of strength development can be made faster by increasing the proportion of C_3S. The hydrated products of C_3A and C_4AF contribute little to the strength of the cement paste, but they react at a much faster rate than the calcium silicates. The reaction of pure C_3A and water is very rapid and produces a weak, yet solid compound. This reaction can be retarded by adding gypsum or calcium sulphate to OPC. The reaction between gypsum and water is also very rapid, and the hydrated product coats the C_3A compound which prevents a 'flash set' [5]. Some proprietary bedding manufacturers reduce the gypsum content of their material. Although these

materials may harden quickly, they do not develop an appreciable strength within a short space of time.

High Alumina cement is another type of cementitious material. The mechanism of its hydration reaction is not given here, but it does develop strength at a faster rate than an unaltered OPC [5]. Some proprietary products contain a blend of OPC and high alumina cement. Most of these products also include a superplasticizer so that the amount of water required to provide a workable mix is reduced. This reduces the quantity of free water in the mixture that must be reacted with or dispersed before the mortar can harden. A proprietary product with this composition was chosen to represent this generic group of bedding materials. This product will be referred to as mortar B.

Workable Properties

Cementitious mortar A was very sensitive to the water content. The manufacturer's recommended water content by mass was 16% which produced a mixture with a 50mm slump immediately after mixing but, a water content of 18% resulted in a collapse slump, while a zero slump occurred at a water content of 14%. Mortar B was slightly less sensitive but only produced a 10mm slump at the manufacturer's recommended water content which was 12%. This product contained fibre glass strands which was considered to reduce the workability. The inert fibre glass strands were approximately 10mm in length. Great care was taken in controlling the quantity of water when mixing. It is recognised that the water/cement ratio is the most influential factor governing the hardened properties [5,7]. Manufacturers usually recommend the quantity of water to be added to yield the optimum strength although this is difficult to control in field conditions.

The workable lives of cementitious bedding materials are very short in order to allow the high strengths to develop quickly. Nearly all proprietary mortars harden in 8 to 15 minutes after adding water at a temperature of 20°C. Most manufacturers produce winter and summer grades of their mortars. Winter grades result in the same hardening time but at a temperature of 5°C. The time taken to mix a 25kg bag of

mortar to an even consistency is approximately three minutes when using a mechanical mixer. This can make it very difficult to place the mortar and level the ironwork before the mortar sets. Additionally, a cementitious mortar will gradually harden throughout its workable life. A mix producing a 50mm slump immediately after mixing may stiffen to a zero slump before the ironwork has been levelled. The short workable life and progressive hardening of the mix can make it difficult to install the ironwork to a high level of workmanship.

Hardened Properties

Fracture of Cementitious Materials: Cementitious materials usually fail by cracking. The relationship between the stress level and crack development is claimed to be well known [8]. Several theories have been developed to describe the strength of cement paste and mortars. Unfortunately, not all theories compare well to the actual behaviour of cementitious products. Griffith [9] developed a theory to describe strength in terms of a limiting direct stress. This criterion predicts that the compressive strength is eight times the tensile strength which is close to actual values.

It has been suggested that failure may occur at a limiting tensile strain, typically between 50 and 150 microstrain [5,10]. It is beyond the scope of this research to determine the limiting criterion so strengths will be expressed as a limiting stress as this is the usual parameter, although reference will be made to tensile strains when discussing the laboratory results in Chapter 5.

Compressive Strength: The strength of a cementitious product is considered to be its most important property [7]. The compressive strength is often quoted as specimens can be easily prepared and tested to measure this value. The specimens are usually 100mm cubes, cast and crushed in accordance with BS1881: Part 116: 1983 [11], although cylindrical specimens are occasionally used.

The rate of development of compressive strength is of particular importance in selecting a proprietary bedding material. Many local authorities and utilities are only interested in this characteristic as they consider that this will provide an estimation of

time required for the bedding material to develop sufficient strength to withstand traffic loading. Local authorities often study this behaviour in their own laboratories to verify data provided in trade literature. Figure 2.2 illustrates the compressive strength development of three cementitious products cured at 20°C. These data were supplied by Derbyshire County Council and Stanton plc. The strength development of a typical OPC mortar cured at 20°C has also been included in Figure 2.2 to provide a comparison.

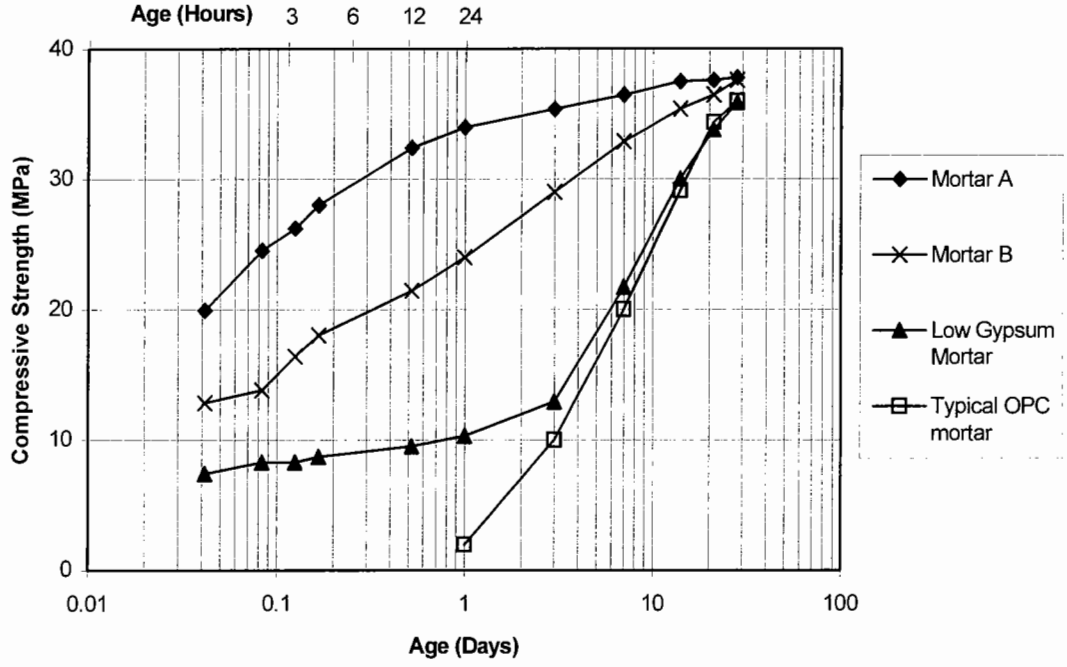

Figure 2.2: Compressive strength development of four cementitious mortars at 20°C

The results illustrate that mortar A had the fastest rate of strength development. Mortar B had a slightly lower rate and required 28 days to achieve its maximum strength. The low gypsum content mortar possessed some strength after initially setting but the subsequent strength development was similar to an unaltered OPC mortar.

Further test were carried out with samples cured at 2°C. It was found that these samples only achieved on average 25% of the compressive strength of the samples cured at 20°C after the same curing period. This can be overcome by using the

seasonal grades of mortar supplied by manufacturers. However, the mortar may be stored at depots for several months so an inappropriate mixture may be used when a reinstatement is made.

Tensile Strength: Materials of a cementitious nature generally have a very low tensile strength. This can be explained by the presence of flaws within the hydrated cement paste. These flaws cause high stresses in the material when the average stress in the whole specimen is comparatively low [5,9]. These localised high stresses are around voids and at bonds between the aggregate and cement paste which cause microscopic fractures. These fractures result in a redistribution of the stresses within a specimen which result in microscopic fractures developing at the next weakest flaw. This process continues until several microscopic fractures develop within a specimen. Eventually, the microscopic fractures join together producing a crack across the specimen, resulting in failure. The direction of this crack is almost always perpendicular to the direction of the load and the failure occurs suddenly. These are typical properties of a brittle material [5]. The tensile strength of a mortar can be increased by adding reinforcement. This can be achieved by blending fibre glass or steel strands with the cement paste. Some proprietary products containing fibre glass strands are claimed to possess tensile strengths in the region of 7 to 9MPa. Proprietary mortar B contained fibre glass strands.

The trade literature does not provide much data on the tensile strength of cementitious bedding mortars, since this has not previously been considered important. It is considered by manufacturers and local authorities that the bedding layer only experiences a compressive stress. It is not thought that a significant tensile stress develops when the iron is loaded by a vehicle wheel. An insufficient compressive strength is often considered to be the cause of failure and most emphasis is placed on this property.

It is difficult to test a cementitious product in direct tension due to the problems associated with gripping the specimen satisfactorily and ensuring there is no eccentricity of the applied load. The standards ASTM C 78-84, ASTM C 496-71 (re-

approved 1979) and BS1881: Part 117: 1983 all prescribe alternative methods such as flexural tests and indirect tensile tests [12,13,14]. However, the different methods produce different results. This is due to differences in stress conditions produced in the samples in each test. Laboratory experiments were carried out to measure the limiting stress and strain at failure of mortars A and B tested in direct uniaxial tension. A description of the apparatus and test method is given in Appendix A.

Samples of the same mortars were also cast into cylinders and a value of tensile splitting strength was determined in accordance with BS1881: Part 117: 1983 [14]. Both tests involved curing the specimens at 20°C and measurements were carried out at various ages; 3hrs, 24hrs, 3 days, 7 days and 28 days. The development of strength in terms of a limiting stress in mortars A and B are shown in Figures 2.3 and 2.4 respectively. The strain at failure for both materials at various ages was determined during the uniaxial tensile test and is shown in Figure 2.5.

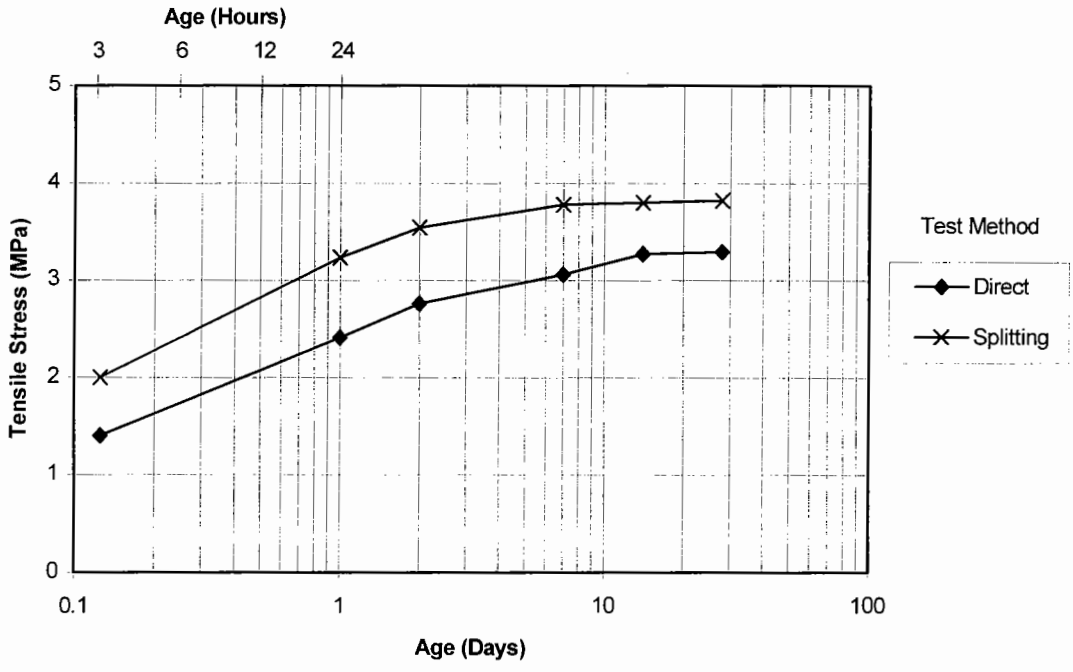

Figure 2.3: Development of tensile strength of mortar A expressed as a limiting stress

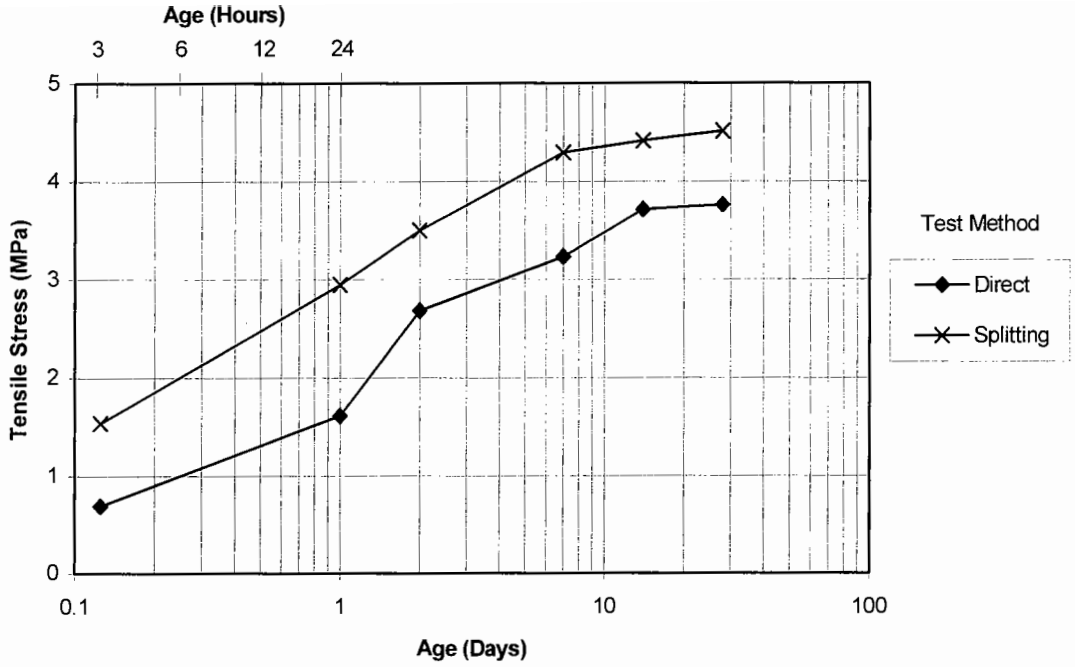

Figure 2.4: Development of tensile strength of mortar B expressed as a limiting stress

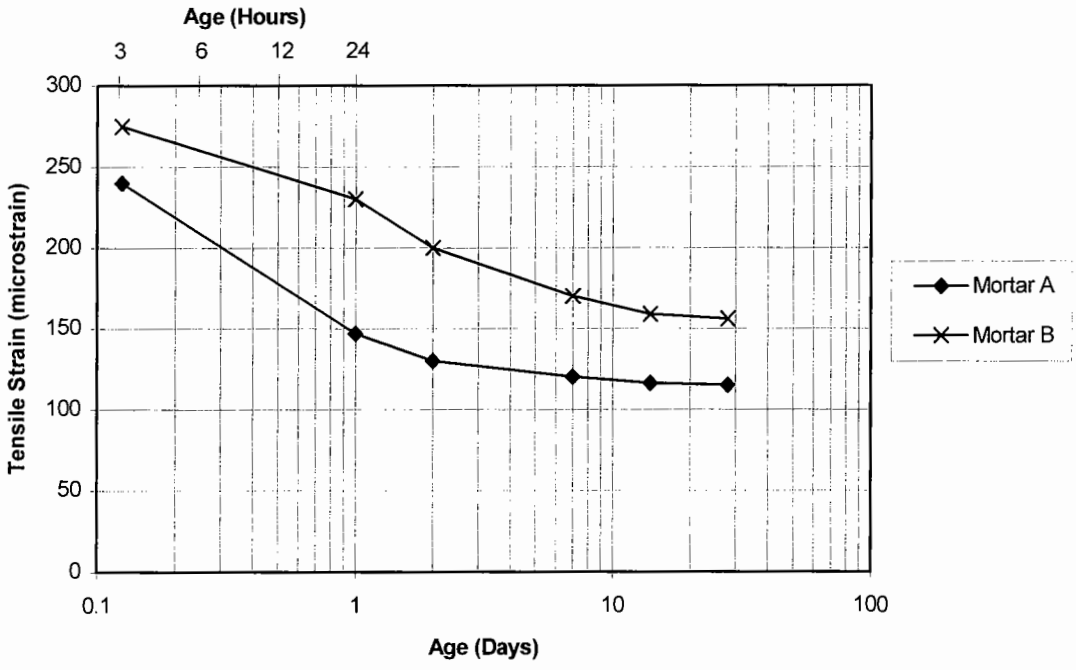

Figure 2.5: Development of tensile strength in both mortars expressed as a limiting strain

The strain at failure decreased with age so it would appear that the materials become weaker with time. However, the strain magnitude due to an applied load is dependant on the static modulus of the material which is described later.

Fatigue Strength: Experiments were carried out to determine the fatigue strength of mortar A. A description and illustration of the apparatus is given in Appendix A. The results from the experiment are shown in Figure 2.6.

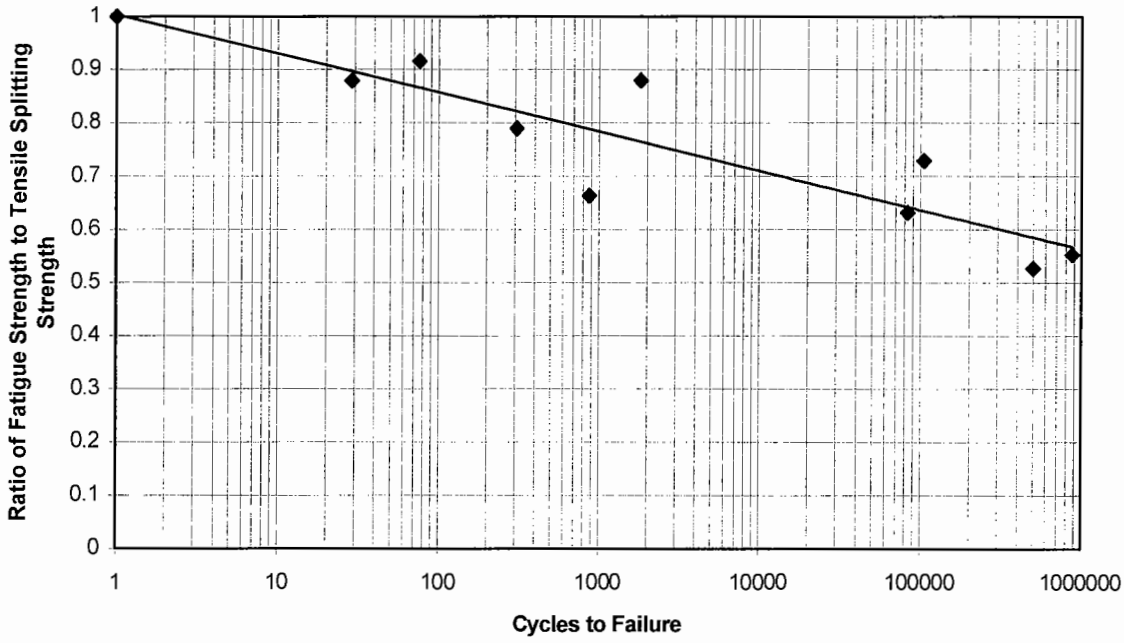

Figure 2.6: Fatigue strength of mortar A determined by an indirect tensile fatigue test

There was considerable variability in the fatigue strength of the specimens tested but the results demonstrate that failure can result after several load cycles at a stress magnitude lower than the tensile splitting strength. These results can tentatively be used to illustrate that the mortar can withstand a maximum of 55% of the tensile splitting strength at 1 million cycles. This trend agrees with other research to study the fatigue behaviour of concrete. These tests have indicated that the fatigue strength at 1 million cycles of concrete in uniaxial tension and compression is 60 and 50% respectively of the short term strength [7]. These data will be referred to when discussing the calculated and measured values of stress and strain.

Static Modulus and Poisson's Ratio: Cementitious materials are generally considered to exhibit non-linear stress-strain characteristics [5] so the modulus of elasticity cannot be referred to as the Young's modulus as this only applies to materials with linear behaviour. The modulus of elasticity is often referred to as the static modulus with cementitious materials [5] and this term will be adopted.

The strengths of bedding materials are usually considered to be the most important factors in providing reliable reinstatements. However, the static modulus usually increases with time in cementitious materials. The distribution of stress in the bedding layer may change with the static modulus. A young bedding mortar may experience a different peak magnitude of stress to a mature bedding mortar. The magnitude of these stresses may be in excess of the strength at these ages. The variations in stress magnitude with static modulus are studied in a sensitivity analysis presented in Section 4.5. Manufacturers' literature only contained data on the compressive strength of their material at various ages, so laboratory experiments were required to determine the elastic properties. A description of the apparatus and the test method used to measure these quantities [15] is given in Appendix A.

The calculated values of the static modulus and Poisson's ratio at various ages for samples of mortar A cured at 20°C are shown in Figures 2.7 and 2.8 respectively. The static modulus can be seen to increase with age. It appears that the maximum value of 21GPa is reached after 7 days. The Poisson's ratio also increases with time and a maximum value of 0.14 was reached after 7 days. Mortar B was found to have a static modulus and Poisson's ratio of 18 GPa and 0.16 at 28 days.

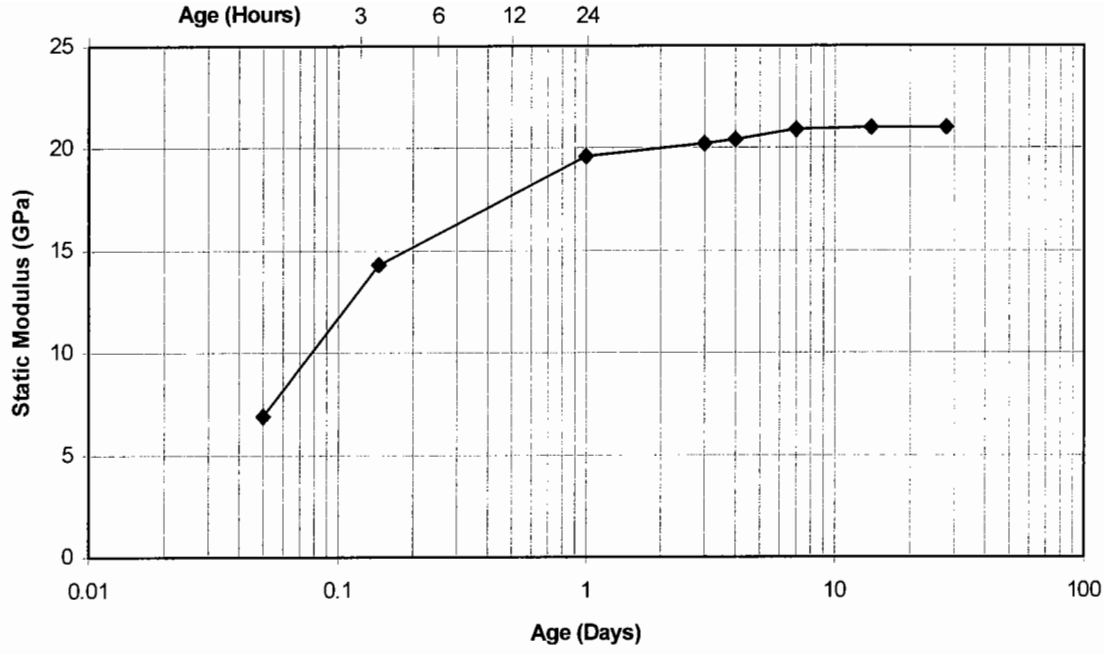

Figure 2.7: Change in static modulus with time measured from cylindrical specimens

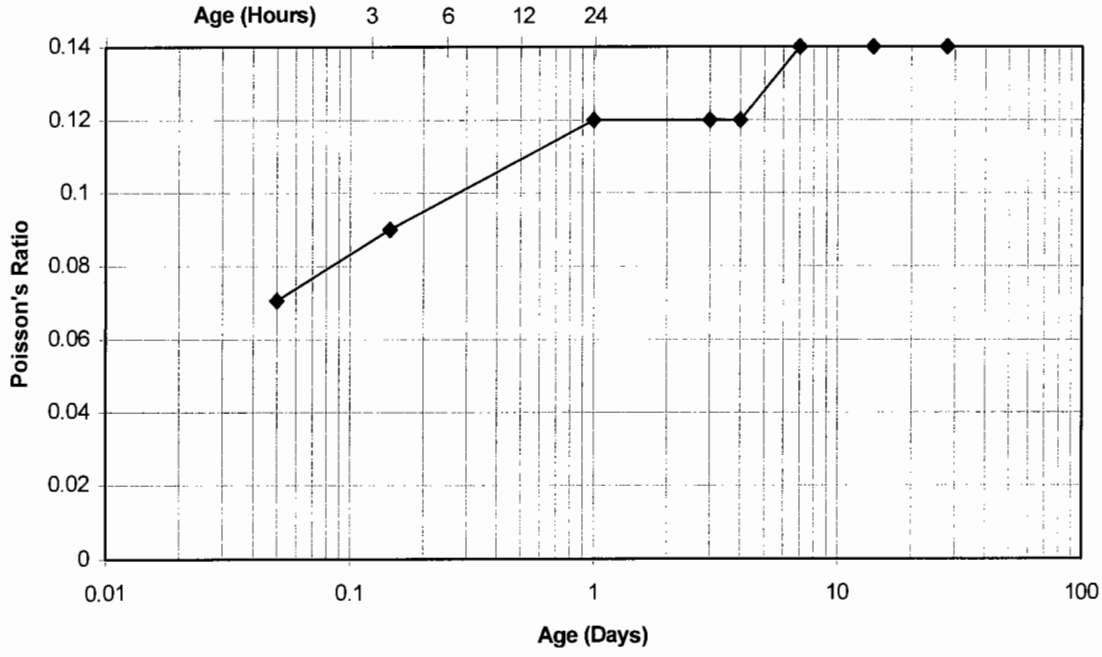

Figure 2.8: Change in Poisson's ratio with time measured from cylindrical specimens

Shrinkage: All cementitious materials shrink to a greater or lesser degree with time. Movements in the horizontal directions of the bedding layer are restrained by friction with the ironwork and brickwork. If the material is unable to move, this will result in tensile stresses developing which could lead to cracking. Experiments were carried out to study the effect of shrinkage using mortars A and B. It was claimed that mortar B would swell in its early life to mitigate the effects of normal shrinkage over its later life. Cementitious materials with this characteristic are known as 'shrinkage compensated' mixtures [5]. Additionally, the fibre glass strands were considered to increase its resistance to cracking. Mortar A did not have this compensation mechanism but was claimed to have low shrinkage properties.

Test Method: The test programme involved bedding four standard ironwork frames onto sheets of plywood with a 25mm thickness of mortar A. Each frame was bedded with a different configuration of the bedding material as shown in Figure 2.9. All ironwork frames have holes located in the flange. It was considered that placing bedding mortar in these holes and above the flange would restrain it from shrinkage and may induce cracking. The holes in the frame illustrated in Figure 2.9a were covered with strips of mild steel. This was to prevent mortar passing to the top of the flange when the frame was levelled to position. This allowed a comparison with the section shown in Figure 2.9b and 2.9c to study whether the restraint provided by the holes had any significant effect. Fibre glass strands were added to mortar A in the section shown in Figure 2.9d to see whether the reinforcement had any effect in reducing cracking. A total of 100g of fibre glass strands was gradually mixed with the mortar. A fifth frame was bedded with mortar B with the same configuration as shown in Figure 2.9e. This enabled a direct comparison of the performance of the two materials.

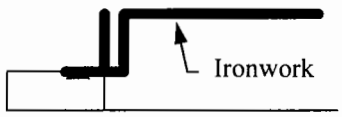

a: Holes in ironwork frame blocked off with strips of mild steel.
No bedding mortar above flange
Mortar: **A**

b: Holes in ironwork frame left open, but no mortar placed above flange
Mortar: **A**

c: Mortar placed above flange and in holes
Mortar: **A**

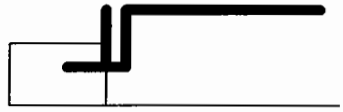

d: Mortar placed above flange and in holes
Mortar: **A** with added fibreglass strands

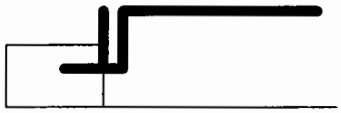

e: Mortar placed above flange and in holes
Mortar: **B**

Figure 2.9: Sections through the bedding configurations used in the shrinkage test

The two bedding materials were mixed with water to the manufacturers' recommendations. A 50mm slump was recorded for the mixture used in Figure 2.9a to 2.9c and a 10mm slump for both mixtures containing fibre glass strands. The presence of fibre glass strands significantly reduced the workability. Each sample was left in the laboratory at an average temperature of 20°C for 28 days. The ironwork covers were not placed within the frames so the development of cracks could be monitored on the internal and external faces of the bedding. The locations of cracks were monitored after 1 day, 3 days, 7 days, 14 days and 28 days. Specimens of both materials were later prepared to quantify their shrinkage. Three prisms of each material with dimensions 100 x 100 x 500mm long were cast and stored at a constant temperature of 20°C. The shrinkage was measured by using a de-mountable mechanical gauge (demec).

Results: A large number of cracks developed in the section shown in Figure 2.9a within the first 24 hours. The cracks had propagated across the full width of the

bedding mortar and were spaced at intervals of approximately 150mm. This is illustrated in Figure 2.10. All these cracks gradually increased in size throughout the remainder of the monitoring period. The mortar A specimen containing fibre glass strands as illustrated in Figure 2.9d contained approximately half the number of cracks after the first 24 hours. However, further cracks developed throughout the test period and the final pattern was almost the same as that shown in Figure 2.10. The other mortar A specimens only exhibited a few cracks initially but developed a similar number and pattern of cracks within 7 days. No further cracks appeared in these samples in the remainder of the test period. The mortar B sample did not develop any cracks within the test period and remained in this condition for another two months.

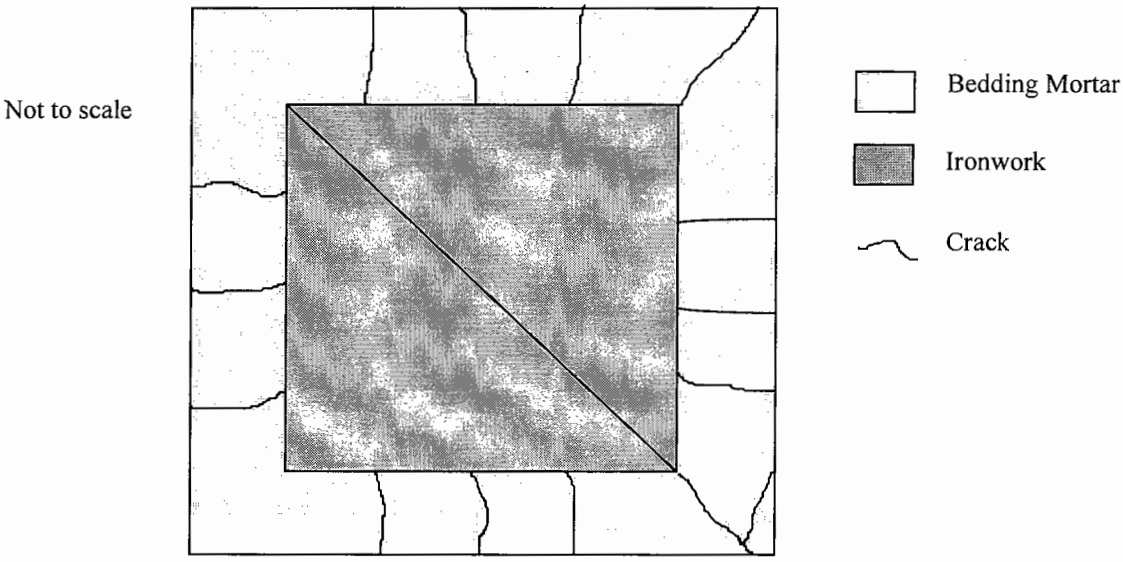

Figure 2.10: Plan view of typical crack pattern that developed in all mortar A samples

The shrinkage of the prisms made from both materials is quantified in Figure 2.11. The specimens made from mortar B expanded within the first day. It began to shrink after this period but at a very slow rate and a net contraction of 52 microstrain was recorded after 58 days. The mortar A specimens shrank inducing an average strain of 149 microstrain after 7 days. It is thought this would explain why cracking occurred in all the mortar A samples after 1 week. The average measurement taken at 58 days was found to be 159 microstrain.

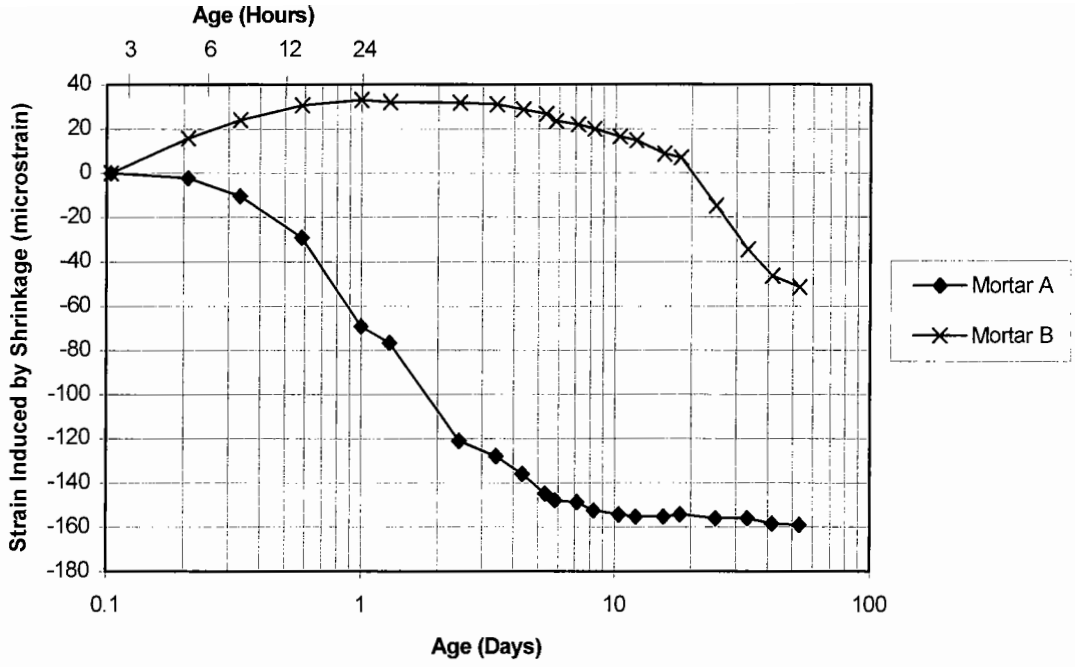

Figure 2.11: Average shrinkage measurements of mortars A and B

Mortar B did not crack during the bedding tests. It also exhibited lower shrinkage than mortar A. The experiments illustrated that mortar A produced the same crack pattern regardless of the bedding configuration and the presence of fibre glass strands. The experiment demonstrated that shrinkage cracks can develop which decrease the integrity of the support to the ironwork and lead to premature failure of a road ironwork installation.

2.2.2 Polymer Resin Based Bedding Materials

Polymer or polymer resin based compounds are also used as bedding materials. These products are not as popular as cementitious products as they are generally five times as expensive and greater care is required in their safe handling. Noxious fumes are produced during mixing and the use of gloves, goggles and barrier creams are recommended by manufacturers. Some products also ignite at temperatures above 30°C.

These proprietary materials usually consist of three components. These are a resin, a hardener and an inert aggregate. The aggregate usually consists of single sized sand

particles no larger than 2mm. The proportions of this mixture have been balanced by the manufacturers to yield optimum strength. The product is normally supplied in quantities of 25kg which produces a volume of 12.5 litres.

Workable Properties

Manufacturers generally supply these materials in winter and summer grades so the time to the initial set is constant throughout the year. This is usually between 20 and 35 minutes but can vary from 15 to 45 minutes at temperatures of 25°C and 0°C respectively when using the appropriate seasonal mixture. The products recommended for bedding ironwork produce a slump of 50mm. Pourable grouts and stiff fillers are also available that produce the same strengths at similar ages but these are not considered to be suitable for the reinstatement of road ironwork.

Polymer resin mixtures remain at the same level of workability before setting. The set is usually very rapid and early strengths develop quickly. These mixtures also form a strong bond to neighbouring materials, so it is imperative that all tools be cleaned before the material sets. However, this bond may be severely impaired if the surfaces are not clean and dry.

Hardened Properties

Compressive Strength: A common characteristic of these materials is a high ultimate strength, often in excess of 75MPa and achieved within three days. Some products can achieve 70 to 80% of the ultimate strength within two hours of mixing, providing the appropriate seasonal grade is used. Figure 2.12 illustrates the compressive strength development of a polymer resin product intended for reinstating road ironwork and which cures at 20°C. This is compared with the strength development of mortar A cured at the same temperature.

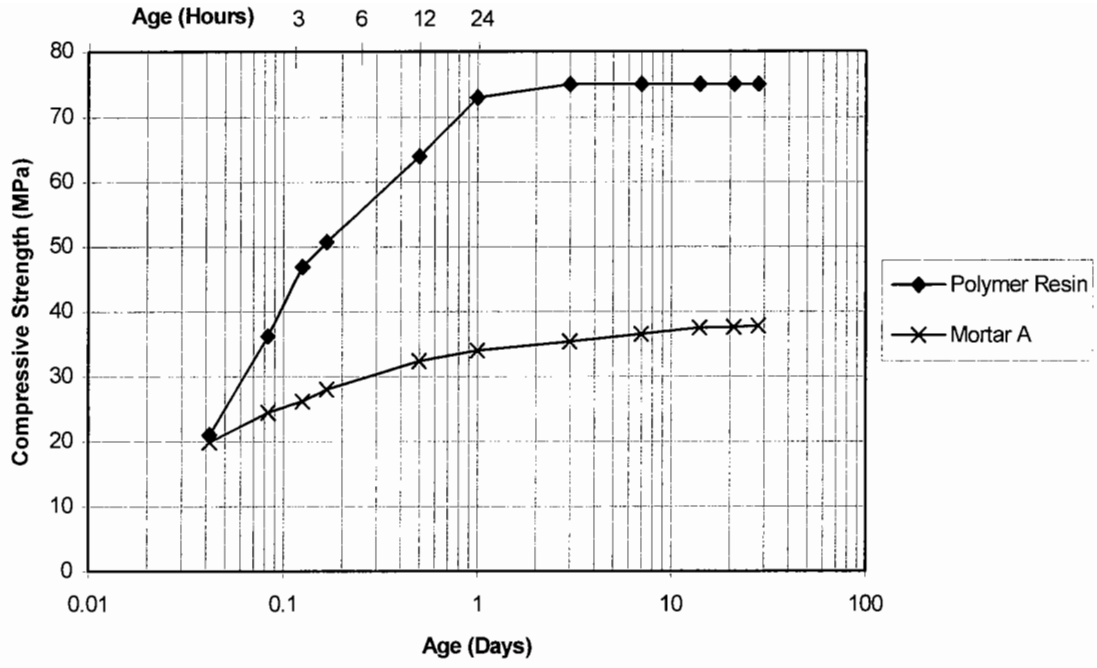

Figure 2.12: Comparison of strength development between a polymer resin product and mortar A at 20°C (Data supplied by Derbyshire County Council)

Tensile Strength: Polymer resin products are not as brittle as cementitious compounds and can exhibit a greater tensile strength. The weakest product studied in this research claimed to have a tensile strength of 13MPa. This data was extracted from manufacturers' literature where the value was obtained by using a standard test method described in BS 6319: Part 2: 1983 [16]. The tensile strength is claimed to develop at a similar rate to the compressive strength.

Static Modulus and Poisson's Ratio: Samples of polymer resin products were acquired and cast into cylinders with a diameter of 150mm and height of 300mm. They were tested by the same method and with the same apparatus as used to determine the elastic properties of the cementitious products [15]. An illustration of results is shown in Figures 2.13 and 2.14.

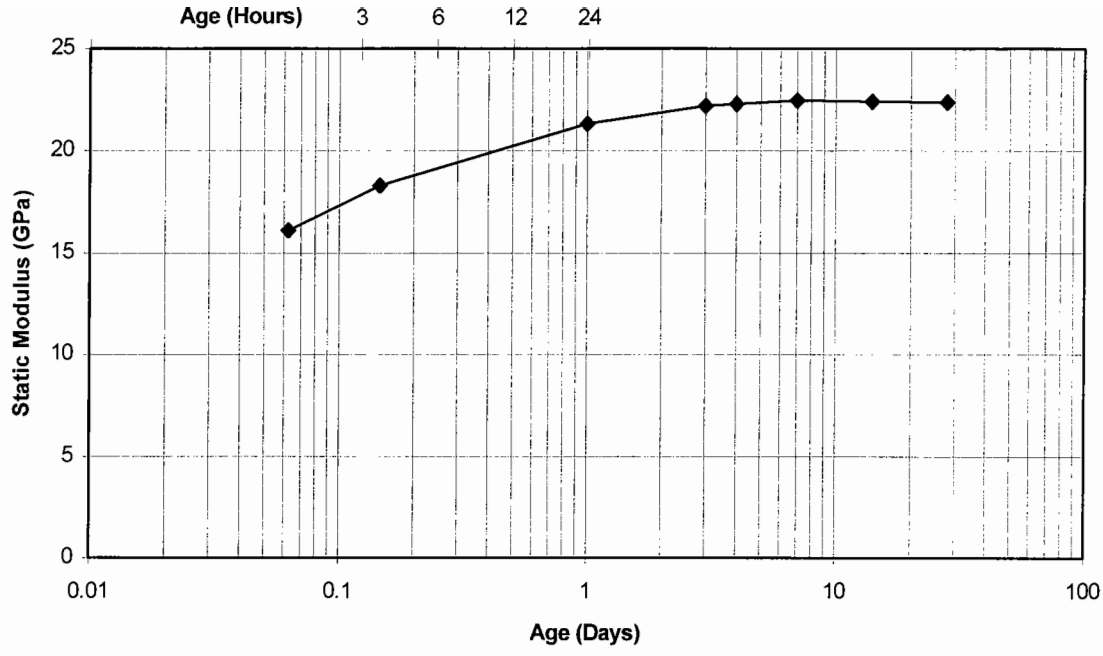

Figure 2.13: Change in static modulus with time measured from cylindrical specimens

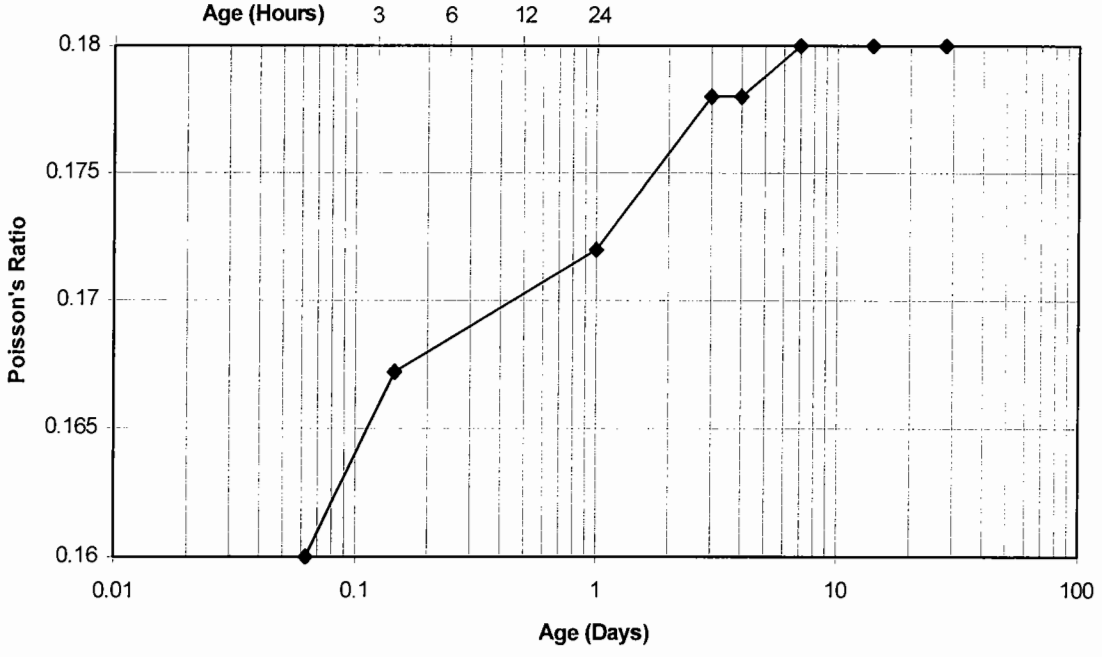

Figure 2.14: Change in Poisson's ratio with time measured from cylindrical specimens

It can be seen that ultimate values of the static modulus and Poisson's ratio were approached at three days after mixing and casting. These were 23GPa for the static modulus and 0.18 for the Poisson's ratio respectively.

Shrinkage: It was considered that a very high level of shrinkage would be required to cause cracking in a bedding layer made with a material having the tensile strength of these products. Consequently, no shrinkage tests were conducted. Manufacturers' literature states that the shrinkage is either negligible or volumetric expansions between 0.25% and 0.5% occur.

2.2.3 High Density Polyethylene (HDPE) Spacers

These products are manufactured ready for installation so site preparation is not required. Discussions with the manufacturer revealed that they were originally developed in Sweden as an alternative to cementitious and polymer resin based bedding materials that develop strength through a chemical reaction which is too slow below temperatures of 0°C for practical use in the Scandinavian climate. The original design of the spacer is an annulus with an internal diameter of 640mm and an external diameter of 800mm. Two types are made each with a different thickness. These are a constant thickness of 10mm and tapered spacer varying from 5mm to 15mm. The tapered spacers are used to accommodate the camber and longitudinal gradient of a road. The spacer is formed in a waffle pattern with channels approximately 10mm wide. The reason for this shape is not clear. It is claimed that this shape reduces the amount of material required in each spacer and also provides shock absorbent properties to protect the underlying chamber. An illustration of a spacer is shown in Figure 2.15.

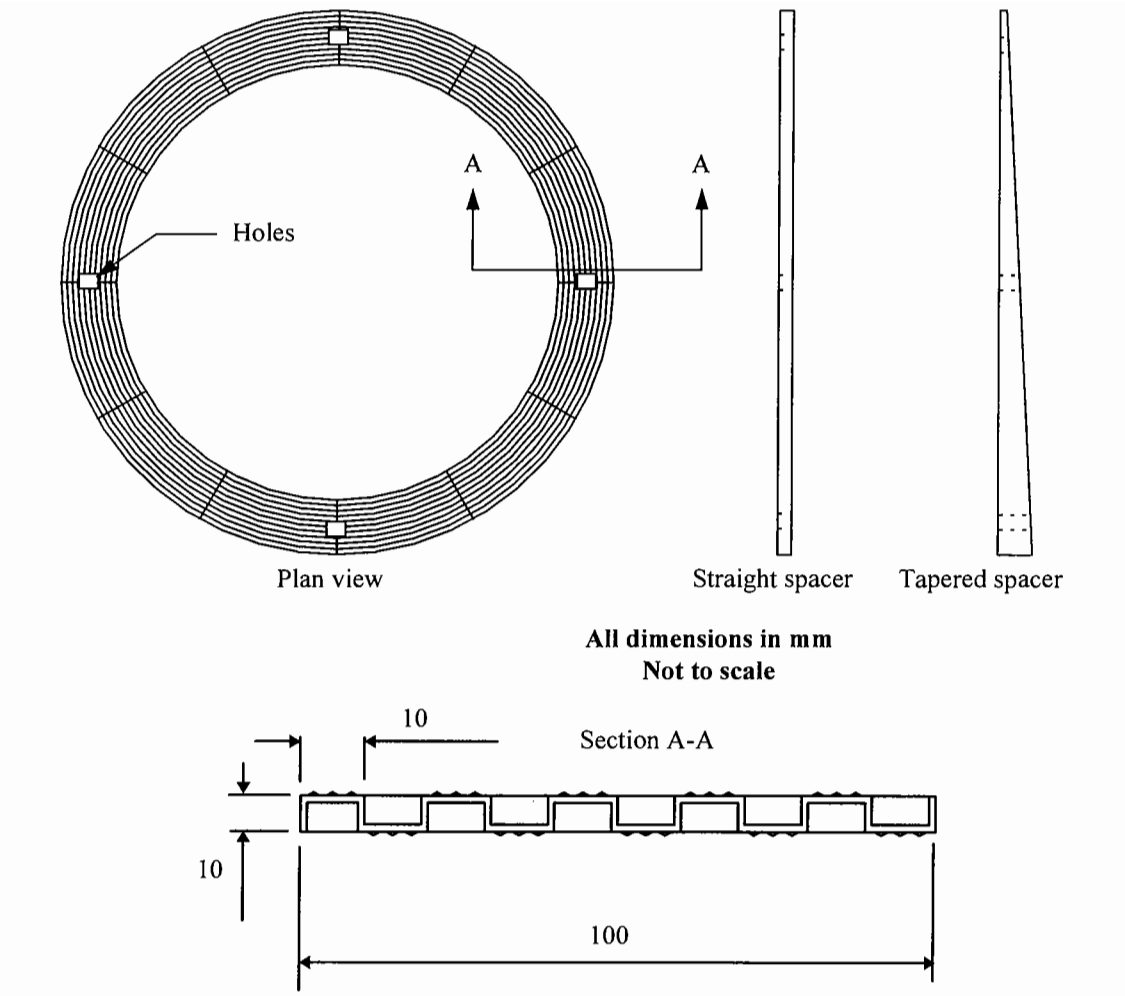

Figure 2.15: Illustration of a HDPE spacer

The method of installation prescribed by the manufacturer simply recommends that the spacers should be laid directly onto the surface of a brickwork or concrete chamber. This provides the support for the ironwork. The number of spacers required depends on how high the ironwork must be raised in order to be level with the surrounding road surface. However, it is recommended that this should not exceed 5 spacers. If the ironwork is still too low, then an additional course of brickwork should be laid on top of the chamber. A stack of spacers can be held together with pre-formed dowels. These are located in holes formed in the spacers. The reinstatement is completed by backfilling with a hot bituminous material. It is claimed the spacers are resistant to temperatures up to 200°C so they should not be adversely affected by this process. This method of reinstatement is claimed to be better than using cementitious or polymer resin products, because reinstatements can

be effected more quickly and a curing period is not necessary, so they can be re-opened to traffic with minimal delay. It is also claimed that a high level of workmanship can be achieved.

These spacers have been used in Sweden since 1972 with apparent success. They were later introduced into the U.K. and initially resulted in reliable reinstatements. It was, however, found by some local authorities that the spacers had worn after a period of two years and had to be replaced. Additionally, the circular design was incompatible with the square and rectangular shapes of ironwork predominantly used in the U.K. The spacers restricted access into manhole chambers and their use was suspended by many water companies.

A square version of the spacer was developed in 1994 to overcome this problem and has been used in field trials by many local authorities. It was found during these trials that the surface of the brickwork chamber on many manholes was uneven. Steps in the surface profile of up to 30mm were measured in the worst cases. The irregularities in the surface profile provided uneven support for the spacers, so the manufacturer recommended that a thin layer of proprietary mortar should be applied to the brickwork. It was argued by local authorities that the use of two proprietary products only made a reinstatement procedure more difficult and that the work was actually taking longer. Northumbrian Water plc also reported that the layer of mortar cracked and deteriorated after six months on some of their reinstatements made with the spacers.

Response to Compressive Load: Experiments were carried out on the circular spacers by the Swedish National Testing Institute [17]. A single spacer was placed on a rigid steel platen and covered by a steel plate with dimensions 800 x 800 x 20mm thick. A loading platen with a diameter of 300mm was placed centrally on top of the steel plate and a compressive load of 392kN was applied by a servo-hydraulic test machine. This is the maximum design load of many ironwork units used in the highway. The thickness of the spacer was measured before and after loading. It was found that no permanent deformation was recorded and there was no evidence of

damage to the spacer. It is considered that the spacers have an adequate compressive strength so this quantity was not measured in further laboratory experiments in this research.

Similar experiments were carried out with the square spacers by Stanton plc. A total of five spacers were placed on an even surface and loaded through a heavy duty ironwork unit. It was again found that the spacers were undamaged after being subjected to a load of 400kN. Measurements of resilient deflections were also taken. It was found that the stack of five spacers deflected by 1.1mm at the maximum load. A settlement of 0.15mm was recorded at the end of the test but this was considered to develop at the interface of the spacers rather than as a deformation within the spacers.

Tensile Strength: A 300mm strip was cut from a 10mm thick spacer and placed in the Zwick test machine as used to determine the direct tensile strengths of mortars A and B. A tensile load was applied at a rate of 0.03MPa per second. This was the same rate of loading used to test the cementitious samples. A total of three specimens were tested yielding an average tensile strength of 24MPa. All of the samples failed suddenly producing a fracture approximately perpendicular to the loading direction.

Modulus and Strain Ratio: The elastic properties of the spacers were measured in the Instron test machine. It was considered that a knowledge of these quantities would be useful for assessing field performance. A description of the method used to determine the elastic properties is given in Appendix A. The elastic properties will be described as the modulus and strain ratio. This is because the elastic properties of the spacers were measured rather than the material itself so it is thought that the expressions Young's modulus and Poisson's ratio are not applicable. The modulus and strain ratio were found to be 16MPa and 0.35 respectively. The interface between the loading platen and the spacers was not lubricated so friction at this point may have reduced the lateral strain so the Poisson's ratio would be a little higher than 0.35.

The behaviour of two installations using the spacers founded on a thin layer of mortar was investigated in the laboratory experiments described in Section 5.5. Field observations of an installation using a spacer are described in Section 3.2.

2.2.4 Quarry Tiles

The nature of fast setting bedding materials only allows small quantities to be mixed and placed before hardening occurs. It is considered that a practical limit is 50kg. This produces a bedding layer 50mm thick when spread over the full width of the walls of a chamber with an opening of 600 x 600mm. In some circumstances the bedding layer may need to be greater than 50mm thick. A typical example would be when a 40mm overlay is applied to the surrounding pavement, and the ironwork has to be raised. An extra course of brickwork can be laid on top of the chamber, but this would raise the ironwork by 75mm. This problem is normally resolved by using a layer of quarry tiles which are nominally 20mm thick. A common method involves laying a 25mm thick layer of bedding material followed by the quarry tiles and a second layer of bedding material prior to placement of the frame. This results in a bedding configuration as shown in Figure 1.1. It has been the experience of some local authorities that there is a large variation in the quality of quarry tiles. Some prove to be far stronger in compression than others. BS 6431: Part 2: 1984 [18] describes the requirements for quarry tiles. The tiles are classified into groups by their ability to absorb water. The highest grade tiles have the lowest water absorption which is less than 6% by mass. This grade of quarry tile is also required to have a compressive strength greater than 20MPa. Lower grade quarry tiles have a greater capacity to absorb water and are only required to have a compressive strength greater than 10MPa. Quarry tiles that were claimed to have low water absorption were acquired and their elastic properties were measured in the Instron test machine. The test method used to measure HDPE spacers was adopted. It was found that the quarry tiles have a modulus and strain ratio of 14GPa and 0.20 respectively, although the strain ratio may be slightly greater, as explained earlier.

The behaviour of two reinstatements with a composite bedding layer using these quarry tiles was investigated in laboratory experiments as described in Chapter 5. A

finite element analysis of this configuration was also carried out and is described in Chapter 6.

2.2.5 Fibrous Boards

Boards consisting of wooden fibres bound within a cementitious mortar have been developed for supporting road ironwork. The boards are manufactured in lengths of 1220mm, 150mm wide and are available in thicknesses ranging from 6mm to 40mm. They can be cut to required lengths using an ordinary hand saw.

Their method of installation is similar to that for quarry tiles, although it is recommended by the manufacturer that they can be used to form bedding layers of any thickness, rather than restricted to applications where thick bedding layers are required. The thickness of the board layer depends on the level the ironwork has to be raised. If two or more boards are required, then it is recommended that they should be stuck together with a cement slurry and be cross lapped at the corners. It is also recommended that the thickness of the mortar layers should not exceed 25mm. The advantages of this system are claimed to be the provision of a reliable reinstatement with a high level of shock absorbency in the bedding layer. This is a relatively new product and has not yet been widely used by local authorities.

The use of proprietary packing units is particularly suited to applications where a quarry tile would otherwise be used. Variations in the strength of quarry tiles may make it an unpredictable material. Experiments were carried out to measure the modulus and strain ratio of the fibrous board by the same method as used to measure these properties for the HDPE spacers. It was found to have a modulus of 15GPa and a strain ratio of 0.22. These are similar values to a good quality quarry tile so it is considered that the manhole structure would behave in a similar fashion if either material was installed, providing the same thicknesses were used.

2.3 Bituminous Materials

Reinstatements are completed by surrounding the ironwork with a bituminous material as illustrated in Figure 1.1. Two main types of bituminous material are regularly used. These are described below.

2.3.1 Hot Rolled Asphalt

Hot Rolled Asphalt (HRA) is a commonly used material in the construction of pavements in the U.K. It is predominantly used to form wearing courses but can also be used for roadbase and basecourse applications. The composition of this material is described in BS594: Part 1: 1992 [19]. This standard specifies the proportions of course and fine aggregate and bitumen content. The principal characteristic of this material is that it contains very little medium sized aggregate which ranges from 2.36mm to 10mm. This results in a 'gap-graded' aggregate structure [4].

A common wearing course formulation for HRA contains 30% course aggregate with a maximum stone size of 14mm. This is referred to as a 30/14 HRA and is frequently used to backfill around ironwork to complete a reinstatement. It is usually compacted by a vibrating roller or vibrating plate.

The material is required to be laid at a temperature of at least 50°C above the Softening Point of the bitumen which is between 45 and 60°C [4]. The higher viscosity below this temperature makes laying and compaction difficult. The quantity of material required to backfill around the ironwork is usually no greater than 300kg. It is difficult to maintain the working temperature in a hot mixture for this small quantity of material. This can be overcome by supplying a larger quantity and using the surplus in other carriageway repairs.

2.3.2 Bitumen Emulsion Mixtures

This is a bituminous material which does not require heating since workability is achieved by the bitumen being in the form of an emulsion in water. The water evaporates when the material is laid and the residual bitumen then performs the same binding role as for hot mixed material. This characteristic makes it particularly

suitable for backfilling around road ironwork as there is no minimum quantity required to maintain workability. Some bedding material manufacturers also produce proprietary emulsion mixtures. These usually consist of 6mm granite chippings blended with the bitumen emulsion. They are usually prepared in 25kg sealed bags or containers. The time taken for the water to evaporate from these products depends on the climate. It has been found that in laboratory conditions it can take several weeks for the mixture to develop an appreciable stiffness. It is considered that this time would be shorter in field conditions due to the effect of wind, assuming a similar temperature, although it is doubtful that all the water would be evaporated within a few hours.

2.4 Ironwork

The majority of ironwork frames and covers manufactured in the last 15 years have been made from spheroidal graphite iron, more commonly referred to as ductile iron. Flake graphite cast iron, otherwise known as grey iron was previously used for ironwork covers and frames.

The difference between the two materials is in the form of the graphite; flakes in grey iron and spheroidal nodules in ductile iron. The difference in the form of graphite significantly affects the mechanical properties of the material. Grey iron is very brittle so thick sections had to be used to ensure adequate strength. Nevertheless, the brittle covers occasionally cracked and failed without warning creating a hazard in the highway. The units were very heavy and costly due to the volume of iron required. Ductile iron became the favourable alternative as this material possesses greater tensile strength, ductility and resistance to impact. This allowed a reduction in the volume of iron required in a road ironwork unit whilst maintaining similar strength. Combined ductile and concrete covers are also manufactured but these products are rarely used in highway applications. All the experimental work in this project has involved the use of ductile ironwork. All ironwork units in the U.K. are manufactured with a frame depth of 100 or 150mm. It is considered by manufacturers that the 150mm deep units are more suitable for heavy load applications.

EN124: 1994 [20] is the current standard which describes the requirements for road ironwork. This replaced BS497: Part 1: 1976 [21] in 1994. The standard describes six classifications of ironwork units. Each grade is specified for use under particular loading conditions. The minimum grade of ironwork unit that can be used in carriageways is the D400 class. Units complying with this grade must withstand a prescribed loading test and incorporate several design features. These features include provision for the stability of the covers within the frame. This is achieved by ensuring the cover seating, the part of the frame which supports the cover, is at least 50mm beneath the surface of the cover. This was included to reduce the risk of the covers being lifted out by passing traffic. This is unlikely during normal service due to the weight of the covers compared to relatively low suction at the road surface generated by passing vehicles. However, if the bedding material deteriorates, the ironwork is no longer evenly supported and is able to rock. It is in these circumstances where the risk of the ironwork cover lifting out of the frame is most likely.

Many ironwork units are installed in urban areas. The standard specifies that they should not cause a nuisance by the cover rattling within the frame. This is achieved by either machining the contact surfaces, using cushioning inserts or by supporting the cover at just three points. Three point suspension is commonly used on U.K. designs of ironwork. Square openings in the carriageway are accomplished by using an ironwork frame supporting two triangular cover units.

Ironwork units are accredited the various grades based on the result of the prescribed load test, which involves applying a load through a loading platen placed centrally on the cover. The dimensions of the loading platen depend on the size and shape of the ironwork unit. A popular design of ironwork in the U.K. has two triangular covers within a single frame which provides an opening of 600 x 600mm. This design would require a platen with a 250mm diameter. The magnitude of the test load varies with the classification. The D400 class has a test load of 400kN.

The initial test is to assess the permanent deformation of the ironwork cover. Load is applied at a rate between 1kN/second and 5kN/second up to 2/3 of the test load and then released. This is repeated 5 times and the permanent deformation is recorded at the centre of the cover. The maximum permissible value is expressed as a formula and depends on the size of the opening and the method of securing the covers within the frame. However, it should not exceed 1mm in all cases [20]. The second test involves loading the ironwork unit in the same manner but to the full test load, and maintaining it for at least 30 seconds. The unit should not show any cracks during the course of this test [20]. These tests are very similar to those described in BS497 which was recently superseded. There has been no evidence during this research that ductile ironwork units have significantly deformed or cracked in use. It is therefore considered that the tests demonstrate that accredited ironwork units possess a suitable degree of strength to be used in the highway.

BS497 did not make any reference to the nature or strength of the bedding material. There has been some consideration of these factors in EN124. The new standard specifies a maximum bearing pressure of 7.5MPa that can be applied through the frame flange onto the supporting surface. This effectively specifies minimum surface area of the underside of the frame. The calculation is based on the specified test load placed centrally on the cover. It is assumed that the load will evenly distribute into the frame and hence to the bedding. This may not be true of the U.K. designs where the cover is only supported at the corners. An uneven distribution of the load into the frame is likely to cause higher stresses in the bedding material at the corners. This was investigated in the laboratory experiments and by using finite element analysis as described in Chapters 5 and 6 respectively.

EN124:1994 is adhered to by all countries within the European Union but the ironwork designs vary significantly. The principal difference is the shape of the ironwork. Units in France and Germany are predominantly circular. This shape is inherently unstable if the contact surfaces between the cover and the frame are uneven. This will result in the cover rattling in the frame when a vehicle passes. The French method to ensure quietness involves placing a cushioning strip along the

contact surface but this is claimed to wear out after a short time. The German approach is to machine the contact surfaces to within a fine tolerance to ensure an even support. Although this approach is successful, it significantly increases the production costs.

Both of these designs support the cover along its entire circumference whereas the U.K. design only supports a cover at its corners. An even distribution of the load into the frame should reduce the magnitude of stress that develops in the bedding material. It is interesting to note that the French and German highway authorities claim they do not experience a high incidence of failure of road ironwork installations. This may be due to the circular design of the ironwork.

The mechanical properties of ductile iron have been measured by Stanton plc. These values were determined by machining specimens with a length of 300mm and a diameter of 8mm from a ductile iron cover. These samples were firmly secured in an Instron test machine and a tensile force was applied. Displacement measurements were taken at regular load intervals by measuring the movement over a known gauge length on the sample using a dial gauge. Additionally, the width of the sample was measured throughout the test using a micrometer. The resulting data was plotted which demonstrated that ductile iron exhibits similar behaviour to mild steel. It was found that the yield strength of the material is 275MPa and it has a Young's modulus of 165GPa and a Poisson's ratio of 0.275. These values were later used in the analytical studies (Table 6.3).

2.5 Manhole Chambers

This research is predominantly concerned with investigating the reason for failure of the support to road ironwork. This is usually located in the bedding material. Occasionally, the supporting chamber is also damaged so a description of these materials and their construction is considered necessary. Many sewers were built in the last century and are still in service. Manhole chambers were built to provide access to the sewers and were constructed from stout brickwork. The bricks were usually laid in traditional English bond. This consists of a row of bricks laid side by

side in a stretcher bond, followed by a row of bricks laid as headers. This is illustrated in Figure 2.16. This results in a wall 215mm (9") thick, which is the length of one brick.

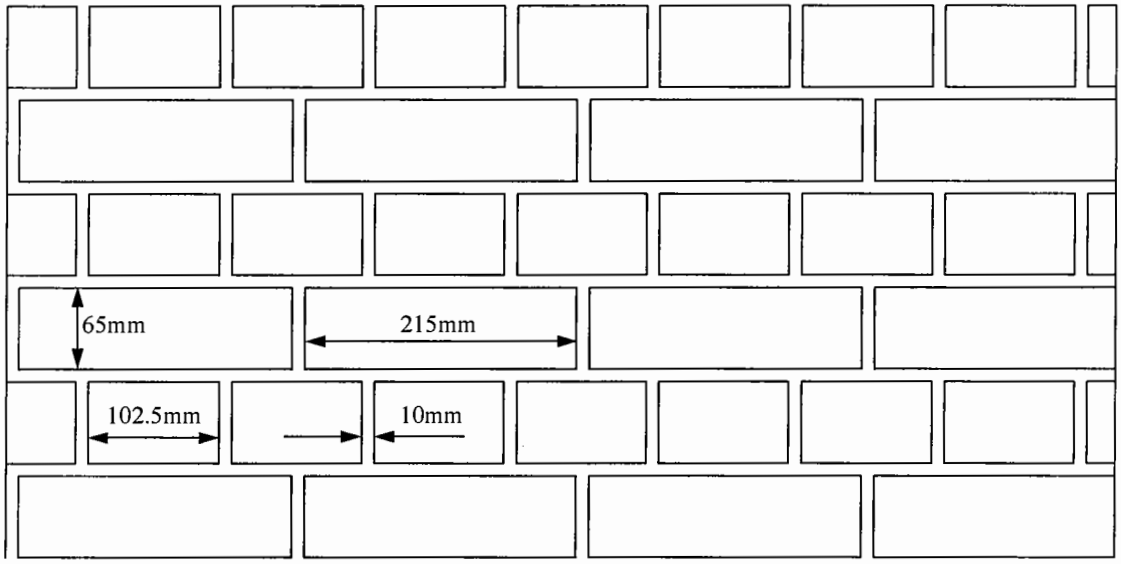

Figure 2.16: Illustration of bricks laid in English bond

Many of these chambers are still in good condition. However, the pipeline has deteriorated in some cases so a complete sewer renewal has been carried out. The depth of the chamber from the road surface varies between manholes. This is to ensure the pipeline is at an even gradient regardless of the vertical alignment of the highway.

Modern construction methods employ circular pre-cast concrete sections to form the manhole chamber. These are often referred to as 'rings' and 'biscuits'. A specification for the dimensions and material properties of these pre-cast units are described in BS5911: Part 1: 1981 [22]. An illustration of a typical construction using these components is shown in Figure 2.17.

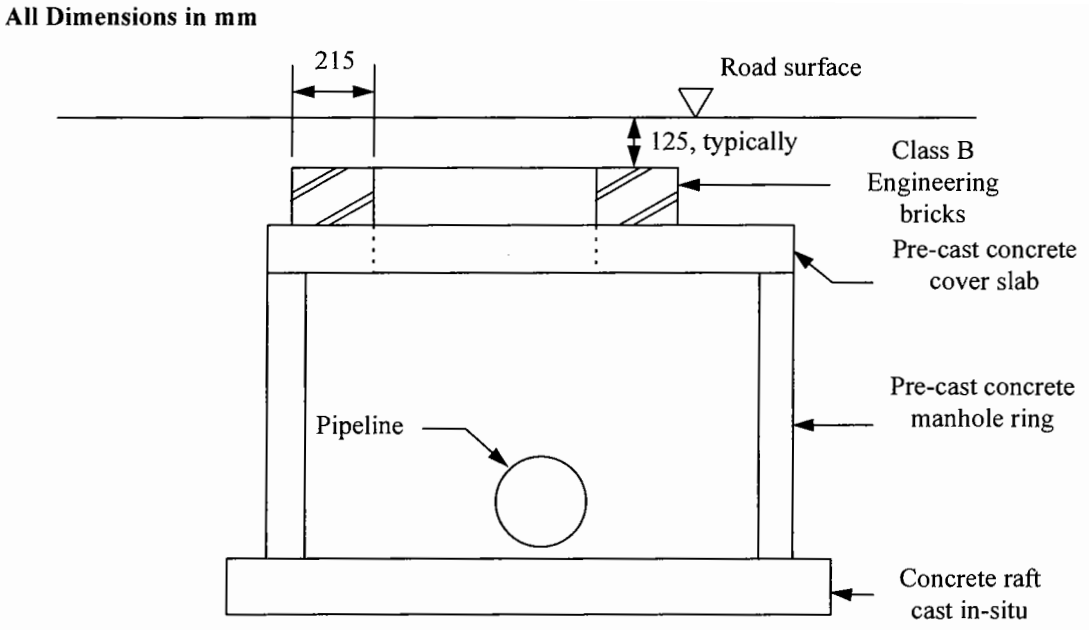

Figure 2.17: Section illustrating modern manhole chamber construction

The surface of the covering slab is usually greater than 150mm below the finished level of the highway but can be as large as 500mm in some cases. The usual practice in these conditions is to lay bricks on top of the covering slab to provide a support for the road ironwork. Class B engineering bricks are nearly always specified by local authorities and a traditional English bond is used. Class B bricks are required to possess a compressive strength greater than 50MPa and a water absorption less than 7% by mass [23].

The older brickwork chambers often increase in width internally with depth to allow ease of access. Standard ironwork units have an opening of 600 x 600mm so brickwork corbels have to be built in order to support the ironwork. The corbels are sometimes rebuilt with modern bricks when the level of the road is altered. Modern bricks usually contain holes or 'frogs' so the strength of the brick may be compromised in corbels. Occasionally bricks are laid on their side in order to achieve the desired finished level. This is illustrated in Figure 2.18. It has been observed in some installations that the brickwork laid in this fashion has failed.

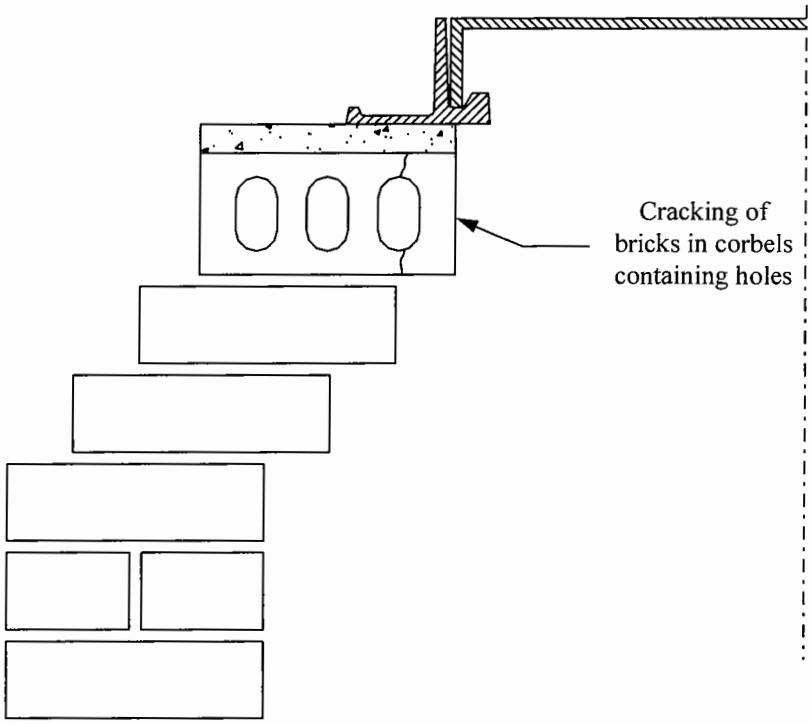

Figure 2.18: Section through a manhole chamber illustrating a brickwork corbel

2.6 Reinstatement Practice

The high incidence of failure of road ironwork installations has long been recognised as a considerable source of expenditure to local authorities and delay to road users. Attempts have been made to reduce the incidence of failure by developing improved methods of installation and specifying bedding materials with certain properties. All of the specifications are based on experience and judgement. No fundamental studies have been made to investigate the failure mechanisms and their causes and the threshold at which they occur. Each method will be described separately.

2.6.1 Preferred Method 7 - Adjustment of Street Ironwork

Several local authorities in England worked together and produced Preferred Method 7 in 1985 [1]. This was a continuation of a series of preferred methods concerning routine highway repairs. It was considered that the use of unsuitable materials and poor methods of installation were the causes of failure of road ironwork installations. The aim of this document was to describe a method of installation that was practical yet resulted in reliable reinstatements. A definition of failure was included in this document. It was stated that a road ironwork installation was considered to have

failed when the level of the ironwork was greater than 20mm beneath the surrounding road surface. However, this did not account for the other failure characteristics as described in Section 1.2.

The details of the method are presented in a flow chart so the prescribed method can be followed for virtually all circumstances that may arise. These include inspection of the condition of the chamber and repairing it if damaged. It also emphasises that all surfaces should be clear of debris before installing the ironwork. The presence of any foreign body is considered to impair the reliability of a reinstatement.

Health and Safety requirements are covered by recommending the use of a winch and cradle to lift the ironwork. Ironwork covers intended for use in the highway weigh at least 50kg. These often have to be handled at floor level where the maximum permissible weight that can be manually lifted is 10kg [24].

The type of bedding material prescribed depends on intended length of closure to traffic. Most reinstatements have to be carried out in a period not exceeding 24 hours. In these cases, the use of a proprietary cementitious bedding mortar or polymer resin product with fast strength development is specified. In circumstances where the manhole can be closed to traffic for longer periods, unaltered OPC mixtures are permitted but these conditions are rare. In all cases, the bedding material must have reached a compressive strength of at least 10MPa before re-opening to traffic. The time taken to reach this strength for a particular material is estimated from the manufacturers' literature or measured in laboratory experiments. It was assumed that the bedding material only experienced a compressive stress and a reliable reinstatement would be achieved if the frame was evenly supported and the bedding material had sufficient compressive strength. The value of required strength was estimated by calculating the contact stress applied by the frame flange as used in EN124 [20]. This calculation assumes that the force applied on an ironwork cover is evenly distributed through the frame flange. It was rounded up to 10MPa to provide a safety margin and is the only specified property for the bedding material. It was considered that a compressive stress in excess of 10MPa would not be experienced.

Preferred Method 7 was adopted by many local authorities when it was first published and was claimed to be successful. However, the use of the winch and cradle was considered to be impractical by many and the method was discontinued.

2.6.2 British Telecommunications plc (BT) Specifications

Two specifications have been published by this utility for the installation of road ironwork and were in use prior to 1995 [25,26]. The first specification described the method of reinstatement although this did not contain a description of the circumstances when ironwork should be reinstated. The method involved placing a 20mm thick layer of mortar onto the surface of the exposed chamber and carefully lowering the frame on to it. The frame was then tamped down until it is level with the carriageway surface. The reinstatement was completed by backfilling with HRA only after the bedding material had hardened. The surface of all chambers was required to be finished 120mm beneath the surrounding road surface. This level was achieved by using Class B engineering bricks.

The second specification described the required properties of a bedding material. All of the required values were determined by judgement as there was no experimental or theoretical work carried out in the drafting of these criteria. The details of the specification are summarised in Table 2.2.

Table 2.2: Summary of required properties for BT specification

Shrinkage	Low (no value quoted)
Initial set time	25 - 45 minutes
Compressive strength at 2 hours [1]	40MPa
Bond Strength at 2 hours [2]	>4.2kN

1. Samples cast and cured at 20°C
2. Measured in accordance with a prescribed test that involves casting a steel plate into a sample of bedding material and measuring the force required in order to remove it.

Only polymer resin based products are able to comply with these criteria and were exclusively used on all BT reinstatements. All the work was carried out by BT personnel who were closely supervised. Such reinstatements proved successful with a low incidence of failure. The company policy was revised in 1995 and recommended that the reinstatements should be made by a contractor and the supervision restricted to random checks. Polymer resin based bedding materials are seldom used by contractors concerned with the reinstatement of road ironwork. It has been considered necessary to specify a cementitious material which the majority of contractors are familiar to maintain the high quality of British Telecom reinstatements. In addition, the polymer resin bonds to the ironwork upon curing and a new unit is required every time a road is re-levelled.

Four proprietary cementitious bedding products were used in trial reinstatements in areas of heavy traffic loading. The performance of these installations was monitored and was used as a basis to select a bedding material for future reinstatements. It is believed that the method of installation will be left to the discretion of the contractors.

2.6.3 Mercury Communications Ltd Specification

This utility produced a specification for the installation and reinstatement of their ironwork in September, 1995 [27]. This standard was based on what is thought to be good practice and Preferred Method 7. The description of the method to be applied is very similar to Preferred Method 7 but the use of a cradle and winch is not stipulated. Additionally, a failure criterion is not included. All Mercury Communications ironwork units have a frame depth of 150mm. The surface of the chamber is required to be 165mm below the carriageway surface, which results in a bedding thickness of 15mm. The level of the chamber may be raised if required by using engineering bricks or quarry tiles.

Two proprietary products are listed for use as the bedding material. These are a cementitious mortar and a polymer resin compound that are both claimed to develop high strengths very quickly. Either material can be used to form the bedding layer.

This standard was only recently introduced so it is not known whether successful reinstatements have been achieved.

2.6.4 Highways Agency Standards

The Manual of Contract Documents for Highway Works [28] contains brief references to the installation of road ironwork. The first reference in Volume 1 describes that the bedding thickness should be between 10 and 25mm although this is rarely applied in practice. The use of proprietary quick-setting mortars are specified to form the bedding layer and a second reference, in Volume 7, specifies that this material should achieve a compressive strength of 20MPa within 2 hours.

The failure threshold of road ironwork installations is included in the Trunk Road Maintenance Manual [29]. It states that hazardous installations should be replaced immediately otherwise installations should only be reinstated if complaints are received. Both of these standards are focused on specifications and tolerances rather than procedures so a description of a method of installation is not included.

2.6.5 New Road and Street Works Act, 1991

This statutory regulation describes the methods and materials to reinstate openings in highways. The specification must be adhered to by all local authorities, utilities and their appointed contractors. It is mainly concerned with the reinstatement of trenches and the installation of pipelines and cables within U.K. highways. The materials and degree of compaction required for this purpose are thoroughly described. The reinstatement of road ironwork is only briefly mentioned. Such installations should only be re-bedded when their level exceeds a tolerance of ±10mm relative to the mean level of the immediately adjacent surfaces [2]. There is no description of recommended methods or materials to be used.

The quality of the bituminous material surrounding the ironwork is considered to be encompassed within this regulation. It is required that this material should be the same as the surrounding wearing course and at least 40mm thick. In many circumstances this would be HRA. It is implied that the use of bitumen emulsion

products are only suitable as a temporary measure. Such materials should be replaced within 10 days. The tolerance for the finished level of all surfacings is ± 6mm.

2.7 Summary

It can be seen that there are several materials that can be used to form the bedding layers for a road ironwork installation. These materials have significantly different properties and it is considered that they would influence the behaviour of the installation under traffic loading. An in-situ study of most of these materials was made in laboratory experiments described in Chapter 5.

Reinstatement specifications have resulted in some improvement in the quality of reinstatements but failures still occur. It is considered that the assumptions made about stress conditions and magnitudes as described in Sections 2.4 and 2.6.1 may not be correct.

3. Field Observations and Experiments

3.1 Introduction

Field observations were made throughout this research. The aim of these observations was to study the methods employed and identify the practical problems associated with reinstating road ironwork. The performance of these installations was subsequently assessed. A case study is presented of three reinstatements made on the A1 trunk road at Sandy, Bedfordshire.

The response of manholes in the field to loading has also been studied. The data gathered from these experiments has allowed an assessment of the interaction between a manhole and a pavement. This has been used to tender some explanations as to why the bituminous surfacing around road ironwork deteriorates at a much faster rate than the rest of the pavement.

3.2 Case Study: A1 Trunk Road, Sandy, Bedfordshire

3.2.1 Site Description

The condition of three reinstatements made on the A1 trunk road at Sandy was monitored throughout the duration of the research. This site has a history of a high maintenance requirement. The manholes provide access to a storm sewer running parallel with the road and are maintained by Anglian Water plc. They are located in the southbound nearside wheel track of the dual carriageway. The position and orientation of the ironwork is illustrated in Figure 3.1. Low speed traffic joins the A1 from St Neots Road as illustrated; this traffic may exert a large twisting force on the middle manhole cover. In addition, the north manhole cover probably experiences large braking forces as traffic slows to leave the A1.

When examined in January 1994 the bedding of the north and middle manholes was seen to have deteriorated resulting in settlement of the ironwork beneath the road surface and cracking of the HRA placed around the outside of the frames. Figure 3.2 illustrates the bedding material of the failed north manhole. It can be seen that the mortar in the bottom right hand corner had completely disintegrated which also

allowed the ironwork to rock. A grey iron unit was in use on the south manhole but the surface had polished under the traffic loading. It was considered that this would impair the skid resistance.

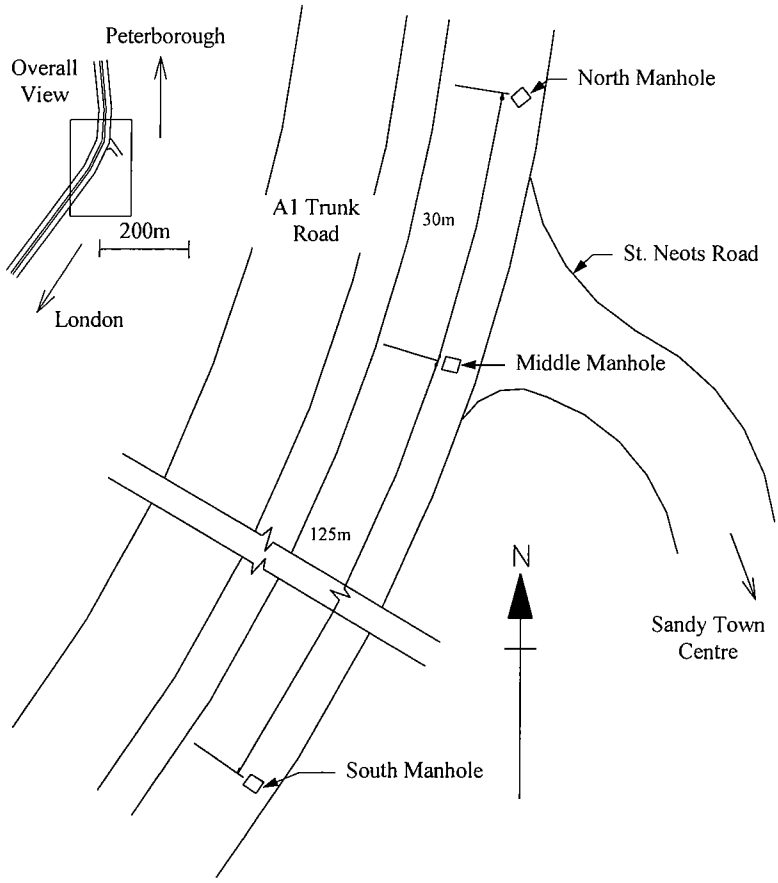

Figure 3.1: Diagram of Sandy test site

Figure 3.2: Bedding material condition of north manhole after failure

3.2.2 Site Visits

Visit No. 1: Reinstatement, 11th January, 1994

A lane closure was arranged to reinstate the ironwork between 10.00 a.m. and 3.30 p.m. The work was carried out by a contractor employed by Anglian Water plc. Bedding mortar A was chosen as the manufacturer claimed that it can develop a compressive strength of over 20MPa within 2 hours which complied with the Manual of Contract Documents for Highway Works [28]. The material only remained workable for approximately 10 minutes after the addition of the water. The contractor successfully managed to mix the mortar and bed the ironwork before it set. Water was mixed with dry powder until the desired workability was reached. The quantity of water was not measured exactly and this resulted in a wet mixture for the north manhole. Each ironwork frame was bedded on a 25mm layer of mortar with another 20mm placed above the flange. The partially completed reinstatement of the north manhole is shown in Figure 3.3. The frames were initially bedded on a large thickness of workable mortar and pressed down until the desired slope and level was achieved. This was indicated by placing a wooden straight edge over the frame.

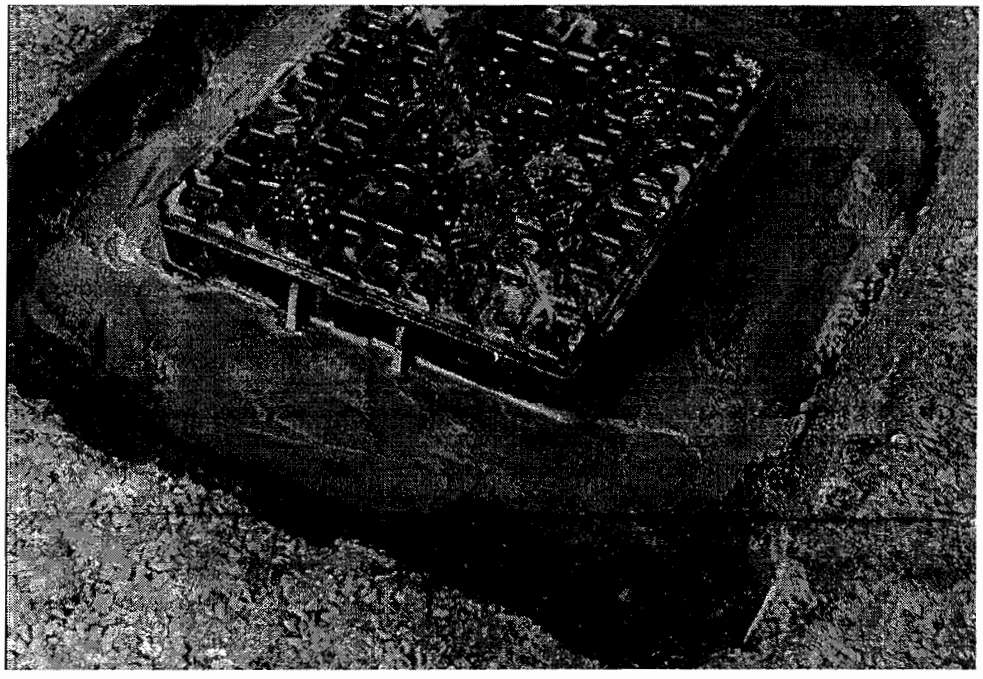

Figure 3.3: Re-bedded north manhole

The reinstatements were completed by backfilling with HRA and compacting with a roller after the mortar had hardened. This operation was carried out three hours after placing the ironwork. Only a small quantity of the material was required so a surplus amount from another maintenance contract was used. Stone chippings were rolled into the HRA to provide a similar skid resistance to the rest of pavement. Care was taken to avoid applying excessive vibrations to the ironwork as this could have damaged the bedding material.

A high level of workmanship was achieved for each reinstatement. The ironwork was evenly supported by the bedding material and it was considered by the contractor and client alike to have an adequate strength. A cylindrical specimen of the bedding material used for the north manhole was made for laboratory measurement of static modulus and Poisson's ratio. These values were 22GPa and 0.17 respectively at 2 days after mixing. This material displayed similar elastic properties after 28 days. Only one sample could be made due to the small quantity of bedding material mixed during the reinstatement.

Visit No. 2: Roadside Inspection, 3rd May, 1994

The condition of ironwork was monitored from the roadside and there was no visible sign of vertical displacement after 4 months in service. However, a small gap of approximately 2mm had appeared between the frame and surrounding backfill material along the leading or northern edge on each installation. The leading edge is on the right hand side of the picture in Figure 3.4. The gap may have been caused by a horizontal movement of the ironwork due to the heavy traffic loading but no corresponding heaving of the HRA on the opposite side of the frame was apparent. There were no other noticeable changes to the surface.

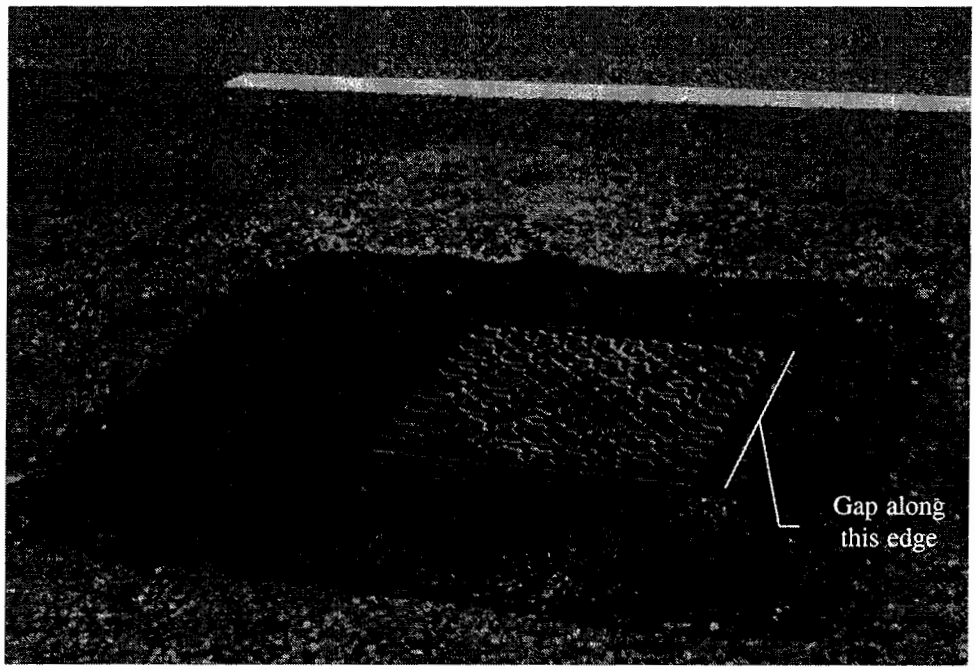

Figure 3.4: Gap on leading edge of ironwork. Traffic flows from right to left

Visit No. 3: Detailed Inspection, 3rd October, 1994

A lane closure was organised to lift the covers of the manholes to allow detailed inspection after 9 months service. Measurements were taken with the Falling Weight Deflectometer (FWD) along this stretch of road and on the covers to investigate the distribution of load through the chamber walls. A description of this machine and the results from this survey are presented in Section 3.4. A theodolite was used to measure the location of several key points on each frame by intersection. This was repeated on future visits to assess movement of the ironwork.

From an initial visual inspection, the gaps that were present on the previous visit had disappeared, although the HRA was beginning to break up along the leading edges as shown in Figure 3.5. Further inspection of the surface revealed hairline cracks in the HRA radiating out from the corners of the frame. This was most evident at the leading corner of the north manhole as illustrated in Figure 3.6. This may represent the onset of the deterioration of bituminous material that characterises the majority of installation failures. Further cracks were noticed along the length of the bitumen sealing between the existing pavement and bituminous backfill of the north manhole. These were again mainly present along the leading edge as shown in Figure 3.7.

The covers of each manhole were lifted to inspect the condition of the bedding mortar. The middle and south manhole had no visible sign of deterioration or cracking. However, the north manhole had a small vertical crack beneath the leading seating. This seating had the smallest bearing area providing support to the cover. This installation also had more cracks in the bituminous material surrounding the frame than the other two manholes. This installation may experience larger forces due traffic turning off the A1 trunk road into St Neots Road.

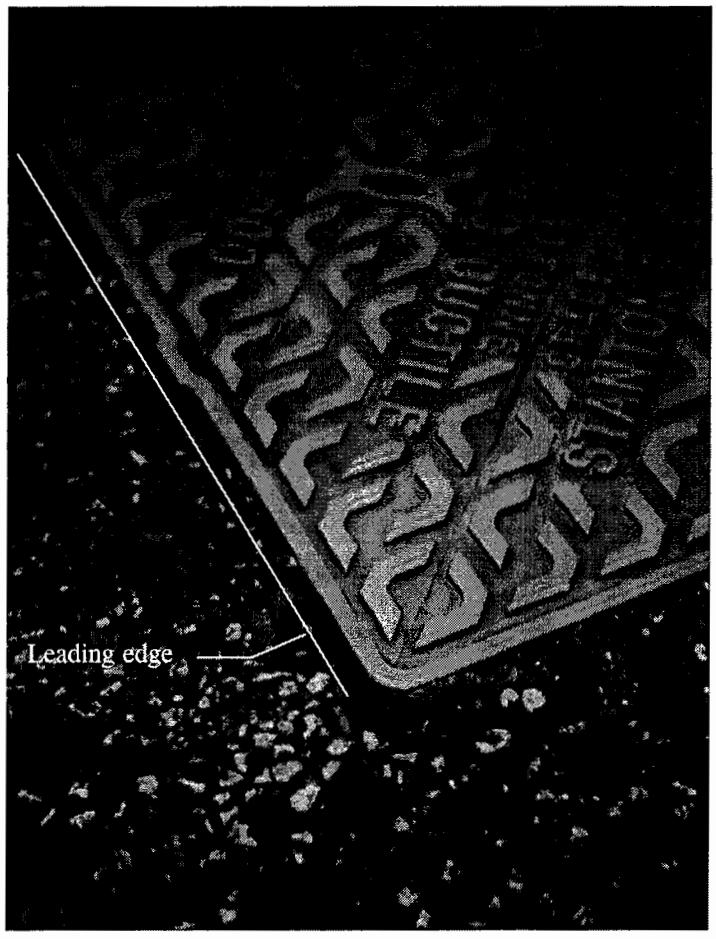

Figure 3.5: Deterioration of the HRA along the leading edge

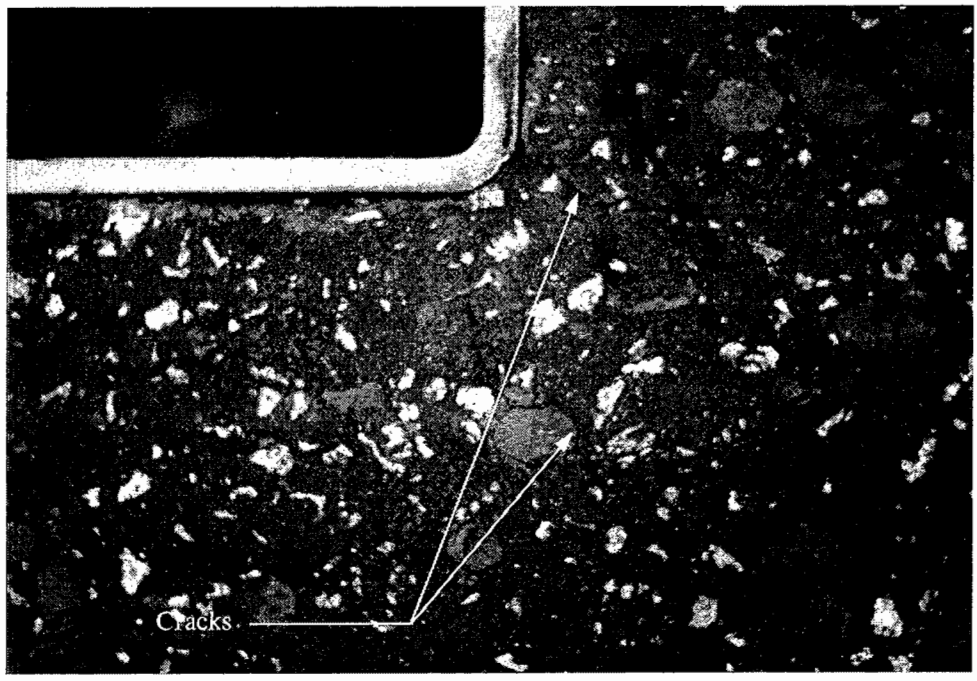

Figure 3.6: Hairline cracks in the HRA around the corners of the frame

Figure 3.7: Cracks along the bitumen sealing on the leading edge. Traffic flows from left to right

Visit No. 4: Roadside Inspection, 19th April, 1995

A visual inspection of the ironwork was carried out from the roadside after 15 months service. The small gap between the leading edge of the frame and the surrounding backfill material had reappeared on the north manhole. Theodolite measurements revealed that the ironwork at all the installations had not moved within the tolerance of the instrument either horizontally or vertically over the previous six months. The narrow gap may be attributed to thermal movement of the backfill material. The opening was first noticed on 3rd May, 1994 but had closed by 3rd October, 1994. This is possibly due to a softening of the bitumen during the summer months and re-compaction by the vehicle wheels or by expansion of the HRA and ironwork. The backfill material will have contracted over the winter months and resisted further compaction due to a higher stiffness at lower temperatures.

A closer inspection of the north manhole revealed that the support to the ironwork had failed. Small resilient vertical movements, only visible through a theodolite, were noticed when a heavy vehicle passed. This installation required reinstating.

Visit No. 5: Detailed Inspection and Reinstatement, 9th May, 1995

A lane closure was arranged on this visit to allow a close inspection and reinstatement after 16 months service. The hairline crack in the HRA radiating from the corner of the frame had increased in length and width on the north manhole as shown in Figure 3.8. The crack length was only 100mm long on 3rd October, 1994. However, this had increased to 300mm and propagated the full width of the reinstated HRA. There had also been a general deterioration of the HRA especially around the leading edge of the frame and at the leading joint of the HRA with the surrounding pavement. This is also shown in Figure 3.8.

Figure 3.8: Deterioration of the HRA surrounding the north manhole

An inspection from inside the manhole revealed a total of 9 cracks in the bedding material. All the cracks were aligned vertically. The crack observed under the leading seating of the frame was still evident but had not increased in width since the previous inspection. All the other cracks were located approximately 150mm from each seating. This is similar to the crack pattern observed during the shrinkage tests as shown in Figure 2.10. The HRA was carefully removed to fully expose the bedding material. This revealed all the cracks had propagated the full width of the mortar and across the chamber wall. This is shown in Figure 3.9.

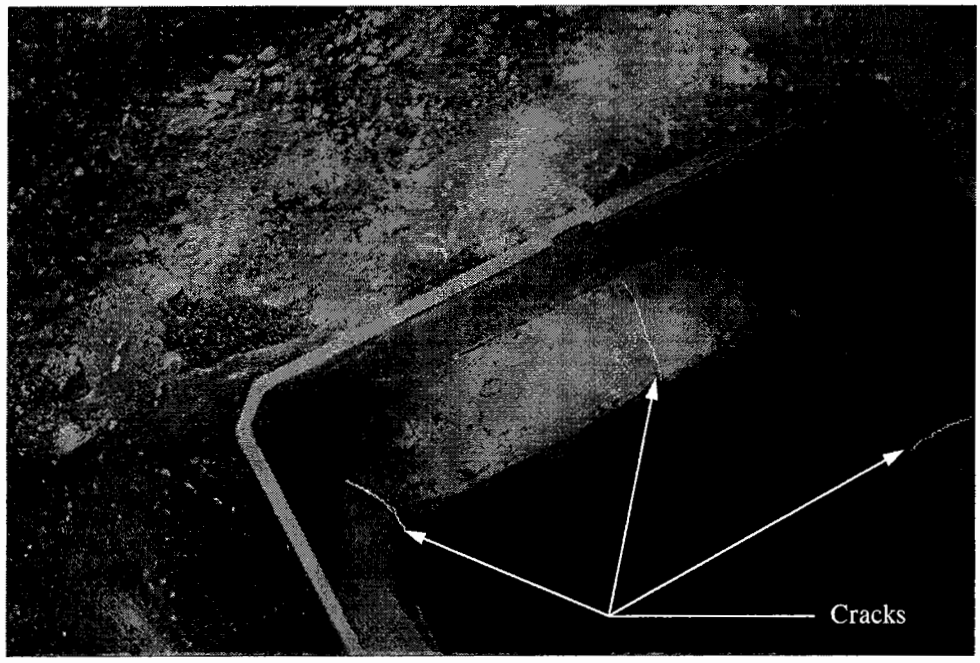

Figure 3.9: Cracks across the full width of the bedding mortar

On removal of the frame, it was noticed that the strip of mortar directly beneath the frame web was heavily crazed with vertical cracks all around the chamber. There did not appear to be a greater concentration around the cover seatings. This is shown in Figure 3.10. Severe cracking of the bedding material would have removed the support for the bituminous surfacing. It is considered that subsequent loading of the bituminous surfacing is likely to have induced cracks in this layer.

Figure 3.10: Severe cracks in the mortar directly beneath the frame web

Following the removal of the bedding mortar it was discovered that the top course of brickwork along the leading edge of the chamber was loose. The bond with the lower course of bricks had disintegrated and the bricks were damaged. It was difficult to determine whether this had caused the cracking of the mortar or vice versa.

A vehicle count was taken by Bedfordshire County Council at this junction on 21st April, 1994. A total of 12,175 vehicles were recorded passing over the north manhole in 24 hours. The number of vehicles with 3 axles or more was 1,007. Only 1,505 vehicles turned into St Neots Road, of which 87 vehicles had more than 3 axles. The estimated total traffic volumes passing over the reinstatement are shown in Table 3.1.

Table 3.1: Estimated total traffic volumes passing over the north manhole during its lifespan of 16 months

Traffic remaining on the A1 southbound		Traffic turning into St Neots Road	
Vehicles with three axles or more (inc. buses)	All other vehicles	Vehicles with three axles or more (inc. buses)	All other vehicles
402,300	5,048,100	57,150	610,650

An inspection of the middle and south manholes revealed no noticeable deterioration of the HRA or bedding material. All the ironwork units at the test site were bedded with the same type and thickness of mortar and to a high level of workmanship. It is considered that the north manhole may have failed before the others due to the high water content of the bedding material during mixing. This has the greatest effect on the physical properties of a cementitious compound and may have impaired the mature strengths [5,7]. It is also thought that the loads applied by passing vehicles may have had an effect. The north manhole experiences the braking force of vehicles turning into St Neots Road which may induce a horizontal tensile stress in the bedding material. This effect is later studied in laboratory experiments and by using finite element analysis. However, it is considered that this effect would have to be substantial as the estimated total number of HGV's turning into St Neots Road over the 16 month period was only 0.93% of the total vehicles passing this point.

A HDPE spacer was used as the bedding material for the reinstatement of the north manhole. This allowed a comparison between the performance of two significantly different proprietary products that experience the same loading regime.

The top course of brickwork was loose and was removed all round the chamber. This was replaced by 40mm thick pre-cast concrete curb units bedded with a 10mm layer of mortar A as used previously. These curb units provided an even support for the HDPE spacer. The finished surface of the curb units was 170mm below the surrounding pavement surface. A single 10mm thick HDPE spacer unit was bedded on top of the curb units with another 10mm thickness of mortar A. The ironwork frame was placed on top of the spacer and tamped level with the surrounding road surface. This is the manufacturer's recommended method of installation. The partly completed reinstatement was left for 30 minutes at this stage to allow the mortar to gain strength. It was considered this would reduce the risk of cracking in the mortar when laying the HRA around the outside of the frame. The partly completed reinstatement is shown in Figure 3.11.

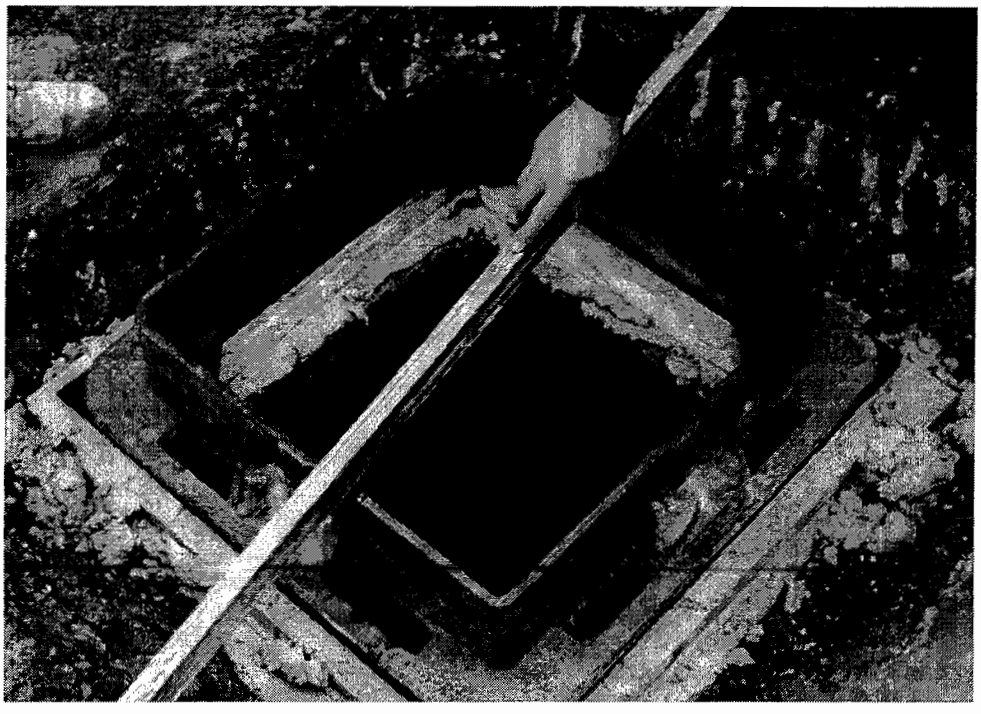

Figure 3.11: Partly completed reinstatement with a HDPE spacer. Spacer directly underneath frame flange

The installation was left for a further 30 minutes after laying the HRA. This was to ensure the HRA had cooled and hardened to an acceptable level before re-opening the carriageway to traffic.

The reinstatement was observed through a theodolite when subjected to traffic loading. It was noticed that there was a small resilient displacement of the frame when loaded by HGV wheels. This effect was not noticed in the surrounding HRA. The frame was monitored for approximately 30 minutes after re-opening the carriageway. No permanent deformation occurred during this time. Subsequent roadside inspections at 3 days and 8 days after reinstatement revealed no obvious signs of deterioration on the surface of the reinstatement.

Visit No. 6: Detailed Inspection and Reinstatement, 23rd October, 1995

A lane closure was arranged to allow a detailed inspection of all three installations. This involved lifting the covers to examine the condition of the bedding material from inside the chambers. It was found that the reinstatement made at the north manhole showed no visible evidence of deterioration to the HDPE spacer, the supporting bedding material or the surrounding HRA. A small gap had appeared between the ironwork and asphalt on this installation 4 months after the reinstatement consisting solely of mortar A was completed, as described in visit No. 2. In addition, cracks later developed in the HRA and along the length of the bitumen sealing, between the reinstated patch and existing carriageway. This had not occurred after bedding the ironwork with the HDPE spacer.

A HDPE spacer provides very little friction with the ironwork compared to other bedding materials, so restraint due to lateral forces is mainly provided by the bituminous material. This was considered to be a possible cause of failure, but there was no evidence of buckling of the asphalt along the trailing edge.

The middle manhole had deteriorated significantly since the last inspection. Hairline cracks were observed in the HRA radiating from the corners of the frame as seen on the north manhole when it was bedded with a cementitious material. Two vertical

cracks were also noticed in the bedding material from inside the chamber. One crack had developed under the leading seating of the frame, closest to the centre of the road, and the other had developed in between the two leading seatings as shown in Figure 3.12.

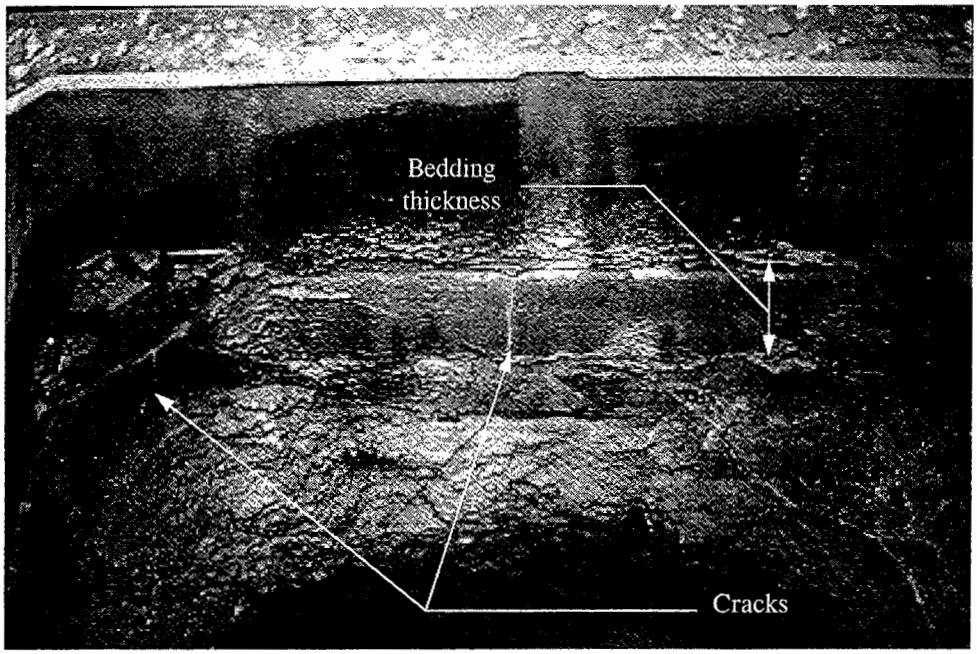

Figure 3.12: Cracks in the bedding mortar of the leading edge in the middle manhole

This installation exhibited a similar pattern of deterioration to the north manhole, although the ironwork frame did not rock under vehicle wheels. It was decided to leave this installation to allow further study of the failure characteristics.

The asphalt surrounding the south manhole had also deteriorated. The cracks were of a similar pattern and distribution to the middle manhole. Additionally, large cracks had developed along the full length of the bitumen sealing on the leading and trailing sides of the reinstatement patch. It was considered that this installation was in a worse condition than the middle manhole, so it was decided to reinstate it using mortar B which contains fibre glass strands. This material was shown to possess a greater mature tensile strength and lower shrinkage than mortar A as described in Section 2.2.1, so may increase its resistance to cracking.

The asphalt was carefully removed to reveal the bedding material underneath. It was found that the mortar was uncracked and showed no sign of deterioration. This manhole is located approximately 125m south of the junction with St Neots Road as shown in Figure 3.1. There is very little slow moving traffic or large lateral forces due to braking or accelerating at this point which may explain why the bedding material did not deteriorate. This is later examined in Chapters 5 and 6. However, there was deterioration of the surrounding asphalt which cannot be attributed to any influence from the bedding material since this remained in good condition.

On removal of the ironwork and bedding material it was found that the brickwork was in good condition and did not require re-pointing. Mortar B was mixed to the manufacturer's recommendation and placed on top of the brickwork. The original ironwork frame was positioned on top of the bedding and tamped down until the desired slope and level was achieved. This resulted in a bedding thickness of 25mm. The mortar inside the chamber was pointed to achieve a smooth finish in order to facilitate future identification of any cracks that may occur. This operation was completed before the mortar hardened which occurred 20 minutes after adding the water. An illustration of the bedded ironwork on the south manhole is shown in Figure 3.13.

Figure 3.13: Ironwork bedded with a cementitious mortar containing fibre glass strands

The reinstatement was completed two hours later by laying HRA around the outside of the ironwork. This was placed in two layers and compacted using a vibrating plate. Care was taken to avoid excessive vibration of the ironwork. A final inspection of the bedding material was made from inside the chamber before re-opening the carriageway. It was found that it had not been cracked when the HRA was placed and compacted.

A roadside inspection was made five months later and it was found that the north and south manholes did not display any visible evidence of deterioration on the surface. Additionally, the cracks in the HRA around the middle manhole had not changed significantly in this period.

Visit No. 7: Roadside Inspection, 6th February, 1996

An examination of the condition of the installations was made from the roadside. It was found that there was no change in the condition of the reinstatement made at the north manhole. However, the hairline cracks observed radiating from the middle manhole had propagated across the full width of the reinstated backfill material and also increased in width. This was the same pattern of deterioration as seen at the north manhole during visit No. 5.

Cracks were observed in the bitumen sealing material between the existing carriageway and reinstated bituminous backfill of the south manhole. This was most noticeable along the edges perpendicular to the direction of the traffic. This was also seen in previous reinstatements.

Visit No. 8: Detailed Inspection, 19th September, 1996

Another lane closure was arranged to allow a close inspection of the bituminous backfill and the bedding material of all three installations and further measurements were carried out using the FWD which are described in Section 3.4. It was found during an initial observation of the north manhole that cracks had developed in the bitumen sealing material and there was a general deterioration of the HRA around the leading edge of the ironwork as observed in the previous reinstatement.

However, an inspection of the bedding layer did not reveal any visible indication of deterioration. Further deterioration had occurred at the middle manhole although the ironwork did not rock under an applied load. Additional cracks were observed in the bituminous backfill radiating from the corners of the ironwork and parallel to the ironwork frame web. There appeared to be greater concentration of these cracks around the leading edge of the ironwork. The cracks running parallel to the frame web were located approximately 100mm from the ironwork. Cracks of this nature had not previously been observed at the north or south manholes prior to reinstatement but were noticed in other field observations. These are illustrated in Figure 1.3a. Further cracks had also developed in the bedding material. These were located in between the seatings along the leading edge.

Further bitumen sealing material had been placed in the joint between the existing carriageway and bituminous backfill of the south manhole since the last visit. However, this material had also developed cracks as seen previously. Additionally, a hairline crack was observed in the backfill material radiating from the leading corner of the ironwork closest to the centre of the road as noticed during previous inspections. An examination of the fibre reinforced bedding material revealed that no cracks had formed and was in the same condition as when it was installed.

3.3 Reinstatement Practice

Several other reinstatements of road ironwork providing access to sewers were observed during the research. All of the installations had failed within two years of a previous repair and exhibited the characteristics described in Section 1.2. The work was carried out by either direct labour organisation (DLO) personnel or appointed contractors. This provided an insight into how the work is actually done and the techniques applied. It also illustrated the practical problems that occur. Most employed a reinstatement method developed from their own experience. None of the specifications described in the last chapter were followed in the reinstatement of road ironwork providing access to sewers.

Great care was taken to divert traffic away from the manholes and the appropriate legislation described in the traffic signs manual, Chapter 8 [30] was adhered to in all cases. All reinstatements began by sawing through the bituminous material around the ironwork. This was always at a distance between 150mm and 250mm from the outside of the ironwork frame, and parallel to the edges. The bituminous material was broken out with a pneumatic hammer to reveal the frame flange and bedding material. The bedding material had deteriorated in most cases so the frame was able to move. All of the frames and covers were lifted out manually, and the failed bedding material was removed. The condition of the chamber was inspected in most cases and damaged brickwork was removed. This was replaced with engineering bricks using an OPC/sand mixture as the mortar. It was considered that rapid hardening bedding products were unsuitable for this application due to their short workable life, despite the relatively short time allowed for the road closure.

Proprietary cementitious bedding products were invariably used to form the bedding layer. It is believed that this material was suitable for this application but very difficult to use. The greatest problem was perceived to be the short workable life and the progressive hardening throughout this period. The bedding material was mixed manually in most cases and took approximately six minutes. By the time the mortar had been placed on the chamber surface it had stiffened considerably. This made it very difficult to tamp the frame down to the required level and ensure even support under the flange. A high level of workmanship was difficult to achieve with such materials. Polymer resin based products were not used in these reinstatements as they were considered too expensive.

The reinstatements were backfilled with HRA in all cases. The small quantity required was often left over from other repairs. The method of compaction varied. In some cases, a 28" vibrating roller was used and the HRA was compacted in a single layer. Some operators considered that the vibrations applied on the ironwork may crack the bedding material underneath, so a vibrating plate was used instead. Care was taken not to apply vibrations to the ironwork in these cases. Others considered that both methods of compaction would inflict some damage to the bedding material

and chose to re-open the road to allow the HRA to be compacted by vehicle wheels, which would provide a less harsh method of compaction. This approach often resulted in an irregular surface finish.

Discussions with highway engineers have revealed that some reinstatements are often carried out quickly to mitigate the disruptive nature of the works to passing traffic. There is usually enormous pressure to re-open the carriageway. In some instances on trunk roads, the police have insisted that the road should be re-opened, regardless of the quality of the reinstatement. Occasionally, the bedding material hardens before the ironwork is properly levelled. The best course of action in this event would be to remove the bedding material and start again. However, materials of a completely unsuitable nature are used to achieve the desired level of the ironwork. Such materials include fragments of the old bedding material and perishable substances, such as newspaper.

It is often perceived that poor installation is the cause of road ironwork installation failures. Although this may affect the longevity of a reinstatement it is emphasised that the workable characteristics of proprietary cementitious bedding materials are not conducive to high quality workmanship.

3.4 Manhole Deflection Characteristics

The existence of a manhole in a pavement represents a discontinuity because of the different structural characteristics of the pavement and the manhole installation. Different resilient and permanent vertical deflections occur generating shear strains at the vertical interface between the two structures. This may have a detrimental effect on materials that bridge over the interface, such as the bituminous surfacing. Field experiments were carried out to study the vertical deflections within a manhole at various depths at a purpose built test site. Subsequent experiments involved measuring the vertical deflection of manholes in public highways relative to the pavement structure.

The vertical deflection characteristics were studied in field experiments using a Falling Weight Deflectometer (FWD). The FWD is a trailer mounted device that applies a dynamic load simulative of a moving vehicle wheel. The magnitude of the load can be varied by altering the height from which the weights are dropped. Velocity transducers or geophones are located at various distances from the loading platen. These instruments are used to calculate deflections through electronic integration. The conventional use of the FWD is in the structural evaluation of pavements to assess serviceable life and assist decision making on maintenance treatments [31]. An illustration of the FWD is shown in Figure 3.14.

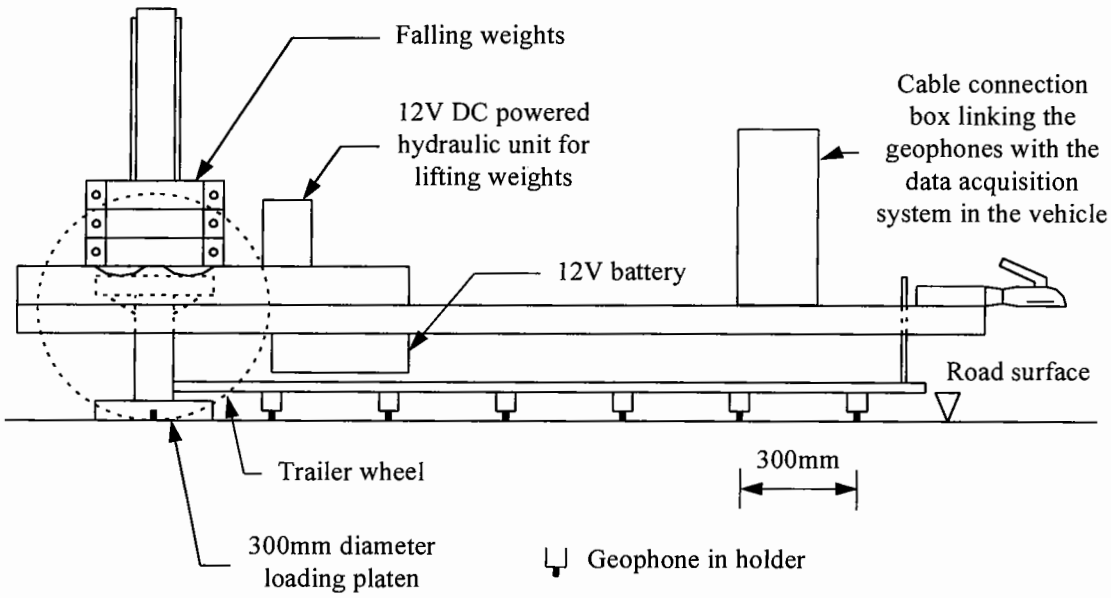

Figure 3.14: Illustration of the FWD

The experiments described here involved the use of the FWD in an unconventional way. The geophones were removed from their usual locations and positioned within a manhole. It was used purely as a machine that is capable of applying full scale loads and recording displacements in field conditions.

3.4.1 Holwell Test Facility

A test facility was constructed in the stock yard at the Stanton plc foundry in Holwell, near Melton Mowbray. The intention of this facility was to allow a variety of experiments to take place without the restrictions imposed on a public highway. A cross section diagram is shown in Figure 3.15.

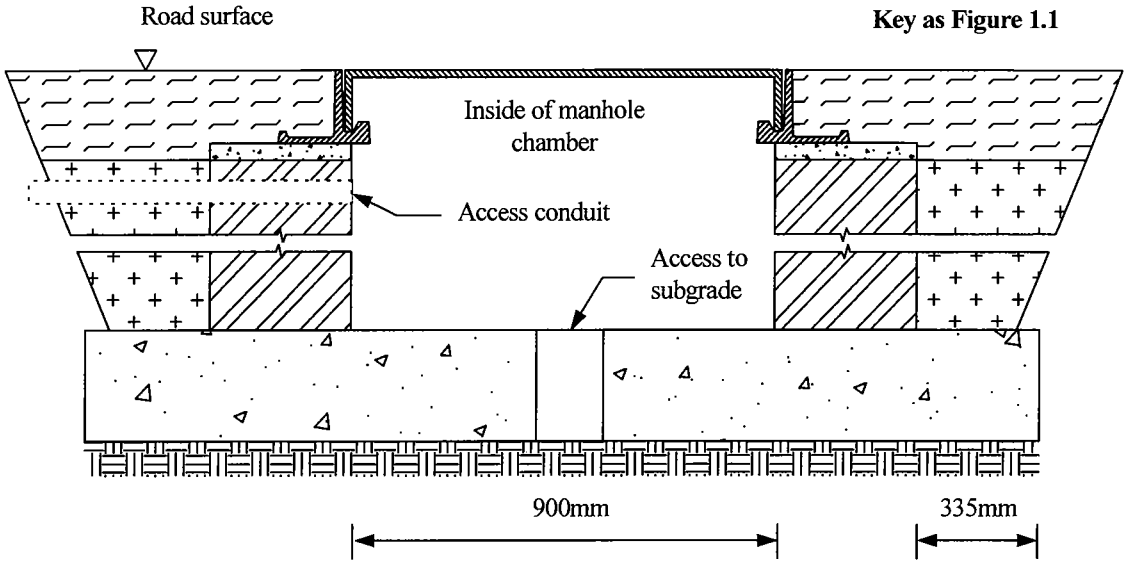

Figure 3.15: Section through the Holwell test facility

The manhole consists of a 2m x 2m x 0.25m thick concrete raft with the surface 1.4m below the surrounding ground level. Holes were formed in the raft to allow access to the subgrade. The chamber was built from Class B Engineering bricks and had internal dimensions of 900 x 900mm. This is slightly larger than a typical manhole opening as the chamber was also used by Stanton plc to test a prototype 900 x 900mm ironwork cover and frame. This was considered to be a standard design for a brickwork manhole at the time of construction. It was later discovered from Nottinghamshire County Council specifications that the width of the foundation slab from its edge to outside of the chamber wall should not exceed 250mm [32]. The exact reason for this detail is not clear, but it is considered that it has been included to reduce material quantities and the size of the hole required to be dug to construct the manhole. The distance from the outside of the chamber wall to the edge of the slab in the Holwell test facility is 335mm as indicated in Figure 3.15. Although this dimension is 85mm larger than the specified maximum it is considered that the facility was not entirely unrepresentative.

The experiment to study the manhole deflection characteristics involved measuring displacements at various depths. The FWD geophones were removed from their usual locations (Figure 3.14) and attached by their magnetic bases to brackets fastened to

the frame flange, the top of the brickwork, halfway down the brickwork, the surface of the concrete raft and on the subgrade. The wires to the instruments were passed through an access conduit and the cover was replaced. Loads of various magnitudes were applied on the cover by the FWD at several locations. The impulse loading was applied six times at each location at three different contact pressures. The typical response from the chamber can be seen in Figure 3.16.

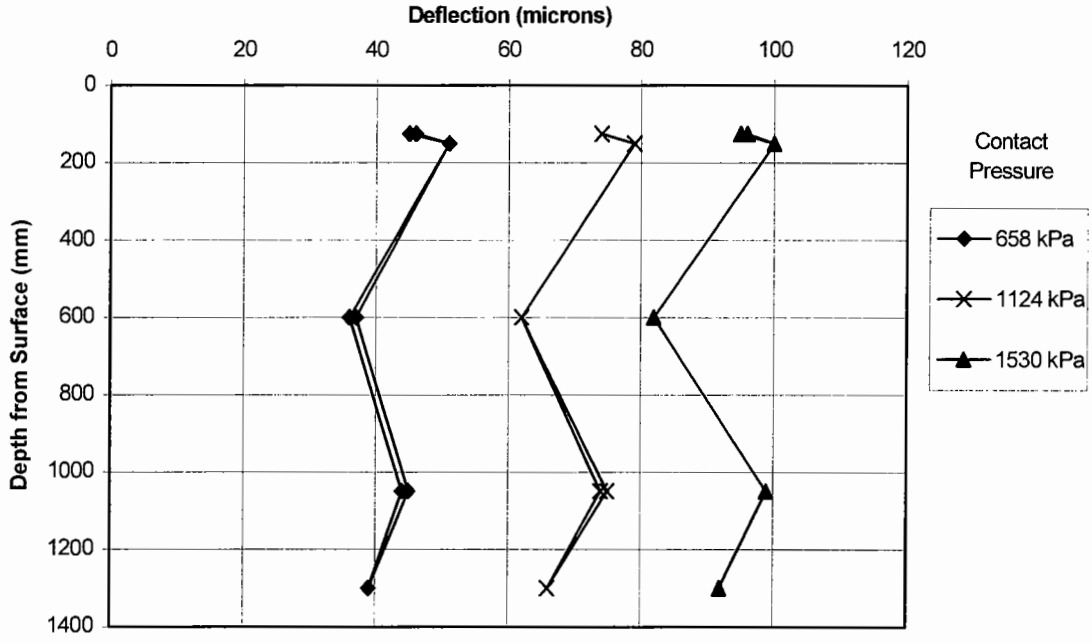

Figure 3.16: Displacement in the Holwell test facility

It can be seen that the deflection remains essentially uniform throughout the depth of the chamber. Hence, the manhole structure generally remained rigid whilst most of the displacement developed in the subgrade.

3.4.2 Test on in-service Manholes

Since the Holwell installation was not typical of highway practice, further experiments were carried out on manholes in public highways. The test method again involved using the FWD. On previous experiments, the wires to the instruments were passed through an access conduit and connected to the FWD. This facility does not exist in manholes found in public highways, so the wires could not be connected to the FWD after the ironwork cover was replaced. This was overcome by applying the

load directly onto the surface of a single wall of the brickwork chamber exposed during a reinstatement. The load was distributed over the wall by a stiff steel beam placed on a soft packing material. It was not considered possible to have a loading platen that would cover all the walls as it would be too heavy to lift manually and an even contact with the entire chamber surface could not be guaranteed. Four geophones were placed around the surface of the brickwork and another in the bottom of the manhole. These were connected to the FWD without the obstruction of the ironwork cover. An illustration of this apparatus is shown in Figure 3.17.

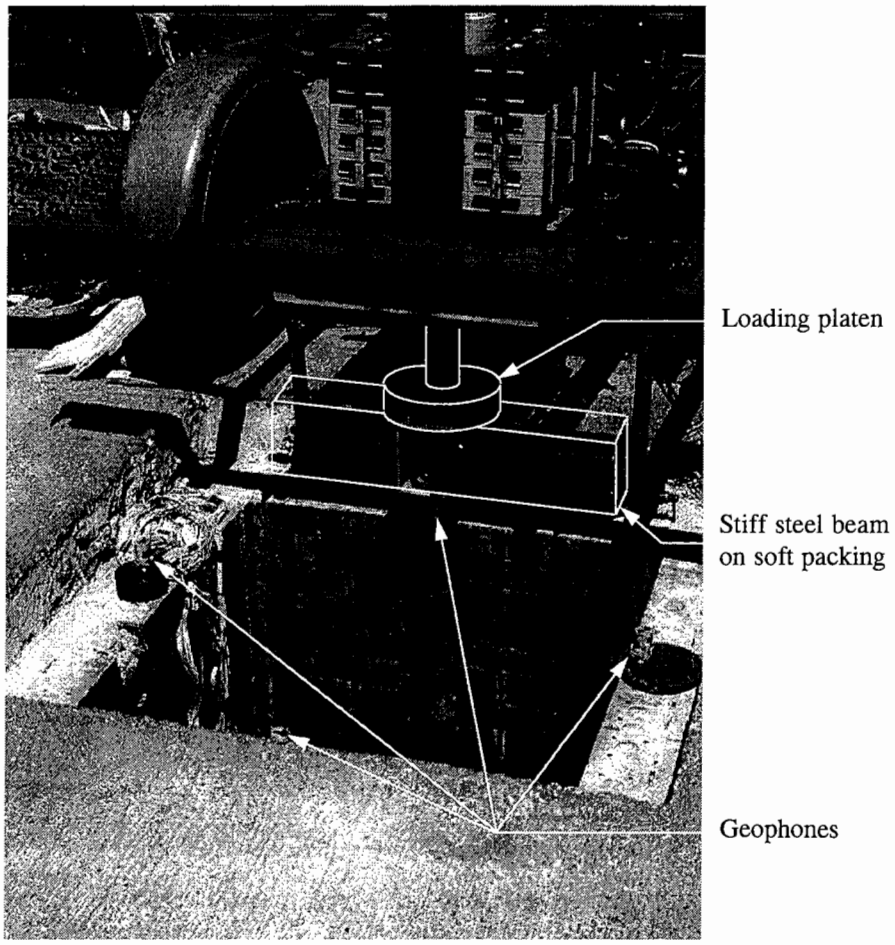

Figure 3.17: Photograph of the test apparatus

A load of 74kN was applied by the platen onto the stiff beam. The displacements were calculated from movements of the geophones and recorded on a portable computer. Although the load was not applied to the chamber symmetrically, by averaging the displacement from the four geophones on the surface and comparing them to the measurements at the bottom of the chamber, it was considered that these

results would provide some indication of whether the effect seen at Holwell was present. Six chambers of different construction were tested. The data from these chambers is shown are Table 3.2.

Table 3.2: Summary of the results from field experiments

Chamber location	Chamber type	Average surface displacement (microns)	Displacement measured at the bottom of the chamber (microns)
1. Kimberley	4m deep brickwork	17	16
2. Long Eaton	2m deep brickwork	32	28
3. Ilkeston	2m deep pre-cast concrete	51	47
4. Ilkeston	2m deep brickwork	45	38
5. Sandiacre	3m deep pre-cast concrete	64	61
6. Sandiacre	4m deep brickwork	67	61

These data show that the average deflection at the surface of the chamber is within 7 microns of the deflection at the bottom of the chamber. This suggests that the chambers generally remained rigid as seen at Holwell with most of the vertical displacement occurring in the subgrade. Additionally, there did not appear to be a trend between the depth and construction of a manhole chamber and the resulting deflection. Consequently, the stiffness of the soil has a strong bearing on the magnitude of surface displacement. It can also be seen that the magnitude of these displacements is small. Nottinghamshire County Council specifications [32] require that manhole chambers are backfilled with a sub-base material. This would provide considerable skin friction and restrain vertical movement of the manhole. It would also provide lateral restraint.

The maximum deflection of a pavement under the action of a wheel usually occurs at the surface, directly underneath the wheel. A pavement structure distributes the applied surface loads onto the underlying layers, so the magnitude of vertical deflection decreases with depth. The magnitudes of vertical deflection at various depths are influenced by the thickness and stiffness of the pavement layers and that of the subgrade [31]. Experiments were carried out by De Beer [33] to measure the deflection of several pavements at various depths when loaded by passing vehicles. Several different pavement constructions were tested and all the results illustrated a similar trend. A typical deflection profile induced by a 70kN load is shown in Figure 3.18.

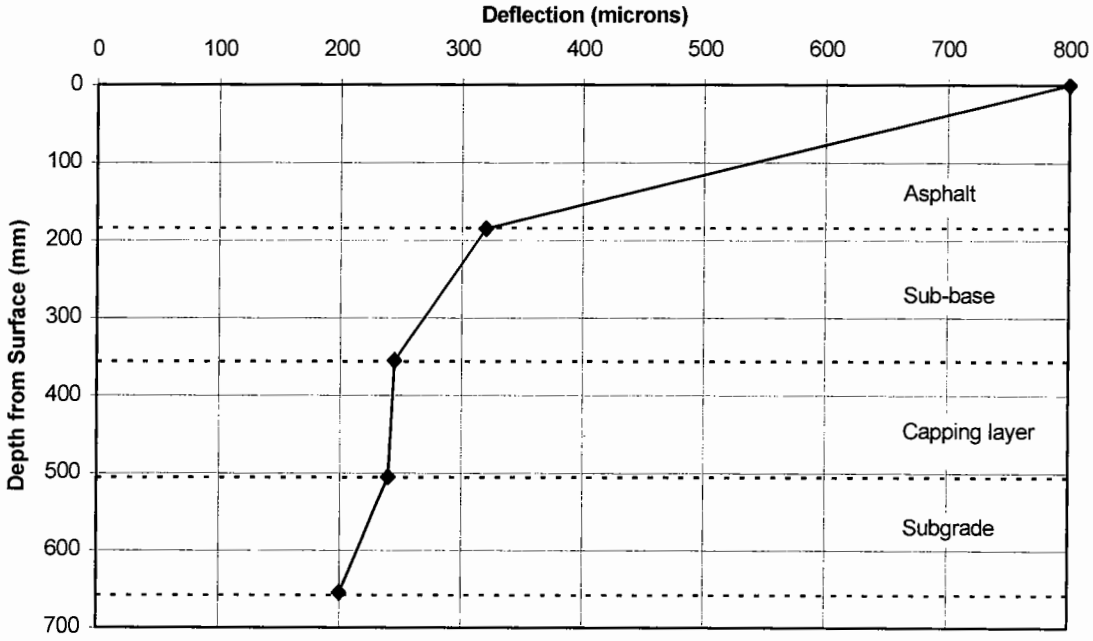

Figure 3.18: Vertical deflection profile through a flexible pavement [33]

It can be seen that the magnitude of the deflection is greatest at the surface and decreases with depth. This is the typical behaviour of a pavement. It can be seen by comparing Figures 3.16 and 3.18 that there is a distinct difference in the vertical deflection profiles between a pavement and a manhole. This would induce a shear force between the two structures. This will be at a maximum when the difference in vertical strain is the greatest. The magnitudes of the vertical displacements of a pavement at a depth greater than 500mm are significantly smaller than at the surface.

The difference in displacement with a manhole at these depths is likely to be small so it would not be likely to cause any damage. Discussions with highway engineers have revealed that there has been no evidence of damage around manholes below these depths.

The difference in displacement is greatest close to the surface. This would affect the bituminous layers of the pavement, often bridging between the two structures. The most damaging effect is considered to occur when loads are applied simultaneously on the manhole and the immediately adjacent pavement. Such loading would be applied by a multi-axle trailer. This is illustrated in Figure 3.19. This loading regime and the resulting shear force is thought to contribute to the deterioration of asphalt around manholes.

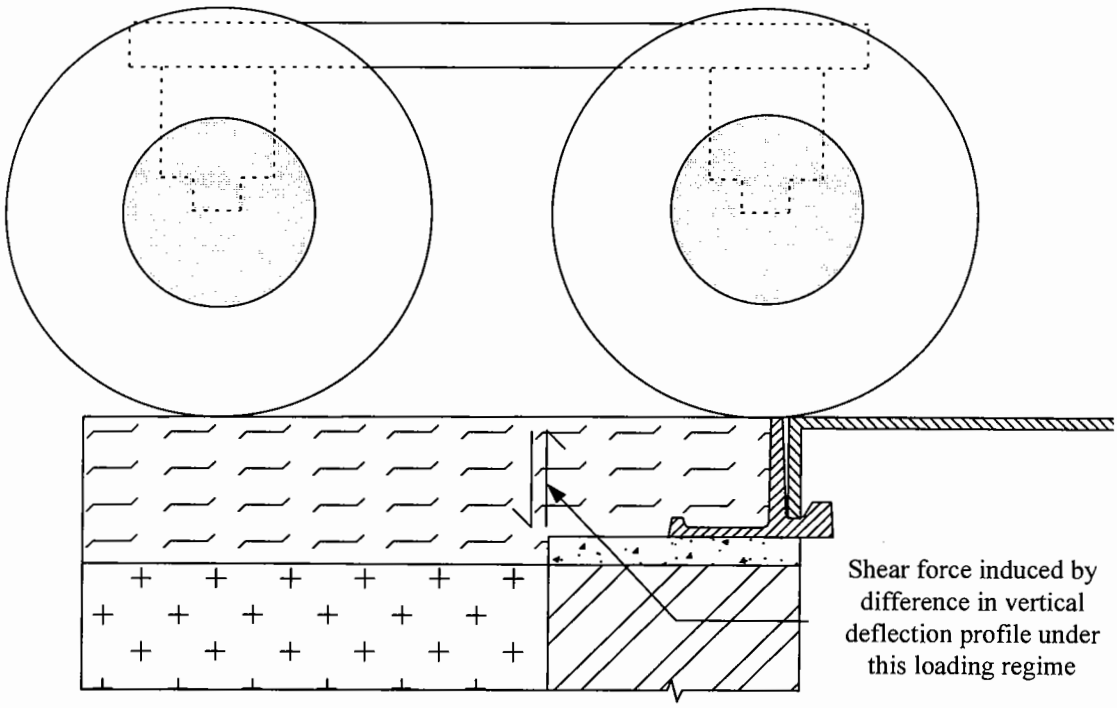

Figure 3.19: Possible worst loading case for bituminous materials around a manhole

Further field experiments were carried out to measure the surface deflection of manholes and the pavement immediately surrounding them. These measurements were recorded using the FWD in a conventional manner. The platen of the FWD was

initially positioned on the ironwork. A load of 49.5kN producing a contact pressure of 700kPa was applied on the cover and the resulting displacement of the platen was recorded. This test was repeated with a larger load which produced a contact pressure of 1100kPa. The load was applied three times for each contact pressure. The FWD platen was moved forward until it was on the bituminous backfill but immediately adjacent to the ironwork and the test was repeated. Further repetitions were made at 0.2m intervals from the second position. The spacing was increased to 0.5m when the platen was 2m away from the ironwork. The final measurement was taken at a distance of 4m from the ironwork. By recording the contact pressure and the displacement of the loading platen it was possible to calculate an in-situ effective stiffness assuming an equivalent linear elastic half space using Boussenesq's equations [34].

viz,

$$d = \frac{qB}{E}(1-\nu^2)I_S \qquad (3.1)$$

where

d = Measured vertical surface deflection underneath the centre of the loading platen

q = Measured pressure applied by loading platen

B = Diameter of the loading platen (300mm)

E = Effective in-situ stiffness

ν = Poisson's ratio (assumed to be 0.4 for entire half space)

I_S = Influence factor, which depends on the shape of the loading platen (1.0 for circular platen)

A total of eight manholes were tested around Long Eaton, Derbyshire and their stiffness was calculated by this method. The manholes were located in pavements of various ages and construction. These are summarised in Table 3.3. The three manholes on the A1 trunk road at Sandy were also tested by this method as mentioned during visit No. 3. It was later repeated at the north manhole when it was reinstated with a HDPE spacer.

Table 3.3: Summary of manhole and pavement constructions tested

Manhole Number	Pavement Construction	Approximate Age
1	Bituminous, no wearing course	Less than 5 years
2	Bituminous, no wearing course	Less than 5 years
3	Bituminous, HRA wearing course	Less than 5 years
4	Bituminous, HRA wearing course	Less than 5 years
5	Bituminous, HRA wearing course	Less than 20 years
6	Rigid, no overlay	Greater than 35 years
7	Rigid, with overlay	Greater than 35 years
8	Bituminous, HRA wearing course	Less than 10 years

The calculated values of effective in-situ stiffness for the pavement around manhole 8 are shown in Figure 3.20. It can be seen that the value of stiffness at the centre of manhole 8 is the lowest and is equal to 180MPa. The ironwork cover is only simply supported at its corners so the vertical deflection at the centre is mainly due to flexure. It can be seen that the stiffness immediately adjacent to the ironwork is approximately 1050MPa. The stiffness rapidly reduces to 560MPa at a distance of 1m and to 420MPa at a distance of 3m from the cover.

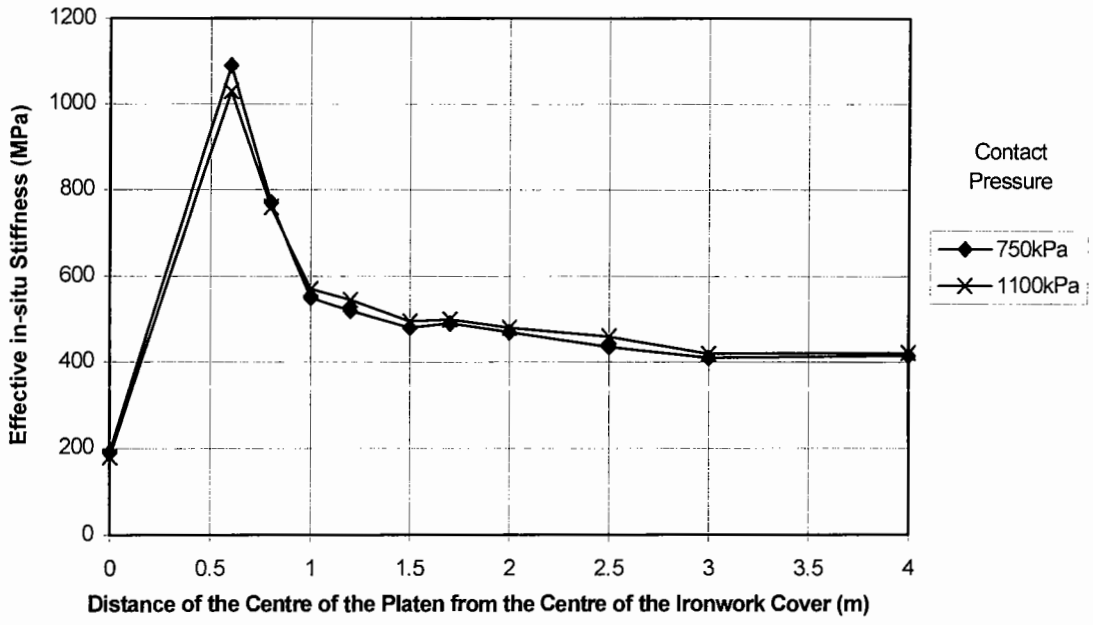

Figure 3.20: Effective in-situ pavement stiffness around manhole 8

These results illustrate that the pavement is stiffer closer to a manhole than at some distance away. Other experiments carried out on flexible pavements produced similar results including the south manhole on the A1 trunk road at Sandy. The stiffnesses next to the manhole were at least 150% larger than those at a distance of 2m.

Manhole 6 was surrounded by a rigid pavement construction. The calculated values of effective in-situ stiffness are shown in Figure 3.21. It can be seen that the difference in stiffness is less noticeable for this type of construction. However, all the calculations of stiffness are lower than those measured on the flexible pavements. It is thought that the subgrade may be particularly soft in this region. The earlier experiments showed that the subgrade strongly influences the displacement of a manhole structure and the same is true of a pavement [31].

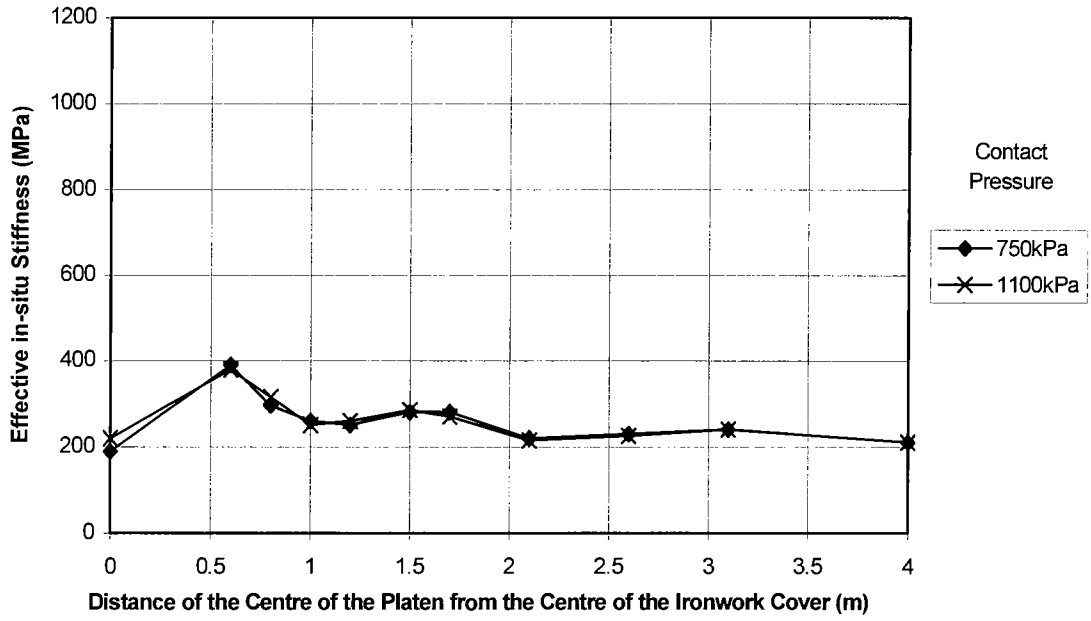

Figure 3.21: Effective in-situ pavement stiffness around manhole 6

The asphalt layer of a pavement can be considered as a beam on an elastic foundation. This layer will bend under an applied load inducing a tensile strain at the bottom of the layer. Tensile strains will also develop at the surface of this layer adjacent to the position of the load. It can suffer from fatigue cracking as a result of repeated applications of tensile strains above a critical level. This is illustrated in Figure 3.22.

If a load is applied next to a manhole, the asphalt directly above the chamber would experience lower vertical displacement due to the higher stiffness in the vicinity of the manhole. The asphalt at this point is effectively partially restrained from vertical movement. This restraint would affect the strains induced in the asphalt. A change in stiffness across such an abrupt interface would induce high tensile strains due to the partial vertical restraint. It has been observed that the strength of the bond between a bituminous material and the ironwork is weak. A lack of restraint would allow the bituminous material to rotate under the action of a nearby load. An illustration of the behaviour of this layer is shown in Figure 3.23. It is considered that a fatigue failure also contributes to the deterioration of the asphalt around manholes, in addition to the differences in vertical displacement distribution.

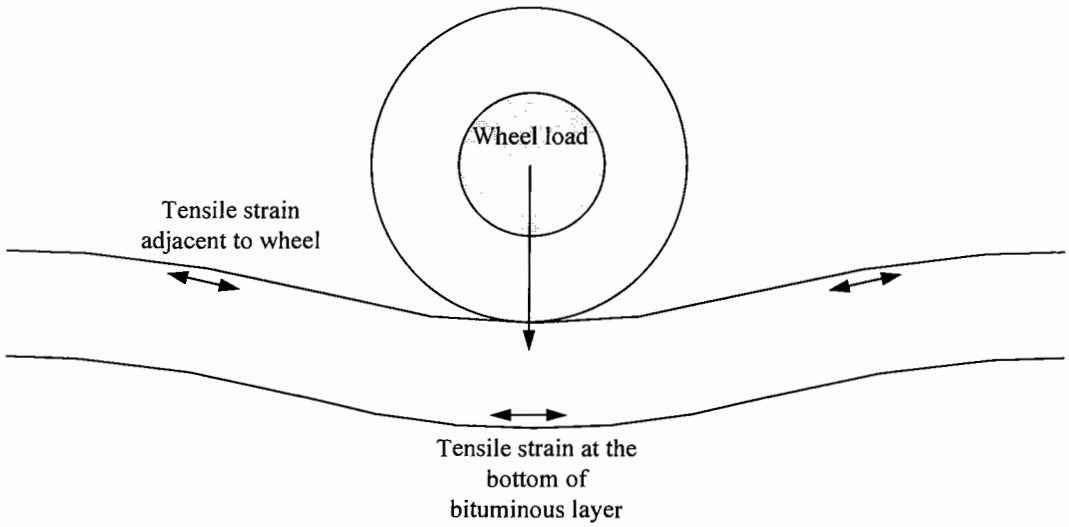

Figure 3.22: Displaced shape of asphalt layer away from a manhole

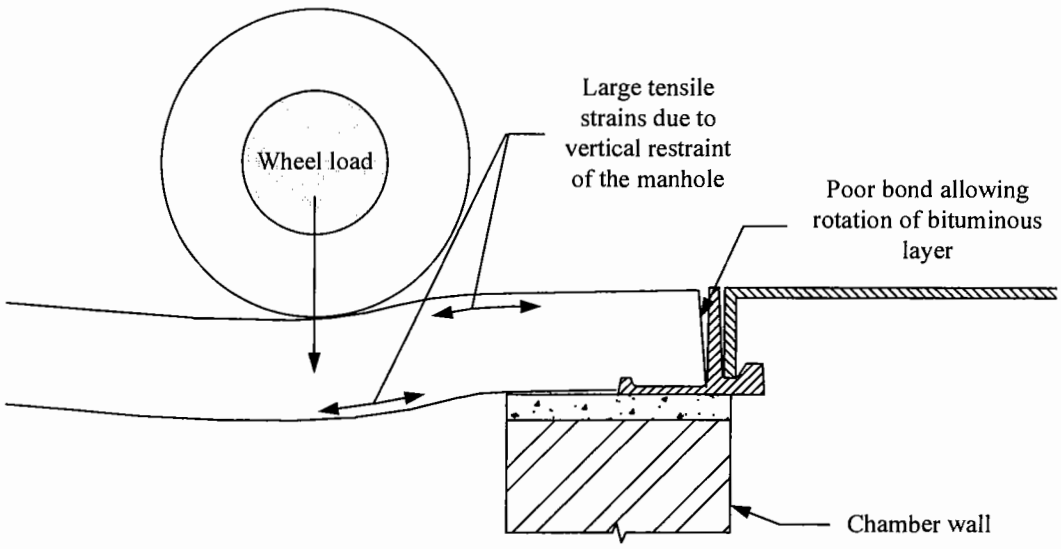

Figure 3.23: Displaced shape of asphalt layer in the vicinity of a manhole

3.4.3 Distribution of Load through the Chamber Walls

A knowledge of the distribution of load through the chamber walls would provide a further understanding of how a manhole interacts with a pavement. The previous experiment with the FWD was repeated at the test site on the A1 trunk road at Sandy. Readings from all the geophones were recorded on a portable computer when the platen was placed on the cover and at various distances from the manhole. This was carried out on all three manholes. Further measurements were taken at a distance of 30m away from each manhole. These data were used to assess the load distribution within the pavement without the influence of the manhole.

The deflection measurements were plotted against their radial distance from the centre of loading to produce a deflection bowl. Figure 3.24 illustrates the deflection bowl when the loading platen was placed on the cover of the north manhole when it was bedded with mortar A. These data are compared with the deflection bowl of the pavement 30m away. The largest deflection occurred directly underneath the loading platen when it was positioned on the manhole cover. The magnitude of the displacement was approximately 500 microns. This result has been omitted as it was primarily due to the cover bending.

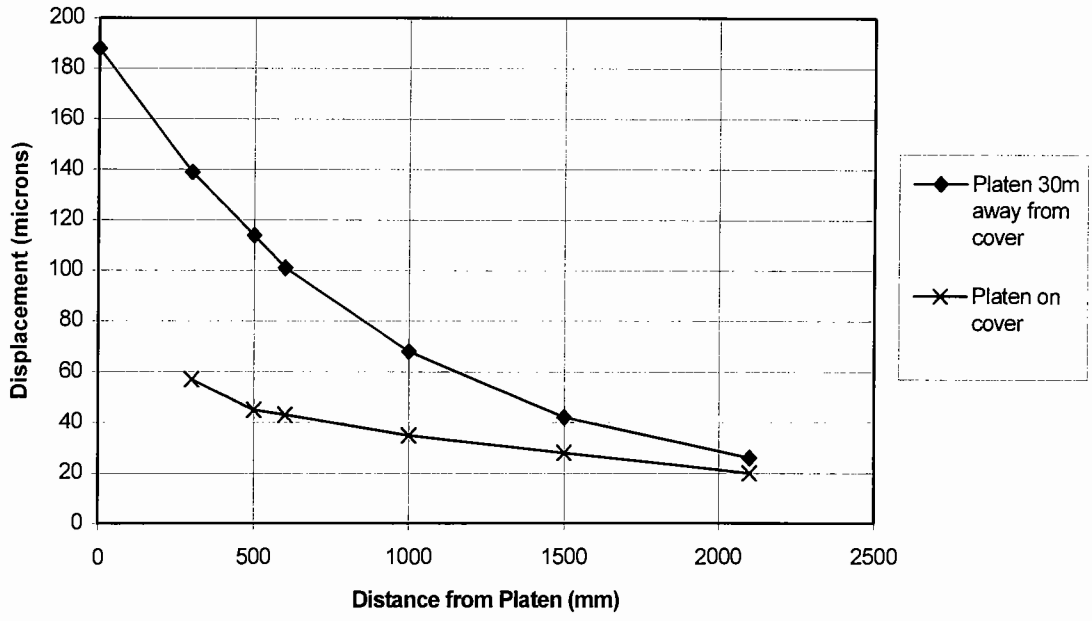

Figure 3.24: Deflection bowl of the north manhole compared to the pavement 30m away

The displacements measured on the pavement surface away from the manhole gradually decrease with distance from the loading platen. This demonstrates that the load is distributed over a wider area with depth. It can be seen that the pavement surrounding the manhole only displaced by a small amount when the load was applied on the manhole cover. This would imply that there is only a small amount of load distribution into the surrounding pavement. Such behaviour would suggest that the manhole displaces almost independently of the pavement. A similar trend in the surface deflection measurements was observed in the field tests in Long Eaton when the load was applied on the cover.

The behaviour of a manhole chamber can be compared to a pile foundation. The ultimate load that can be carried by a pile is dependant on its base resistance and shaft resistance. The base resistance is the product of the base area and the ultimate bearing capacity at the base level. The shaft resistance or 'skin friction' is the product of the perimeter area of the shaft and the average ultimate shearing resistance per unit area [34]. Manholes generally have a large base area and perimeter area compared to a pile so it is presumed that a manhole provides a very strong foundation, providing it has not been built on a very soft soil. Evidence from load tests on instrumented piles has indicated that most of the load is supported by skin friction on the upper part of the pile when only loaded to a fraction of its bearing capacity [34]. Such a condition may be analogous to a manhole under the action of a vehicle wheel. Due to the large perimeter area of a manhole, the shearing stress in the backfill would be low, so a small vertical deflection would be seen on the surface. This is seen in Figure 3.24. Additionally, a low displacement at the base of the manhole would result as shown in Table 3.2 in Section 3.4.2.

3.5 Theoretical Calculations of Vertical Displacement

Previous experiments have suggested that the in-situ effective stiffness of a pavement around a manhole is considerably greater than it is some distance away. The greatest value was found to be at the position of the chamber wall. If the stiffnesses could be matched then the high strains that are considered to develop in the asphalt would be

reduced. This could be achieved by using a low stiffness bedding material. Theoretical calculations were carried out to determine the desired stiffness of a bedding material to achieve this effect. This was done with the ELSYM5 computer program [35].

This program is used for determining stresses, strains and displacements in a pavement structure with up to five layers. It assumes that the materials exhibit linear elastic behaviour and are isotropic. Each layer is also assumed to be homogeneous and cover a semi-infinite area.

The purpose of the calculations was to determine a stiffness of bedding material that would provide a better compatibility in the displacements at the surface of the two structures. The surface displacement of a pavement is affected by many variables, so a sensitivity study was carried out incorporating changes in layer thicknesses and stiffnesses. The values chosen are considered to be the extremities of each variable. Manholes provide access to buried pipelines, so it is likely there would be a trench reinstatement in the pavement next to the manhole. Pipelines are usually bedded on pea gravel and backfilled with a sub-base material with a bituminous surfacing [2]. The depth of the pipeline will vary, but is generally buried at depths between 2m and 4m [2,32]. Further analyses were carried out with a sub-base extending to these depths. The results generated from all these calculations provided an indication of the range of surface displacement that can be found in pavements. These are shown in Table B.1 in Appendix B. This table also indicates the values applied to each variable. A series of calculations were carried out to determine surface deflections for various configurations of manholes. These results and the variables included in these analyses are shown in Table B.2 in Appendix B.

It is shown in all calculations that the manhole is stiffer than the pavement. This is the same observation noted in the field experiments. It would be impractical to have several bedding materials compatible with a small range of pavement stiffness as this is usually unknown. However, the stiffness of a bedding material could be matched to an average pavement stiffness. The average pavement displacement was determined

from the results shown in Table B.1. This value is 0.975mm. Additionally, the average manhole displacement was extracted from the data in Table B.2 and was found to be 0.018mm. The manhole configuration yielding the closest surface displacement to the average was No. 2 as indicated in Table B.2. This manhole has a chamber depth of 2m founded on a subgrade with a stiffness of 20MPa. The stiffness of the bedding material in this configuration was altered until the surface displacement was within 5 microns of the average pavement displacement. This value of stiffness was equal to 0.1MPa when a Poisson's ratio of 0.14 was applied. This is the desired stiffness of a bedding material to provide a better compatibility of displacement.

ELSYM5 assumes that each layer extends across a semi-infinite area which is not an entirely realistic representation of a manhole. It is appreciated that this stiffness value would not be compatible in all circumstances, and the result cannot be quoted to a high degree of accuracy due to the assumptions made in the calculations. However, it can be inferred that a bedding material with a lower stiffness than existing cementitious or polymer resin products would be more suitable. These products typically have a mature static modulus between 20 and 25GPa. The modulus of a HDPE spacer was measured and was found to be 16MPa, so it is thought that there would be a reduction in the difference of displacement between the two structures when this material is used. A slight reduction in the effective in-situ stiffness was measured at the north manhole at the Sandy test site when it was reinstated with a single HDPE spacer. Additionally, it took longer for cracks to develop in the surrounding HRA than when it was reinstated with mortar A. Laboratory experiments were carried out to assess the performance of these spacers and were compared to reinstatements made with cementitious mortars. The results from these experiments are presented in Chapter 5.

An alternative approach would be to use a chamber fabricated from a material of a lower stiffness than concrete or brick. It would not be practical to recommend the replacement of existing chambers with such a material, but this approach may be used in new construction or major sewer renewals. A proprietary product has been developed by Danelaw Ltd from recycled plastic. Several chambers have been

installed in the field and have appeared to withstand traffic loading satisfactorily. A FWD survey of a comparable nature to the experiment described in Section 3.4.2 was carried out. It was found that the chambers had a very similar in-situ effective stiffness to the surrounding pavement.

3.6 The Effects of Raised and Sunk Ironwork

It has been noted from the field observations that it is very difficult to place ironwork at exactly the same level as the existing road surface. The recommended tolerance has been set at ± 5mm to the surrounding level [1]. It is thought that this value has been determined through practice and judgement. In some circumstances it may not be possible to achieve an even surface profile. An example of this condition would be in the middle of a highway where a ridge is present for surface water drainage. This is illustrated in Figure 3.25.

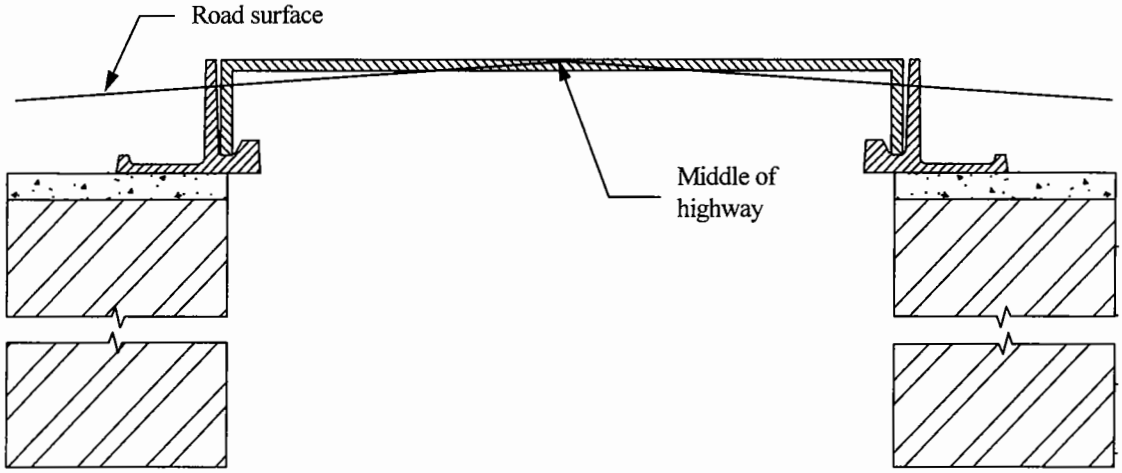

Figure 3.25: Example of where road ironwork cannot be set at the same level as the surrounding pavement

It is considered that the loads applied on raised or sunken ironwork would be different from those applied on perfectly level ironwork. Surface irregularities would introduce dynamic forces applied by vehicles in addition to the static force. It would be useful to know the magnitudes of these loads so the worst loading case could be determined.

Experiments were carried out by Stanton plc to study this effect but an unsuitable method of data recording was used so the results proved to be inconclusive. Other

research has been carried out involving the measurement of forces applied by HGV wheels on the vehicle and the forces experienced at the pavement surface [36]. Data from these experiments have been used to develop models to simulate vehicle loads. The models take into account several variables such as the vehicle suspension stiffness and tyre stiffness. A similar approach involves only using the tyre stiffness and assuming the suspension is rigid. This would overestimate the maximum load applied due to a surface irregularity but is considered to be satisfactory as this would provide an additional safety margin. The dynamic force due to a step in the surface profile is:

$$F = Kd \tag{3.2}$$

where

F = Dynamic component of force induced by surface irregularity

K = Tyre stiffness (typically = 3.5MN/m) [36]

d = Step height between ironwork and surrounding surface (Positive values denote the ironwork is above the surrounding level of the pavement)

This force is in addition to the static force applied by a wheel. A 5mm upwards step would result in a dynamic load of 17.5kN, so the total load for a 40kN static load would 57.5kN.

3.7 Summary

The field observations have shown that a standard method of installation is not used in current practice. Many DLO personnel or contractors employ methods that they believe will result in reliable reinstatements. Good quality workmanship can be achieved but it is difficult with cementitious mortars that have a short workable life. However, it was seen at the test site on the A1 at Sandy that good quality workmanship alone will not prevent failure. It would appear that the disintegration of the bedding material is due to inadequate properties.

Field experiments have provided possible reasons for the deterioration of the bituminous layer immediately surrounding the ironwork. It was found that the

vertical displacement profile of a manhole is incompatible with a pavement and the effective in-situ stiffness increases around a manhole. This behaviour is likely to induce high tensile strains in the bituminous layers which would reduce its fatigue life. This may be overcome by using a HDPE spacer to form the bedding layer. Early indications from the north manhole at Sandy suggest this may be a practical solution.

4. Equipment Development

4.1 Introduction

The field experiments revealed several practical problems in achieving quantitative in-situ measurements inside a road ironwork installation. It was considered to be very difficult to install instrumentation within a manhole and take measurements when it was re-opened to traffic. In addition, the magnitude of the load applied by passing vehicles could not be easily determined. It was decided to build a test facility in the laboratory that was simulative of field conditions where experiments could be carried out under carefully controlled conditions. By understanding the behaviour of manholes in the field it was possible to incorporate these features into the design of the laboratory test facility. A description of the development of this apparatus is given below.

4.2 Prototype Facility

4.2.1 Description

A prototype was constructed before designing the main laboratory test facility. This allowed an assessment of how simulative conditions could be achieved in the laboratory. It also allowed a study of the various types of instrumentation and data acquisition systems that would be applicable to these experiments. The prototype test facility consisted of a brickwork chamber built on the laboratory strong floor. It was constructed from Class B Engineering Bricks and 3:1 ratio of sand and OPC respectively laid in English bond. The height of the chamber was 1400mm with internal dimensions of 600 x 600mm. These internal measurements are the standard size of a manhole at the surface [22,32]. The chamber walls were 215mm (9") thick which is the length of a single brick.

A standard Stanton M-Way ironwork frame was bedded on to the top of the chamber with proprietary mortar A. The thickness of this mortar was 50mm, and an additional thickness of 20mm was placed above the flange around one corner. Embedment strain gauges specifically intended for embedding in cementitious materials were placed in the bedding close to the seatings, 10mm above the surface of the brickwork.

These instruments are identical to normal strain gauges but are encapsulated within a block of epoxy resin. The surface of the block is coated with sand particles to aid bonding to the surrounding material. They were the only known instrument that could provide a reasonably accurate measurement of strain within a cementitious specimen. Each gauge had dimensions of 25 x 5 x 3mm thick and they were all aligned to measure horizontal strains across the width of the mortar. An assessment of their accuracy of strain measurement is described in Section 4.4.2. An illustration of the prototype test facility is shown in Figure 4.1 which indicates the position of the embedment strain gauges. The gauge label is prefixed with the letter P to denote prototype facility in the discussion of the results.

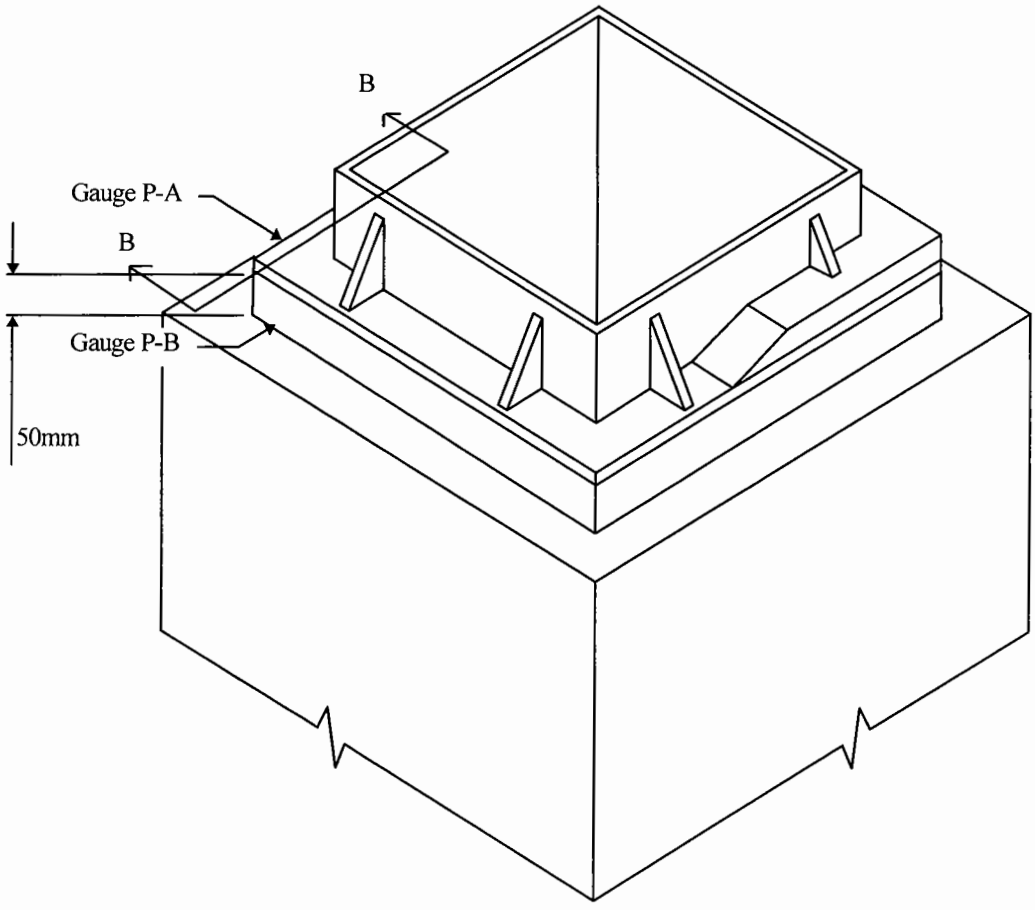

Figure 4.1: Illustration of the prototype facility

The first experiments involved loading the installation through a 300mm diameter platen placed on the ironwork cover at various locations. The strain gauges were calibrated to provide an output in microstrain using a gauge factor provided by the

manufacturer. The readings were taken at steps of approximately 5kN to a maximum value of 80kN and recorded on a datalogger. This load was applied slowly through a hydraulic jack at each platen position. The load was applied for eight loading cycles and three loading cycles were applied prior to recording the output to allow the loading platen and cover to settle.

The second experiment involved removing the cover and applying loads up to 120kN directly onto one of the cover seatings through a rigid bracket. Loads were applied to the seatings in the corners with and without mortar above the flange in separate experiments. A second loading bracket was made to apply loads at an angle of 15° to the vertical and these experiments were repeated. The maximum load had to be restricted to 50kN in these experiment as the chamber began to rotate about its base at higher loads. Sections through the chamber illustrating this apparatus can be seen in Figures 4.2a and b. The readings were again taken at intervals of 5kN over 8 loading cycles for each experiment.

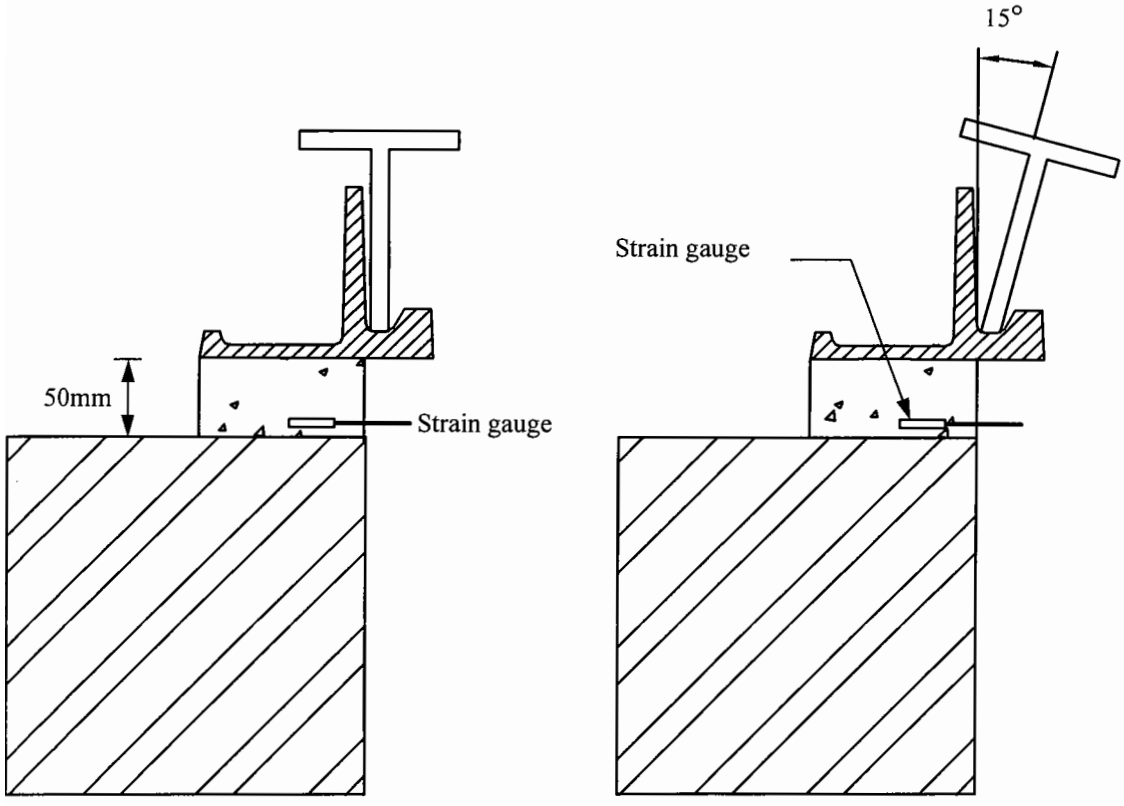

(a) Section B-B in Figure 4.1
Vertical load

(b) Section B-B in Figure 4.1
Angled load

Figure 4.2: Sections through the prototype facility

4.2.2 Results

The output recorded by gauges P-A and P-B is shown in Figure 4.3. These results were recorded when the loading platen was placed on the corner of the ironwork cover directly above these gauges. This loading position induced the largest output from these instruments.

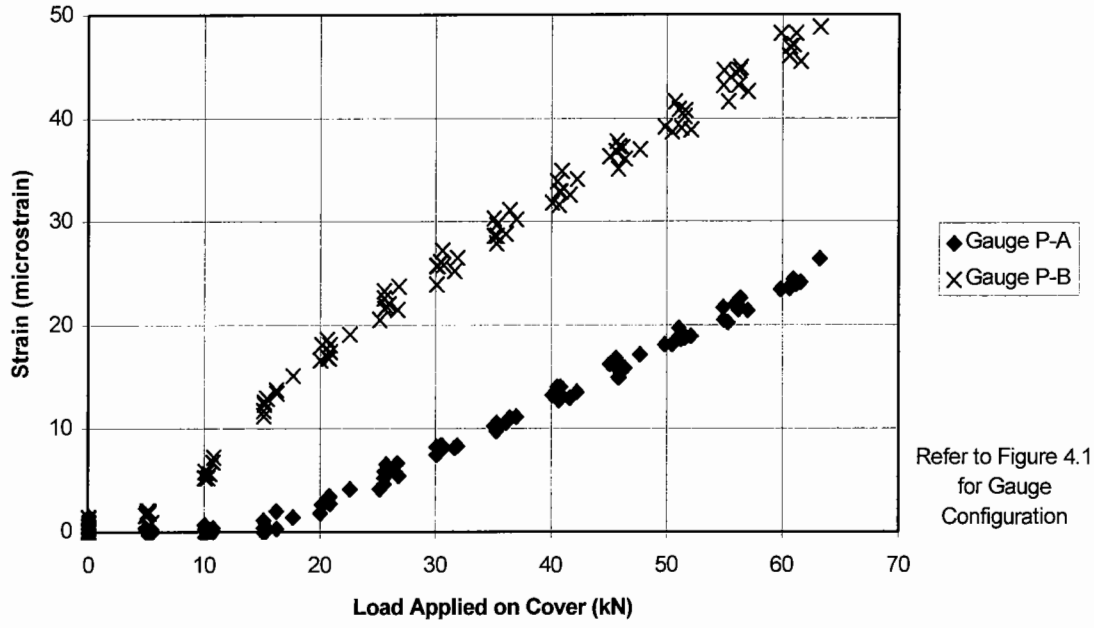

Figure 4.3: Results recorded when loaded through a 300mm diameter platen placed on the cover

Figures 4.4 and 4.5 show the output from the same gauges when the load was applied to the seating through a vertical and angled bracket in separate experiments. The data collected from other instruments located in the opposite corner with bedding material above the flange produced similar results.

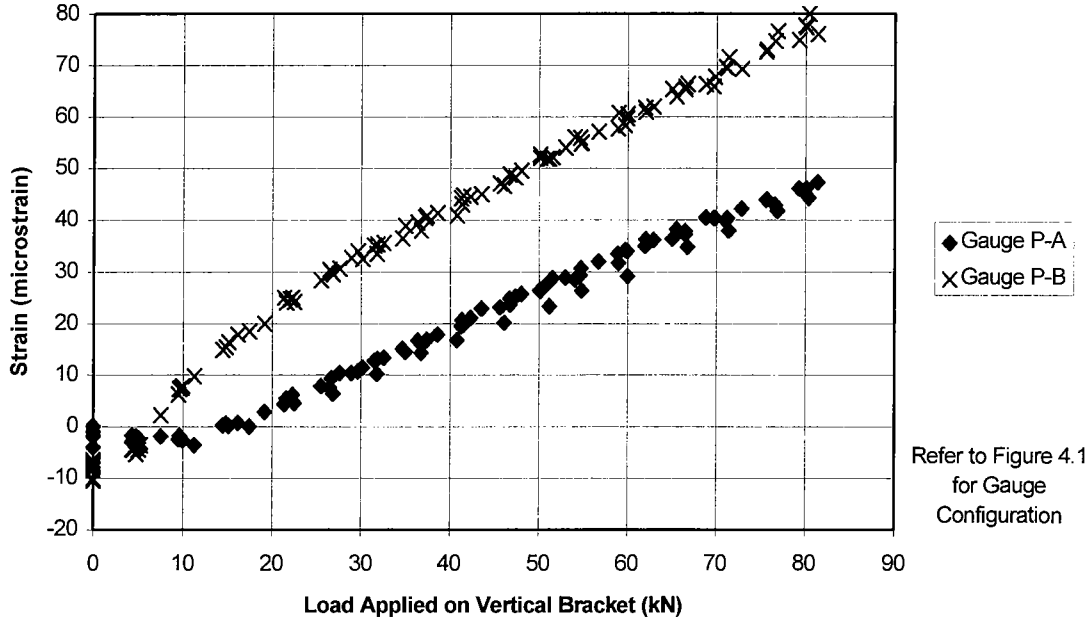

Figure 4.4: Results recorded when loaded through a bracket mounted vertically in the cover seating

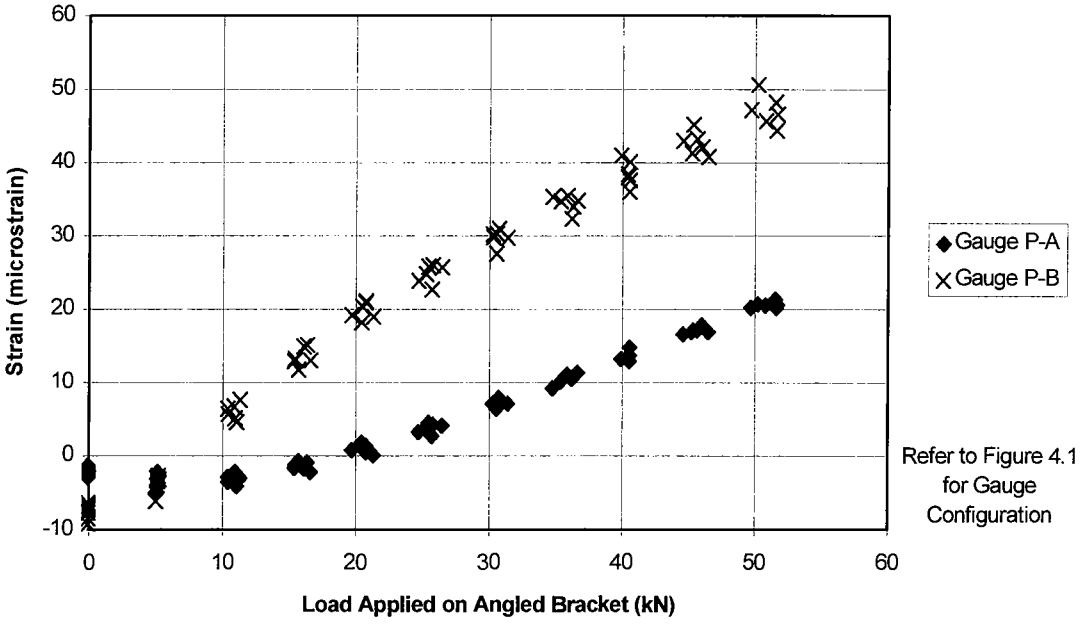

Figure 4.5: Results recorded when the loaded through a bracket mounted at 15° to the vertical in the cover seating

All of the experiments indicated that a tensile strain developed across the width of the bedding material when load was applied to the ironwork. Although these strains are

small, it is interesting to note that tension did develop in the bedding material, since it has previously been thought to be entirely in compression.

4.2.3 Review of Prototype Facility

On completion of the experiments, an assessment of this test facility was made. The shortcomings were identified so they could be mitigated in the design of the main laboratory test facility. These are discussed below.

Scale Effects

It was thought that using full scale components provided the most realistic simulation. Building a half scale model would be difficult as this would require custom made ironwork castings that may not be an exact likeness. Additionally, the aggregate in the proprietary bedding mortars would not be at the appropriate scale and may affect the results. From these considerations it was decided that the laboratory test facility should be built at full scale.

Confinement

Observations from the A1 test site revealed that the failure of the bedding and of the bituminous material immediately surrounding the ironwork are not necessarily related. A study of the behaviour of the bituminous materials would require a pavement structure typical of an urban environment to be built around a chamber. These pavement layers should be built at full scale to be compatible with the manhole.

Loading

The load was applied to the prototype test facility through a hydraulic jack connected to a loading frame. It was difficult to move the position of this jack as the loading frame was fastened to the laboratory floor. It was considered useful to know the position of the load causing most damage to an installation. Hence, it was decided that the load should be capable of application at any point on the surface of an installation.

Temperature Effects

The air temperature in the laboratory was studied over the duration of these tests and was found to vary between 18 and 21°C. This would not significantly affect the behaviour of brickwork, bedding mortar or iron but may affect the bituminous material. It was decided to monitor the temperature variations during experiments with the laboratory test facility.

Foundation

It was noted in Section 3.4.2 that most of the vertical deflection of a manhole develops in the subgrade. The prototype test facility was built on the laboratory strong floor which provided negligible vertical deflection. It was considered that this effect should not be neglected in the laboratory test facility otherwise misleading results may be recorded. The subgrade could be simulated by placing the manhole on a layer of material that would provide the required vertical deflection. Two chambers could be built on different materials to represent different subgrade conditions. The selection of such materials is described in Section 4.3.3. Additionally, the chambers should extend to a depth of at least 1500mm to provide a reasonable similarity to field conditions. It was decided to form the foundations to each chamber at the bottom of a pit and backfill with clay to form the support for the pavement. This would result in chambers 1900mm deep.

4.3 Laboratory Test Facility Development

4.3.1 Preparation

A redundant test pit built beneath floor level existed at the south end of the laboratory. The dimensions of this pit were 4.1m x 2.1m x 1.9m deep. The size of the pit allowed two manhole chambers to be built, so each could be founded on a layer of material with a different stiffness to represent two subgrade conditions. This would be easier than building a large tank above ground level and ensuring that the walls were sufficiently stiff to provide negligible outward movement. The walls and floor of the pit were constructed from 150mm thick reinforced concrete. It was considered that such construction would not move by an appreciable amount under the action of the applied load. The water table is estimated to be only 1m below the surface in this

region of the laboratory. However, the pit was waterproofed during construction with a plastic membrane and the walls and floor were found to be dry on inspection.

Investigations were made into selecting suitable materials to simulate the subgrade stiffness. It was intended to select materials that represented subgrades with stiffnesses of 30MPa and 175MPa. These values were chosen to represent typically 'soft' and 'stiff' subgrades at a depth of 2m below the pavement surface [37]. The original proposal was to build one chamber deeper than the other. The shorter chamber would be supported by a thickness of compacted clay. This thickness would provide a difference in stiffness between the two installations. However, this method was not suitable as preliminary calculations found that a large thickness of the available silty-clay would be required to provide the desired difference in stiffness. Instead, it was decided to represent the subgrades with layers of rubber. Each layer covered one half of the pit floor so the backfill material had the same support conditions as the manhole.

4.3.2 Chamber Design

The field experiments described in Section 3.4.2 indicated that a manhole chamber generally remains rigid under load, regardless of the materials from which it is built. Additionally, there does not appear to be a higher incidence of failure of the road ironwork supported by chambers built from brickwork when compared to concrete chambers. It was decided that both chambers should be built from brickwork as these could be fitted into the rectangular pit more easily than circular pre-cast concrete units because of their square shape. Each brickwork chamber was constructed from Class B Engineering bricks and had internal dimensions of 600 x 600mm. The thickness of the walls increased from 215mm to 317mm at depths below 1.5m from the surface. Each chamber was supported by a concrete slab foundation with dimensions of 1300 x 1300 x 150mm thick. All of these details complied with Nottinghamshire County Council specifications [32].

It was decided to position the chambers towards one side of the pit, so a small area of pavement could be built adjacent to them. This would allow a study of the behaviour

of the bituminous materials when the load was applied on the manhole, and at a distance of up to 1m away. It was thought that such investigations would allow a better understanding of how the manhole interacts with the pavement, and how the damage to the bituminous materials could be ameliorated. The proximity of the pit walls was thought to have some effect on the behaviour of the pavement and manholes. Efforts were made to reduce the friction by covering the pit walls with heavy duty polyethylene sheets. It was considered there would still be some boundary effects so field verification experiments would be required. These are described in Section 7.7.

4.3.3 Rubber Selection

An estimation of the load that would be experienced at the base of the manhole was made before determining suitable rubber types and thicknesses. The loading frame was designed to apply a peak load of 120kN. The load experienced under the manhole foundation was anticipated to be 30% less due to skin friction of the chamber walls. The resulting 84kN load was expected to be evenly distributed by the concrete raft foundation.

Vertical displacements of both subgrades were calculated under this load regime by assuming an equivalent elastic half space using Boussinesq's equations [34]. It was assumed in these calculations that the manhole remained rigid and the load was applied directly onto the subgrade. A Poisson's ratio of 0.35 was applied in all calculations. Further calculations were carried out with the elastic layer analysis computer program: ELSYM5 [35]. These calculations again assumed the manhole remained rigid and only the subgrade layer was simulated. The results are shown in Table 4.1.

Table 4.1: Estimations of vertical deflection by two methods

Method	Displacements for two Subgrade Stiffnesses (mm)	
	30MPa	175MPa
Boussinesq	2	0.4
ELSYM5	2.1	0.4
Average	2.05, say 2	0.4

Previous laboratory experiments carried out by others have used a similar technique to simulate the subgrade [38]. However, a natural rubber or synthetic equivalents have always been used. These materials are expensive and it was estimated that it would cost approximately £10,000 to use this kind of rubber to produce the simulative conditions in the laboratory test facility. Other types of rubber and closed cell sponges exist that are far cheaper. Samples were obtained and cut into squares of 215 x 215mm. The dead weight of the manhole structure was calculated from unit weights and volumes of the component materials. This was equal to a load of 1kN acting over an area of 215 x 215mm. The applied load on a sample of this size was calculated from the expected vertical stress at the bottom of the chamber. This was equal to 2.5kN. The dead weight and applied load were also calculated for the situation when load is applied on the backfill. This was found to be approximately equal to the values under the manhole chamber.

Each rubber sample was placed in a stiff steel box with internal dimensions of 215 x 215mm and covered with a stiff loading platen. The box provided the confinement that was expected at the base of the pit. Two LVDT's were placed on the platen to measure the vertical displacement of the rubber. The test apparatus was placed in an Instron test machine and a steady load of 1kN was applied for at least 15 minutes. This allowed the rubber to settle within the box under the equivalent dead weight of the manhole chamber. The load was gradually increased to a maximum of 12kN. The resulting displacements were recorded at 0.3kN intervals. An illustration of the apparatus is shown in Figure 4.6.

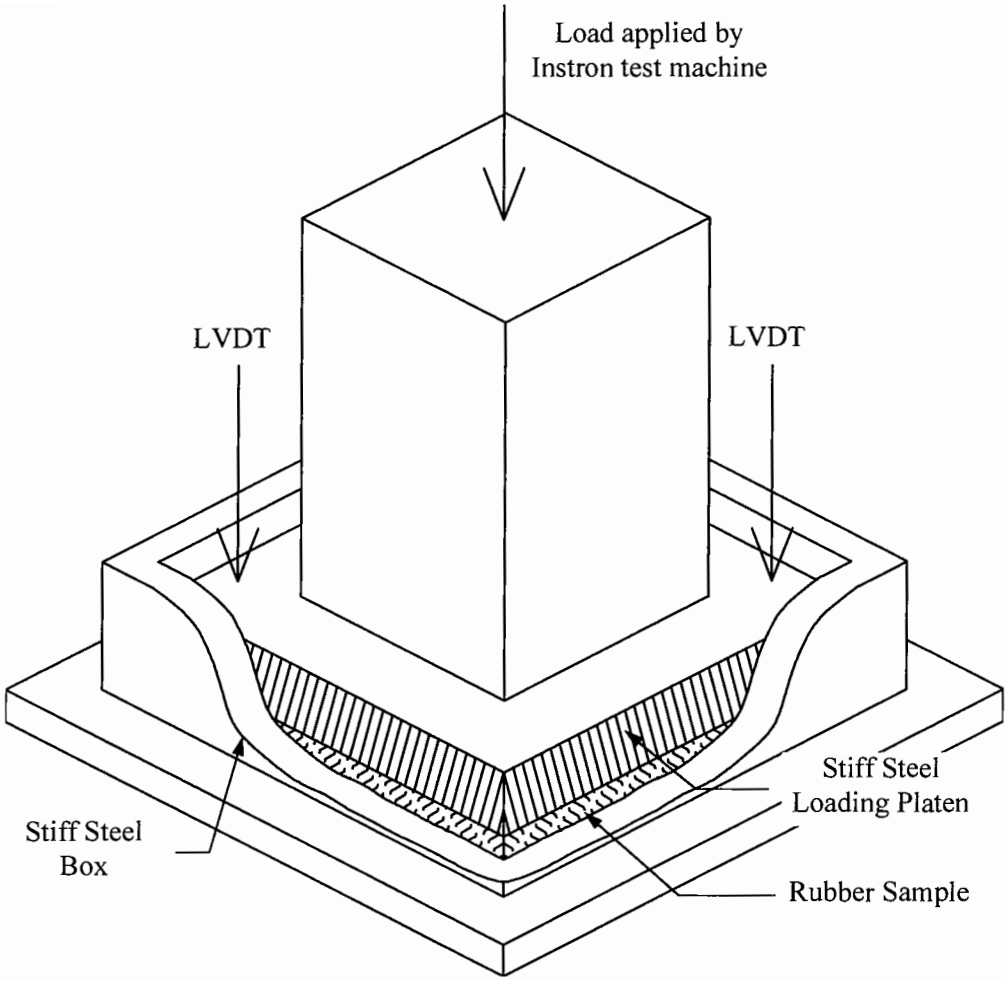

Figure 4.6: Apparatus used to measure rubber displacements

Rubber samples demonstrating a suitable displacement under this initial test were subjected to repeated loading between 1kN and 3.5kN at cycles of 5Hz. It was found there was a negligible difference in the displacements between the two rates of loading.

The displacement behaviour of a 12mm thick sample of Hemsell rubber is shown in Figure 4.7. It can be seen that the sample displaced by 2.15mm between loads of 1kN and 3.5kN. This material was selected to represent a subgrade with a stiffness of 30MPa. The manufacturer's literature estimated creep to be negligible.

A 3mm thick sample of Neoprene rubber displaced by 0.9mm between 1kN and 3.5kN. No other marginally stiffer materials were available. The neoprene rubber sample exhibited non-linear behaviour; increases in displacement diminished with

increases of load. The displacement of this sample between 10kN and 12.5kN was equal to 0.4mm, the required amount. The vertical stress was calculated at 10kN and used to estimate the area required to give the same stress at 1kN. Four squares measuring 100 x 100mm were removed from the original test piece to create a mesh sample of the required area. An 18mm thickness of stiff Wisaform board was placed on top of the rubber. This was to ensure an even load distribution over the mesh. The mesh sample was tested by the two methods described previously and produced a displacement of approximately 0.4mm between loads of 1kN and 3.5kN. A graph of the results is shown in Figure 4.7.

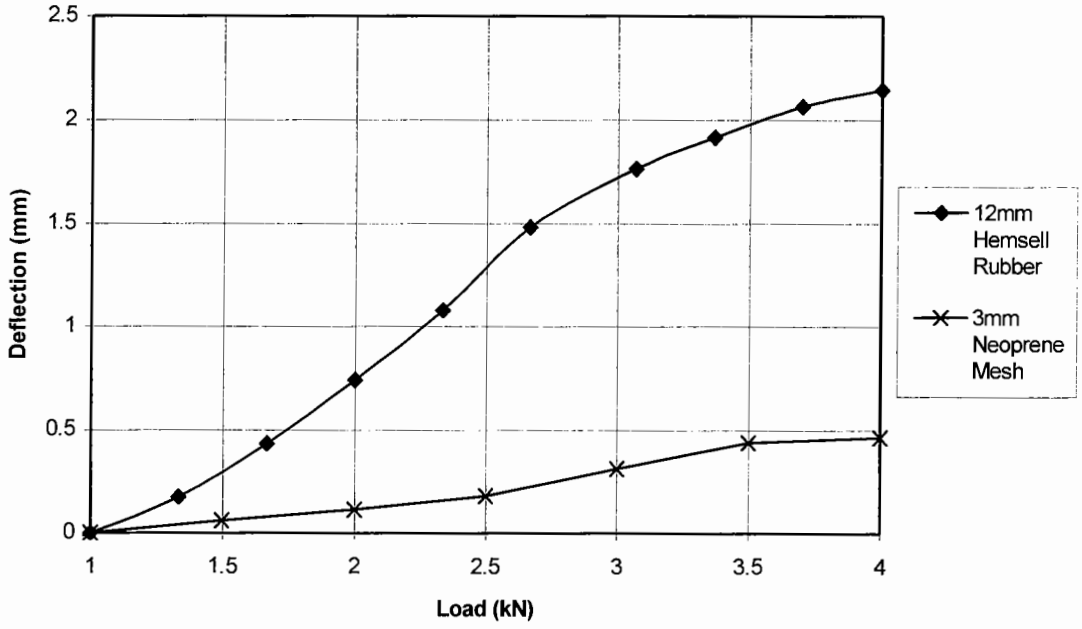

Figure 4.7: Displacement of 12mm thick Hemsell rubber and 3mm thick Neoprene mesh rubber under prescribed loads

The neoprene rubber has been estimated to creep by 30% over an indefinite period by the manufacturer. This was verified in a laboratory experiment complying with BS4443: Part 3: 1988 [39]. The creep was accommodated by using a 6mm thick neoprene mesh which produced a displacement of 0.6mm between the test loads. This material was adopted to represent a subgrade with a stiffness of 175MPa. The Wisaform board would be required to provide an even load distribution over the mesh. All the materials in the pit would have to be placed on top of this board which was

wrapped in plastic to prevent water penetration. Both rubber materials were waterproof and their behaviour should not have been affected by the presence of damp clay.

4.3.4 Rubber Layer Commissioning Tests

Further tests were carried out to measure the displacement of both rubber layers in-situ before backfilling with clay around the chambers. This involved applying a dead weight of concrete slabs and steel beams amounting to 35kN on top of each chamber. The displacement of the surface of the rubber layer near to the chamber was measured relative to the pit floor for each case. The in-situ measurements of load and deflection were compared with values measured in the Instron test machine. A summary of the results from both methods is shown in Table 4.2.

Table 4.2: Summary of data from deflection experiments under 35kN in-situ load

Hemsell rubber representing a subgrade of 30MPa resilient modulus		
Displacement measured in Instron machine (mm)	Displacement measured in-situ (mm)	Difference (mm)
0.45	0.41	0.04
Neoprene sponge representing a subgrade of 175MPa resilient modulus		
0.11	0.09	0.02

The difference in displacements determined by both methods was less than 0.05mm, so it was considered that the rubber layers were behaving as expected.

The influence of the rubber layers were again measured in-situ nine months after placing the backfill materials. The vertical displacement at the surface of each chamber was measured relative to a stable datum. The chamber surfaces were exposed during a reinstatement. An ironwork unit supported by a single HDPE spacer was placed on the surface and loaded at its centre by the loading frame. The vertical displacement of the chamber was measured at three points as illustrated in Figure 4.8.

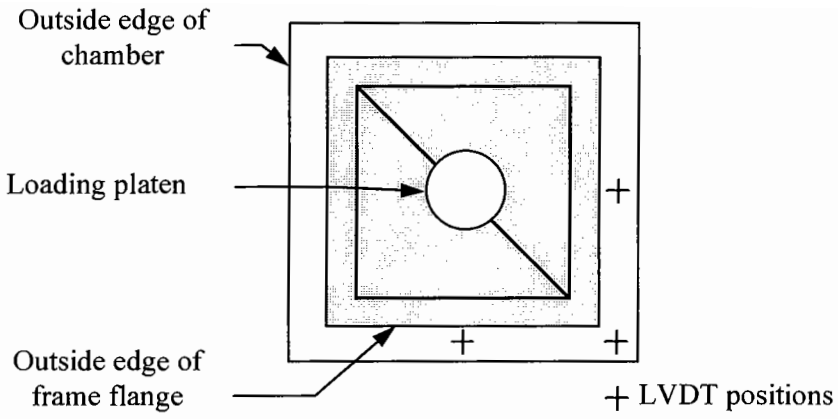

Figure 4.8: Plan view of in-situ displacement measurement apparatus

It was not considered that the load was evenly distributed onto the chamber surface as the ironwork frame carried load at its corners. This is discussed further in Chapters 5, 6 and 7. The measurements from the three LVDT's were averaged to provide an indication of the difference between the vertical displacements of the two chambers. The average values of displacement for both chambers were recorded at intervals of 5kN up to a maximum of 80kN are shown in Figure 4.9.

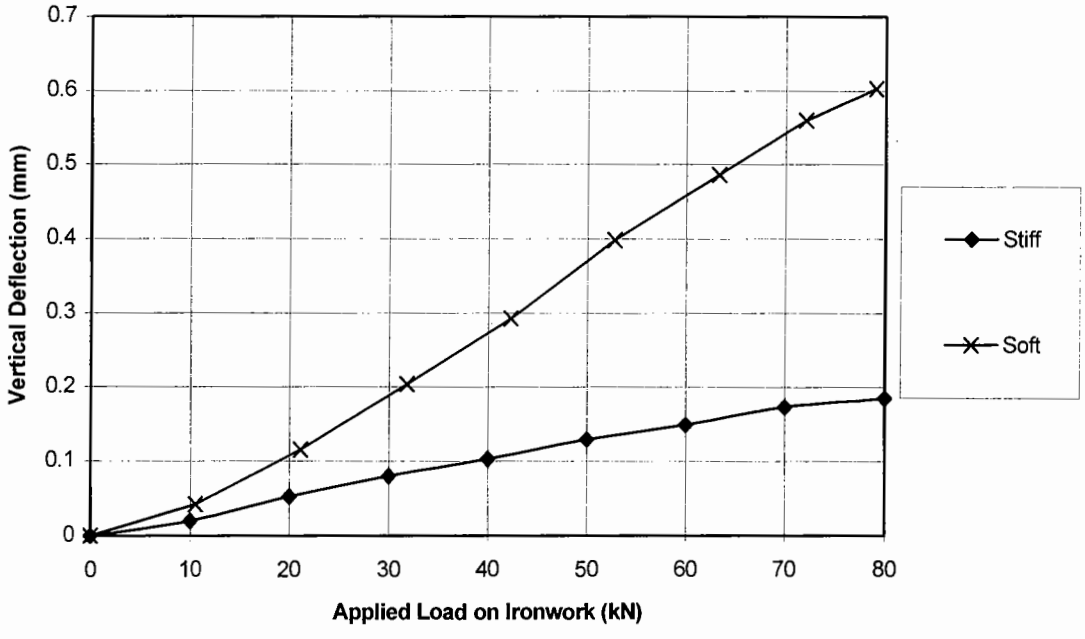

Figure 4.9: Average in-situ displacement measurements

It can be seen that the installation with soft foundations experienced a larger displacement than the installation with stiff foundations so the rubber layers were still

behaving as expected nine months after completing the laboratory test facility. It is considered that these values of displacement cannot be compared to the previous measurements with any confidence due to the uneven load distribution at the surface of the chamber.

4.3.5 Backfill Material and Pavement Construction

A layer of silty-clay was placed and compacted in 35mm lifts on top of the rubber layers to a depth of 1350mm. Bricks prior to firing, known as 'Green' bricks, were used for this purpose and were compacted a layer at a time using a pneumatic hammer. Cone penetrometer tests were carried out at various depths to ensure an even degree of compaction. A force of 412N +/-25N was required to insert the cone to the full depth of 50mm. A core of compacted clay was taken from the pit to measure the California Bearing Ratio (CBR) [40]. A value of 3% was recorded.

A 300mm thickness of Type 1 crushed Granite sub-base was placed on top of the clay and compacted with a vibrating roller and pneumatic compaction hammer in small areas. This was placed in 75mm layers. The final 240mm layer consisted of 28mm dense bitumen macadam (DBM) which was compacted with a 28" vibrating roller and finished level with the laboratory floor. A typical urban road would usually only consist of a 200mm thick DBM, but with a 40mm thick surfacing of HRA. It was considered unnecessary to complicate the construction by using two materials, so the full thickness was produced by the DBM. This material was placed in three layers of equal thickness to ensure a suitable degree of compaction.

4.3.6 Loading Frame

It was decided from the experiments with the prototype test facility that the position of the load should be easily adjustable. This was accomplished by applying the load through a moving wheel running across the width of the pit. This method of loading allowed a study of how the stress and strain at various points in the pavement and manhole structure varied as the wheel moved. A second method of loading was devised so that the loads could be applied through a fixed platen. This method was suitable for repeated load tests. It was considered that the loading frame made the test

facility extremely versatile and capable of applying loads in all the required modes. An illustration of the steel loading frame is shown in Figure 4.10.

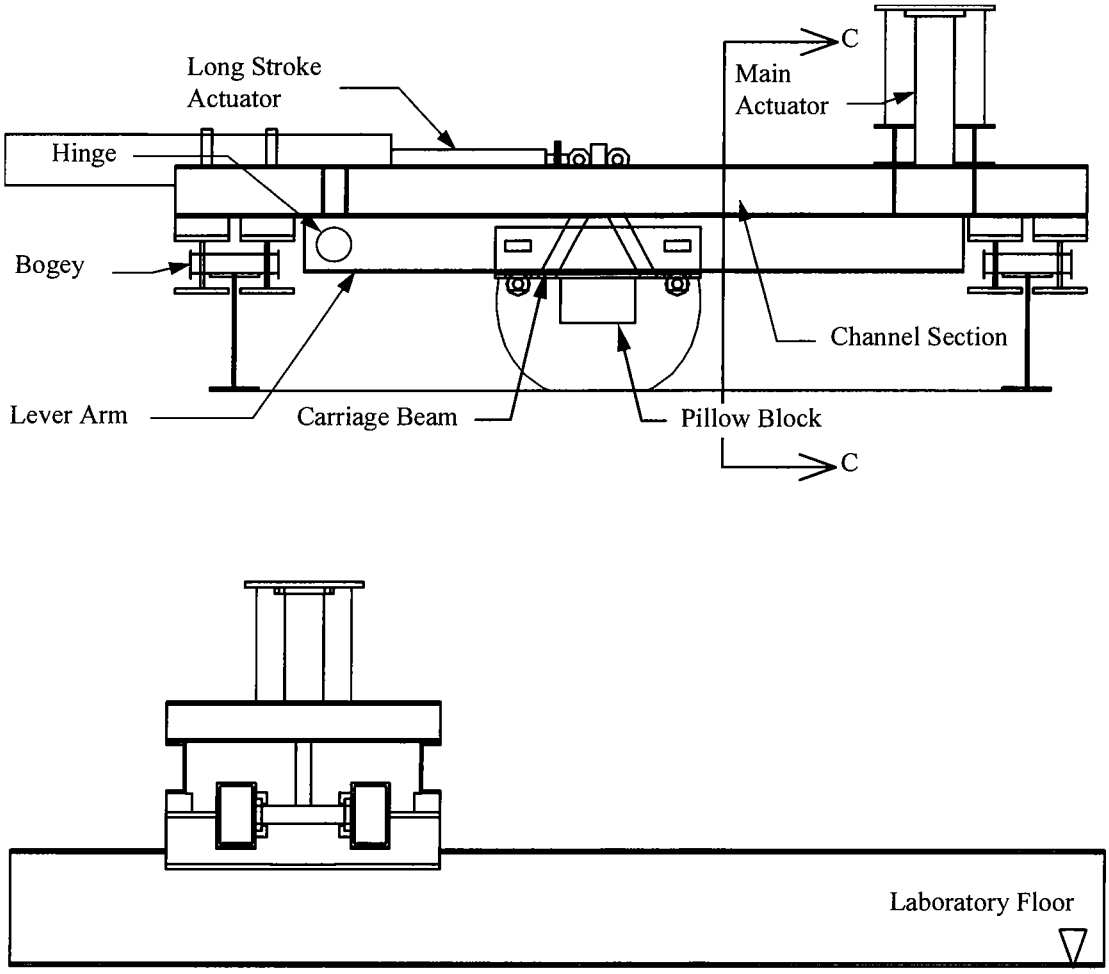

Figure 4.10: Illustrations of the laboratory test facility loading frame

The wheel is mounted in a carriage that can be moved across the width of the pit by a long stroke actuator. Load is applied to the carriage and wheel through the lever arm, consisting of two lengths of Rectangular Hollow Section steel (RHS), positioned either side of the wheel. These beams are connected by hinges to two channel sections positioned on the outside of the lever arms. A stationary hydraulic actuator applies load to the lever arms at the opposite end. The channel sections are fastened to bogies that run along supporting beams either side of the pit. These beams are fastened to the laboratory floor. Each loading cycle takes ten seconds to complete in the rolling wheel mode. The advantage of this design is that there is a minimum

number of moving parts. It has been found with other wheel tracking devices that a large number of moving parts complicates the design.

The initial design involved attaching strain gauges to the wheel carriage, and calibrating under known loads for use as a load cell. The load measured at the wheel would then be used to control the force applied by the actuator. Unfortunately, the carriage beam was stiffer than anticipated and the resulting strains were too small for accurate control. Attempts were made to fabricate thin load cells from ¾" mild steel plate to be inserted in between the carriage beam and the pillow blocks. However, the plate warped significantly during milling. This problem was finally overcome by placing a standard load cell in the connection between the main actuator and lever arms. A wire was also attached to the wheel carriage which turned a potentiometer as the wheel moved. This provided a ramp voltage proportional to the position of the wheel and was used to adjust the force applied by the actuator. This allowed a constant force to be applied to the wheel as it moved along the length of the lever arm.

The second mode of operation was to apply loads to the manhole structure through a stationary platen. This allowed a study of how the bedding and backfill materials deteriorated under repeated loading. The loading platen was clamped directly to the lever arms. The height of the stationary platen was such that the lever arms did not touch the wheel carriage during this method of loading.

The entire loading frame was mounted on bogies to allow movement along the length of the pit. This movement was only possible between tests, when the lever arms were raised. The steelwork was designed to BS5950: Part 1: 1990 (Amendment 1) [41], using a partial safety factor of 1.6 for all applied loads. Photographs of the laboratory test facility during construction are included in Appendix C.

4.3.7 Loading Frame Commissioning Tests

Commissioning tests were carried out before starting the experimental programme to ensure that the loading frame was working as intended. The first tests involved studying the load applied through the moving wheel. It was important to ensure that the applied load was constant as the wheel moved along the lever arm. Measurements of the wheel position and the load applied to the lever arms were recorded using a Schlumberger 3531D datalogger. The load measurement was taken from the load cell inserted in the connection between the lever arms and the main actuator. These data were used to take moments about the hinge of the lever arm and calculate the load applied by the wheel. An illustration of the calculated load applied by the wheel is shown in Figure 4.11. This experiment was repeated before testing each reinstatement and similar results were recorded.

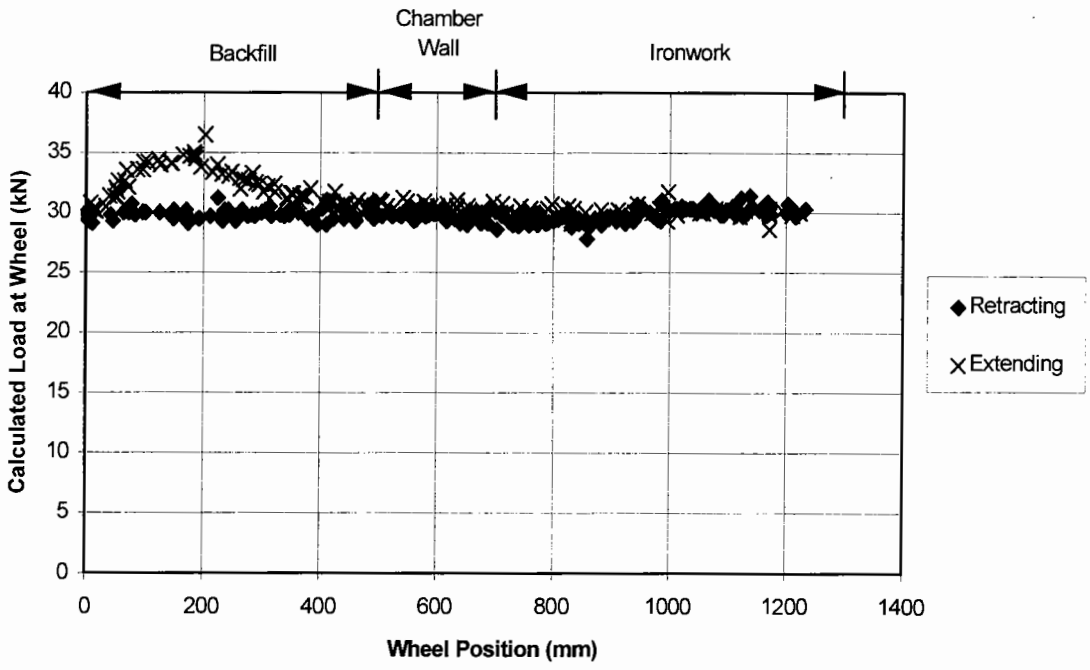

Figure 4.11: Calculated magnitude of load applied by the moving wheel

It can be seen that the load remains virtually constant as the wheel is retracted by the long stroke actuator, but a variation in load is experienced when the wheel is located on the backfill and travelling in the opposite direction. This can be attributed to the hydraulic delivery required by the long stroke actuator which moves the wheel backwards and forwards. A larger delivery of fluid is required when the actuator is

extending as part of the cylinder is filled with the piston rod when it is retracting. The larger delivery reduces the pressure at the servovalve on the main actuator below 500psi. Servovalves do not work efficiently below this pressure so the main actuator was unable to retract immediately thus causing an increase in the load applied to the wheel.

The variation in load would affect the readings from the instruments so the results presented in Chapter 5 are for the wheel retracting only. It can also be seen in Figure 4.11 that the constant magnitude of load is 30kN. This is 10kN lower than the intended design load as the tyre bulged severely at higher loads. However, the purpose of the rolling wheel tests was to identify likely failure mechanisms without causing any damage to an installation. A load of 30kN was found to produce measurable strains in the bedding material and the surrounding bituminous material.

The repeated loading method was found to work satisfactorily. Sinusoidal loads of 40kN could be applied at frequencies up to 6Hz. However, the support to the main actuator required bracing at these loading rates. Greater magnitudes of load could be achieved at lower frequencies without causing the loading frame any distress. All structural members, and connections including the carriage beams and bearings were selected to withstand 120kN.

4.4 Instrumentation

Various types of instruments were used in the laboratory experiments to study the behaviour of the bedding, ironwork and bituminous material. A description of each type of instrument is given below.

4.4.1 Strain Gauges

Strain gauges were mounted on the surface of the ironwork frame at the top edge and between seatings. They were used to study the flexure of the ironwork frame. These instruments measured strain over a 10mm gauge length. Their resolution is influenced by many factors, including interference by electrical equipment and the data acquisition method. It is considered that a resolution of ± 1 microstrain could be

achieved with the combination of gauge and data recording device used in these experiments. The accuracy of the instruments is principally affected by the bond between the gauge and the test specimen. Care was taken to ensure that the surface of the ironwork was de-greased and the adhesive was uniformly spread across the surface of the gauge. This was achieved by applying pressure onto the gauge with a clamp until the adhesive hardened.

4.4.2 Embedment Strain Gauges

These instruments were found to be useful in the experiments with the prototype facility. They were used in all the subsequent experiments in the laboratory test facility to study the behaviour of the bedding and bituminous materials. The location and orientation of these instruments are described in the presentation of the results given in Chapter 5.

A resolution of ±1 microstrain was also achieved with embedment strain gauges. However, great care had to be taken with their installation. It was essential that no voids were present around the gauges as this would have affected the accuracy of strain measurement. This was achieved by pressing each gauge into the workable bedding material to ensure a uniform bond with the base and sides of the gauge. Bedding material was then placed on top of the gauge and a slight pressure was applied onto the surface to ensure an even contact.

The data recorded from these instruments were used to identify likely failure mechanisms in the bedding layer. These data had a strong bearing on the findings from this research. It was considered to be very important to confirm that a suitable bond formed between the instruments and the surrounding material. A poor bond may have resulted in a lower measurement of strain than was actually present in the parent material. Two verification experiments were carried out to assess the accuracy of the strain measurements. The readings from these strain gauges were compared to other instruments and with theoretical calculations.

The first experiment involved casting three gauges in the centre of a 100mm cube of proprietary mortar A. The gauges were aligned at 45° to each other and were placed in the horizontal plane. This cube was allowed to cure for seven days before testing. Most of the results presented in Chapter 5 are concerned with measurements of horizontal tensile strains. It was considered to be particularly useful to investigate the accuracy of strain measurement in this plane.

The cube was crushed in accordance with BS1881: Part 116: 1983 [11] and the resulting strains were recorded on the same datalogger used with the laboratory test facility. A cylinder was cast from the same batch of material and was cured in the same environment. The static modulus and Poisson's ratio were measured immediately afterwards by the method described in Section A.3 [15]. It was found to have values of 20.5GPa and 0.13 respectively. Knowledge of these values allowed a calculation of horizontal strain due to a uniaxial compressive force. It was considered that the horizontal strain at the centre of the cube was not restrained by the loading platens. The calculated and measured values of strain are plotted against compressive stress in Figure 4.12.

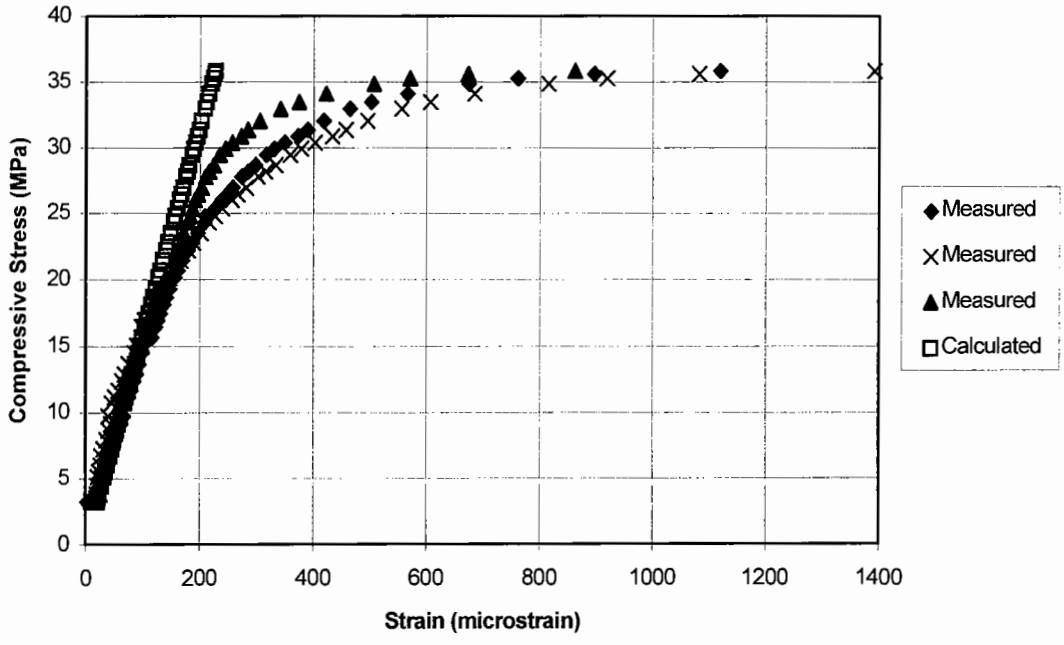

Figure 4.12: Comparison of calculated and measured strains from cube crushing experiment

The results illustrate that all three embedment strain gauges measured the horizontal tensile strain within a tolerance of ±2 microstrain and provided a close comparison with the theoretical calculations when the compressive stress was no greater than 20MPa. The gauges were installed by the method described previously and it was found that they had all formed a continuous bond when they were broken out of the failed cube.

The second experiment involved comparing the strain measured by a single embedment strain gauge with a LVDT measuring displacement over a known gauge length. A sample of cementitious mortar B which contains fibre reinforcement was cast into a beam measuring 100 x 100 x 500mm long. An embedment strain gauge was placed at the centre of a face of the beam and 5mm from the surface. This beam was also allowed to cure for seven days before testing. A LVDT was placed on the surface of the beam, over the embedment strain gauge. The specimen was loaded in a 4-point beam bending test machine so that the instruments were on the bottom face of the beam. Fibre reinforced bedding material was used as it was thought that it would be able to withstand larger tensile strains. Additionally, this material was used in later experiments so a knowledge of the performance of embedment strain gauges in such a material would be useful. A total of 11 load cycles were applied before the beam cracked. An average peak tensile strain of 98 microstrain was measured by the embedment strain gauge. The surface displacement measured by the LVDT was used to calculate an average strain of 106 microstrain. This embedment strain gauge was also found to have formed a continuous bond with the surrounding material along all surfaces.

A study of the strains measured in the first pair of installations tested in the laboratory test facility allowed an investigation of the repeatability of the embedment strain gauges. These reinstatements involved using the same bedding configuration on each chamber which consisted of a Chieftain 600 x 600 x 100mm deep frame bedded on a 75mm thick bedding layer which contained 20mm thick quarry tiles. It was found that the measurements recorded in the installation with hard foundations agreed with the values recorded at the same positions in the installation with soft foundations

within a tolerance of ±20%. The embedment strain gauge positions are indicated in Figure 5.1. For example, the peak strain recorded by gauge T1-B in the installation with hard foundations was 70 microstrain, whereas the peak strain measured at this location in the installation with soft foundations was 58 microstrain. It was later found that the stiffness of the foundations had a negligible effect on the behaviour of the bedding layer. This study provided evidence that repeatable measurements were possible from these instruments to a reasonable level of confidence. Additionally, the embedment gauges used in the experiments described above did not reveal any evidence of damage on removal from the specimens and the resistance remained unchanged. This indicated that reliable measurements were achievable.

Both of the previous experiments to assess the performance of embedment strain gauges described above illustrated that the values of strain measured by the embedment strain gauges provided a close comparison with calculated strain magnitudes, and those determined using a LVDT. This comparison was used to determine the accuracy of the strain readings which was found to be ±5%.

The accuracy and repeatability of embedment strain gauges is considered to be heavily influenced by the degree of contact with the surrounding material. The gauges were broken out of the bedding material on completion of experiments in the laboratory test facility and it was found that a uniform contact had been achieved. These instruments were installed by the method described earlier.

4.4.3 Inductance Strain Coils

These instruments can also be used to measure strain. They consist of a coil of wire wrapped around a non-metallic core. The instruments are installed in pairs and an AC signal is supplied to one coil which induces an electromagnetic coupling in the other coil. The strength of the coupling is related to the spacing between the instruments which is converted into a voltage by a Bison instrument [42]. This instrument was purposely developed for use with strain coils. The intensity of the coupling, and hence the voltage, changes when the spacing between the coils is altered. This would occur due to a strain in the surrounding material. A calibration was made before

installing to measure the change in the voltage induced by the coils when they were moved apart or closer together. This information is used to provide a measurement of strain.

A pair of inductance strain coils were installed 25mm from the bottom of the bituminous layer, 500mm away from the outside of the chambers. These instruments are severely affected by the close proximity of metallic objects which distort the magnetic field. This made the instruments unsuitable for use near the manholes where the ironwork cover and frame were present. An embedment strain gauge was used to measure strain 25mm from the bottom of the bituminous material at a distance of 50mm from the chamber walls.

The inductance strain coils were not removed during the experiments with the laboratory test facility and it was found that the peak strain magnitude remained unchanged throughout the test programme. From this evidence, it is considered that highly repeatable results were achieved with these instruments.

4.4.4 Pressure Cells

A pressure cell contains a thin diaphragm which flexes under an applied load. Four strain gauges are attached to this diaphragm and are connected to form a Wheatstone bridge. The gauges are orientated so two gauges measure a tensile strain and the other two measure a compressive strain. This yields the largest output from a Wheatstone bridge. The output is calibrated against a known level of pressure before installation. This factor is used to convert recorded measurements into pressure [43]. The presence of a measuring device in a soil mass disturbs the stress and strain distribution in its locality. Investigations were made to compare the measurements recorded by these instruments in-situ with the calculated value of stress when the instrument was not present [43]. This behaviour was studied when the instruments were installed in Keuper Marl (silty clay) and Meldon Dust (crushed stone varying in size from 9.5mm to dust) under a variety of load regimes. It was found in all cases that the difference between the recorded and calculated values of stress was no greater than 9%. Further

experiments revealed that an applied stress in a direction perpendicular to the pressure cell diaphragm produced an error of no greater than 4% [43].

Pressure cells were buried in the sub-base and clay layers of the backfill material at various depths. These instruments allowed a study of the stress distribution caused by the applied wheel load at various positions, both on the ironwork and the backfill. They were located at distances of 200mm and 500mm away from the outside of each chamber and were orientated to measure vertical stress. Great care was taken when installing these instruments to ensure that the diaphragm was horizontal and was evenly supported. Fine gravel was packed around each instrument installed in the sub-base layer. The locations of the pressure cells and the other instruments in the backfill are shown in Figure 4.13.

These instruments were not reinstated during the test programme and constant peak recordings were maintained, so it is considered that these instruments are also capable of providing repeatable measurements.

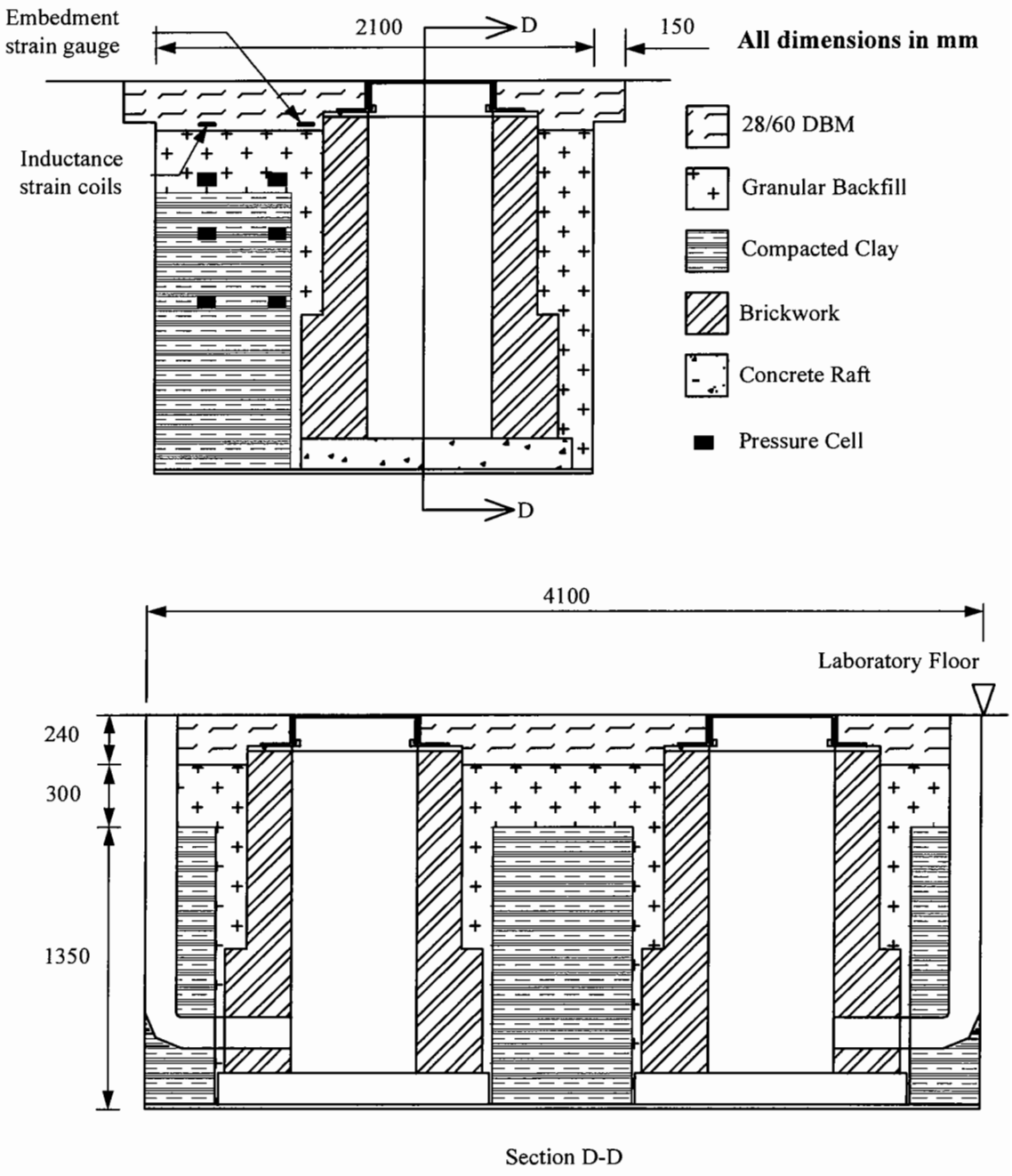

Figure 4.13: Cross section views through the laboratory test facility pit

4.4.5 Datalogging Systems

The outputs from all of the instruments in the laboratory test facility were recorded on a datalogger which had proved to be an efficient method of recording readings from the prototype facility. This device allowed the data to be transferred to a computer and studied within a spreadsheet. A Schlumberger 3531D datalogger was used to record measurements during the rolling wheel tests. It can capture data from up to 80

channels and store the information on a floppy disc. However, it cannot capture data at a fast rate and was unsuitable for the repeated load tests. Measurements were taken from several instruments located in the backfill, bedding material and ironwork. The datalogger was set up so that the wheel position and one other channel were recorded constantly for 400 cycles. This was repeated for all channels. During the time it took to record the value of the second channel, the wheel only moved 2mm from its recorded position. The resulting data provided information on how the output from each instrument varied as the wheel moved across the surface.

The results presented in Chapter 5 illustrate the magnitudes of strain measured by the instruments installed in the laboratory test facility. The Schlumberger 3531D datalogger scanned each channel 20 times and recorded the average value. Each point in the figures illustrated in Chapter 5 represents an averaged recording. Occasionally, the recorded data contained a random value which does not appear to agree with the overall pattern of the results. It is thought that during the averaging process electrical interference caused the datalogger to record a single value that was significantly different to the rest of the data, thus influencing the average measurement resulting in a random value. The resulting data point is usually clearly erroneous.

Measurements were recorded with another datalogging system during the repeated load tests. The load was cycled at a rate of 5Hz during these experiments. The second system allowed data to be captured every millisecond but it could only receive an input from a maximum of eight channels. This was overcome by taking several sets of reading from different channels.

4.4.6 Instrument Commissioning Tests

Further commissioning tests were carried out to ensure that the instruments and dataloggers were functioning correctly. All of the instruments were connected to each datalogging system and left for 30 minutes without applying any load. It was found that none of the measurements drifted during this period. Subsequent experiments involved comparing the recorded values to measurements taken with an oscilloscope. The difference was found to be negligible.

4.5 Sensitivity Analysis

The intention of the laboratory test facility was to study the strains that develop in the bituminous and bedding materials for various road ironwork and bedding configurations. This would provide some indication of how these installations behave when loaded and highlight the likely mechanisms of failure. A sensitivity analysis was carried out to study the effects of common variables within road ironwork installations on the magnitudes and distribution of stresses within the bedding material. The results from this analysis were used as an aid to develop an experimental programme.

4.5.1 Description of Analysis

A two-dimensional plane strain finite element analysis was chosen as the tool for this purpose. It was considered that the use of the elastic layer analysis programs such as ELSYM5 would be unsuitable due to the assumptions made about the boundary conditions. Two-dimensional finite element analyses were considered to provide sufficient detail without over complicating the issue. The sections used in the analyses were programmed to behave as plane strain. The most common variables in road ironwork installations are listed below. These were determined from field observations and discussions with highway engineers.

- Static modulus of the bedding layer
- Bedding thickness
- Angle of applied load
- Inclusion of quarry tiles within the bedding layer
- Effect of mortar above frame flange

Static Modulus of the Bedding Layer

Cementitious mortars are the most commonly used materials to form the bedding layer. This material has been shown to increase its static modulus with age as described in Section 2.2.1. The distribution of stress in the bedding material may change with static modulus. A young bedding material may experience a different peak magnitude of stress to a mature bedding material. The magnitude of these

stresses may be in excess of the strength at these ages. It was considered that by altering this variable, it would be possible to see whether a reinstatement would be more likely to fail at an early or later age. The static moduli used in the analyses were 6.7GPa, 13.6GPa and 21GPa to represent different ages.

Bedding Thickness

This is the most common variable so its effect was considered worthy of investigation. The thickness of the bedding layer is varied to ensure the surface of the ironwork is level with the surrounding road surface. Analyses were carried out with bedding thicknesses of 10mm and 50mm to represent typically thin and thick layers.

Angle of Applied Load

The angle of load applied by a wheel will change if a vehicle is braking or accelerating. This may alter the stress distribution and magnitude within the bedding material. It has been estimated that a heavy goods vehicle can de-accelerate at a rate of nearly 0.5g during an emergency stop [44]. By applying Newton's second law, the direction of the resultant load can be determined.

Vertical force = $F_V = m.g$ Horizontal force = $F_H = m.a$

where m = mass applied on one wheel where a = deceleration due to breaking

g = acceleration due to gravity = $9.81 m/s^2$ $0.5(9.81)\ m/s^2$

so $F_V = 9.81m$ and $F_H = 4.905m$

giving a resultant load during an emergency stop which is 25° to the vertical. Further calculations were carried out with the load applied at 15° to the vertical to represent normal braking. Both of these calculations were compared to a vertical loading case.

Inclusion of a Quarry Tile in the Bedding Layer

A two-dimensional model was created with a 20mm thick quarry tile included in the bedding layer. The thickness of the bedding material above and below the quarry tile

was 20mm and 25mm respectively. This model provided a comparison to the thick bedding layer section.

Effect of Mortar above the Flange

Bedding material is sometimes placed through holes and on the upper surface of the frame flange. It is considered by some highway engineers that the presence of this mortar would restrain the ironwork from lateral movements. However, it is thought by others that this may induce a high tensile stress in the bedding material placed within the holes when a horizontal component of load is applied which would lead to failure. A model was created with a 50mm thickness of bedding material and a further 20mm thickness placed above the flange so comparisons could be made to the section with a thick layer of bedding material.

Figures 4.14 and 4.15 illustrate sections where the bedding thickness is 50mm and 10mm respectively and the effects of including a quarry tile were assessed using the section illustrated in Figure 4.16. The section with mortar above the flange is shown in Figure 4.17. A section through the frame of a Chieftain 600 x 600 x 100mm deep cover seating was used in all the analyses as this is the most common type of ironwork unit installed in practice although the ironwork cover was omitted to simplify the analyses. All loads were applied directly to the seating on the ironwork frame. The load was applied through a number of very stiff elements positioned in this region to simulate a uniformly distributed load. This is illustrated by the small red area shown in Figure 4.18. The length of the cover seating was measured and was found to be 20mm. The magnitude of the vertical component of force was 2.875kN. The was equivalent to a 57.5kN force acting over a unit thickness. This was considered to be the largest magnitude of applied force as discussed in Section 3.6.

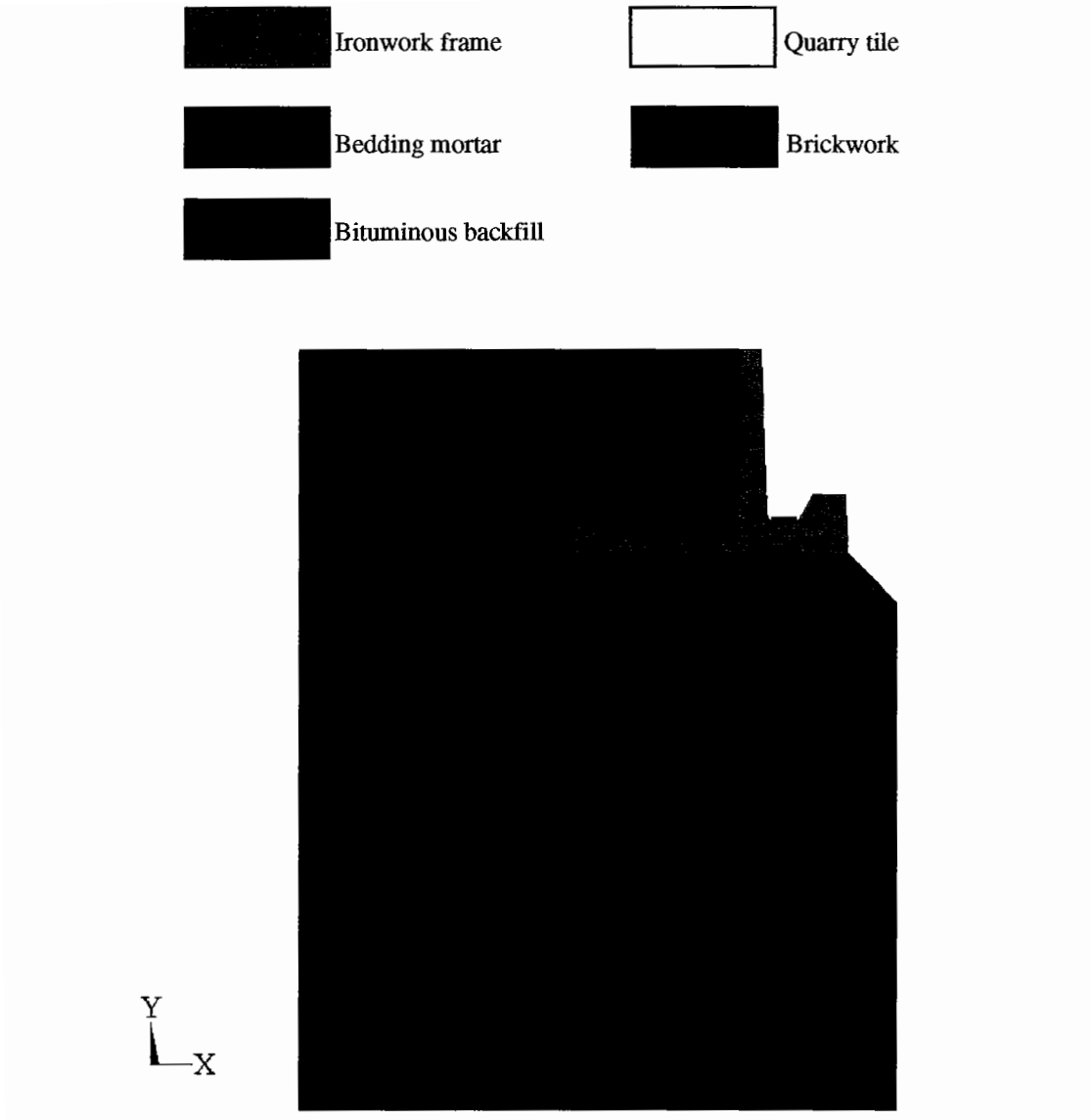

Figure 4.14: Section with a thick layer of bedding material (Model A)

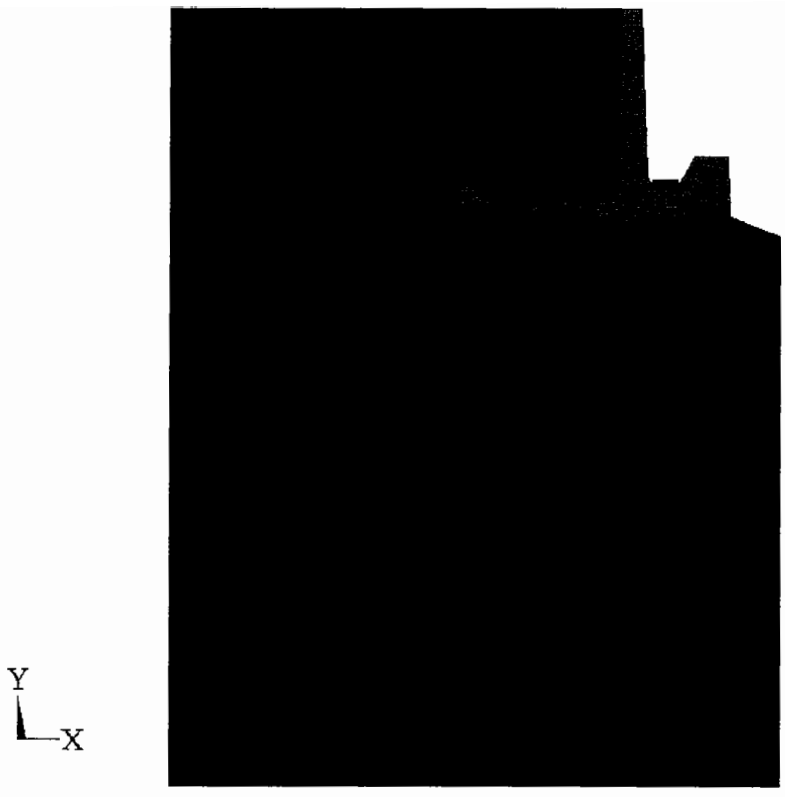

Figure 4.15: Section with a thin layer of bedding material (Model B)

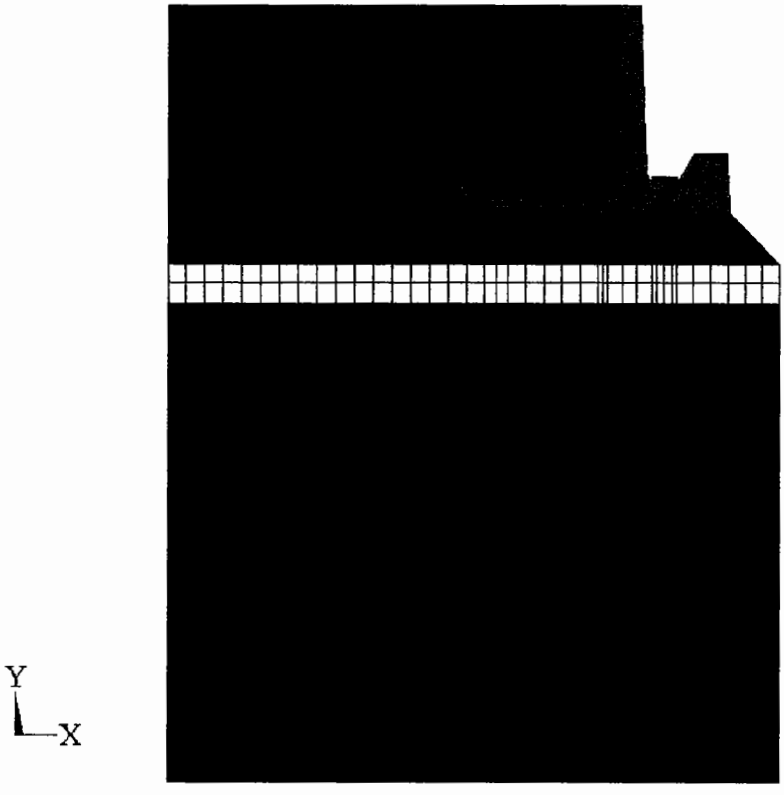

Figure 4.16: Section including a quarry tile (Model C)

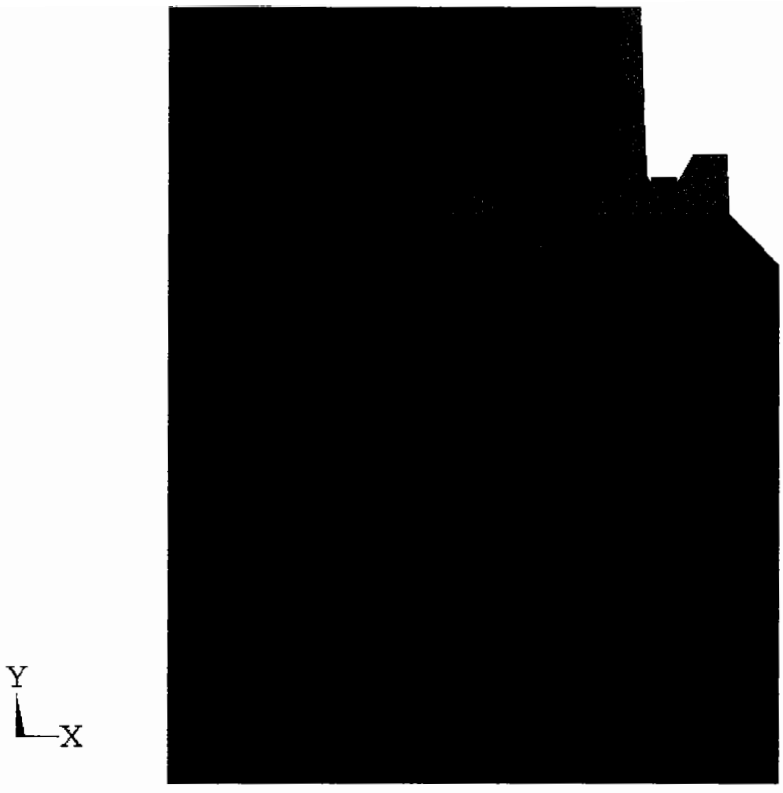

Figure 4.17: Section with bedding material above the flange (Model D)

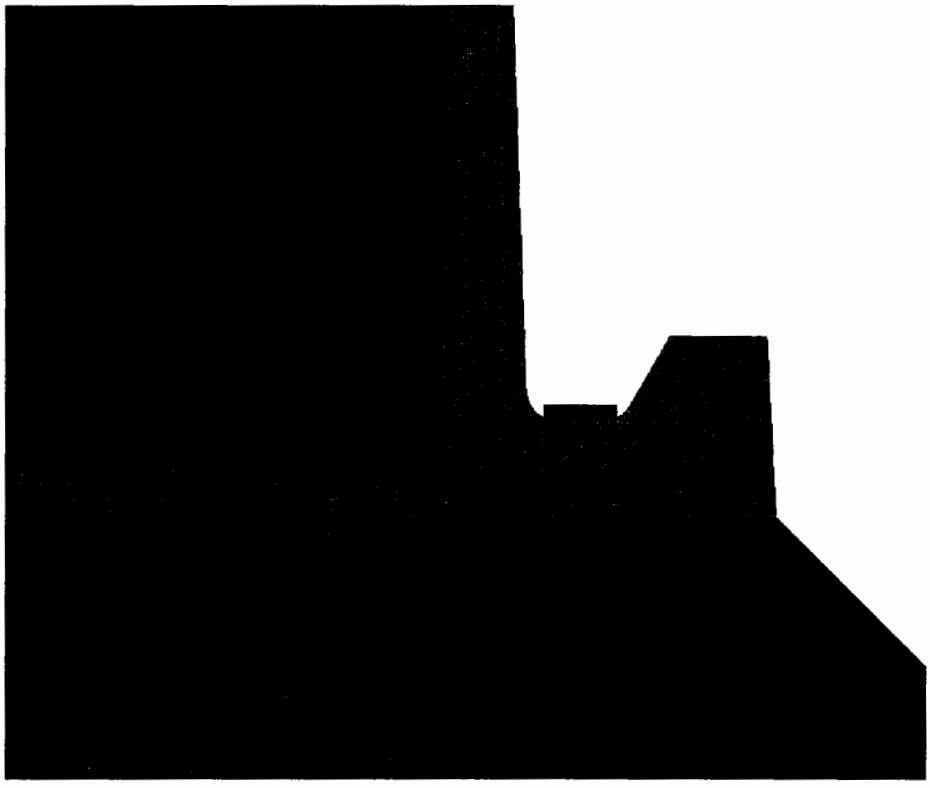

Figure 4.18: Illustration of stiff elements in the cover seating

The idealised structure was fully restrained in both the horizontal and vertical directions at the base of the brickwork. This is not a realistic representation of a typical manhole but was required for the purpose of the analyses. The restrained base only appeared to affect stresses within the bottom five rows of elements and not at any other point in the structure. It is emphasised that these analyses were only a sensitivity study to allow comparisons to be made. The comparisons were only relative observations and it is felt that the analyses were not accurate enough to quote absolute values of stress. The creation of the models for these analyses and their solution was carried out by Strucom Ltd who provide a commercial service using the ANSYS computer program. All of the materials were assumed to exhibit linear elastic behaviour which also simplified the analysis. The displacement behaviour of each of the component material is discussed in Section 6.2.2. It can be seen from the experimental data presented in this section that all the materials exhibited linear behaviour to a high level of confidence. Further analyses were carried out with three-dimensional models using the ANSYS computer program. A discussion of these analyses and the limitations of this program are presented in Chapter 6.

4.5.2 Results

Maximum Principal Stress

The experiments to measure the direct tensile strength of cementitious mortars described in Section 2.2.1 revealed that all the specimens failed in a direction perpendicular to the direction of loading. This has been observed by others and would suggest that shear stresses have no effect on the behaviour of this material [45]. Additionally, the failure of cementitious materials is considered to be related to the stress magnitude as also described in Section 2.2.1 [8]. It would appear that the failure stress in a road ironwork installation is related to the principal stresses. It was observed during an initial study of the maximum principal stress distributions that a region of high tensile stress developed close to the bottom of the bedding layer in all the analyses. It is therefore considered that maximum principal stress would be a useful indicator in comparing the performance of each section. Figure 4.19 illustrates the maximum principal stress in a section with a 50mm thick bedding layer which has a static modulus of 21GPa and is loaded vertically. A summary of the peak maximum principal stress calculated in each section is shown in Table 4.3.

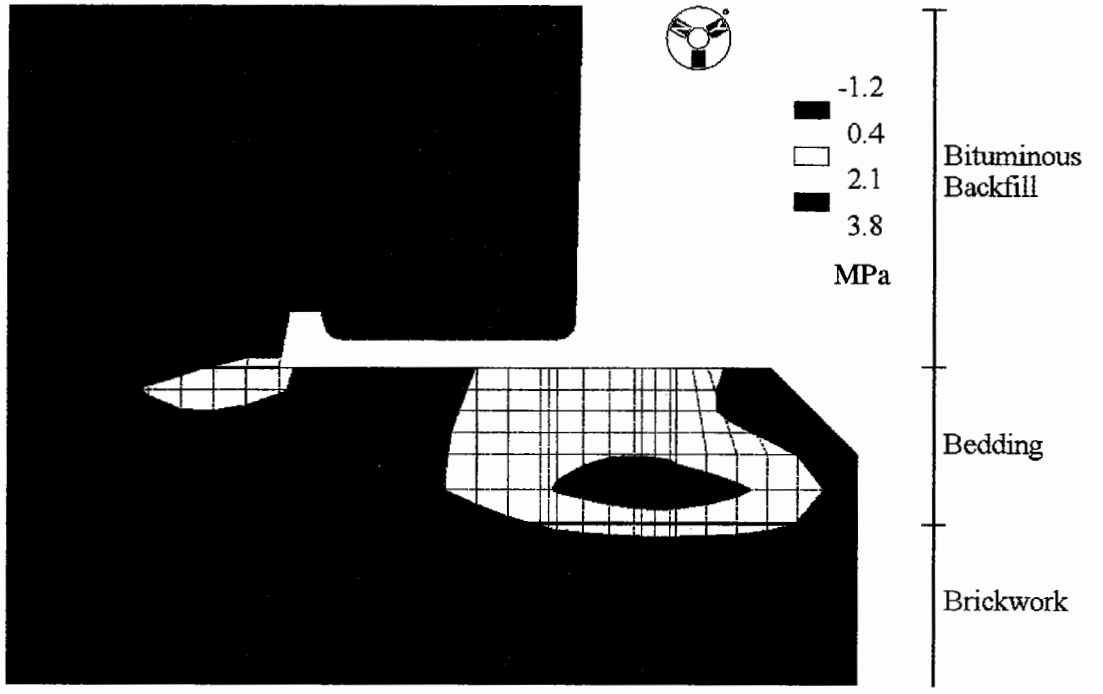

Figure 4.19: Maximum principal stress distribution illustrating a region of high tension near the bottom of the bedding layer

Table 4.3: Summary of peak maximum principal stress calculated in each section

Ref. Number	Bedding Thickness (mm)	Static Modulus of the Bedding (GPa)	Angle of Applied Load to the Vertical (Degrees)	Quarry Tile included	Mortar above the flange included	Peak value of Maximum Principal Stress (MPa)
1	Composite	6.7	0	Yes	No	2.0
2	Composite	6.7	15	Yes	No	2.0
3	Composite	6.7	25	Yes	No	1.9
4	Composite	13.6	0	Yes	No	2.9
5	Composite	13.6	15	Yes	No	2.9
6	Composite	13.6	25	Yes	No	2.8
7	Composite	21.0	0	Yes	No	3.4
8	Composite	21.0	15	Yes	No	3.2
9	Composite	21.0	25	Yes	No	3.0

Table 4.3 continued: Summary of peak maximum principal stress calculated in each section

Ref. Number	Bedding Thickness (mm)	Static Modulus of the Bedding (GPa)	Angle of Applied Load to the Vertical (Degrees)	Quarry Tile included	Mortar above the flange included	Peak value of Maximum Principal Stress (MPa)
11	10	6.7	0	No	No	1.9
12	10	6.7	15	No	No	1.4
13	10	6.7	25	No	No	1.0
14	10	13.6	0	No	No	5.3
15	10	13.6	15	No	No	5.1
16	10	13.6	25	No	No	4.9
17	10	21.0	0	No	No	6.6
18	10	21.0	15	No	No	6.4
19	10	21.0	25	No	No	6.1
21	50	6.7	0	No	No	2.0
22	50	6.7	15	No	No	1.3
23	50	6.7	25	No	No	0.6
24	50	13.6	0	No	No	3.1
25	50	13.6	15	No	No	3.0
26	50	13.6	25	No	No	2.8
27	50	21.0	0	No	No	3.6
28	50	21.0	15	No	No	3.5
29	50	21.0	25	No	No	3.3

Table 4.3 continued: Summary of peak maximum principal stress calculated in each section

Ref. Number	Bedding Thickness (mm)	Static Modulus of the Bedding (GPa)	Angle of Applied Load to the Vertical (Degrees)	Quarry Tile included	Mortar above the flange included	Peak value of Maximum Principal Stress (MPa)
31	50	6.7	0	No	Yes	2.0
32	50	6.7	15	No	Yes	1.6
33	50	6.7	25	No	Yes	1.2
34	50	13.6	0	No	Yes	3.2
35	50	13.6	15	No	Yes	2.9
36	50	13.6	25	No	Yes	2.8
37	50	21.0	0	No	Yes	3.7
38	50	21.0	15	No	Yes	3.4
39	50	21.0	25	No	Yes	3.3

Effect of the Static Modulus of the Bedding Material

The static modulus had a great influence on the peak values of maximum principal stress in the bedding material. The peak maximum principal stress was related to the static modulus of the bedding material as illustrated in Figure 4.20. This effect was most pronounced in the section with a 10mm thick bedding layer (Model B, No.s 11 to 19).

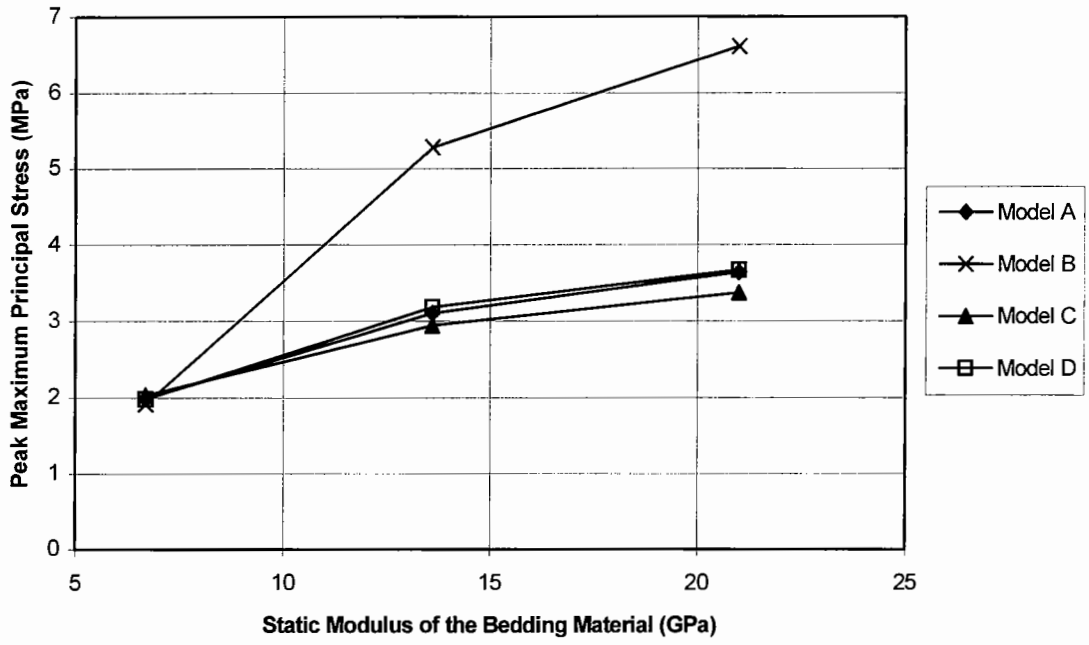

Figure 4.20: Variations of peak maximum principal stress with the static modulus of the bedding

The experiments described in Section 2.2.1 illustrated that cementitious bedding materials have some tensile strength after initially setting but it does not increase significantly. The analyses indicate that the largest tensile stresses develop in mature mortars which typically have a static modulus of 21GPa. It is thought that the bedding is most at risk after the development of stiffness and strength is complete. This compares well to field observations as most installations do not fail immediately after re-opening to traffic.

Effect of the Bedding Thickness

The bedding material thickness also had a significant effect on the peak maximum principal stress. The peak values in the analyses with 10mm thick bedding layers were all greater than the analyses with 50mm thick bedding layers. This was the pattern for all comparable analyses with common values of static modulus and loading angles. Figure 4.21 illustrates the variation in peak maximum principal stress with bedding thickness for two values of the bedding static modulus. It can be seen that there is an inverse relationship.

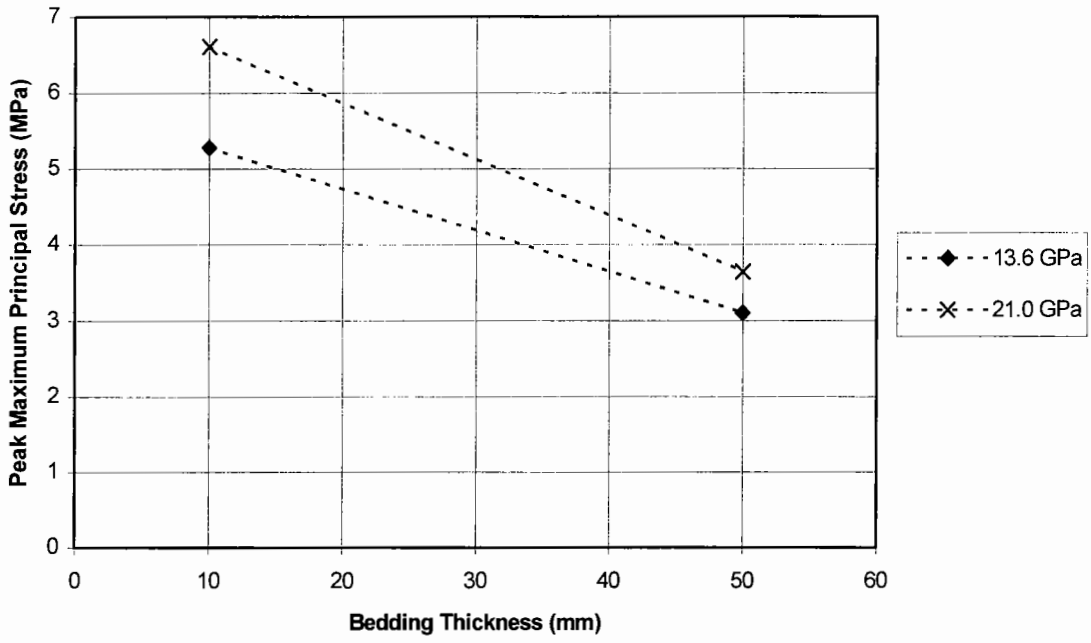

Figure 4.21: Variation of peak maximum principal stress with the bedding material thickness

Effect of the Loading Angle

The loading angle was varied on each model illustrated in Figures 4.14 to 4.17. It was found that the vertical loading case produced the greatest maximum principal stress in all the analyses. Variations in the angle of the applied load only had a small effect. The change in the peak values of maximum principal stress are shown in Figure 4.22.

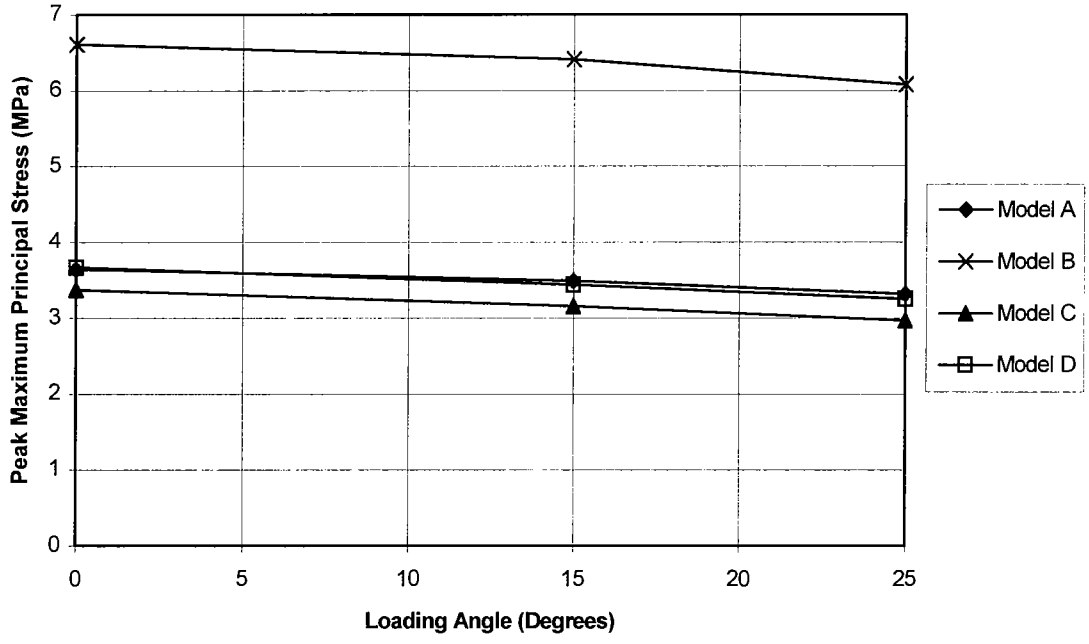

Figure 4.22: Variations of peak maximum principal stress with the loading angle

The direction of the angled load was towards the centre of gravity of the models. If the opposite side of the manhole is considered; the mirror image of the sections shown in Figures 4.14 to 4.17, the load would be applied at -25°, acting away from the centre of gravity. It is considered that the load applied in this direction could have a damaging effect. This is discussed later in Chapters 5 and 6.

Effect of Quarry Tiles

The presence of the quarry tile affected the distribution of the maximum principal stress. It was found that the highest value manifested itself in the layer of mortar beneath the quarry tile whilst the quarry tile experienced relatively low stresses. The magnitude of the stress in the bedding material was generally lower than the values calculated in the comparable sections with a thick layer of bedding material.

Effect of Bedding Material placed above the Flange

Minor differences of stress distribution beneath the flange were noted between all the analyses with and without bedding material above the flange but there was a slight reduction in the magnitude for the section with bedding material above the flange. A

small region of high tensile stress was noted to occur within the hole in the frame flange, but this was lower than the peak value that developed in the bedding material underneath the flange.

Minimum Principal Stress

The minimum principal stress indicates the largest compressive stress in an element. All the sections produced similar minimum principal stress distributions and there were only small differences in the peak magnitudes. The largest compressive stress magnitude in the bedding material was located directly underneath the cover seating. This decreased with distance from this point. The minimum principal stress distribution in a section with a 50mm thick bedding layer which has a static modulus of 21GPa and is loaded vertically is illustrated in Figure 4.23. This is the same model used to illustrate the maximum principal stress in Figure 4.19.

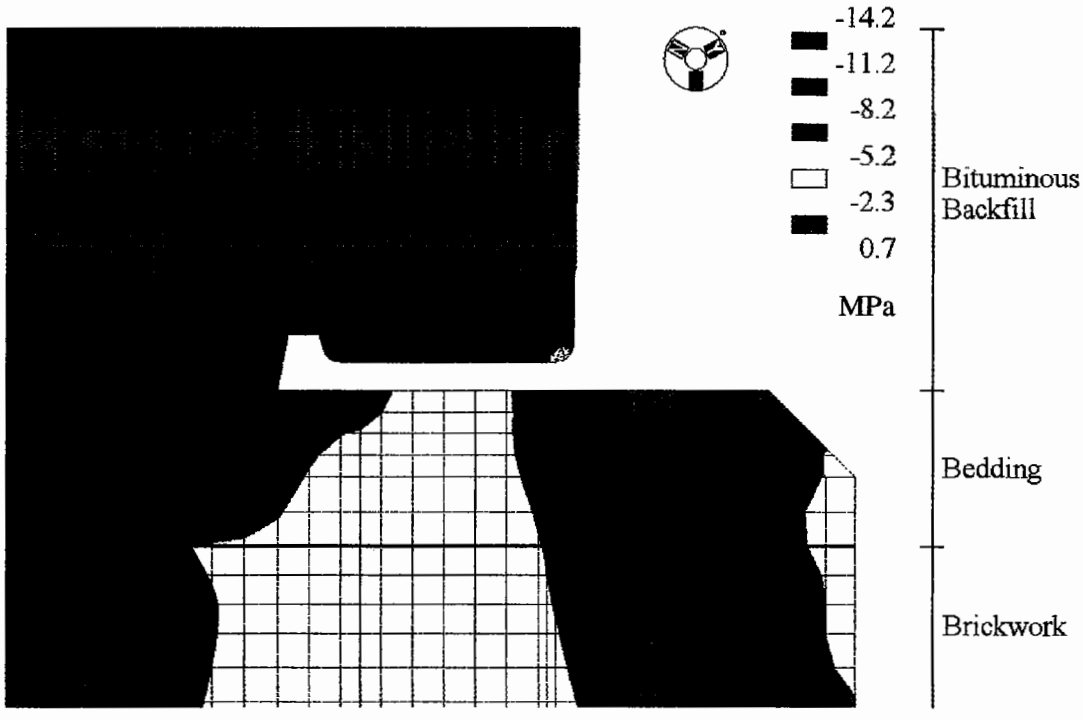

Figure 4.23: Typical minimum principal stress distribution

4.5.3 Summary of Results

It was found that changes in the static modulus of the bedding material produced the greatest variations of maximum principal stress in this layer. The largest stresses occurred in the analyses with the highest values of static modulus. The bedding layer thickness also had a significant effect and would be worthy of investigation in the laboratory test facility.

4.6 Experimental Programme

Before starting the experiments in the laboratory test facility, it was important to decide which combinations of ironwork and bedding material should be tested. It was intended to test numerous common bedding configurations that were significantly different from each other. This would provide an indication of any common failure mechanism and the threshold at which it occurred. The two-dimensional finite element analyses illustrated that the greatest variation in the bedding material tensile stress was due to changes in the static modulus of this material, with the largest values developing in a mature bedding material. This is convenient as it would be difficult to reinstate the ironwork, backfill, connect the instruments and apply loads before the bedding material developed a mature static modulus. The laboratory safety policy only permits the compaction of bituminous materials outside normal working hours.

The bedding thickness was also indicated as an influential variable and this was included in the experimental programme. The analyses only provided results indicating relative magnitudes, so it was considered that the other variables should not be excluded from the programme. Consideration was given to configurations including quarry tiles, mortar above the flange and the angle of applied load. The brickwork chambers were finished 175mm beneath the laboratory floor. This allowed either a 100mm deep frame and 75mm thick bedding layer, or a 150mm deep frame and a 25mm thick bedding layer to be placed so that the ironwork cover was level with the surrounding surface.

The first two installations consisted of a thick bedding layer of mortar A which contained a quarry tile. The elastic properties of good quality quarry tiles were found

to be similar to fibrous boards (Section 2.2.5) so this configuration provided information on the behaviour of composite bedding layers in general. These installations were replaced with a configuration with a 25mm thickness of mortar A to allow a comparison of their behaviour. Additionally, installation No.4 included a 20mm layer of bedding placed over the flange to allow a study of a configuration where the frame flange was encapsulated in the bedding. The behaviour of a 25mm bedding thickness configuration was further studied by using mortar B which contained fibre glass strands. These experiments provided a comparison with installations 3 and 4. Two reinstatements were made using square HDPE spacers. This allowed a comparative study of the behaviour of the bedding layer when a material with significantly different elastic properties was installed. Additionally, the HDPE spacers allowed an investigation into how the bedding material affected the strains in the surrounding bituminous layer.

The brickwork level was raised for the last two reinstatements so that the bedding material thickness could be reduced to 10mm, as this was the worst case as calculated by the sensitivity analysis. These configurations were installed with a new design of ironwork and bedding material. These were developed from the findings of the previous installations and the three-dimensional finite element analysis. A discussion of their development and results obtained from these laboratory test facility are given in Chapter 7. A summary of the configurations tested is shown in Table 4.4.

Table 4.4: List of configurations tested in the laboratory test facility

Installation No.	Manhole Foundation	Ironwork Type	Bedding Material and Configuration
1	Stiff	100mm deep Chieftain unit (EN124: 1994 D400 Class [20])	75mm layer of mortar A containing a 20mm thick quarry tile
2	Soft	100mm deep Chieftain unit (D400 Class)	75mm layer of mortar A containing a 20mm thick quarry tile
3	Stiff	150mm deep Chieftain unit (D400 Class)	25mm layer of mortar A
4	Soft	150mm deep Chieftain unit (D400 Class)	25mm layer of mortar A with another 20mm placed above the flange
5	Stiff	150mm deep Chieftain unit (D400 Class)	25mm layer of mortar B with another 20mm placed above the flange
6	Soft	150mm deep Chieftain unit (D400 Class)	25mm layer of mortar B
7	Stiff	150mm deep Chieftain unit (D400 Class)	2 HDPE spacers placed on a thin layer of mortar A
8	Soft	100mm deep Chieftain unit (D400 Class)	5 HDPE spacers placed on a thin layer of mortar A
9	Stiff	100mm deep new design	10mm layer of new mortar
10	Soft	100mm deep new design	25mm layer of new mortar

Each installation was initially loaded by the rolling wheel. The wheel was tracked in 5 positions as shown in Figure 4.24. This was carried out on both installations and allowed a study of how the strains in the bedding and bituminous materials varied as the wheel moved across the pit. This information provided an indication of the position of the load causing the most damage.

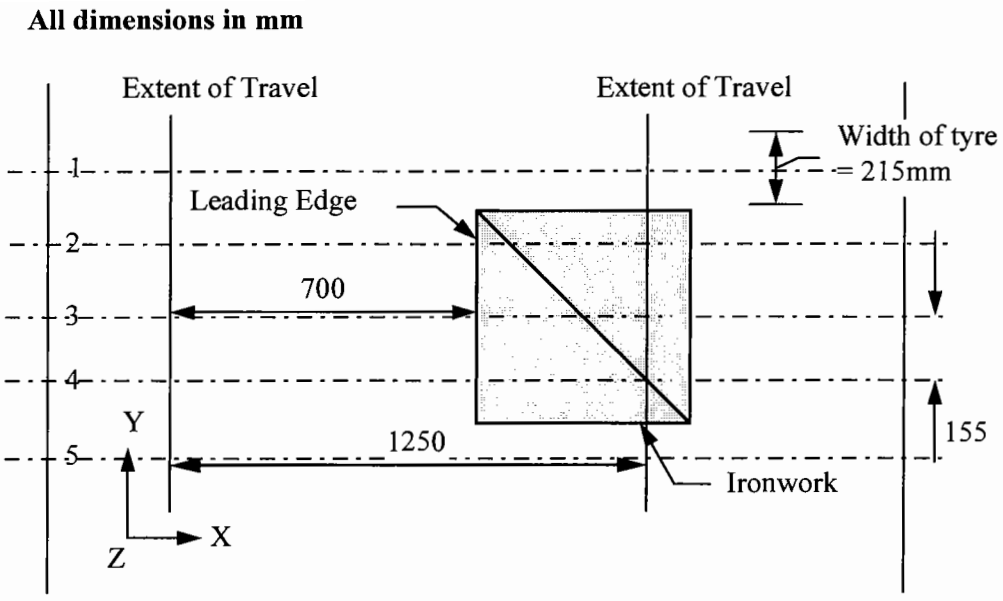

Figure 4.24: Plan view of a manhole installation indicating wheel paths

Initially, the wheel was positioned in Tracks 1 and 5 so that the edge of the tyre was 5mm away from the edge of the ironwork. This allowed a study of how the wheel affected the bedding material without touching the ironwork. Secondly, the edge of the tyre was run along the edge of the ironwork cover in Tracks 2 and 4. The wheel passed over the corner of the ironwork in these positions so the load would be mainly concentrated onto one seating and the bedding material underneath this point. The instruments in the backfill material were positioned along the centre line of the manholes. The wheel was finally positioned in Track 3 to study the output from these instruments and to gather further data from the embedment strain gauges in the bedding material. The wheel was tracked for approximately 500 passes before readings were taken. This enabled the ironwork cover to settle into the frame and allow an initial compression of the backfill.

Each installation was also subjected to a repeated plate load test. The platen was positioned at the location where the highest strains were recorded when loaded by the wheel. A sinusoidal load oscillating at 5Hz was applied for 1 million cycles. The peak magnitude of the load was varied between tests and is indicated in the description of the results. These tests allowed a study of any change in the instrument readings which were compared to any deterioration observed during the test. All of

the installations were loaded in this manner. The instrument layout in the bedding was changed throughout the experimental programme to investigate possible failure mechanisms that had been indicated from previous reinstatements. The positions are indicated in the description of the results in Chapter 5.

4.7 Summary

Careful consideration was applied to the design of the laboratory test facility and it is believed that it provides a close simulation of field conditions. It was also thought that the apparatus was sufficiently versatile to facilitate all tests required for this research. An experimental programme was developed to encompass a wide range of different bedding configurations. It was thought that this range would highlight any common failure mechanism and the threshold at which it occurred. The results from these investigations are presented in the next chapter.

5. Laboratory Test Facility Results

5.1 Introduction

The prototype test facility illustrated that tensile strains developed in the horizontal plane of the bedding material. A sufficiently large strain may lead to the development of vertical cracks in this layer as seen in the field. This was further investigated in these laboratory experiments. Each configuration presented in Table 4.4 was loaded through the rolling wheel and the fixed loading platen. Readings were taken from the instruments located on the ironwork frame and in the bedding and bituminous materials during these experiments. A study of these data allowed an understanding of how road ironwork configurations behave and helped to identify likely causes of failure.

5.2 Test 1: Bedding Layer Containing a Quarry Tile (Installations 1 & 2, Table 4.4)

The use of quarry tiles is a common method of ensuring the ironwork is placed level with the surrounding pavement when a thick bedding layer is required. These instances occur when an overlay is applied to a pavement as described in Section 2.2.4. It was also noted in Section 2.2.5 that quarry tiles have very similar elastic properties to fibrous boards so this configuration provided information on the behaviour of composite bedding layers in general.

A Standard Chieftain 600 x 600 x 100mm deep ironwork unit was bedded on top of each chamber. These units comply with EN124: 1994 [20] and are rated as class D400. Proprietary cementitious mortar A was used to form the bedding layer. The bedding layers were 75mm thick in total with the inclusion of a 20mm thick quarry tile in the middle. The quarry tile was evenly bedded on a 30mm thick layer of bedding material covering the entire width of the chamber walls.

Several embedment strain gauges were placed in the bedding material of both installations to measure strains in three mutually perpendicular directions, immediately underneath and in between seatings. A further study of the sensitivity

analysis revealed that the largest calculated strains developed in the bottom layer of bedding material, so the majority of gauges were placed in this region, although additional gauges were located in the top layer. The arrangement of the gauges was identical for each installation and a plan view is shown in Figure 5.1. The annotation will be referred to in the presentation of these results.

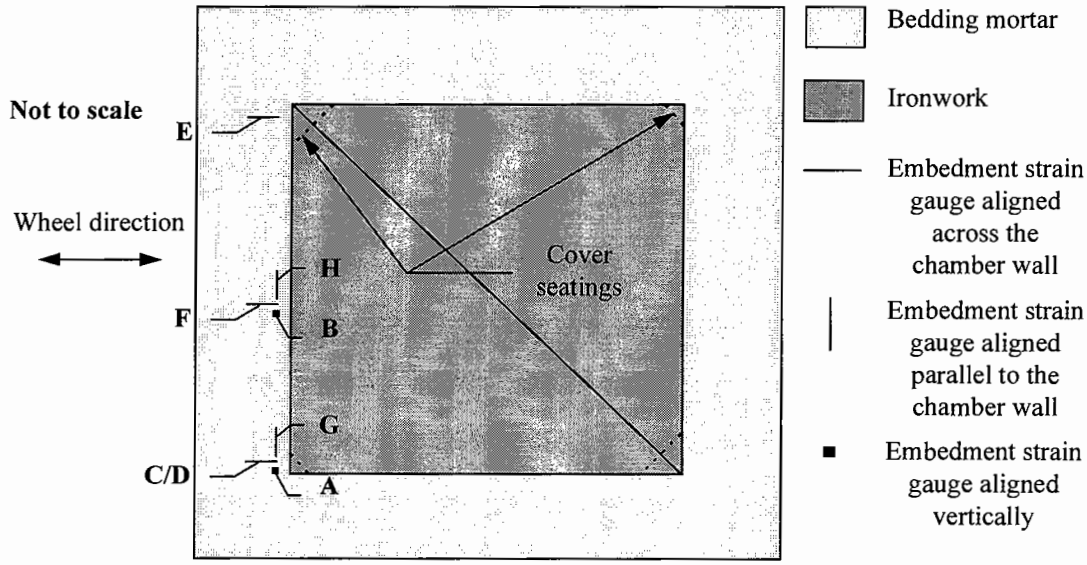

These instrument labels will be prefixed by T1 to denote Test 1.

Figure 5.1: Plan view of the embedment strain gauge layout for installations 1 & 2

5.2.1 Rolling Wheel Test Results

Bedding Material

The results from embedment strain gauge T1-A in the installation with stiff foundations are shown in Figure 5.2. This instrument was mounted vertically, directly underneath the bottom left hand seating as shown in Figure 5.1. The x-axis of the chart refers to the wheel tracks (Figure 4.24). The largest strains measured by this instrument occurred when the wheel was positioned in Track 4. Measurable strains were recorded when the wheel was 250mm away from the edge of the ironwork. The wheel was less than 50mm away from the edge of the brickwork chamber and bedding material at this point. The peak compressive strain of 98 microstrain occurred when the wheel was on the ironwork cover, directly above the seating. The magnitude decreased as the wheel travelled across the cover. A similar response but of a smaller magnitude, was measured when the wheel was positioned in Track 3. Negligible response was obtained for the other wheel tracks.

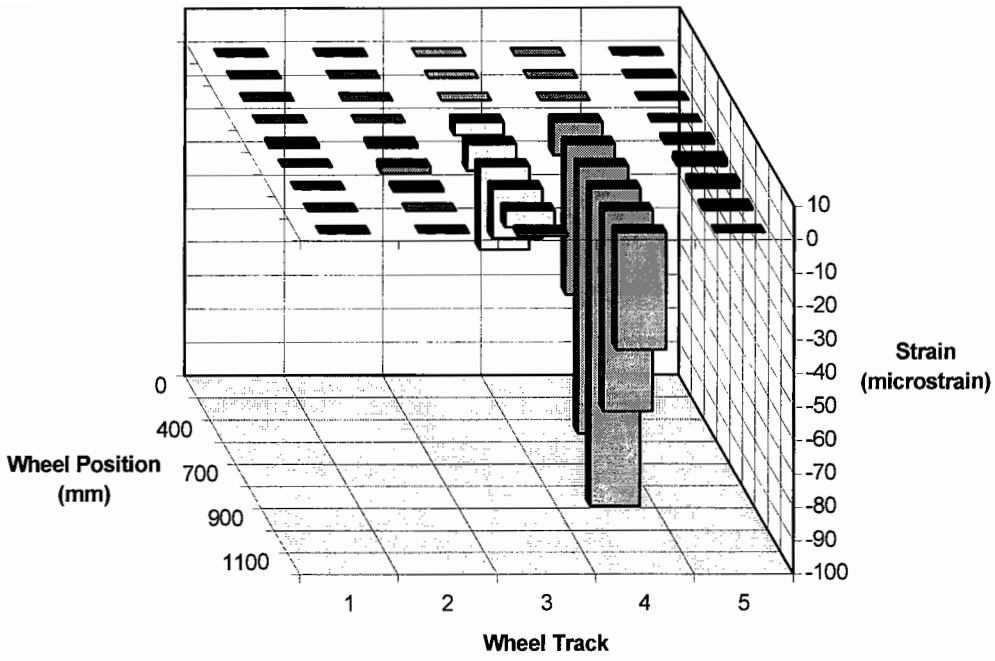

Figure 5.2: Vertical strain measured by gauge T1-A in the installation with stiff foundations (No.1)

The strain measured by embedment strain gauge T1-B, positioned between two seatings is shown in Figure 5.3. A peak compressive strain of 70 microstrain was measured by this gauge when the wheel was positioned on the edge of the ironwork cover in Track 3. Compressive strains were also recorded in Tracks 2 and 4. The maximum values were recorded when the wheel was positioned on the edge of the ironwork. The compressive strain magnitude diminished in all wheel tracks as the wheel moved across the cover. Strains were measured in wheel Tracks 1 and 5 but the values were considerably lower than those recorded in Track 3.

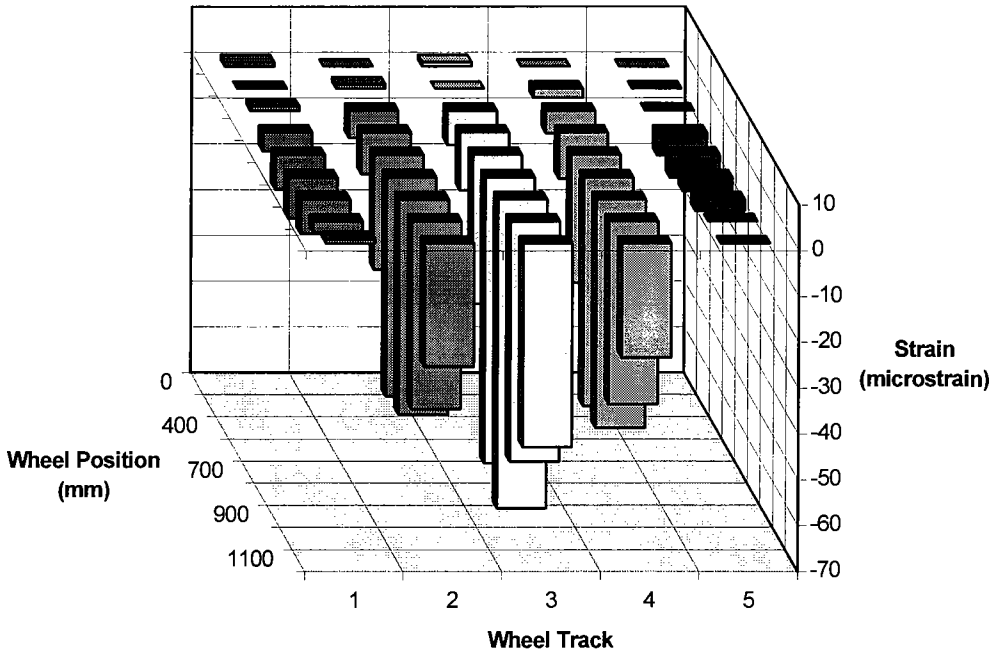

Figure 5.3: Vertical strain measured by gauge T1-B in the installation with stiff foundations (No. 1)

A similar pattern of results emerged from testing the installation with soft foundations (No.2). However, vertical tensile strains were measured by gauge T1-A when the wheel was on the backfill. The results from this gauge and embedment strain gauge T1-C when the wheel was positioned in Track 4 are shown in Figure 5.4.

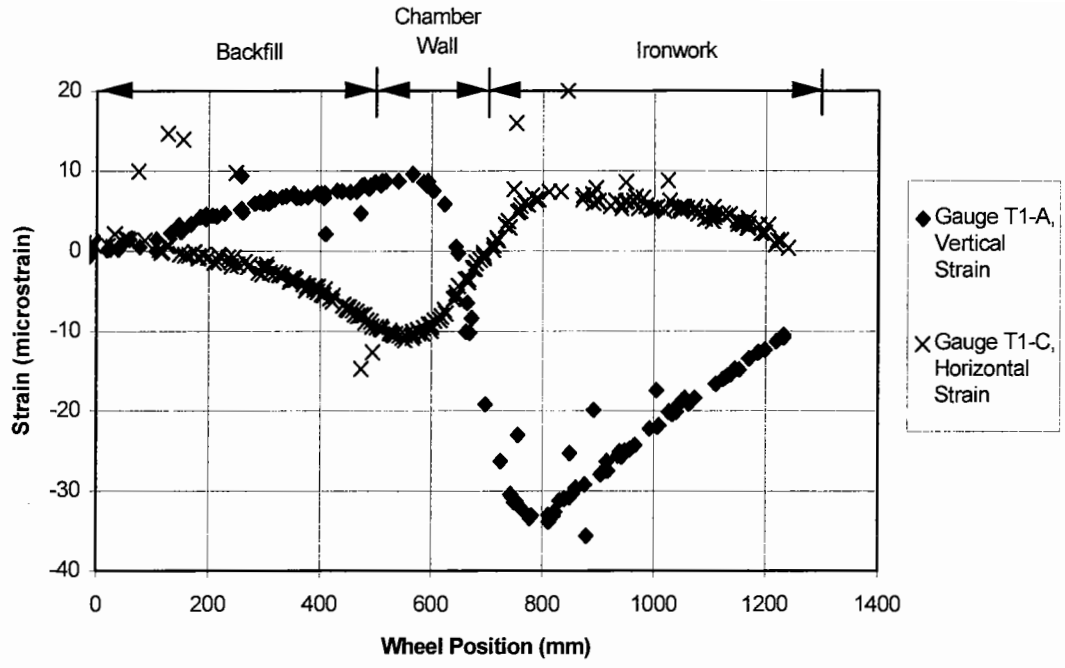

Figure 5.4: Vertical and horizontal strain measured by gauges T1-A and T1-C in the installation with soft foundations (No. 2) when loaded in wheel Track 4

It can be seen that the vertical strain increases to a value of 10 microstrain when the wheel is above the outside of the chamber wall. This value drops to a compressive strain of 35 microstrain when the wheel is positioned on the edge of the ironwork cover. This effect may be due to the soft foundations causing a larger deflection of the backfill than the stiff foundations. This may cause a rotation of the bedding material and induce tension in the vertical plane along the internal edge of the bedding. This effect was studied further in later reinstatements.

Embedment strain gauge T1-C (Figure 5.1) measured horizontal strain across the width of the bedding next to gauge T1-A. Figure 5.4 illustrates that gauge T1-C measured a tensile strain when gauge T1-A measured a compressive strain. This may be attributed to the Poisson effect. These data were measured by instruments positioned in the lower layer of bedding material, underneath the quarry tile. Figure 5.5 illustrates the output measured by embedment strain gauge T1-D (Figure 5.1) in the installation with soft foundations. The instrument was also mounted horizontally and was located directly above gauge T1-C in the bedding material above the quarry tile.

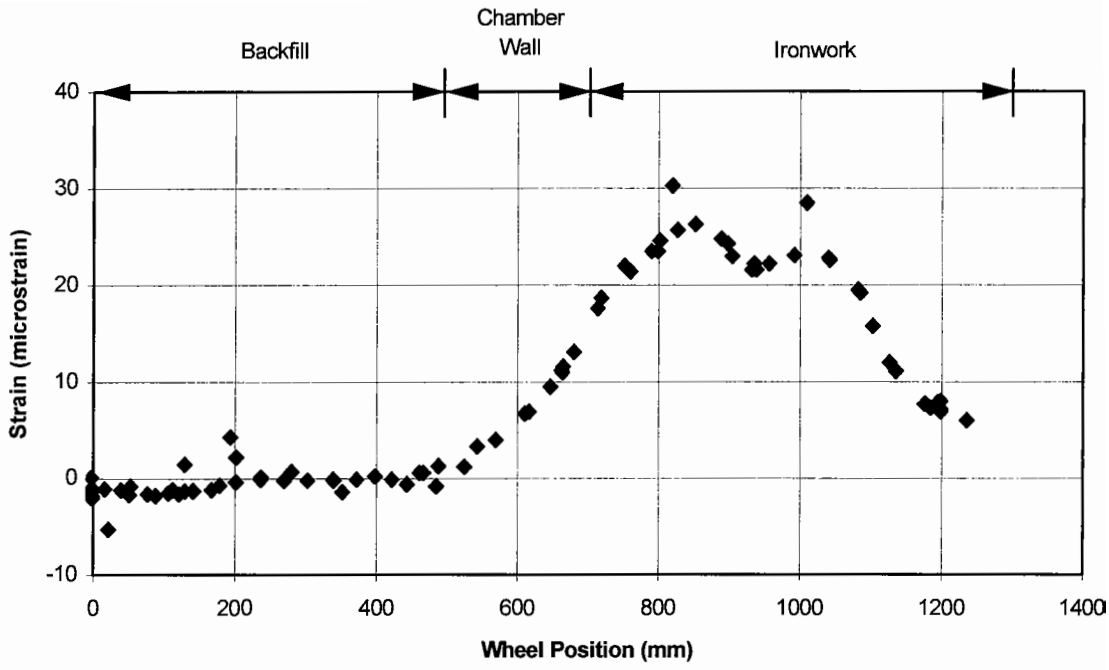

Figure 5.5: Horizontal strain measured by gauge T1-D in the installation with soft foundations (No. 2) when loaded in wheel Track 4

The peak tensile strain measured by this instrument was 26 microstrain. This was measured when the wheel was positioned on the corner of the cover directly above the bottom left hand seating. The load from a seating will distribute over a wider area with increasing depth, so it will be confined to a small area in the top layer of bedding. This is a possible reason for a larger tensile strain in the top layer than in the bottom layer. The instruments at this location measured the largest tensile strain in both installations. These results show that tensile strain develops in the bedding as seen in the prototype test facility. The direct tensile tests on cementitious bedding mortar specimens illustrated that cracks develop perpendicular to the direction of the load. A sufficiently large horizontal tensile strain would cause vertical cracks to develop in the bedding layer as discovered in the field.

Gauge T1-E was placed in the bottom layer of the bedding underneath the top left hand seating as shown in Figure 5.1. This gauge was also aligned to measure strain across the width of the mortar. The results from this gauge in the installation with soft foundations when the wheel was positioned in Track 2 are shown in Figure 5.6.

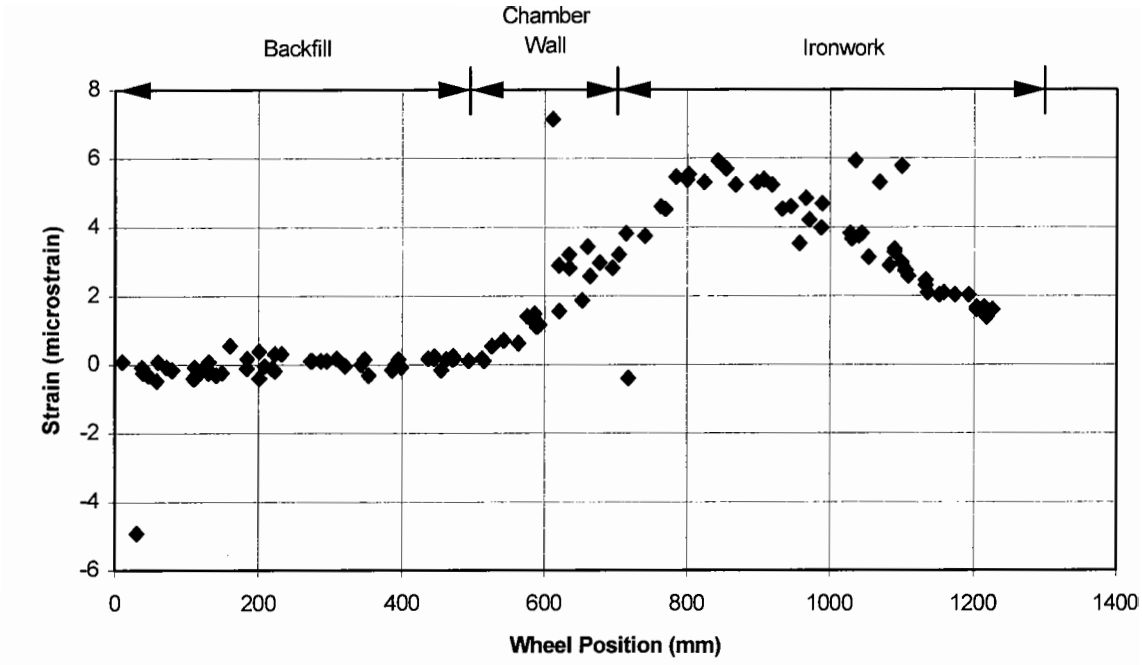

Figure 5.6: Horizontal strain measured by gauge T1-E in the installation with soft foundations (No. 2) when loaded in wheel Track 2

It can be seen that a peak of 6 microstrain was recorded when the wheel was positioned over the corner of the ironwork which is smaller than the measurements recorded by gauge T1-C. The bearing area of the seating above gauge T1-E is approximately twice as large as the seating above gauge T1-C, so there is a lower concentration of load at this point. This may explain the lower strain measurement. Virtually no strain was measured by gauge T1-E when the wheel was positioned in Track 1. Similar results were recorded by gauge T1-C when the wheel was positioned in Track 5.

The bedding layer was placed across the full width of the chamber wall, as often done in practice. Load can be applied to the bedding when the wheel is positioned over the chamber wall. The strain recorded by embedment strain gauge T1-F in wheel Track 3 in the installation with soft foundations is shown in Figure 5.7. This instrument was positioned in the bottom layer of bedding, in between two seatings and aligned to measure strain across the width of the mortar.

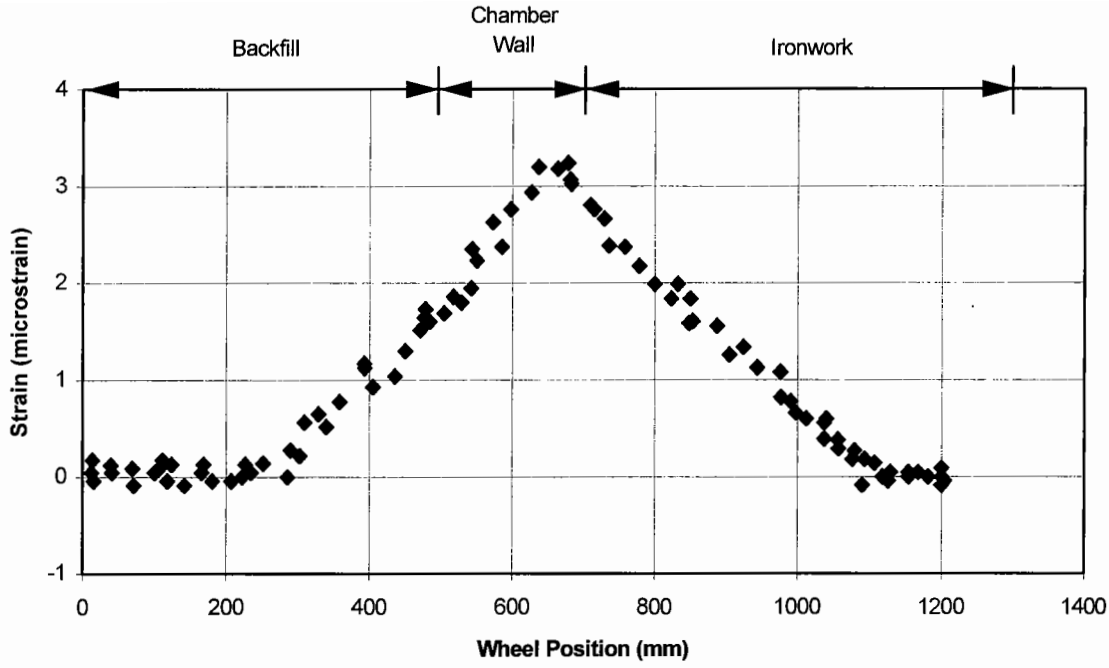

Figure 5.7: Horizontal strain measured by gauge T1-F in the installation with soft foundations (No. 2) when loaded in wheel Track 3

It can be seen that the peak magnitude is smaller than those recorded by gauges T1-C and T1-E. Gauge T1-F measured a tensile strain when the load was applied on the surface above the instrument. A similar trend was seen in the installation with stiff foundations. This gauge was 165mm beneath the surface so the load would have distributed over a wide area at this depth. Gauges T1-C and T1-E measured their largest strains when the wheel was on the corner of the ironwork. The load was carried by the cover seating at this position which was 65mm above these instruments. Additionally, the distance between gauge T1-D and the seating was only 20mm. These results indicate that a high concentration of load produces a large tensile measurement. It would appear likely that the bedding would suffer the most damage when load is applied above the bottom left hand seating. It is considered that the bearing area of the seating has a strong influence on the magnitude of tensile strain in the bedding directly underneath.

The strain measured by gauge T1-G in the installation with soft foundations is shown in Figure 5.8. These results were recorded when the wheel was positioned in Track 4.

This gauge was aligned to measure strain parallel to the chamber wall and was positioned in the bottom layer of the mortar underneath the bottom left hand seating as shown in Figure 5.1.

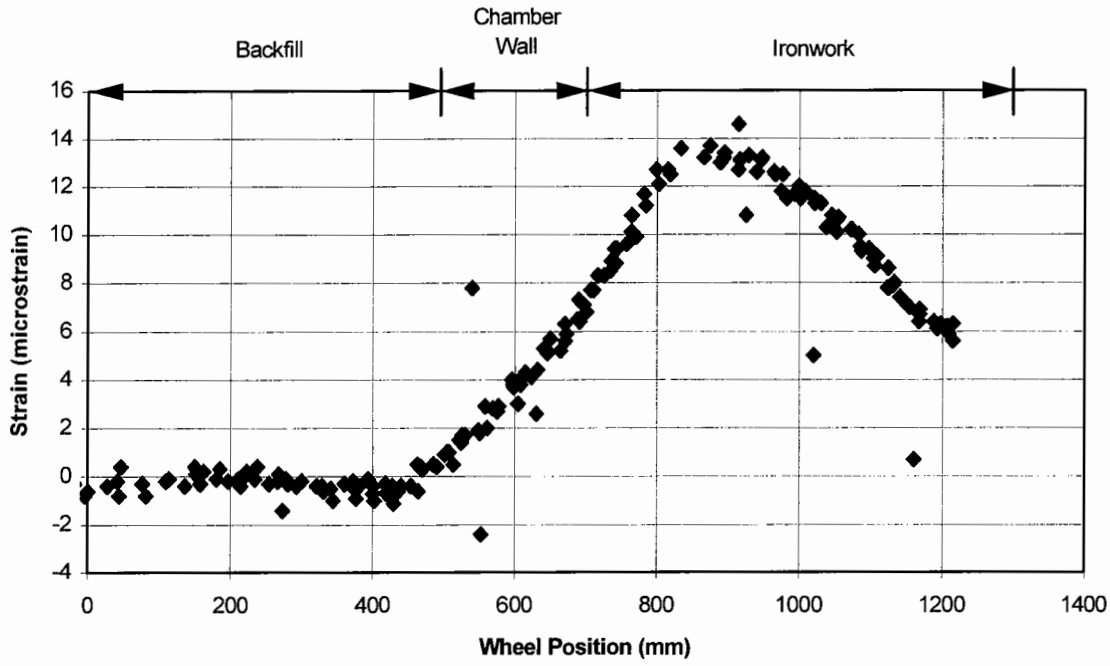

Figure 5.8: Horizontal strain measured by gauge T1-G in the installation with soft foundations (No. 2) when loaded in wheel Track 4

This gauge measured a tensile strain as the wheel moved across the chamber wall and onto the ironwork. The largest tensile strain of 14 microstrain occurred when the wheel was completely on the ironwork cover and above this corner. The tensile strain reduced as the wheel moved across the cover. A similar trend occurred when the wheel was tracked along the centre line of the chamber (Track 3) but the maximum tensile strain was only 4 microstrain. This was the largest measurement of tensile strain in the bottom layer of the bedding for both installations.

The ironwork frame may be considered as a beam on an elastic foundation. Loads are applied to the corners of the frame when the wheel is on the cover which may result in bending. The ironwork has a Young's modulus of 165GPa which is much greater than the bedding material which has a mature static modulus 21GPa. The frame also had a greater depth than the bedding layer so its flexural rigidity was much greater. It

is considered that the neutral axis of bending for the composite would be within the ironwork frame due to this difference. If the neutral axis is within the ironwork then the region below will be in tension which includes the bedding material assuming a good bond in between. Only a small tensile strain was recorded by gauge T1-G. However, if the bedding layer was thinner, the moment of resistance would be reduced which would result in a larger tensile strain. The strain at this point was measured again in later reinstatements.

Another method of inducing tension due to flexure of the bedding material occurred when the wheel was tracked along the centre line of the installation. The length of bedding material along the leading edge was loaded in two modes. It was loaded centrally when the wheel was positioned on the chamber wall, immediately adjacent to the ironwork inducing a sagging bending moment. However, a hogging moment resulted when the wheel was positioned on the ironwork cover and the bedding was loaded through the cover seatings. The strain measured by embedment strain gauge T1-H in the installation with soft foundations, mounted parallel to the chamber wall and in between seatings is shown in Figure 5.9. The results from this instrument are compared with the strain measured at the top of the ironwork frame in between seatings.

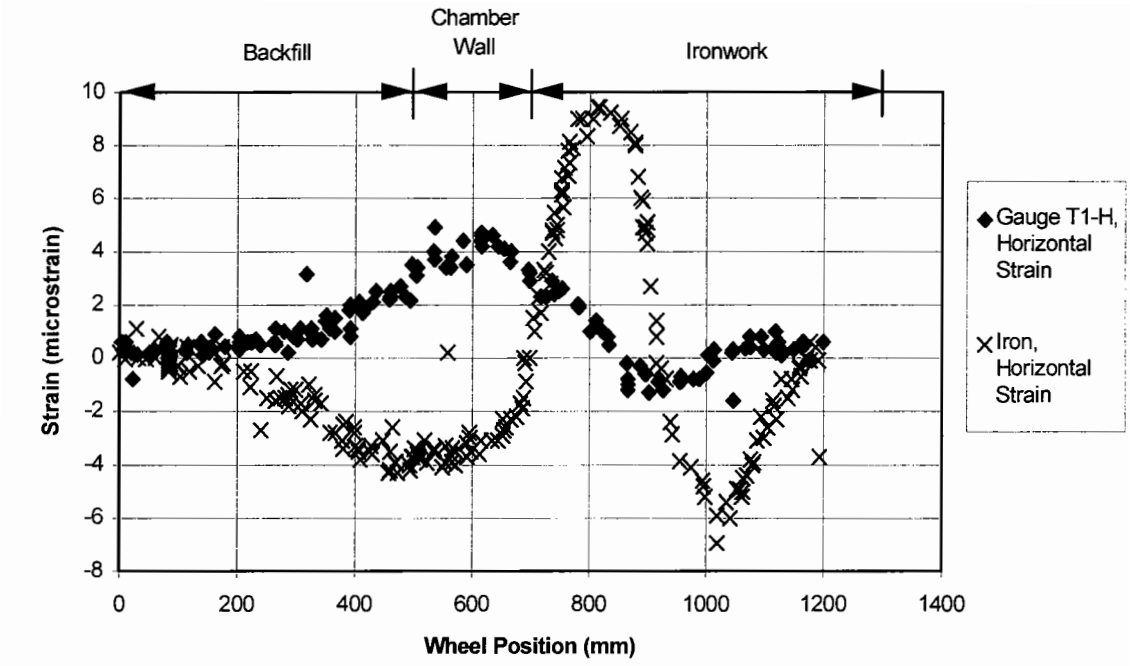

Figure 5.9: Horizontal strain measured by gauge T1-H and at the top of the ironwork frame in the installation with soft foundations (No. 2) when loaded in wheel Track 3

The peak tensile strain in the bedding occurred when the wheel was immediately adjacent to the ironwork cover but was only 5 microstrain. The strain gauge mounted on top of the ironwork frame measured a small strain but of the opposite sense to those seen in the bedding. This indicates that the iron and bedding bend together under an applied load. It was considered that this mechanism should have resulted in a larger tensile strain in the bedding. ELSYM5 was used to calculate the strain at this position. The layers defined in the program consisted of the frame web, bedding material including the quarry tile and brickwork. The appropriate thicknesses and stiffnesses were attributed to each layer and the horizontal strain was calculated for both load cases. The physical properties of the materials are shown in Table 6.3. The ANSYS finite element analysis program was also used to provide an estimation of the horizontal strain at this point. A two-dimensional model was created with the same profile as the bedding configuration used in the laboratory test facility, as seen from the inside of the chamber. Both programs indicated strains of the same order of magnitude and these are summarised in Table 5.1. The large moment of resistance as

previously mentioned is considered to be attributable to the small tensile strain measurement. Other common bedding configurations have thinner layers and may be susceptible to this failure mechanism. This was also studied in later reinstatements.

Table 5.1: Summary of the results of flexural strains measured in the bedding mortar, and estimations by two methods

	Strain developed due to sagging moment (microstrain)	Strain developed due to hogging moment (microstrain)
Measured in laboratory test facility	5	-1
Calculated by ELSYM5	3	-2
Calculated by ANSYS	9	-6

Backfill Material

The locations of the instruments in the backfill material are shown in Figure 4.13. The output from the instruments at the bottom of the DBM layer when the wheel was located in Track 3 is shown in Figure 5.10. These data are taken from experiments on the installation with a soft foundation.

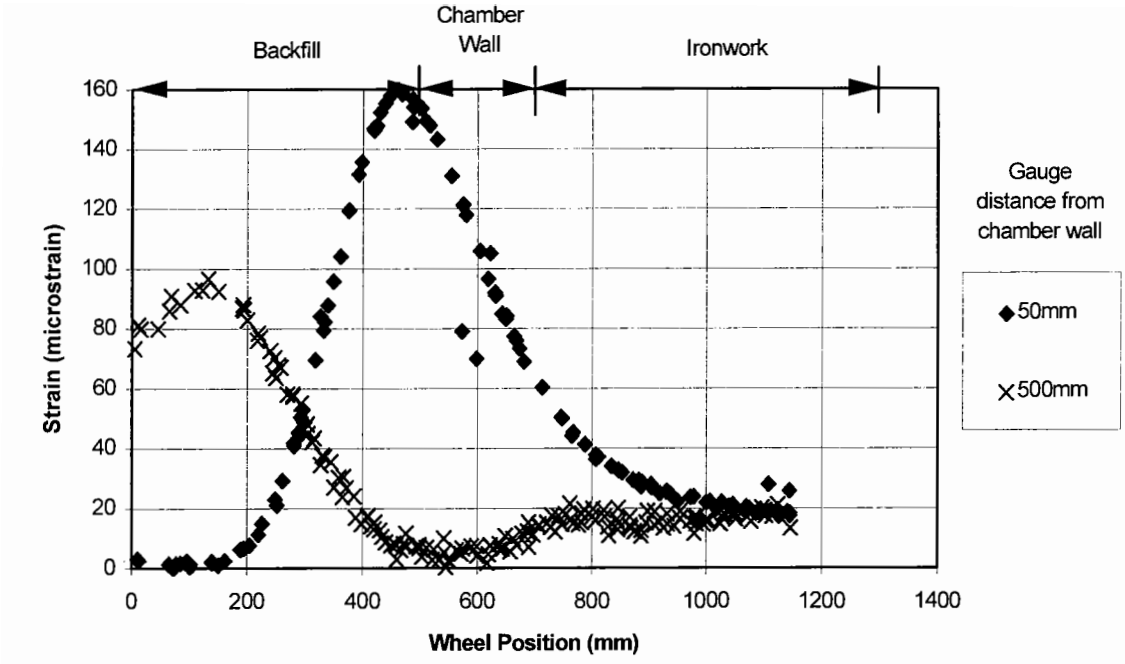

Figure 5.10: Horizontal strains measured by instruments positioned 25mm from the bottom of the DBM layer in the installation with soft foundations (No. 2)

The peak tensile strains occurred when the wheel was directly above the instruments. It can be seen that the largest strain of 160 microstrain was measured by the embedment strain gauge 50mm from the edge of the chamber. Strains were still measured by this instrument after the wheel had passed onto the ironwork. The strain measurement is considered to be larger closer to the manhole compared to some distance away due to a difference in the effective in-situ stiffness as described in Section 3.4.2. This was investigated in later experiments by measuring surface deflections at various positions on the laboratory test facility. Additionally, the bituminous layer may adopt the bending moments of a beam on an elastic foundation. The ends of the beam influenced by a wheel load at some distance from a manhole are restrained from rotation by the surrounding pavement. This is illustrated in Figure 5.11a. However, the bituminous material around an ironwork unit does not form a strong bond with the outside of the frame. This has been noticed in field observations. Hence a rotation of the bituminous layer at this point is possible, causing a greater tensile strain to develop in the bottom of the layer. This is shown in Figure 5.11b.

This pattern was noticed in both installations. The larger tensile strain around the ironwork may be the cause of cracking of the bituminous material. This effect was also studied in later experiments.

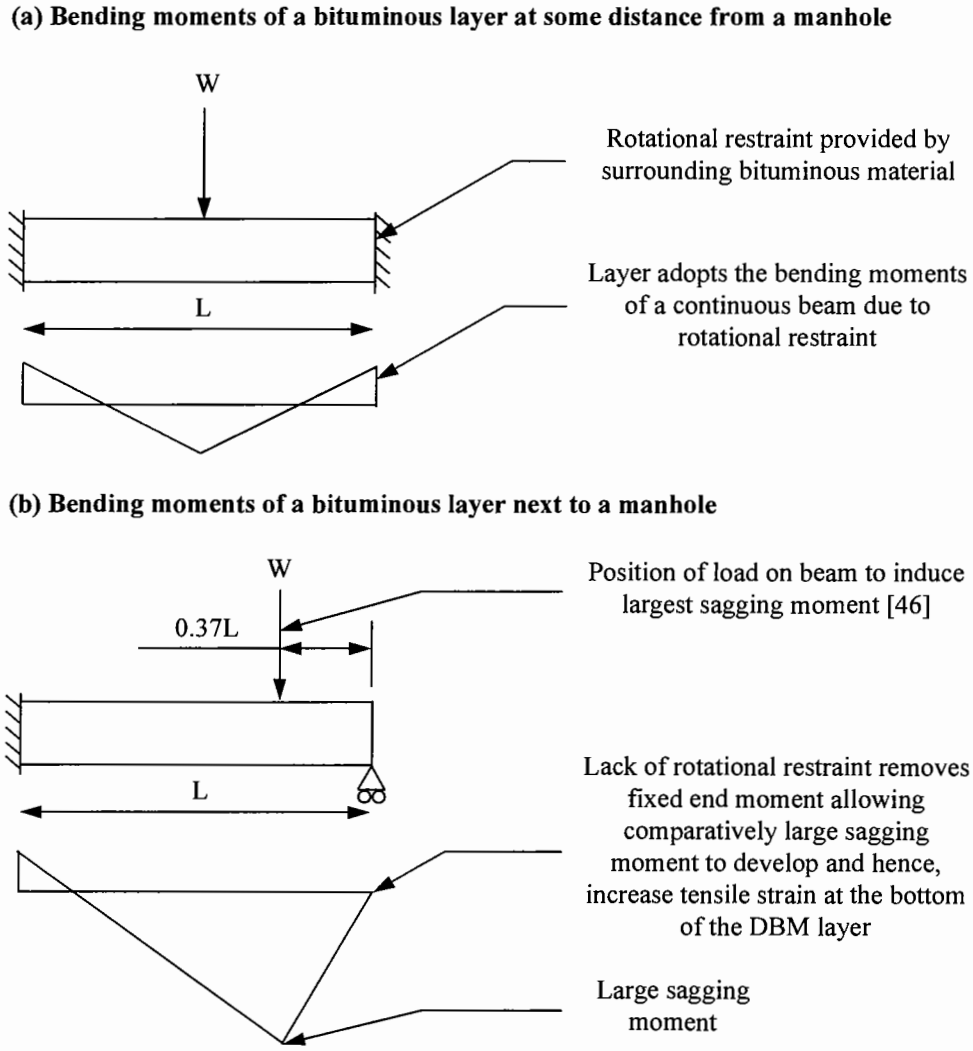

W = Applied load, assumed to be a point load in this example for simplicity

L = Length of DBM under the influence of the load

Figure 5.11: Illustrative example of the difference in maximum bending moments due to a change of restraint conditions

5.2.2 Repeated Load Test Results

The rolling wheel tests indicated the position of the load inducing the largest tensile strain in the bedding layer. This occurred when the wheel was above the bottom left hand corner of the ironwork cover. Mortar A has a mature compressive strength of 38MPa and a static modulus of 21GPa. The approximate vertical strain at failure under uniaxial compression was calculated to be 1800 microstrain. The largest compressive strain measured was 98 microstrain so it was thought that a compressive failure was unlikely. It is thought that a tensile failure was the most likely cause of cracking in the bedding which would result in vertical cracks as seen in the field. The fixed platen of the loading frame was placed at the most sensitive position. This was the first repeated load test to be carried out so the load was restricted to 30kN. This was applied at 5Hz for 1 million cycles and the strains measured by the instruments in the bedding material and on the ironwork frame were recorded at approximate intervals of 150,000 cycles.

The output from embedment strain gauge T1-D in the installation with soft foundations measuring horizontal strain above the quarry tile and underneath the seating is shown in Figure 5.12.

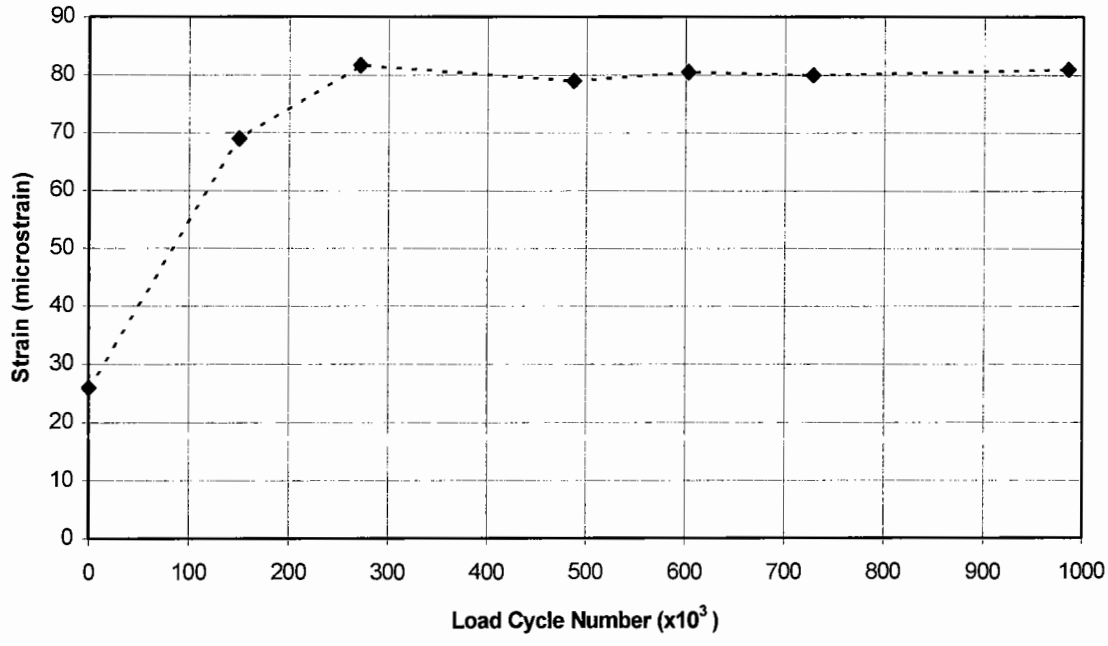

Figure 5.12: Horizontal strains measured by Gauge T1-D in the installation with soft foundations (No. 2)

This gauge displayed the largest tensile strain in the mortar during the rolling wheel tests. The magnitude of this tensile strain was 26 microstrain at the beginning of the repeated load test. After 150,000 load applications, this strain had increased to 69 microstrain. A further increase to 82 microstrain was recorded after 272,000 load applications. The level of strain then remained constant for the remainder of the test. Embedment gauge T1-C also exhibited an increase in strain. The initial reading was a tensile strain of 8 microstrain, increasing to 23 microstrain after 272,000 load applications. No further increases were recorded for the remainder of the test. During the test, there was also a reduction in the compressive strain from 85 microstrain to 73 microstrain measured by gauge T1-A.

There was also an increase in the flexure of the frame. The output from the strain gauge measuring horizontal strain at the top of the frame, in between seatings is shown in Figure 5.13.

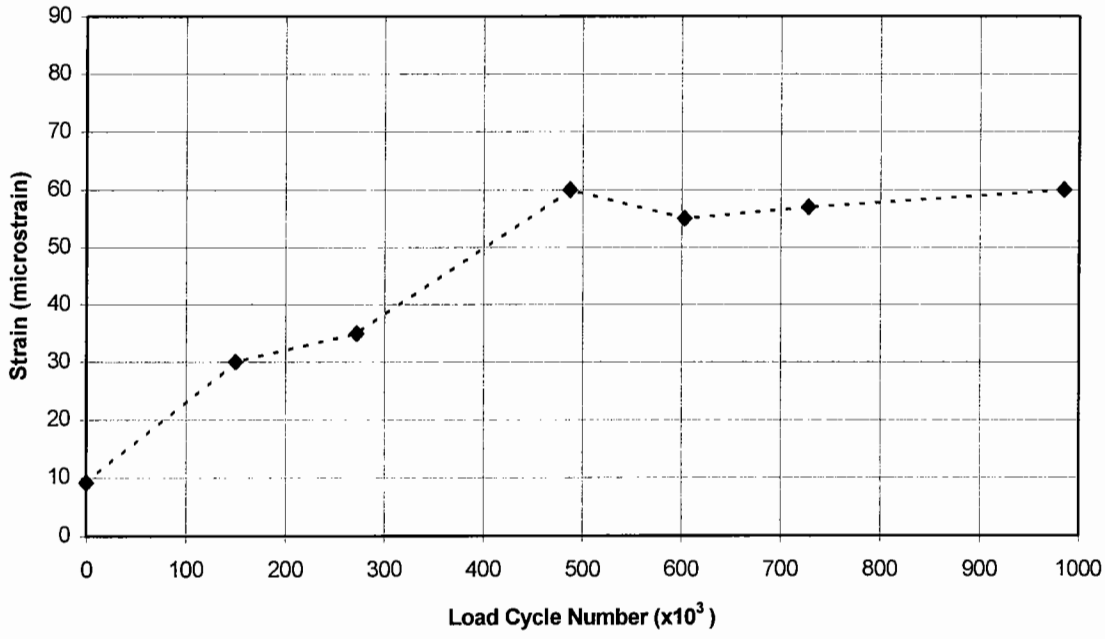

Figure 5.13: Horizontal strain measured by strain gauge at the top of the frame, in between seatings in the installation with soft foundations (No. 2)

The tensile strain measured by this instrument increased from 10 microstrain at the start of the test to 35 microstrain after 272,000 cycles. The bedding material forms the foundation to the ironwork frame. Cracking of this support would allow greater flexure of the frame.

A repeated load test was carried out on the installation with stiff foundations. The same load regime was applied for 1 million cycles and readings were taken at approximate intervals of 150,000 cycles. The instruments in the same positions demonstrated the trends seen previously. However, the increases were smaller and did not occur until the installation had received 700,000 cycles.

An inspection of the bedding material inside both manholes was made at the end of the test. It was found that a vertical crack had developed through the full depth of the bedding underneath the bottom left hand seating. Other full depth cracks were noticed passing through the joints between quarry tiles close to this corner. Cracks were not evident in the quarry tiles. The cracks would have a significant effect on the distribution of the load. This may explain the increases in horizontal strains measured underneath the seating.

Both installations demonstrated similar trends and strain magnitudes under both loading regimes. It would appear that the stiffness of the supporting foundation has a negligible effect on the behaviour of the bedding layer.

5.3 Test 2: 25mm thick Bedding Layer (Installations 3 & 4, Table 4.4)

A circular saw was used to cut through the DBM layer above the outside edge of both chambers after testing was completed with the first configuration. The ironwork and bedding layers were removed and were replaced with another common ironwork and bedding configuration. This consisted of a standard Chieftain 600 x 600 x 150mm deep ironwork unit bedded on a 25mm thickness of cementitious mortar A spread across the full width of the chamber. An additional thickness of 20mm was placed above the frame flange on the installation supported by soft foundations so the flange was entirely encapsulated within the bedding. These reinstatements were completed

by backfilling and compacting a proprietary bitumen emulsion product around the outside of the ironwork. This product contained 6mm granite chippings. This configuration allowed a comparison between the behaviour of the thick bedding previously tested with that having an average thickness. The installation procedure was similar to examples of good practice that are followed on site.

Embedment strain gauges were placed in the 25mm thickness of mortar to measure strains in various directions and at various positions. A plan view of the arrangement of the instruments where the results have been presented is shown in Figure 5.14. This was identical for both installations. The positions included underneath the bottom left hand cover seating and in between seatings. Another embedment strain gauge was placed in the mortar passing through a hole in the frame flange in the installation with soft foundations. Some of the gauges were located in the same region as the previous experiment. In these cases, care was taken to ensure that the instruments were installed at exactly the same location and distance from the top of the brickwork chamber. Load was applied in the same regime as in the previous experiments.

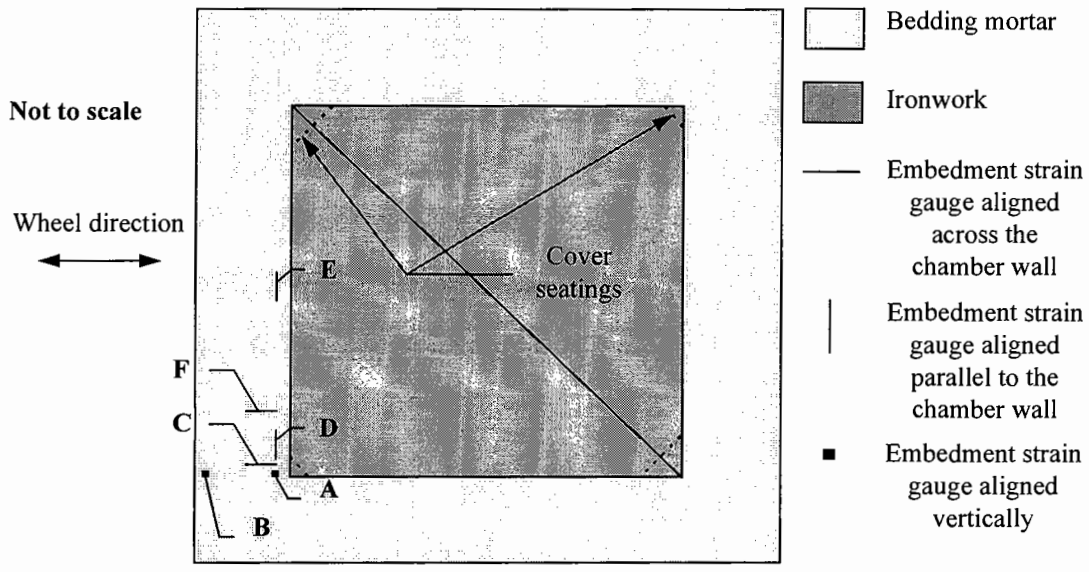

These instrument labels will be prefixed by T2 to denote Test 2.

Figure 5.14: Plan view of the embedment strain gauge layout for installations 3 & 4

5.3.1 Rolling Wheel Test Results

Bedding Material

Figure 5.15 illustrates the output from gauge T2-A in the installation with stiff foundations. This instrument was mounted vertically under the bottom left hand seating. The data has been presented in the same format as Figure 5.2.

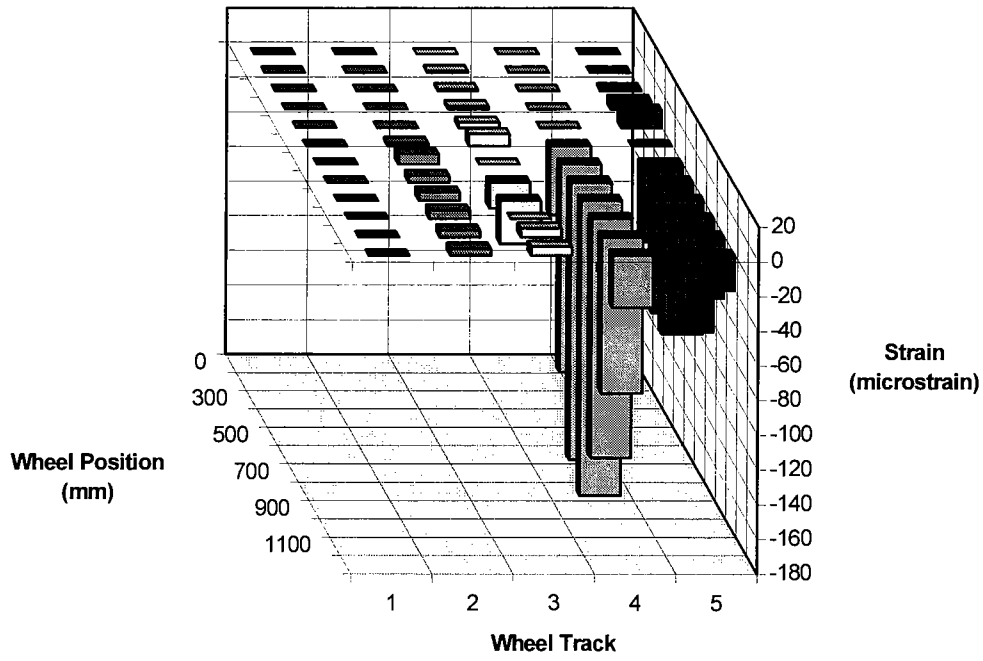

Figure 5.15: Vertical strain measured by gauge T2-A in the installation with stiff foundations (No. 3)

It can be seen that the measurements follow the same trend as seen in the last configuration. Both sets of results illustrate that load applied on the cover is not evenly distributed onto the bedding layer. The applied load had the greatest influence over this gauge when the wheel was positioned on the bottom left hand corner of the ironwork cover.

The largest compressive strain was 170 microstrain which was larger than the peak recorded in the configuration containing a quarry tile. The vertically mounted instrument was closer to the cover seating in the second configuration so it is thought that it would be subjected to a higher concentration of load. Despite the larger

measurement, it is not considered sufficient to cause a compressive failure of the bedding material.

The output recorded by the same gauge in the installation with soft foundations exhibited a similar response to the gauge in this position in installation No. 2. Tensile strains were again noticed when the wheel was located above the outside edge of the chamber. The largest tensile strain of 7 microstrain measured by gauge T2-A occurred when the wheel was located in Track 4 as shown in Figure 5.16.

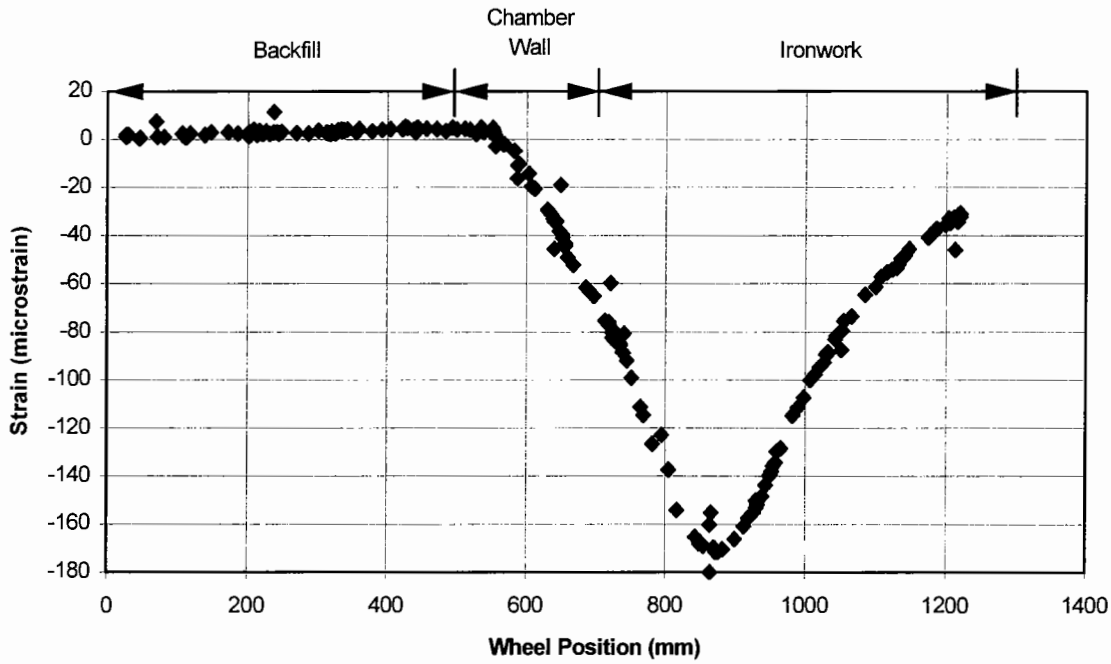

Figure 5.16: Vertical strain measured by gauge T2-A in the installation with soft foundations (No. 4) when loaded in wheel Track 4

Another vertically mounted gauge was placed in the bedding of both installations close to the outside edge of the chamber. This instrument is labelled as gauge T2-B in Figure 5.14. The measurements from this instrument when the wheel was located in Track 4 of the installation with soft foundations are shown in Figure 5.17.

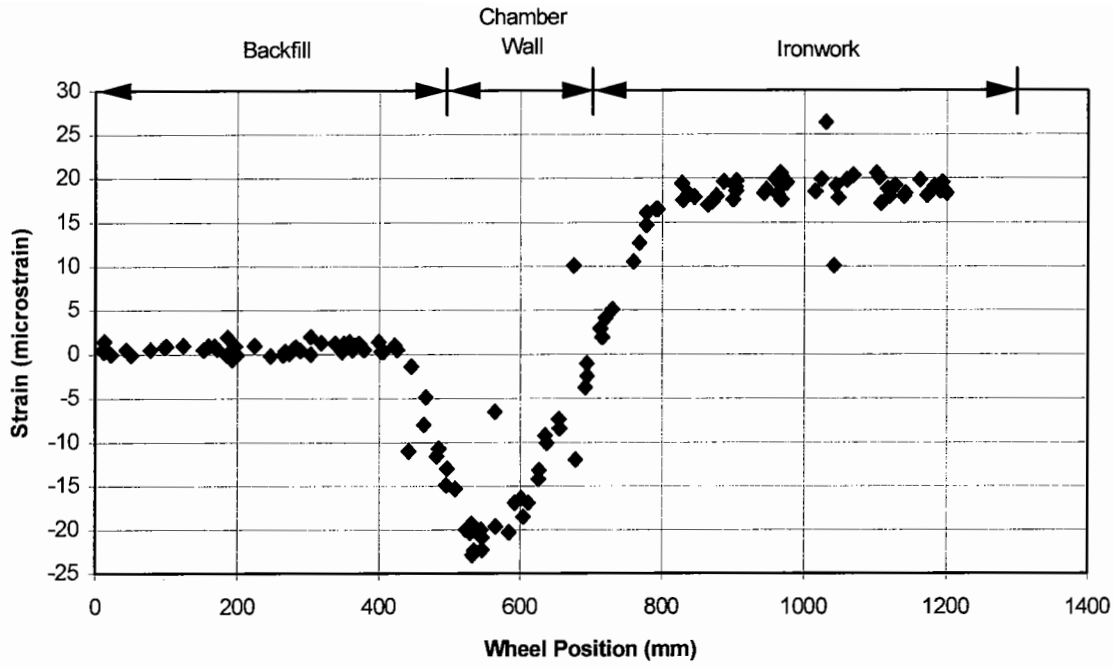

Figure 5.17: Vertical strain measured by gauge T2-B in the installation with soft foundations (No. 4) when loaded in wheel Track 4

A compressive strain of 23 microstrain was recorded when the wheel was above the outside of the chamber and a tensile strain of 19 microstrain was measured after the wheel had moved onto the ironwork. This was in the opposite sense to the strains recorded by gauge T2-A at these wheel positions. The output from gauge T2-B in the installation with stiff foundations produced a similar pattern of results as seen in Figure 5.17 but the peak compressive and tensile strains were only 4 and 5 microstrain respectively. The difference in the compressive strain magnitudes may be attributable to a difference in the effective in-situ stiffness between the backfill and the manhole which is later shown to be greatest on the installation with soft foundations. It is therefore considered that the bedding layer rotates. This is illustrated in Figure 5.18.

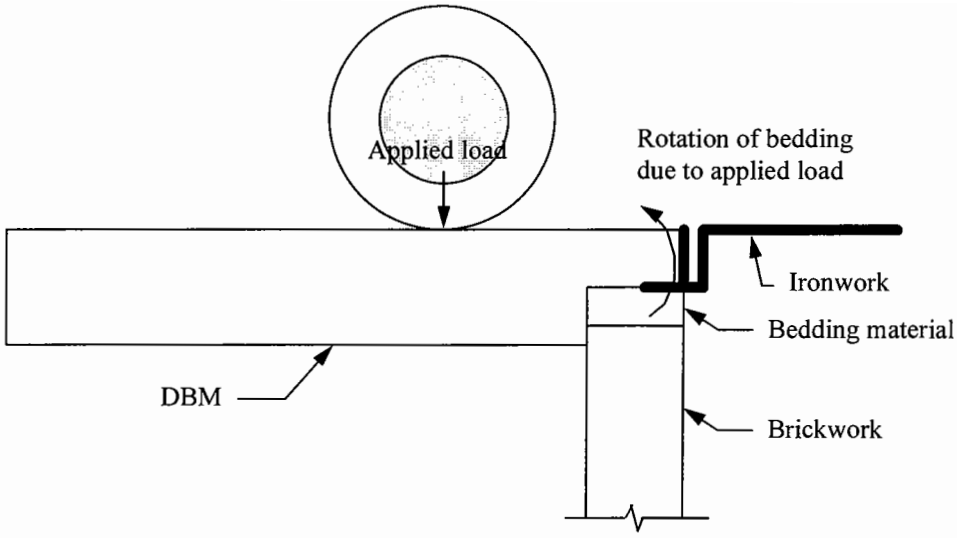

Figure 5.18: Vertical tension induced in the bedding due to a difference in effective in-situ stiffness

A comparison between gauges T2-A and T2-B illustrated that the magnitude of the peak vertical compressive strains increased closer to the corner of the ironwork. From these results it is again considered that the load is concentrated over a small area around the cover seating. Gauge T2-A was set 20mm away from the inside face of the bedding material so it may not be measuring the largest compressive strain present in the bedding. Later experiments involved fastening an ordinary strain gauge to the exposed surface of the bedding underneath the cover seating.

The cover seatings were unsupported in all the reinstatements so the frame web may have twisted when load was applied on the ironwork cover. This may have resulted in uplift of the frame flange. The reaction to the uplift would be provided by the materials placed above it. The mortar above the flange would have provided some restraint which is likely to have induced the tensile strain as seen in Figure 5.17. It was noted from previous experiments and field observations that the frame does not form a strong bond with a cementitious bedding material and would explain the small tensile strain recorded in the reinstatement without mortar above the flange. It is thought the restraint was provided entirely by the bituminous backfill in this installation.

The strain measured by gauges T2-A and T2-C in the installation with stiff foundations when the wheel was positioned in Track 4 are shown in Figure 5.19. Gauge T2-C was located underneath the bottom left hand cover seating and aligned to measure horizontal strain across the width of the bedding layer.

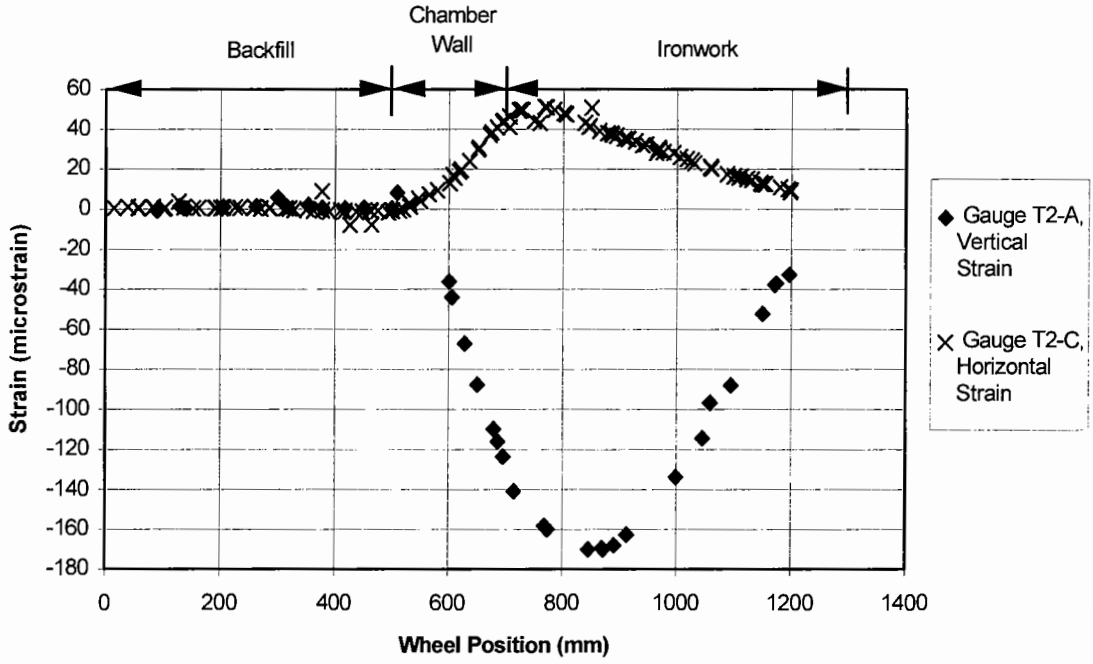

Figure 5.19: Vertical and horizontal strain measured by gauges T2-A and T2-C in the installation with stiff foundations (No. 3) when loaded in wheel Track 4

The data again illustrates a similar trend to the configuration containing a quarry tile, but the peak magnitudes are larger. The largest tensile strain recorded by gauge T2-C was 53 microstrain and this occurred when the wheel was on the corner of the ironwork cover. This was the largest tensile strain recorded in this configuration. This trend was previously thought to be attributed to the Poisson effect. However, the ratio of the peak strains was 0.31 which is considerably larger than the value measured in the Instron test machine which was 0.14. Although a horizontal tensile strain would occur due to a vertical compressive force it is considered that the Poisson effect is only partially attributable to these measurements. A strain gauge measures a tensile strain due to an elongation of the gauge. This would occur due to a translation in a plane parallel to the gauge or a rotation in a perpendicular plane. This would suggest that the bedding layer was bending across the width of the mortar.

The gauge at this location in the installation with soft foundations produced similar results when the wheel was positioned in Track 4 but the peak tensile strain was only 32 microstrain. The presence of mortar above the flange would have increased the flexural rigidity of the bedding layer which may be related to the lower strain measurement at this point.

A peak tensile strain of 27 microstrain was measured by gauge T2-D in the installation with stiff foundations. This instrument was located next to gauge T2-C but aligned to measure strain in the horizontal plane parallel to the chamber wall. An illustration of the output from this gauge is shown in Figure 5.20.

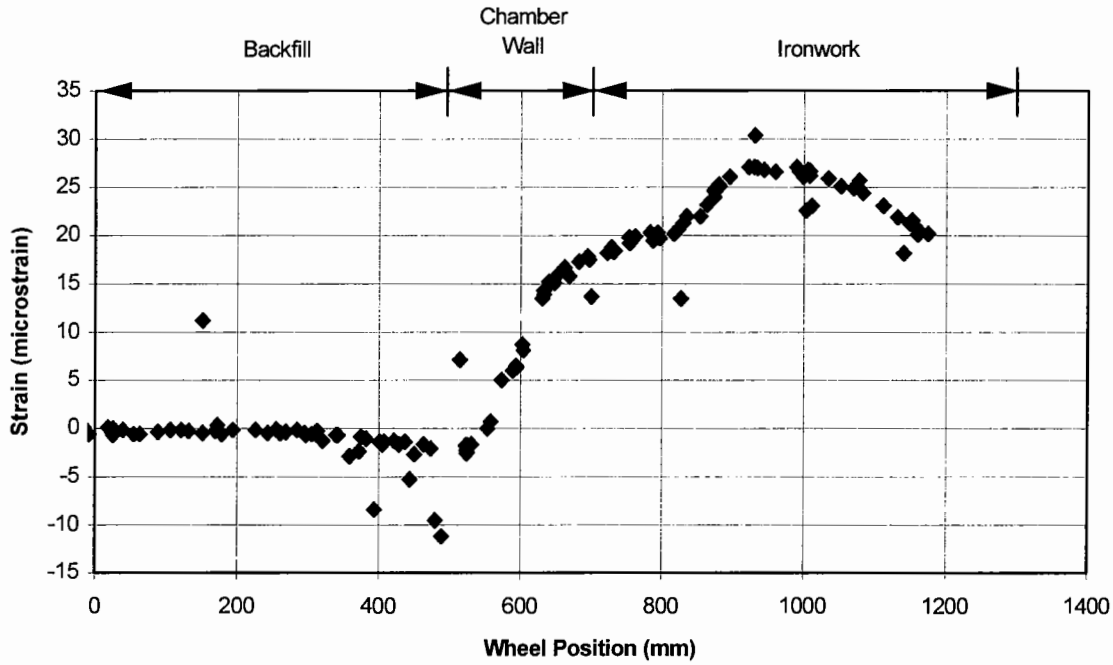

Figure 5.20: Horizontal strain measured by gauge T2-D in the installation with stiff foundations (No. 3) when loaded in wheel Track 4

This measurement was also considered to be caused by the Poisson effect and flexure of the bedding. A peak tensile strain of 17 microstrain was recorded by this gauge in the installation with mortar above the flange (No. 4). Evidence from three common bedding configurations illustrated that tensile strains develop in the horizontal plane, 10mm from the surface of the brickwork. In all cases, the magnitude of the peak

value was inversely proportional to the overall bedding thickness. This provides confidence in the suggestion that the bedding layer bends under load as it has been seen that the peak value reduced with a larger flexural rigidity.

The flexure of the bedding and iron in between two seatings when the wheel was positioned in Track 3 was also investigated in these installations. The output from gauge T2-E (Figure 5.14) and a strain gauge mounted on the top edge of the iron above this point is shown in Figure 5.21. These results were recorded in the installation with stiff foundations.

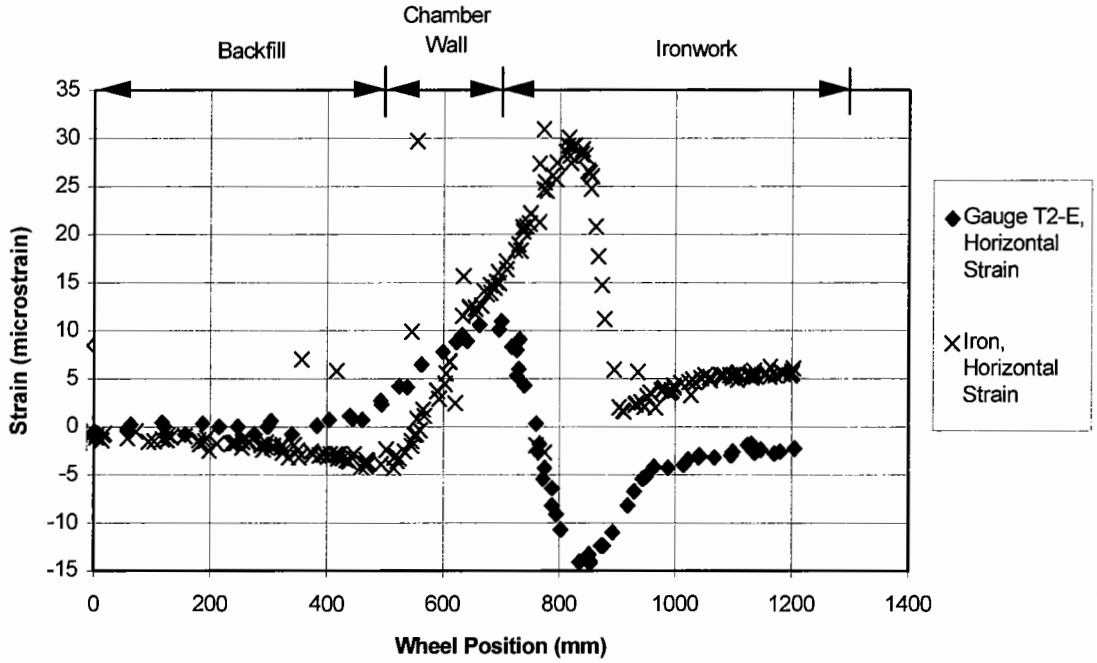

Figure 5.21: Horizontal strain measured by gauge T2-E and at the top of the ironwork frame in the installation with stiff foundations (No. 3) when loaded in wheel Track 3

The peak value of tensile strain in the bedding was 10 microstrain which developed when the wheel was immediately adjacent to the ironwork. This mechanism produced a larger tensile strain than the previous configuration probably due to lower flexural rigidity of the bedding layer but it is lower than the tensile strains seen under the bottom left hand corner of the ironwork. It is considered that the mechanisms

operating in this corner are more likely to cause cracking of the bedding by virtue of the larger tensile strains.

Backfill Material

Installations 1 & 2 were the first to be tested and the ironwork was bedded before placing the bituminous layer in the pit. The DBM was placed in a single operation so there was a continuous aggregate structure throughout this layer. The second experiments (No. 3 & 4) involved cutting through the DBM around the outside edge of each chamber. This allowed the ironwork and bedding configuration to be changed. It is thought that an abrupt interface between the two bituminous materials may have affected the behaviour of the DBM layer. Additionally, the proprietary bitumen emulsion product had a different stiffness to the DBM which may have also affected the behaviour of this layer.

Readings were taken from the instruments at the bottom of the bituminous layer when the wheel was tracked along the centreline of each installation. The measurements recorded in the installation with the soft foundations are shown in Figure 5.22. These are the same instruments that provided the data illustrated in Figure 5.10.

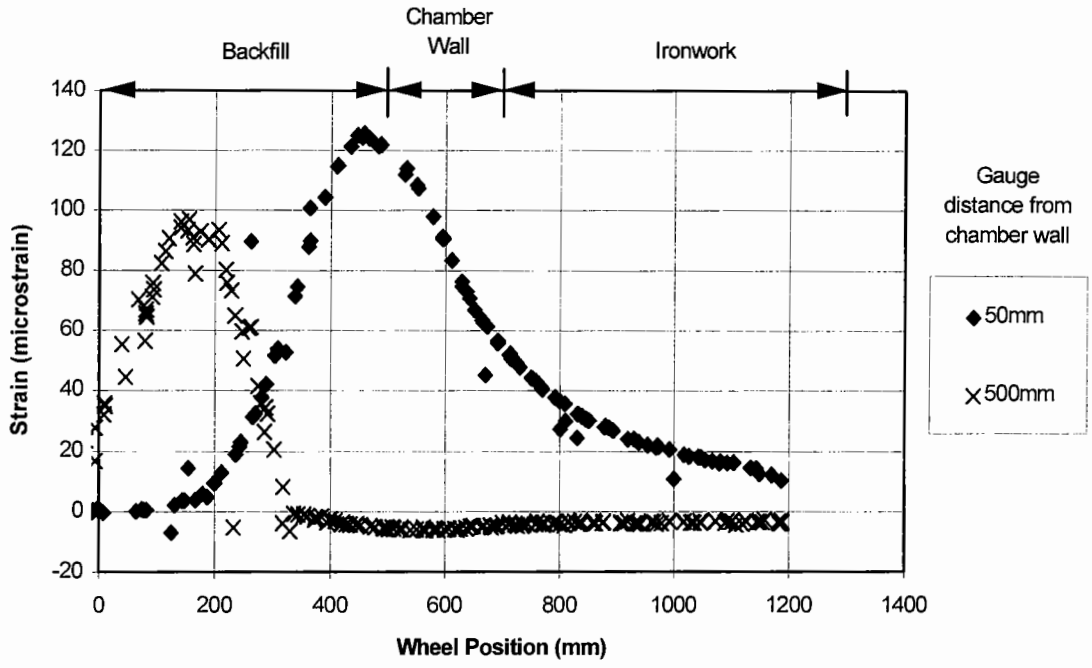

Figure 5.22: Horizontal strains measured by instruments positioned 25mm from the bottom of the DBM layer in the installation with soft foundations (No. 4)

The results from the previous bedding configurations illustrated that the strain close to the outside of the chamber wall was significantly larger than the values 500mm away. However, the results from this configuration showed a reduction in the strain measured close to the manhole. This had reduced from 160 to 127 microstrain for the installation with soft foundations. The air temperature measured at laboratory floor level was found to be 19°C during this experiment. The temperature during the previous experiments was 21°C which may account for the difference in peak magnitudes. However, the instruments were located 215mm beneath the surface so it is considered that the difference is not entirely attributable to a temperature change. It was considered that the large difference in strains previously measured was due to lack of rotational restraint through poor bond with the ironwork and a difference in the effective in-situ stiffness between the manhole and the surrounding backfill. The effect of cutting through the bituminous layer created a discontinuity in the aggregate structure. This lack of continuity between the DBM and reinstated material may have allowed the manhole to displace independently of the backfill and reduce the DBM strain. This is illustrated in Figure 5.23.

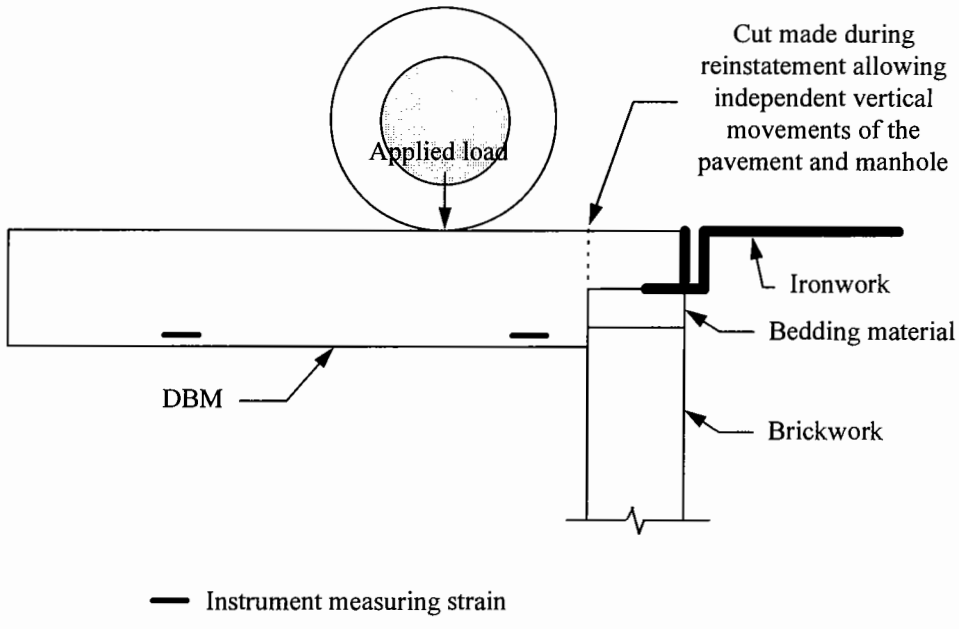

Figure 5.23: Effect of a cut in the DBM layer

Surface deflections of the pit were measured relative to the surrounding laboratory floor at the positions illustrated in Figure 5.24. Additional experiments were carried

out to study the movement of the laboratory floor immediately surrounding the pit. It was found that there was no vertical deflection of this region so the measurements can be quoted with reference to a stable datum. LVDT's were positioned at various locations on the surface and aligned to measure vertical movements in a series of tests. An additional experiment was carried out to measure horizontal movement of the ironwork frame at the location shown in Figure 5.24. All of the measurements were recorded at a distance of 50mm from the edge of the tyre, which was positioned in wheel Track 3.

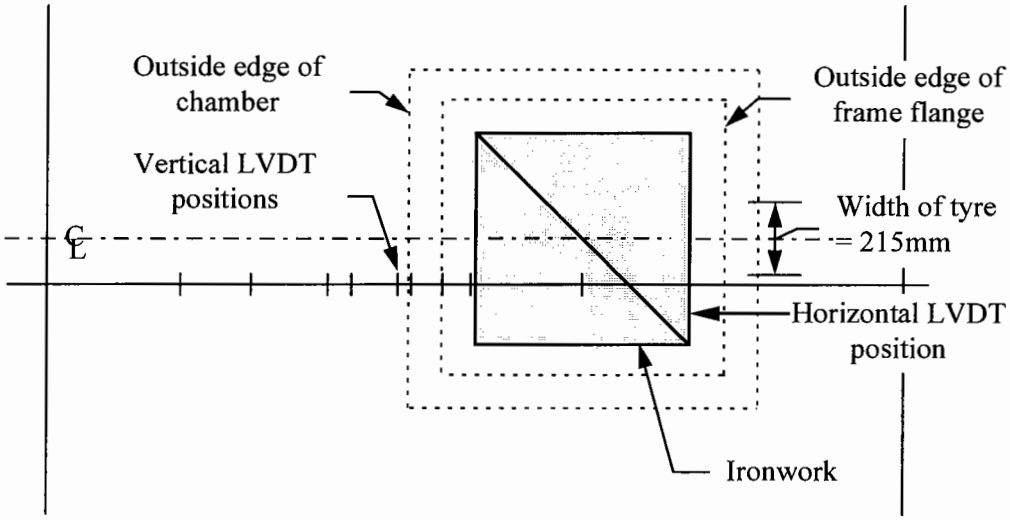

Figure 5.24: Plan view illustrating the LVDT positions used to measure vertical and horizontal displacements on each installation

It was found that the greatest vertical measurements occurred when the wheel was immediately adjacent to an instrument. The peak values have been plotted against their position on the surface to produce a deflection profile across the width of the pit. The results from the installation with soft foundations are shown in Figure 5.25.

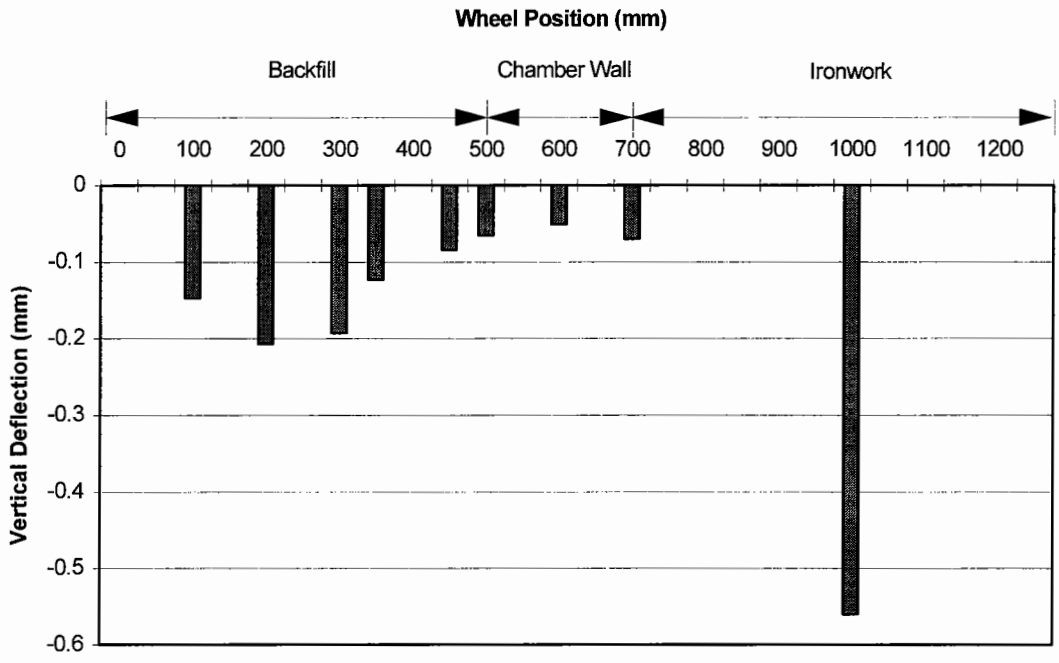

Figure 5.25: Vertical deflection profile measured on the installation with soft foundations (No. 4) when loaded in wheel Track 3

The results illustrate that the largest vertical deflection occurred when the wheel was at the centre of the ironwork cover. It can also be seen that there is a difference between the vertical deflection recorded on the backfill and above the chamber wall. These results illustrate the same effect as seen in the field; the effective in-situ stiffness is greatest above the chamber wall. This provides confidence in the simulative properties of the laboratory test facility. A similar trend was recorded on the installation with stiff foundations but the vertical deflections were approximately 25% smaller. It would appear that the greatest difference in the effective in-situ stiffness is apparent on the installation with soft foundations. The difference in overall stiffness between the manhole and surrounding backfill combined with the lack of rotational restraint of the DBM would account for the larger strains measured in the bottom of this layer close to the manhole.

The LVDT placed on the top edge of the ironwork web on the installation with soft foundations recorded a heave of the surface as the wheel approached the chamber. This may be related to the vertical tensile strain measured by gauge T2-A. A surface

heave was also recorded by the LVDT located above the centre of the chamber after the wheel had moved onto the ironwork. This was most evident on the installation without mortar above the flange. An illustration of these displacements is shown in Figure 5.26. Horizontal movements of the ironwork frame web at the location shown in Figure 5.24 were also recorded on both installations. The results are shown in Figure 5.27.

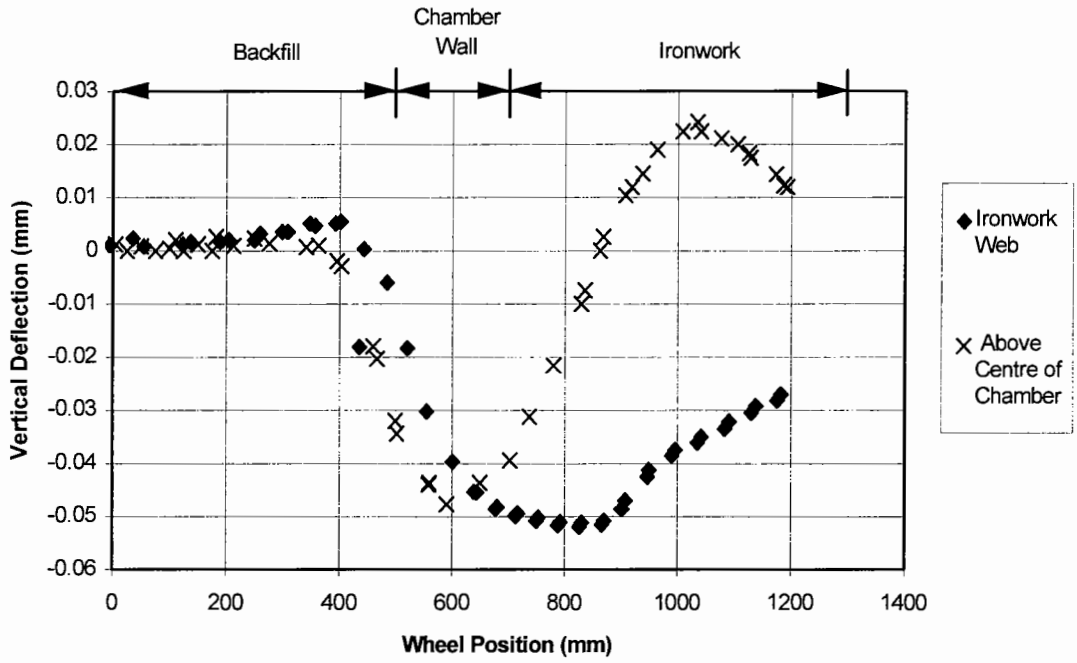

Figure 5.26: Vertical deflections recorded on top of the ironwork web and above the centre of the chamber on installation with stiff foundations (No. 3)

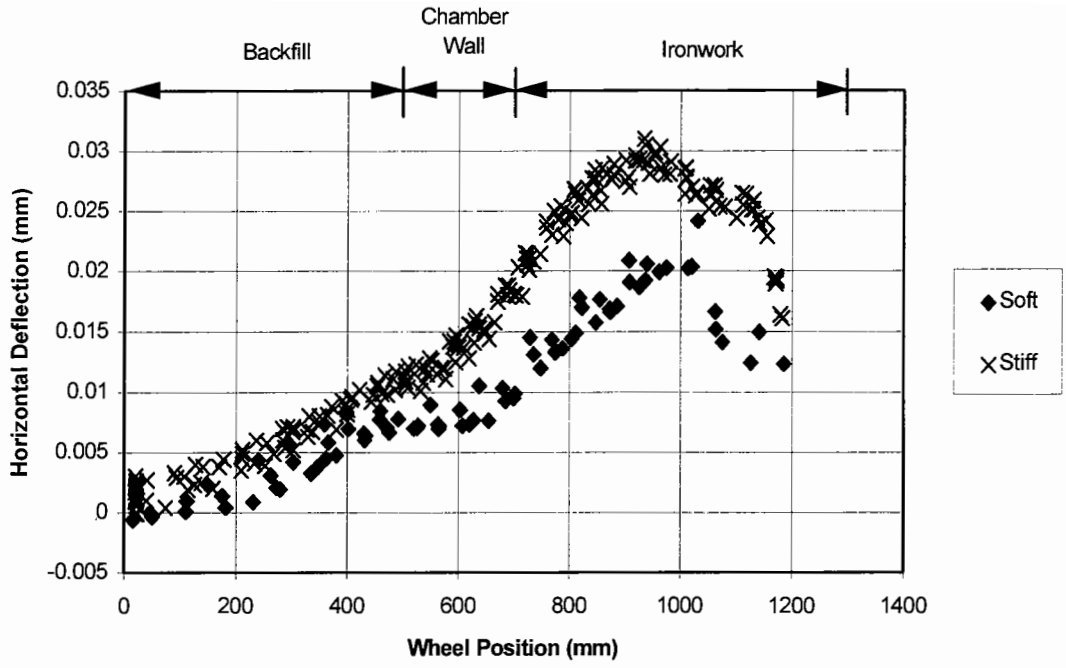

(Positive values denote movement from right to left in Figure 5.24)

Figure 5.27: Horizontal deflections of the ironwork frame web recorded on both installations when loaded in wheel Track 3

Both installations demonstrated that the frame web moved closer to the centre of the manhole as the wheel moved onto the ironwork cover. This was most noticeable in the installation without mortar above the flange. Additionally, this reinstatement yielded the largest surface heave above the centre of the chamber which is directly above the outside of the frame flange. This may be due to the frame twisting at its corners when load is applied to the cover. Such motion would be restrained when the frame flange is encapsulated within the bedding as the results imply. This would account for the vertical tensile strain measurement recorded by gauge T2-B as previously considered. An uplift of the frame flange in an installation without mortar above the flange may cause a large shear strain to develop in the bituminous material. This may result in the development of vertical cracks parallel to the frame web which has been seen in the field.

5.3.2 Repeated Load Test Results

The rolling wheel tests indicated that the bottom left hand corner was again the most sensitive loading position on both configurations. A loading platen designed to apply loads at 25° to the vertical was positioned over this corner on each installation. A vertical load varying between 0 and 35kN was applied for 2000 cycles with the direction of the load acting towards the centre of the chamber. Readings were taken from all the instruments and compared to values recorded when the installation was loaded with the vertical loading platen at the same magnitude and at this location. It was found that there was a negligible difference in the readings between the experiments, including the output from gauge T2-F located in a hole in the frame flange close to this corner (Figure 5.14). This instrument recorded a tensile strain of 11 microstrain in both experiments so it is considered that the angle of the applied load does not significantly affect the strain distribution and magnitude. The vertical platen was used to apply a 35kN load at a rate of 5 Hz for 1,000,000 cycles and measurements were recorded every 100,000 cycles. The magnitudes of strain did not change throughout the duration of each test but some measurements were considerably greater than those measured during the rolling wheel experiments.

An inspection of the bedding material was made on completion of the tests. It was found that two vertical cracks had developed, both approximately 150mm away from the corner where the load was concentrated. This is illustrated in Figure 5.28. The cracking of the bedding would have altered the load distribution so the measurements of strain in this layer would be different compared to an uncracked layer. It is considered that these cracks developed at the start of the repeated load test before the initial readings were taken as there were disproportional differences in the strain measurements recorded in the rolling wheel test and at the start of the repeated load test. The peak magnitude of the horizontal tensile strain was 53 microstrain in the installation with stiff foundations. It was considered that this installation would require fewer load applications than the previous configuration to cause cracking. A similar crack pattern occurred in the previous bedding configurations, and similar patterns have been seen in the field.

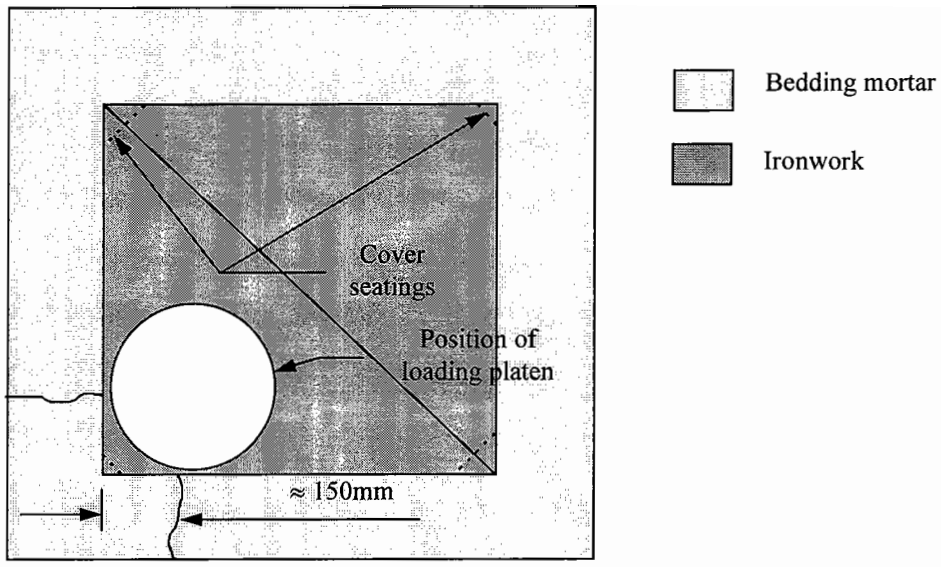

Figure 5.28: Plan view of the crack pattern after repeated load test

5.4 Test 3: 25mm thick Bedding Layer using Mortar B (Installations 5 & 6, Table 4.4)

The previous ironwork and bedding configurations have illustrated that tensile strains develop in the bedding layer. The largest tensile strains were measured in the horizontal plane underneath the cover seating in the frame with the smallest bearing area. These were measured when the wheel was positioned on the cover directly above this corner. The evidence suggests that tension develops due to a combination of the Poisson effect and bending of this layer as the peak tensile strain measurement was inversely proportional to the overall bedding thickness and hence the flexural rigidity of bedding layer.

All of the installations exhibited vertical cracks in the bedding layer after a repeated load test. These may have resulted due to flexure or shrinkage so it would appear that bedding material A has insufficient tensile strength. Both installations were replaced using mortar B to form the bedding layer. This material contains fibre glass strands and has been shown to develop a greater tensile strength than mortar A. The same configurations used in Test 2 were used but mortar was placed above the flange on the installation with the stiff foundations instead. The static modulus of mortar B (18GPa) had been found to be marginally smaller than for mortar A (21GPa) so larger strain measurements were expected from these experiments. Embedment strain

gauges were installed in each bedding layer. The arrangement was the same for both installations and those discussed below are illustrated in a plan view in Figure 5.29. The reinstatements were backfilled with 30/14 HRA. This material was compacted with a vibrating plate.

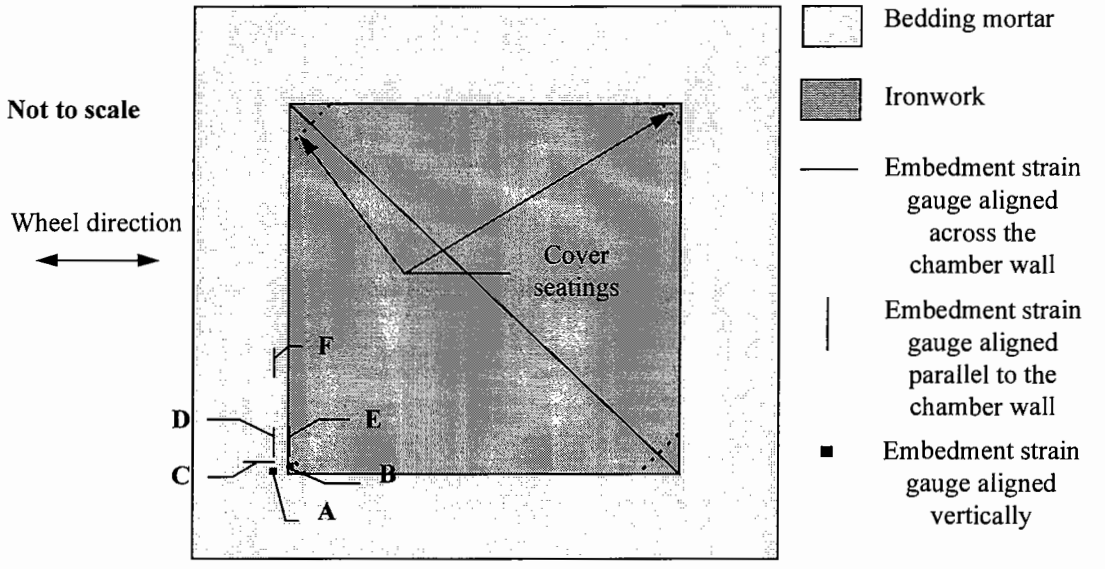

These instrument labels will be prefixed by T3 to denote Test 3.

Figure 5.29: Plan view of the embedment strain gauge layout for installations 5 & 6

It was noticed that cracks developed in the bedding material 150mm from the loaded corner during repeated load tests on the previous configurations. This pattern of cracking was similar to that seen during the shrinkage tests described in Section 2.2.1 but embedment strain gauges were installed at this location to study the transient behaviour at this point. All of the previous installations demonstrated that the highest strains are located close to the corners. Strain gauges were attached to the exposed surface of the bedding immediately underneath the bottom left hand seating which had the smallest bearing area. The output from these instruments were compared to the embedment gauges which were set 20mm away from this surface.

5.4.1 Rolling Wheel Test Results

Bedding Material

The strains measured by gauges T3-A and T3-C in the installation with soft foundations are shown in Figure 5.30. These values were recorded when the wheel was positioned in Track 4. This figure also illustrates the strain measured by gauge

T3-B mounted on the surface of the bedding directly underneath the bottom left hand seating and aligned to measure vertical strain.

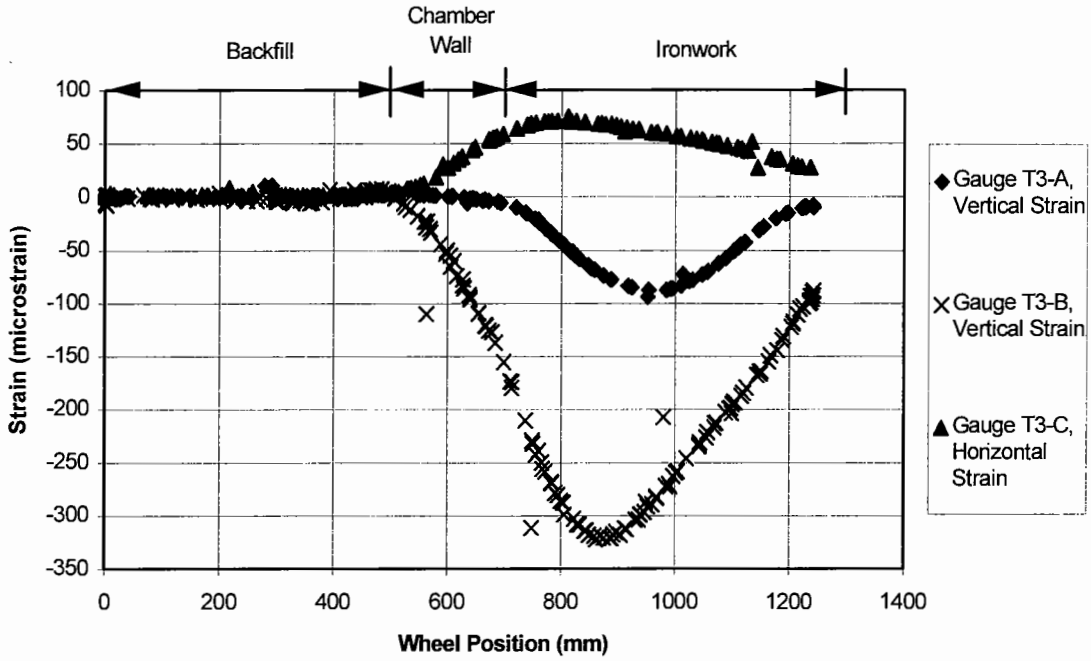

Figure 5.30: Vertical strains measured by gauges T3-A and T3-B and horizontal strain measured by gauge T3-C in the installation with soft foundations (No. 6) when loaded in wheel Track 4

Gauge T3-B measured a peak compressive strain of 323 microstrain whereas gauge T3-A only recorded a peak of 92 microstrain. This measurement indicates that there is a very high concentration of load immediately beneath the seating. However, this magnitude of compressive strain is well below the strain expected in a compressive failure. This gives further confidence that the bedding material cracks due to tensile strain or stress. The peak tensile strain measured by gauge T3-C was 65 microstrain. A similar trend was seen in the installation with stiff foundations but the tensile peak magnitude was slightly lower. This reinstatement had mortar above the flange so it is considered that the increased flexural rigidity of this layer provided a larger restraint to bending as seen previously. Vertical tensile strains thought to be induced by a difference in effective in-situ stiffness also developed in the installation with soft foundations when the wheel was located adjacent to the chamber, although the magnitudes were no greater than 8 microstrain.

Horizontal tensile strains also developed parallel to the chamber wall. The output from gauge T3-D and a strain gauge T3-E, mounted on the surface of the bedding underneath the bottom left hand corner are shown in Figure 5.31. These measurements were recorded in the installation with soft foundations when loaded in Track 4.

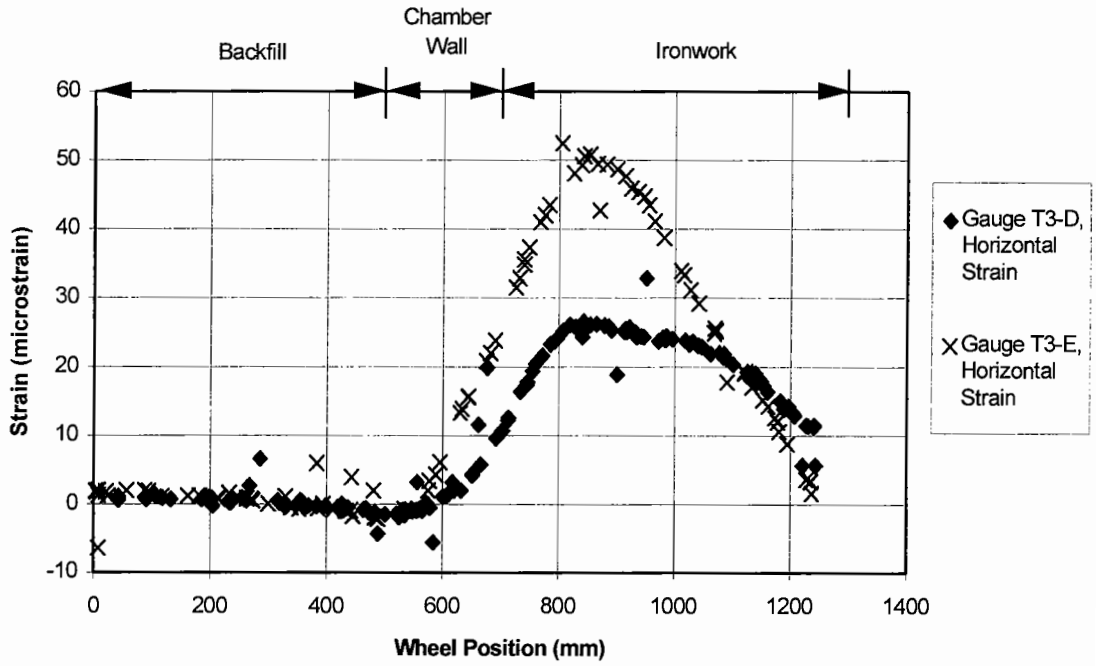

Figure 5.31: Horizontal strain measured by gauges T3-D and T3-E in the installation with soft foundations (No. 6) when loaded in wheel Track 4

Larger tensile strains were recorded on the surface of the bedding underneath the cover seating. These measurements illustrate the same trend as seen with the vertically mounted gauges; a greater resilient strain is induced on the surface of the bedding immediately underneath this cover seating. A similar trend was recorded by gauges T3-D and T3-E in the installation with stiff foundations. The peak magnitudes were lower in this reinstatement as seen in the previous configuration with mortar placed above the flange.

The gauge positioned 150mm from the corner with the smallest seating area (gauge T3-F) measured its largest tensile strain when loaded in Track 4. The peak magnitude

was 38 microstrain which was recorded in the installation with soft foundations. The measurements recorded by this gauge are shown in Figure 5.32.

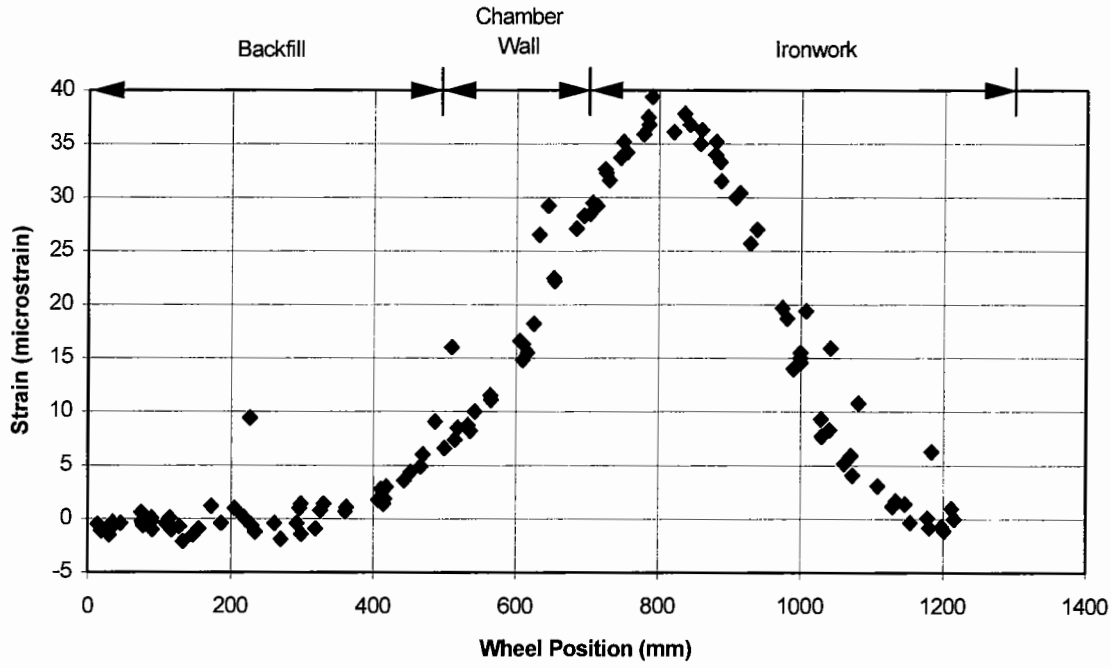

Figure 5.32: Horizontal strain measured by gauge T3-F in the installation with soft foundations (No. 6) when loaded in wheel Track 4

Although tension was measured at this point it was not as great as the region directly underneath the seating. It is considered that cracking would occur under the seating first. If cracks did develop in this area then the load may be redistributed over the bedding layer inducing higher strains at some distance from the corners. These strains may cause secondary cracking at these locations. However, it has been found that the shrinkage of the bedding material generates cracks at distances of 150mm from the corners as described in Section 2.2.1.

Backfill Material

An air temperature of 18°C was recorded at laboratory floor level during these experiments. The measurements from the instruments placed close to the bottom of the DBM layer recorded a similar pattern of results as seen in the second configuration. It appears that a cut in the bituminous material above the outside edge

of the chamber reduces the strain otherwise induced by a difference in the effective in-situ stiffness of the support to the DBM.

Vertical displacements of the surface of the pit were recorded at the same locations as the previous experiment (Figure 5.24) and a similar pattern of results emerged. Horizontal movements of the frame web were also recorded. This was most evident in the installation supported by soft foundations which did not have mortar placed above the flange.

5.4.2 Repeated Load Test Results

Repeated load tests were carried out on each installation adopting the same method as used previously. None of the strain magnitudes in either bedding layer changed during the tests. An inspection of the bedding layers at the end of each test did not reveal any cracks. This evidence appears to demonstrate that a bedding material with tensile reinforcement increases the longevity of a reinstatement.

5.5 Test 4: HDPE Spacer Bedding Layer (Installations 7 & 8, Table 4.4)

Field experiments and previous tests have indicated that the difference in the effective in-situ stiffness between a manhole and the backfill may be reduced by using HDPE spacers to form the bedding layer. This may result in a reduction of the large tensile strains in the bottom of the DBM layer. Both installations in the laboratory test facility were reinstated with this product. Two spacers were used in the bedding layer in the installation with stiff foundations whilst five spacers were used in the installation with soft foundations. This is the manufacturer's recommended maximum thickness.

A 10mm layer of proprietary mortar A was used to provide an even support to the HDPE spacers. This is also in accordance with manufacturer's recommendations as described in Section 2.2.3. Embedment strain gauges were placed in this layer to monitor its behaviour. Discussions with engineers from Northumbrian Water plc revealed that cracks had developed in this region with some of their installations. Strain gauges were not attached to the spacers as it was considered that they have

adequate strength as they did not fail when loaded through an ironwork unit. These experiments were also described in Section 2.2.3. A plan view of the positions of the embedment strain gauges where the results have been presented is shown in Figure 5.33. This was identical for both reinstatements. The cementitious bedding layer was too thin to allow embedment strain gauges to be installed vertically. All of these instruments were aligned to measure horizontal strains. Both installations were initially loaded by the rolling wheel as described in Section 4.6.

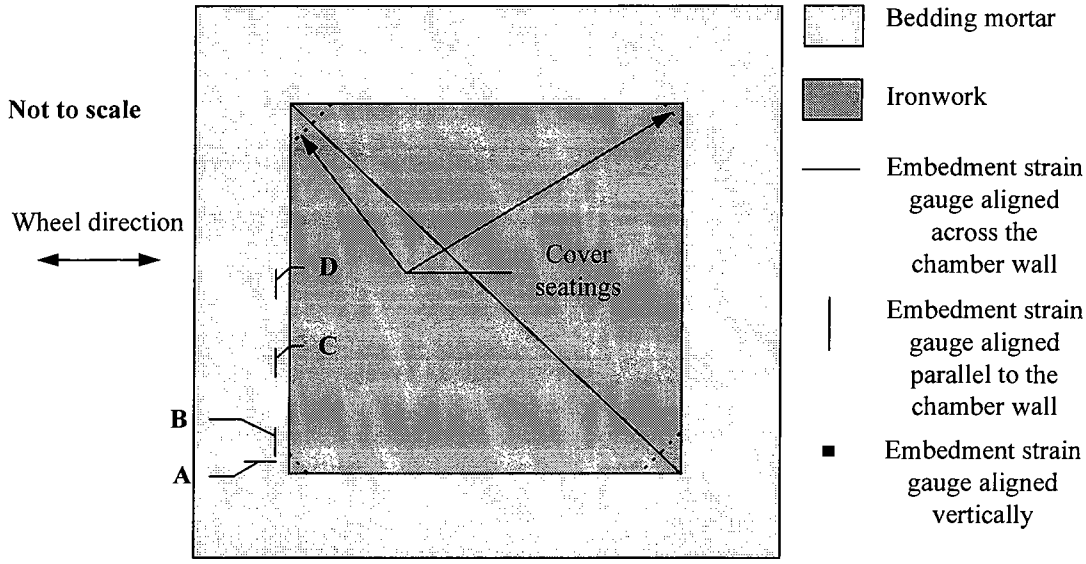

These instrument labels will be prefixed by T4 to denote Test 4.

Figure 5.33: Plan view of the embedment strain gauge layout for installations 7 & 8

5.5.1 Rolling Wheel Test Results

Bedding Material

The embedment strain gauges recorded similar values of strain in both configurations. The thickness of the HDPE spacers did not appear to affect the behaviour of the thin cementitious bedding layer. Figure 5.34 illustrates the strain measured by Gauge T4-A in the installation with soft foundations. These results were recorded when the wheel was positioned in Track 4.

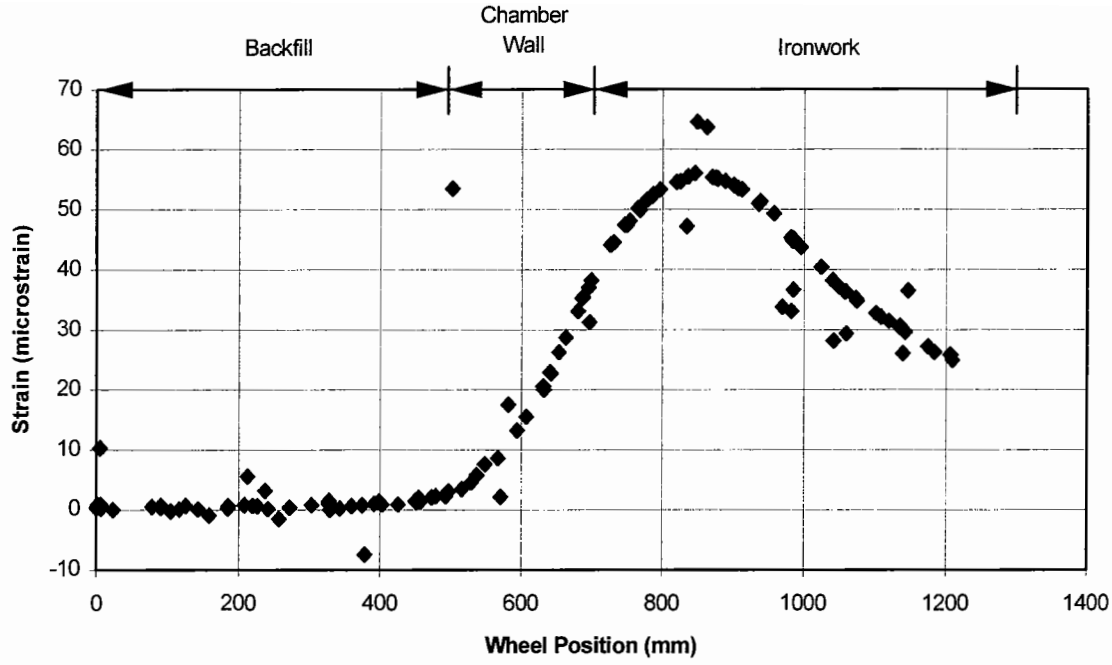

Figure 5.34: Horizontal strain measured by gauge T4-A in the installation with soft foundations (No. 8) when loaded in wheel Track 4

A large tensile strain still developed at this point in the bedding layer regardless of the HDPE spacers. The peak tensile strain measurement was 56 microstrain. A similar trend was recorded for the installation with stiff foundations which had a peak value of 51 microstrain at the same wheel location. Marginally smaller peak values were recorded when the wheel was positioned in Track 3.

Gauge T4-B in both installations also recorded its largest tensile strain when the wheel was positioned on the corner of the ironwork cover above this instrument. The results recorded in the installation with stiff foundations are shown in Figure 5.35.

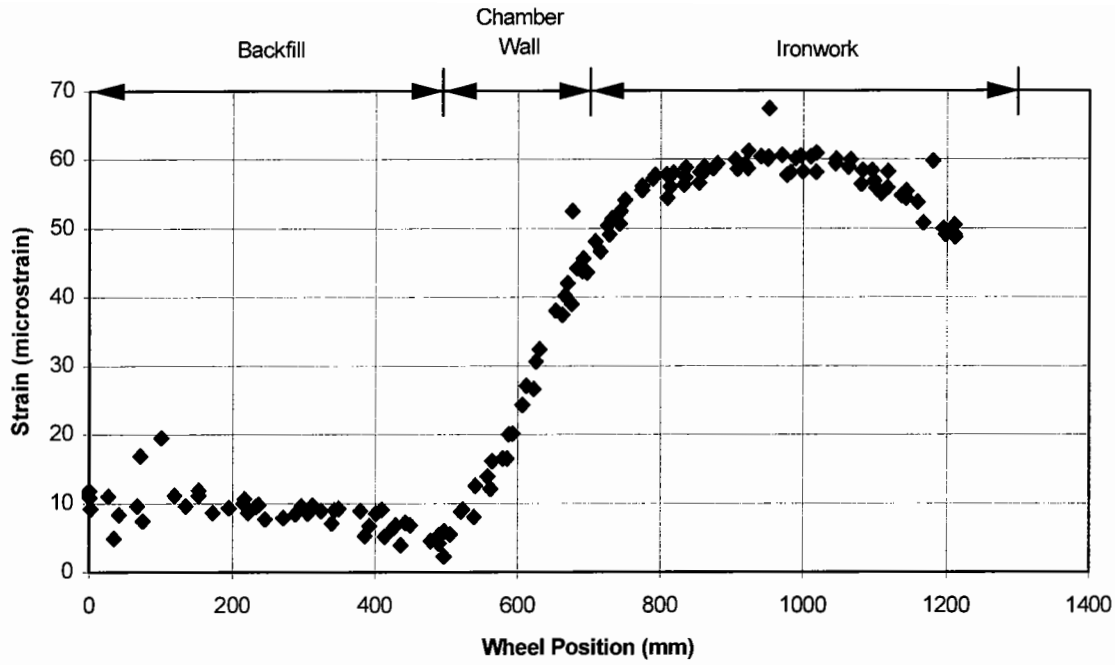

Figure 5.35: Horizontal strains measured by gauge T4-B in the installation with stiff foundations (No. 7) when loaded in wheel Track 4

The peak tensile value was 60 microstrain. The installation with soft foundations recorded a peak value of 54 microstrain. These instruments also recorded slightly smaller peak values when the wheel was positioned in Track 3. It would appear that large tensile strain measurements were not as sensitive to the position of the load in these reinstatements.

Gauge T4-C located 150mm from the corner also recorded a tensile strain as the wheel moved onto the ironwork cover in Track 4. However, the largest strain was 24 microstrain which was measured in the installation with stiff foundations.

The strain gauge attached to the top of the frame, in between two seatings also recorded a large tensile strain as the wheel moved onto the ironwork in Track 3. These strain measurements and those recorded by gauge T4-D in the installation with soft foundations are shown in Figure 5.36.

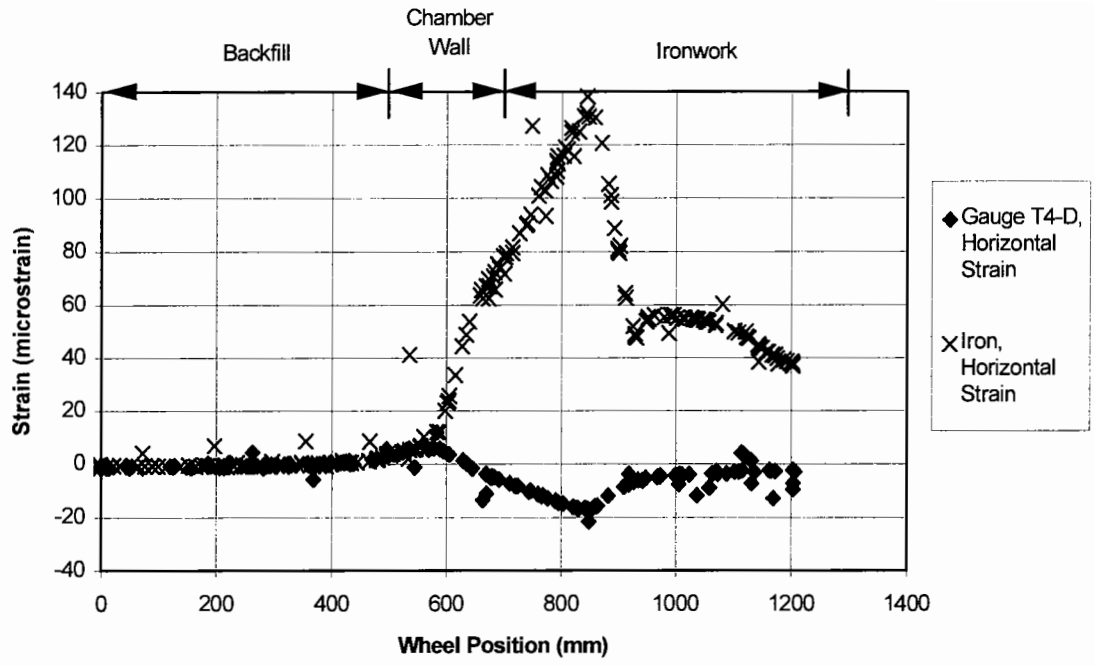

Figure 5.36: Horizontal strains measured by gauge T4-D and at the top of the ironwork frame in the installation with soft foundations (No. 8) when loaded in wheel Track 3

The largest tensile strain recorded on the frame was 130 microstrain. The equivalent gauge on the installation with stiff foundations measured 94 microstrain. Measurements from the previous configurations were between 5 and 30 microstrain. It is considered that the lower stiffness of the HDPE spacers allowed increased flexure of the ironwork frame web.

It is evident from the results that tensile strains develop in the thin layer of supporting cementitious bedding material. The magnitudes of these strains are equivalent to those measured at the same locations in the previous configurations. These results demonstrate that the likelihood of cracking in the thin layer of cementitious mortar will not be reduced by the presence of HDPE spacers in the bedding layer.

Backfill Material

The strains measured in the bottom of the DBM layer illustrated the same pattern of results as previously seen in both installations. The HDPE spacers had no effect on

the strains at these locations. Vertical and horizontal surface deflection measurements were taken at the same locations as used in previous experiments (Figure 5.24). Figure 5.37 illustrates the deflection profile recorded on the installation with stiff foundations.

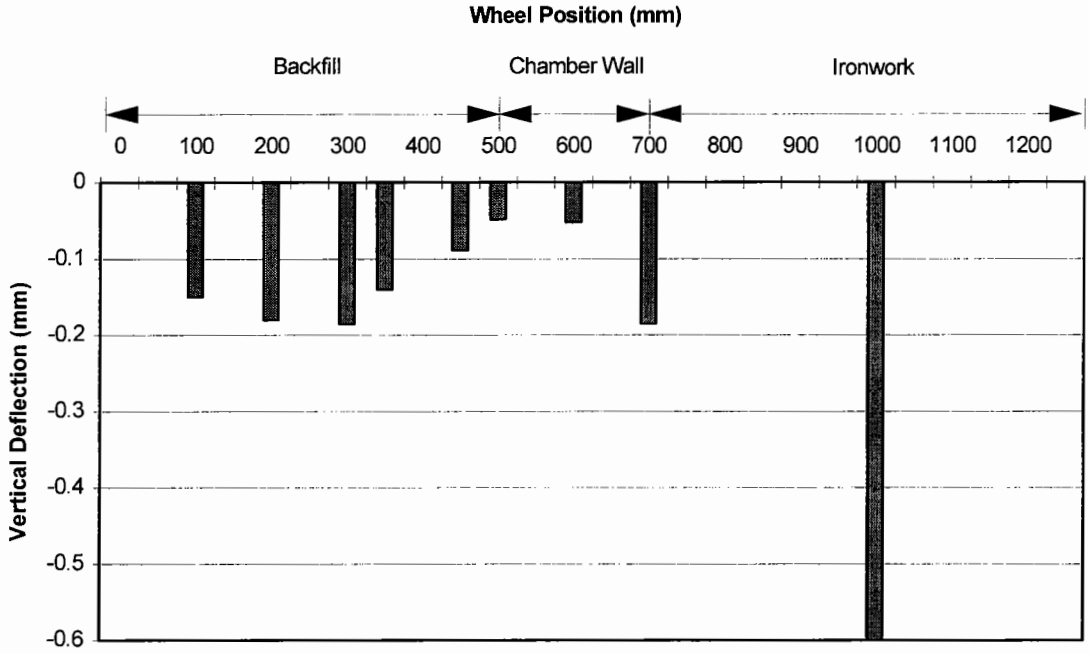

Figure 5.37: Vertical deflection profile measured on the installation with stiff foundations (No. 7) when loaded in wheel Track 3

A vertical deflection of 0.18mm was recorded when the wheel was positioned over the inside edge of the chamber. This was the same as the vertical deflection of the backfill at a distance of 300mm from the chamber so it would appear that two HDPE spacers achieved the desired effect. However, the vertical deflection was only 0.05mm when the wheel was over the outside edge of the chamber. The vertical deflection profile measured on the installation with soft foundations is shown in Figure 5.38.

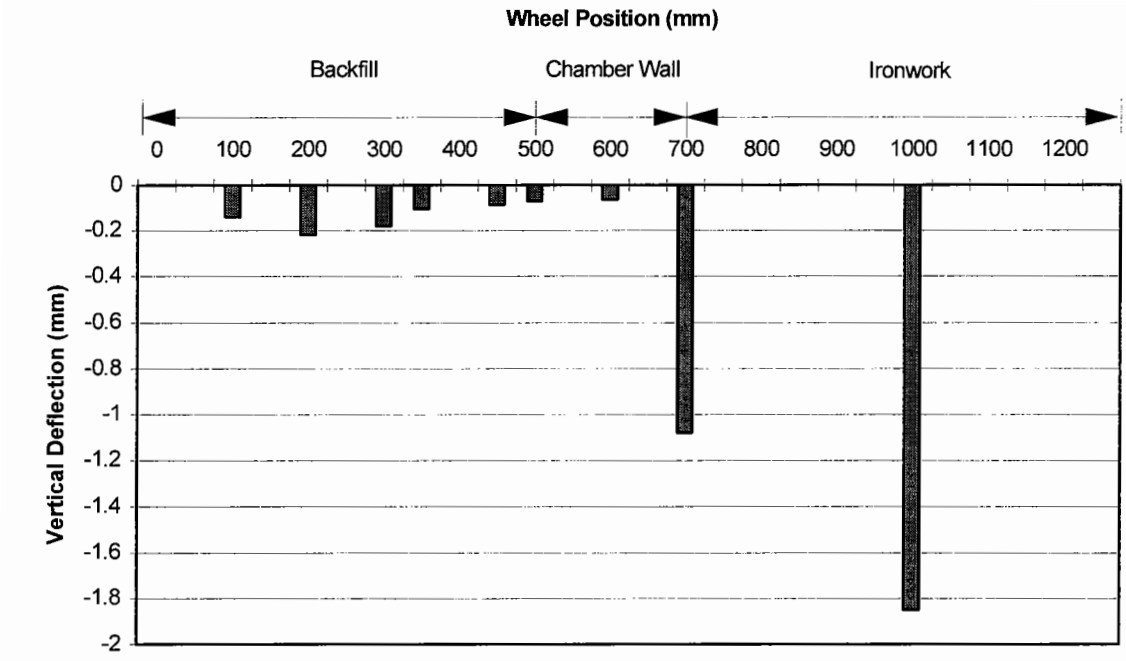

Figure 5.38: Vertical deflection profile measured on the installation with soft foundations (No. 8) when loaded in wheel Track 3

The vertical deflections recorded when the wheel was above the inside edge of the chamber and on the ironwork cover were far greater than the peak vertical deflection of the backfill. However, only a small vertical deflection was again recorded above the outside edge of the chamber wall which was similar to the values recorded in previous configurations. The proprietary HDPE spacers were only 100mm wide therefore only covered half of the chamber wall. The bituminous backfill above the outside of the chamber wall did not have the benefit of the soft support so a reduction in the difference in overall stiffness was not achieved in this region.

Inward horizontal movements of the frame web were also recorded. The measurements from the installation with soft foundations are shown in Figure 5.39.

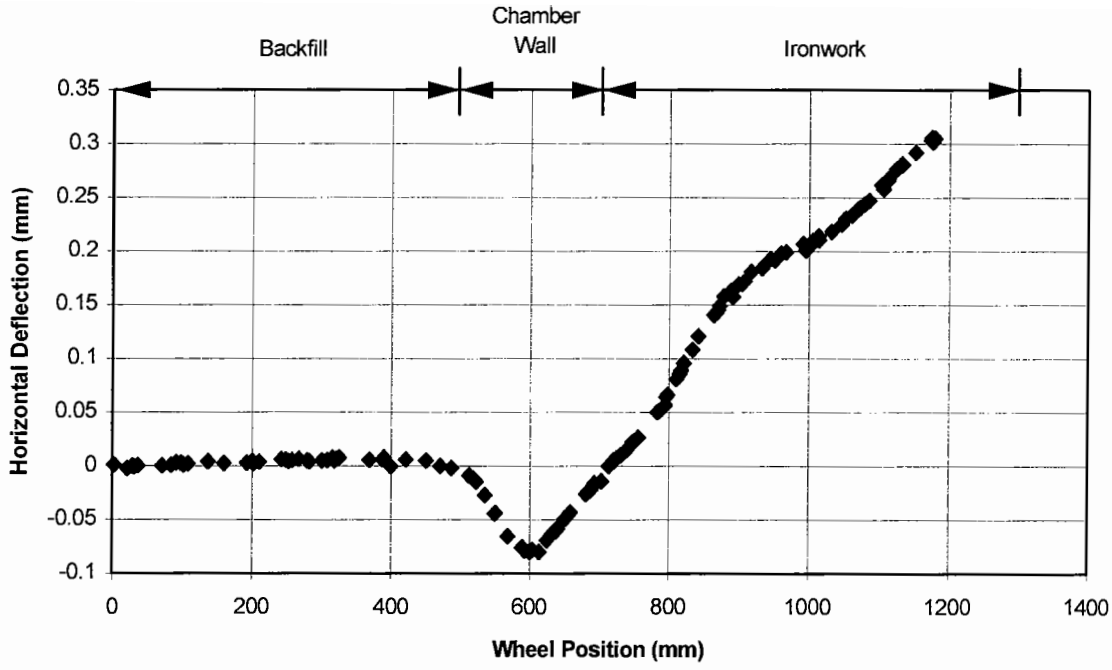

(Positive values denote movement from right to left in Figure 5.24)

Figure 5.39: Horizontal deflection of the ironwork frame web recorded on the installation with the soft foundations (No. 8) when loaded in wheel Track 3

The frame web moved towards the centre of the manhole when the wheel was positioned on the ironwork cover. The peak displacement was 0.3mm and a peak surface heave of 0.1mm was recorded above the outside of the frame flange on the reinstated bituminous material. These measurements again imply that the frame twisted when load was applied on the cover. The low stiffness of the HDPE spacers would have provided less restraint to this motion than the cementitious bedding layers which resulted in these large surface displacements.

5.5.2 Repeated Load Test Results

Each installation was loaded with the fixed loading platen for 1 million cycles. The magnitude of the load was 35kN. The strain measured by gauge T4-B in both installations decreased at 100,000 cycles to approximately 30 microstrain which was half its former value. There was also an increase in the strain measured along the top edge of the frame. An inspection of the cementitious component of the bedding layer revealed vertical cracks directly underneath the seating and at a distance of

approximately 150mm away from the loaded corner. Cracks also developed in the bituminous backfill of the installation on the soft foundations. These cracks were located parallel to the frame web, next to the loaded corner and directly above the outside edge of the frame flange. These cracks appeared on the surface after approximately 500 cycles. The HDPE spacers were inspected on removal from the laboratory test facility. It was found that there was no evidence of wear or distress.

HDPE spacers only appear to achieve the desired effect when no more than two spacers are laid. Only one HDPE spacer was used in the reinstatement in the A1 at Sandy which took longer to reveal evidence of deterioration than the mortar A installation at this site. The experimental results have shown that five spacers induced large horizontal and vertical deflections of the ironwork. This was considered to be attributable to the cracking of the bituminous backfill after a low number of loading cycles. It would appear that this number of spacers offers a far from reliable reinstatement. Additionally, neither installation significantly reduced the peak tensile strains in the cementitious bedding material. This limits the use of HDPE spacers to a narrow range of bedding thicknesses so it is not considered to be a versatile bedding material. The Test 5 results (installations 9 &10) will be discussed in Section 7.6.

5.6 Summary

All the configurations installed in the laboratory test facility demonstrated that horizontal tensile strains develop in the bedding. The magnitude of these strains relative to those in the vertical direction indicate that the Poisson effect is not the sole cause of these measurements. However, these strains were inversely proportional to the bedding thickness and hence, to the flexural rigidity of this layer. It is considered that the bedding layer bends under the action of an applied load. This was measured by instruments aligned across and parallel to the chamber walls. The largest compressive strain measured was 323 microstrain so it is thought that a compressive failure is unlikely, especially when proprietary bedding materials generally have high compressive strengths.

Surface measurements of displacement revealed that the ironwork frame appears to twist which would cause uplift of the flange. This motion would be restrained by materials placed above it. Vertically mounted embedment strain gauges were placed in the bedding material close to the outside edge of the chamber in some reinstatements. These gauges recorded tensile strain in the configurations with mortar above the flange when the wheel was located on the cover. It is likely that this strain was induced by an uplift of the frame flange. The bituminous backfill material would also provide some restraint to this motion. However, a sufficient movement would cause cracks to develop parallel to the web and above the outside edge of the flange. Such cracks appeared in the test with five HDPE spacers and have been observed in the field.

6. Finite Element Analysis

6.1 Introduction

The laboratory test facility provided data on the strain distribution and magnitudes in the bedding layer of common road ironwork installations and the surrounding backfill. These experiments revealed that tensile strains develop in the bedding material. However, these measurements were recorded at discreet positions and may not be the largest values of strain that developed within each configuration. This was investigated by finite element analysis which provided calculated values of strain at all points within the region analysed. This was a useful supplement to the laboratory experiments. Three-dimensional models of some of the configurations tested in the laboratory were created. These included the prototype test facility, the composite bedding layer containing a quarry tile and the 25mm thick bedding layer with and without bedding above the flange as described in Section 4.2 and Chapter 5. The elastic properties of mortar A were applied to the cementitious component of the bedding layer in these models. It was evident from the laboratory and field experiments that bedding layers formed with mortar A were more likely to fail than those formed with mortar B.

The calculated and measured values of strain were compared at the positions where the embedment strain gauges were installed in the laboratory experiments for verification purposes. This exercise allowed an assessment of the level of confidence that could be placed in the analyses.

Cementitious materials are most commonly used to form the bedding layer and are considered to fail at a limiting stress as discussed in Section 2.2.1. The finite element analyses also provided calculated values of stress. The peak magnitudes and directions were compared to the tensile and compressive strengths of mortar A and the characteristics of failed installations as seen in the laboratory and field. These comparisons were used to consider the most likely causes of failure. Knowledge of the peak stress magnitudes was later used to specify some of the required properties of an improved bedding material as described in Chapter 7.

The behaviour of the ironwork frame was also investigated in the analyses. This information was used to study the distribution of load on to the bedding material and to discuss the likely effects on the bituminous material. This exercise revealed shortcomings in the design of the frame. A description of the analyses followed by a presentation of the results is given below.

6.2 Analysis Description

6.2.1 Geometry

The laboratory test facility indicated that bending occurs in the bedding in planes across and parallel to the chamber wall. A two-dimensional analysis would only allow an investigation of bending in one of these planes so three-dimensional analyses were used to study this behaviour. It is considered that the two-dimensional analyses presented in Chapters 4 and 5 only provided a simplified study so the data can only be used for qualitative purposes.

The results from the laboratory test facility illustrated that the strains measured by gauge T1-A (Figures 5.1 and 5.2) rapidly diminished as the rolling wheel moved across the cover. Additionally, this instrument recorded a compressive strain no larger than 3 microstrain when the wheel was positioned in Track 2 (Figure 4.24). This trend was also recorded by instruments in this position in later reinstatements. Other results demonstrated that negligible bending of the frame and bedding occurred in between the two leading seatings. This was presented in Figures 5.9 and 5.21. This was further studied using two-dimensional finite element analysis and ELSYM5 as described in Section 5.2.1 and summarised in Table 5.1. It is therefore considered that a load applied at one corner of the ironwork has a negligible influence over an adjacent corner.

Each frame studied in the laboratory test facility included two designs of cover seating which had a different bearing area. It became apparent that a smaller bearing area resulted in a larger strains in the bedding layer. Owing to the small distribution of load away from the cover seating and the lack of bending in between seatings, it was considered that the structure could be approximately described as having four

planes of symmetry. The analysis was, therefore, simplified by only studying an eighth of the structure (half of a corner) which included the cover seating with the smallest bearing area. However, it recognised that the results would only be valid around this type of cover seating, which is considered to be the worst case. Appropriate restraints were applied along the boundaries which thus approximate to planes of symmetry. The planes of symmetry are illustrated in Figure 6.1 and the applied boundary conditions are given in Table 6.1. A total of four models were created using the same geometry as some of the configurations tested in the laboratory experiments. These are summarised in Table 6.2.

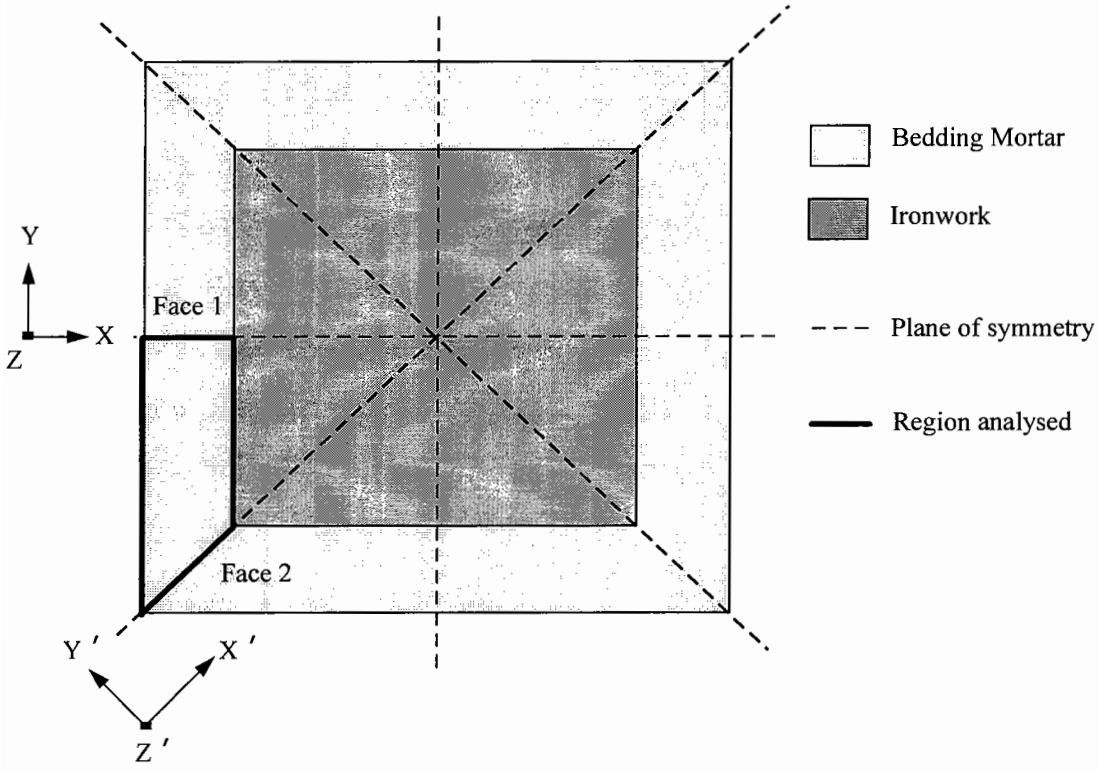

Figure 6.1: Plan view of the region studied

Table 6.1: Applied boundary restraints

Face 1	Translations	Rotations
X	Free	Fixed
Y	Fixed	Free
Z	Free	Fixed
Face 2		
X ′	Free	Fixed
Y ′	Fixed	Free
Z ′	Free	Fixed

Table 6.2: Summary of configurations modelled in analyses

Model No.	Bedding Thickness	Ironwork Type	Laboratory Experiment Reference (Table 4.4)
1	50mm	Stanton M-Way (150mm deep)	Prototype facility
2	75mm including a 20mm quarry tile	Chieftain 600 x 600 x 100mm deep	Test 1 (Both installations, Nos. 1 & 2)
3	25mm	Chieftain 600 x 600 x 150mm deep	Test 2 (Installation with stiff foundations, No. 3)
4	25mm with a further 20mm placed above the flange	Chieftain 600 x 600 x 150mm deep	Test 2 (Installation with soft foundations, No. 4)

Each bedding configuration was supported by a series of elements representing the brickwork. The field observations revealed that the brickwork layer remains largely undamaged unless it is built in a corbel as discussed in Section 2.5. Additionally, there was no evidence of damage to any of the brickwork chambers used in the laboratory experiments on completion of testing, so it was considered that an analysis of the full depth of the chamber would not provide useful information. Only the top

215mm of brickwork was simulated in each model which is equivalent to three courses of bricks. This was the same depth of brickwork as used in the two-dimensional analyses. Full vertical restraint had to be applied at the base of the brickwork to achieve equilibrium in the calculations. It was considered that this boundary condition may have influenced the calculated stresses and strains. This was observed in the two-dimensional analyses presented in Section 4.5 by a region of high compressive stress at the base of the model. However, the full restraint applied to the base of the model only affected the bottom 50mm of brickwork. A similar effect occurred in the three-dimensional analyses but should not have significantly affected the behaviour of the bedding and ironwork due to the distance between the base of the brickwork and these components of the model.

The field and laboratory evidence has shown that the ironwork cover does not suffer any damage apart from surface polishing during normal service, so this component was omitted from these models. Loads were applied directly on the cover seating instead. The ironwork frame distributes load onto the bedding so great care was taken in the creation of this component in the model. Web stiffeners, seating details and all the holes in the frame flange were included in addition to applying the appropriate thicknesses of the ironwork around the frame. A study of the behaviour of the entire bituminous layer would require the backfill materials to be incorporated into the analyses which would increase the complexity of the models and the cost of the solution, so it was also excluded from these analyses.

6.2.2 Material Behaviour

Ironwork

Experiments were carried out in the laboratory test facility to study the response of ductile iron to an applied load. Strain gauges were attached to a stiffening rib at the centre of the covers used in the first configuration. A load was gradually applied through the stationary platen located at the centre of the ironwork cover to a maximum of 40kN and then slowly reduced. The response from the strain gauges was recorded at intervals of approximately 7kN over four loading cycles. This is illustrated in Figure 6.2.

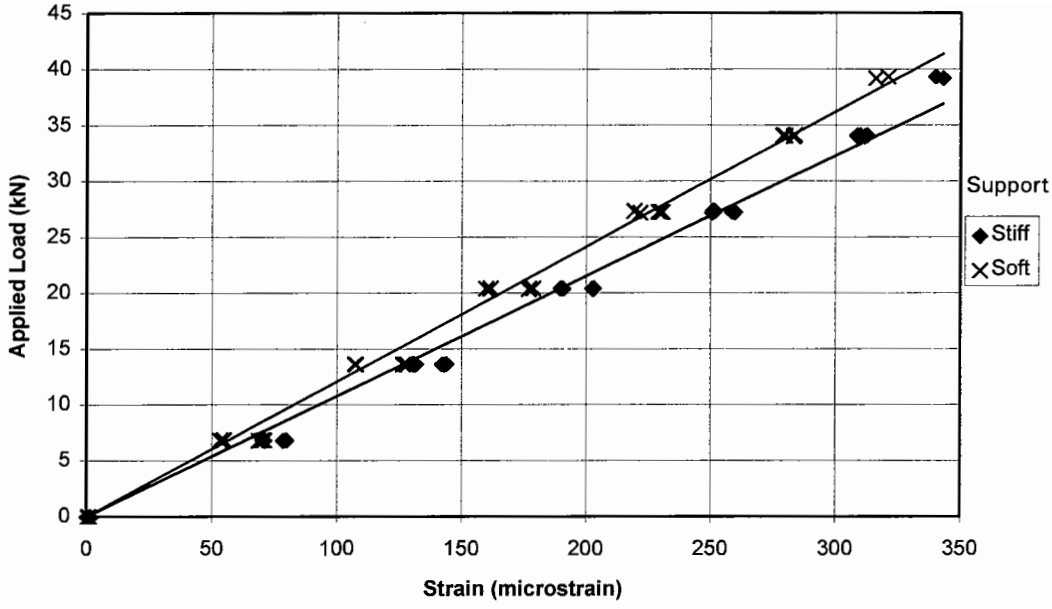

Figure 6.2: Response of the ironwork covers to an applied load

These experiments illustrated that the covers exhibited a linear elastic response. It is considered that the material properties of the ironwork could be assumed to be linear elastic without severely compromising the accuracy of the results. The elastic properties of ductile iron were supplied by Stanton plc and are given in Table 6.3.

Bedding Material

Further experiments were carried out to study the response of the bedding used in the first configuration in the laboratory test facility. A load was applied in a similar manner as described above when the stationary platen was located on the corner of the ironwork cover above embedment strain gauges T1-A and T1-D (Figure 5.1). The resulting strains measured by these instruments were recorded at intervals of approximately 7kN. The response from gauges T1-A and T1-D are shown in Figures 6.3 and 6.4 respectively.

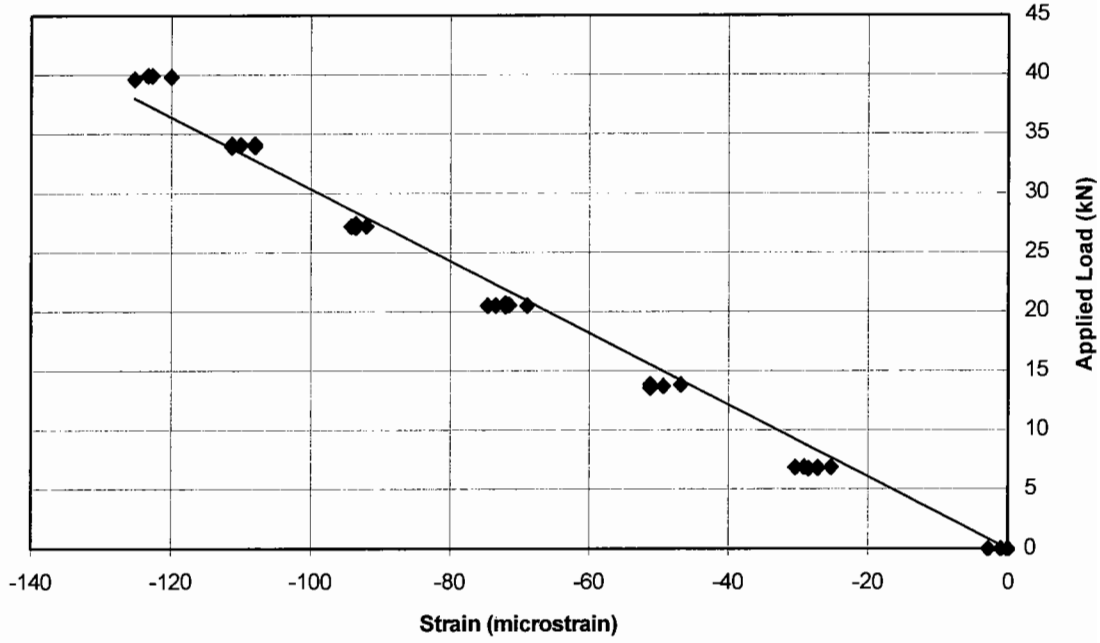

Figure 6.3: Response recorded by Gauge T1-A under an applied load

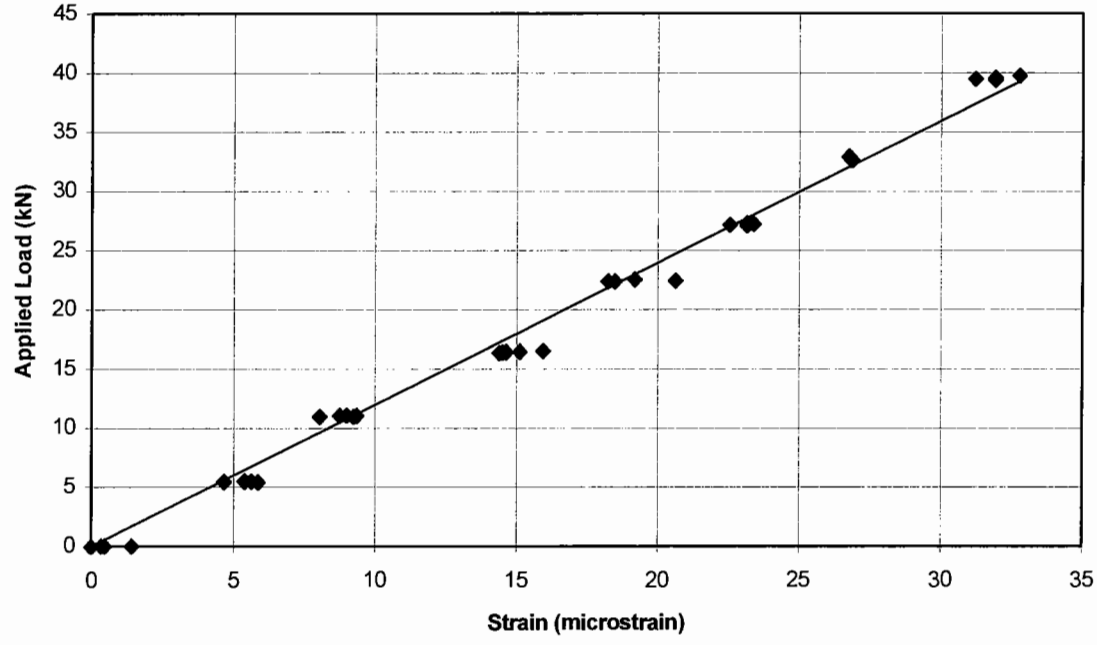

Figure 6.4: Response recorded by Gauge T1-D under an applied load

Both instruments measured a virtually linear elastic response to the applied load during these experiments. However, it is considered that cementitious materials do not possess linear characteristics, as mentioned in Chapter 2, so the term static modulus was applied instead of Young's modulus. The non-linearity in cementitious

materials is considered to be attributable to creep [7]. The test method used to determine the static modulus [15], described in Appendix A, prescribes that a sample should be subjected to several loading cycles before recording displacements. This mitigates the effects of creep so that the subsequent loading curves only exhibit a small curvature and can be approximately described as linear elastic. The various configurations installed in the laboratory test facility were subjected to at least 200 passes of the rolling wheel before measurements were recorded from the instrumentation. This includes the results illustrated in Figure 6.3 and 6.4 so it is considered that the in-situ bedding material exhibited linear behaviour to a reasonable level of confidence.

Displacement measurements were recorded by two LVDT's during the experiments to determine the direct tensile strength of bedding materials. The results from these experiments were described in Section 2.2.1 and a description of this test method is given in Appendix A. The displacement measurements were used to calculate the tensile strain in the specimen and were plotted against the applied stress. The response of a mature sample of bedding mortar A is shown in Figure 6.5.

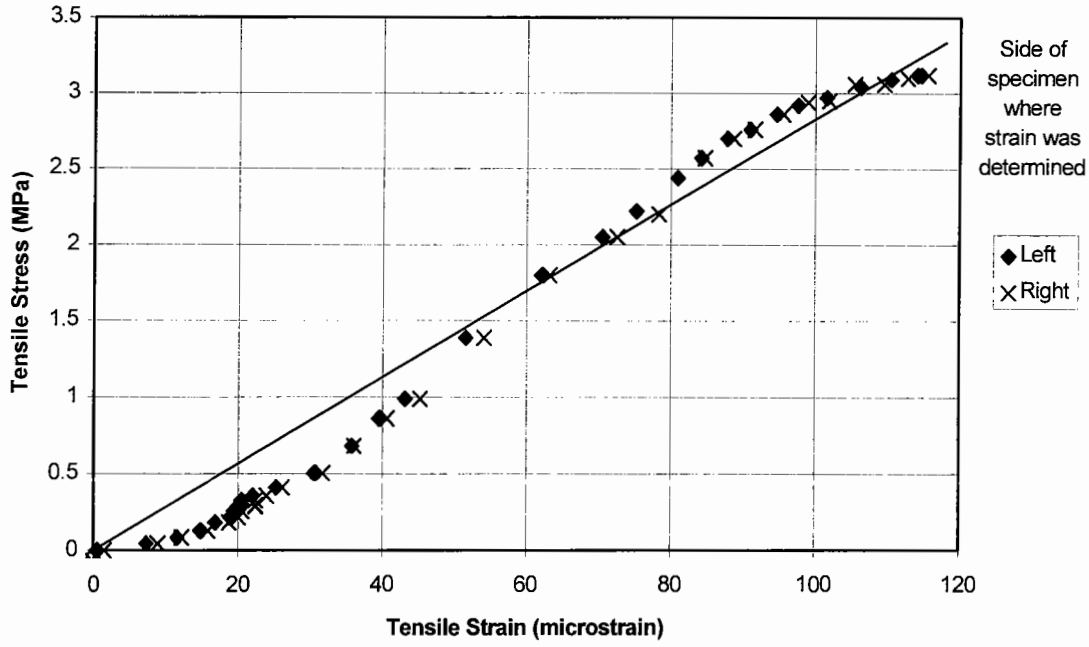

Figure 6.5: Response of a mature sample of bedding mortar A during a direct tensile test

The results indicate that mortar A can exhibit non-linear behaviour. Values of the modulus were calculated at various positions on this loading curve and it was found to vary approximately between 5 and 50GPa. However, these results were determined from a monotonic test where creep strains would have significantly influenced the displacement behaviour. This is not equivalent to the loading regime experienced by the bedding layer in the laboratory test facility.

Figure 2.7 illustrated that the static modulus and Poisson's ratio of mortar A reached mature values of 21GPa and 0.14 respectively after 7 days. This experiment was repeated during an assessment of the performance of embedment strain gauges described in Section 4.4.2 and similar values were recorded, which provides confidence in the repeatability of this result. Laboratory experiments did not commence until at least seven days after the installation of each configuration so it is considered that bedding layers in the laboratory test facility had achieved mature elastic properties.

It is thought from the results presented in Figures 6.3 and 6.4 that the mature elastic properties of bedding mortar A can be approximately described as linear elastic without severely affecting the accuracy of the results. The mature elastic properties of cementitious mortar A were adopted and these are shown in Table 6.3.

Brickwork

The supporting brickwork generally exhibits no evidence of damage as previously discussed so it was thought to be an unnecessary complication to adopt non-linear characteristics to describe the behaviour of this layer. Values of the elastic properties were extracted from literature [47] and are shown in Table 6.3.

Table 6.3: Summary of the elastic properties used in the analyses

	Modulus of Elasticity(GPa)	Poisson's ratio
Ironwork	165	0.275
Quarry Tile	14	0.22
Bedding Mortar	21	0.14
Brickwork	14	0.2

6.2.3 Loading

The ironwork cover was excluded from the analyses as previously described. Load was applied to each model through the cover seating which simulated the effect of the cover applying load to the frame. Two load cases were applied to each model and separate solutions were calculated. The first case involved applying a vertical load and the second case involved applying the load at 25° to the vertical with the direction of the loading acting away from the centre of gravity of the model. Both load cases are illustrated in Figure 6.6. The two-dimensional analyses described in Section 4.5 revealed that an angled load acting in this direction may cause a rotation of the ironwork and bedding which could have a damaging effect. Such circumstances would arise if a vehicle was breaking heavily on the ironwork cover as discussed in Section 4.5.1. The load applied by a vehicle wheel can vary due to irregularities in the surface profile of a highway as discussed in Section 3.6. The greatest applied force was estimated to be 57.5kN by using equation 3.2 so a vertical component of load of 28.75kN was applied in all load cases. This is equivalent to a 57.5kN vertical load applied across the whole seating. This is considered to be the worst loading case expected in the field.

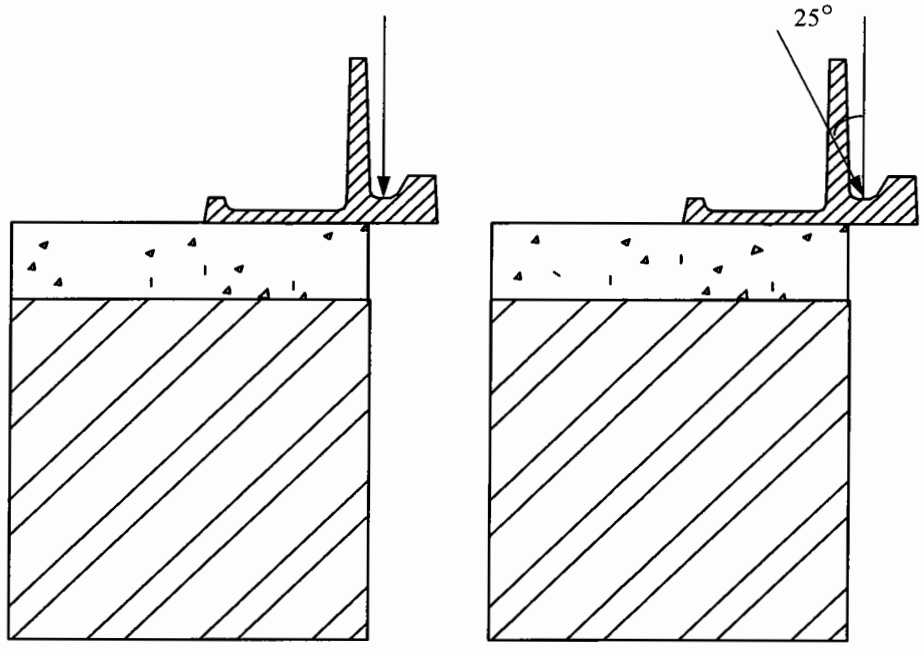

Load case 1 **Load case 2**

All angled load cases are parallel to Face 2 (Figure 6.1)

Vertical component of load = 28.75kN in all load cases

Figure 6.6: Section through manhole illustrating load cases used in the three-dimensional finite element analysis

6.2.4 Element Type

A mesh was applied to each model using three-dimensional brick shaped elements (ANSYS reference: SOLID 45) [48]. These elements had a node at each corner which allowed translations in three mutually perpendicular directions so each element had 24 degrees of freedom (DoF). The complexity of a model, hence its cost of solution, is heavily influenced by the total number of the DoF. By including rotational DoF at each node the cost of solution would have approximately doubled. It was considered that a suitable mesh density would have mitigated any errors due to this approximation.

6.2.5 Mesh Details

The laboratory experiments illustrated that the principal area of interest in the bedding is underneath the cover seatings of the ironwork frame. The laboratory results also illustrated that large compressive strains were measured on the surface of the bedding at this point which significantly reduced in magnitude at a small distance away. A fine mesh was applied to this region of the model with the sides of each element measuring between 8 and 10mm. The element size was increased towards the

extremities of the model where the resulting stresses and strains were thought to be small and the accuracy was less important. The length of a side of an element in these regions varied between 20 and 50mm.

A Stanton M-way frame was bedded on the prototype facility which contained rectangular holes in the frame flange. A relatively simple mesh was applied in this model (No. 1, Table 6.2) as the cubic elements could easily be fitted around the holes as shown in Figures 6.7 and 6.8. The bedding thickness in this model was 50mm as used in the prototype test facility.

Model 2 was created to simulate the bedding layer containing a quarry tile installed in the laboratory test facility. This configuration involved modelling a Chieftain 600 x 600 x 100mm deep frame which contained oval holes in the frame flange. Care had to be taken to avoid excessive distortion of the element shapes around these regions as illustrated in Figures 6.9 and 6.10. The resulting mesh densities are probably much finer than necessary in these regions but it was required to avoid excessive distortions which would have severely affected the results. The ratio of the height to the width of an element is known as the aspect ratio. The recommended maximum aspect ratio in the ANSYS computer program is 20:1 [48]. The elements used in these analyses offer a very poor approximation when they are stretched beyond this limit. The fine mesh located in the bedding material underneath the holes in the frame flange limited the maximum element size at the extremities of the model. Some of the elements at the bottom of the brickwork were stretched close to the limit.

Model 3 is illustrated in Figures 6.11 and 6.12. This geometry was used to study the behaviour of the installation with a Chieftain 600 x 600 x 150mm deep frame bedded on a 25mm thickness of mortar A. The results from the laboratory experiments using this configuration are described in Section 5.3. This frame also contained oval holes in the flange hence the mesh is similar to Model 2.

Further layers of elements were added above the frame flange of Model 3 to create Model 4. This geometry represented the configuration with bedding mortar above the flange and is illustrated in Figures 6.13 and 6.14.

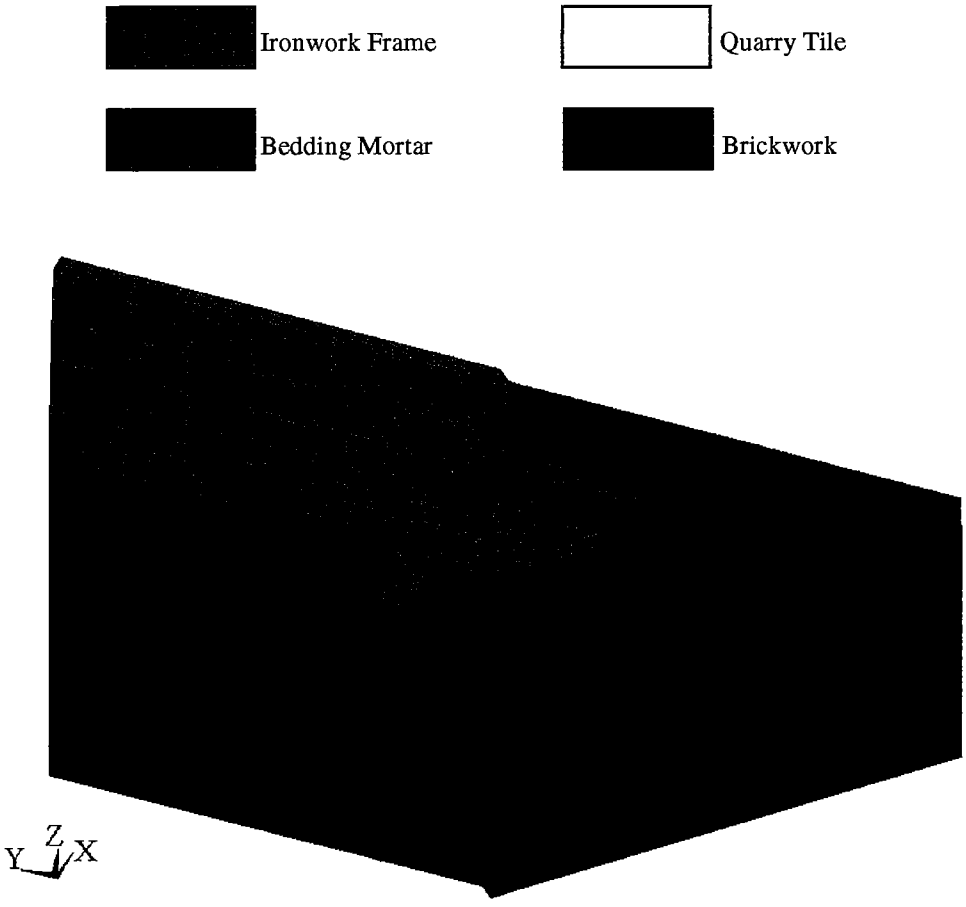

Figure 6.7: Inside view of Model 1. M-Way frame bedded on a 50mm thickness of mortar A

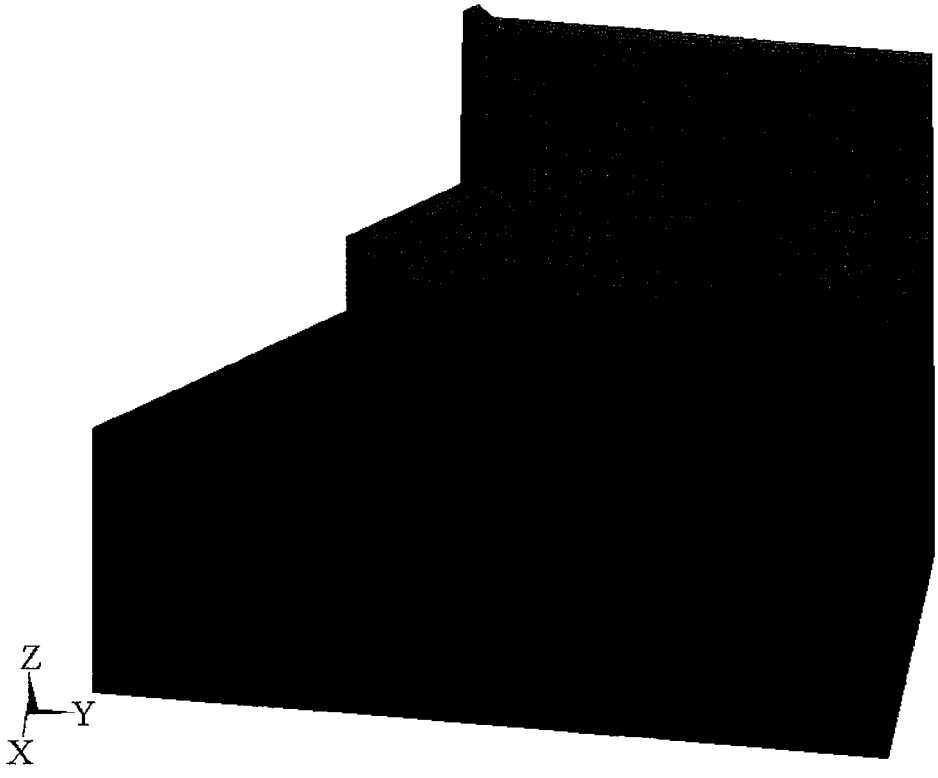

Figure 6.8: Outside view of Model 1. M-Way frame bedded on a 50mm thickness of mortar A

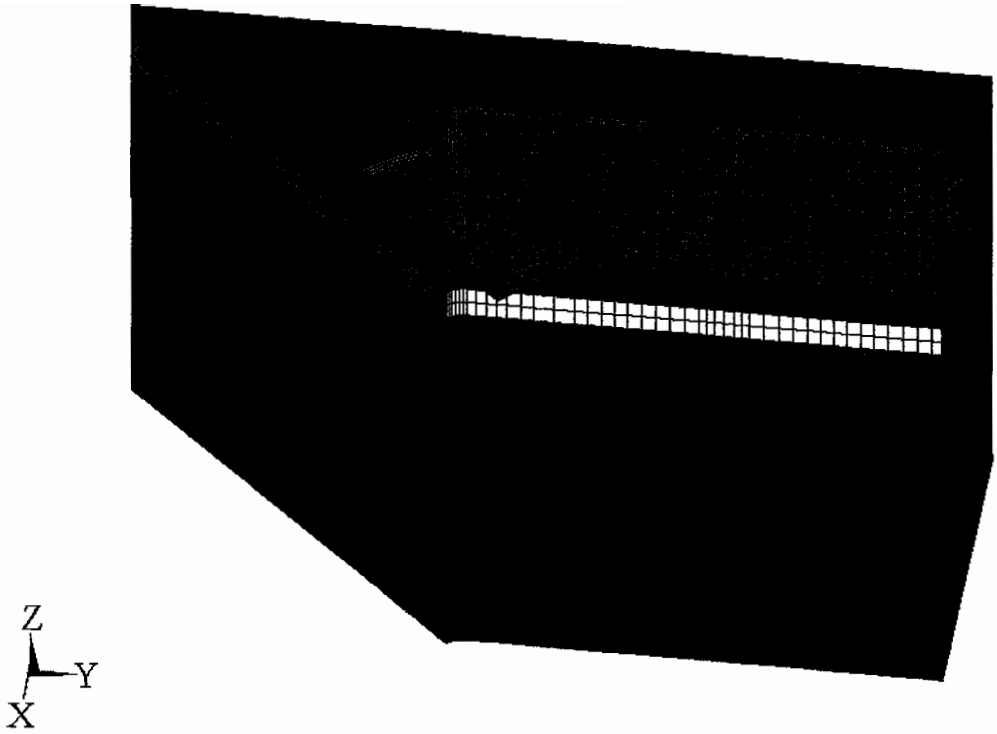

Figure 6.9: Inside view of Model 2. Chieftain 600 x 600 x 100mm deep frame bedded on a 75mm thick layer of mortar A including a 20mm thick quarry tile

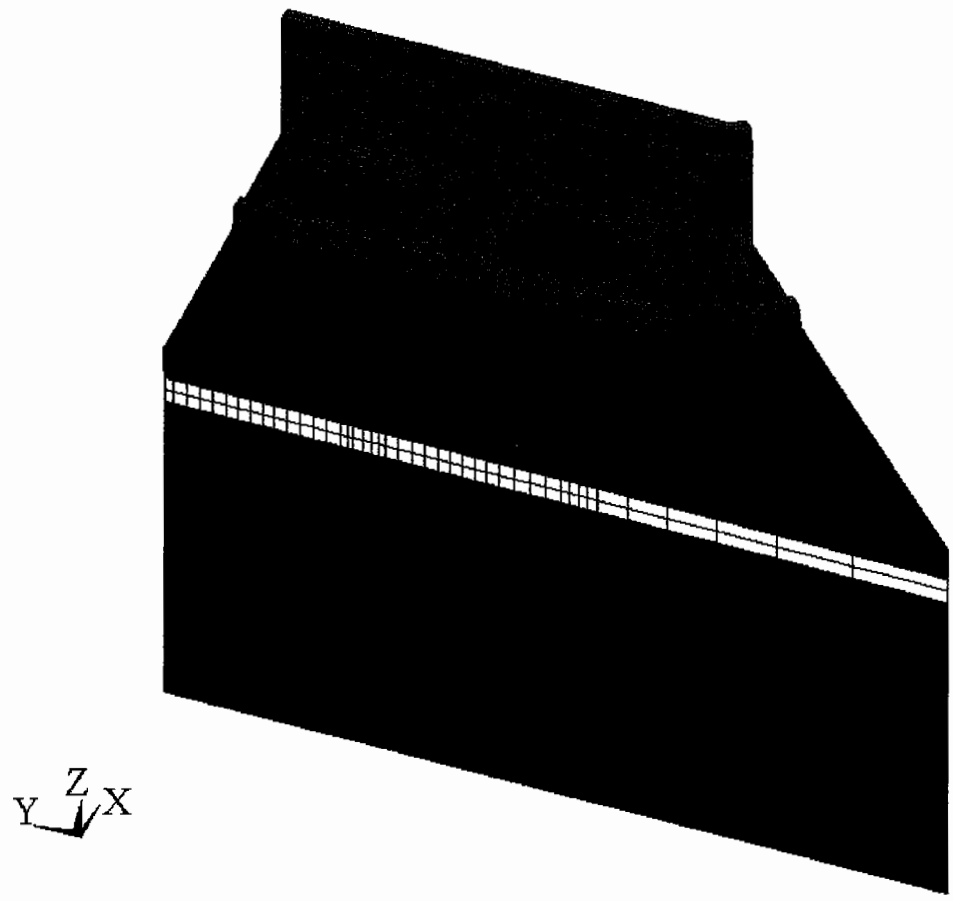

Figure 6.10: Outside view of Model 2. Chieftain 600 x 600 x 100mm deep frame bedded on a 75mm thick layer of mortar A including a 20mm thick quarry tile

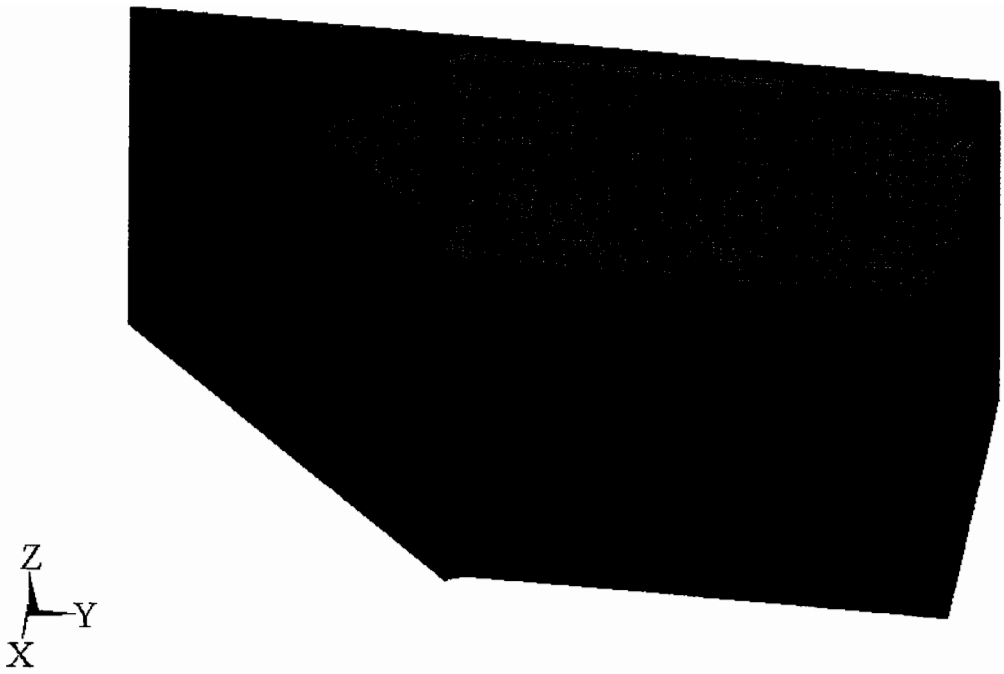

Figure 6.11: Inside view of Model 3. Chieftain 600 x 600 x 150mm deep frame bedded on a 25mm thickness of mortar A

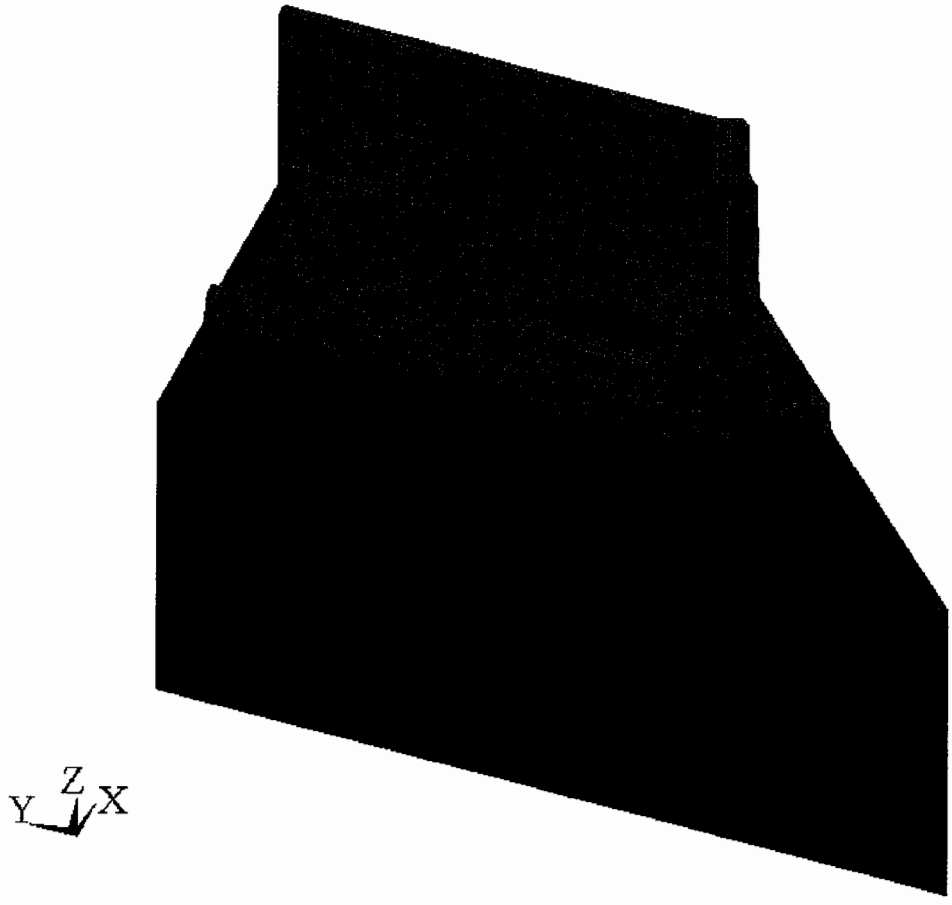

Figure 6.12: Outside view of Model 3. Chieftain 600 x 600 x 150mm deep frame bedded on a 25mm thickness of mortar A

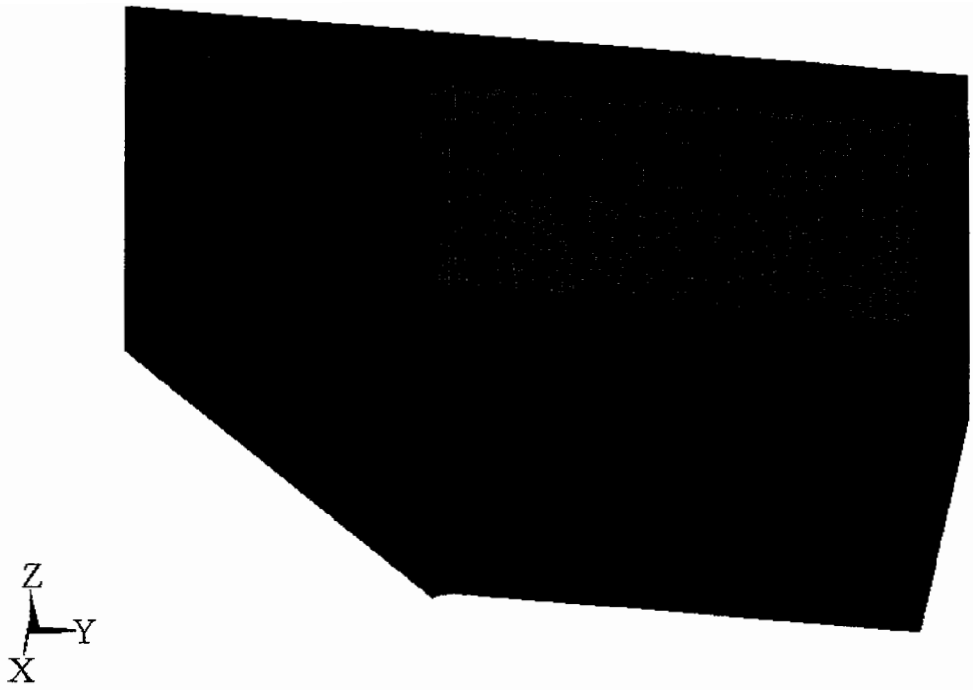

Figure 6.13: Inside view of Model 4. Chieftain 600 x 600 x 150mm deep frame bedded on a 25mm thickness of mortar A with a 20mm thickness of bedding above the flange

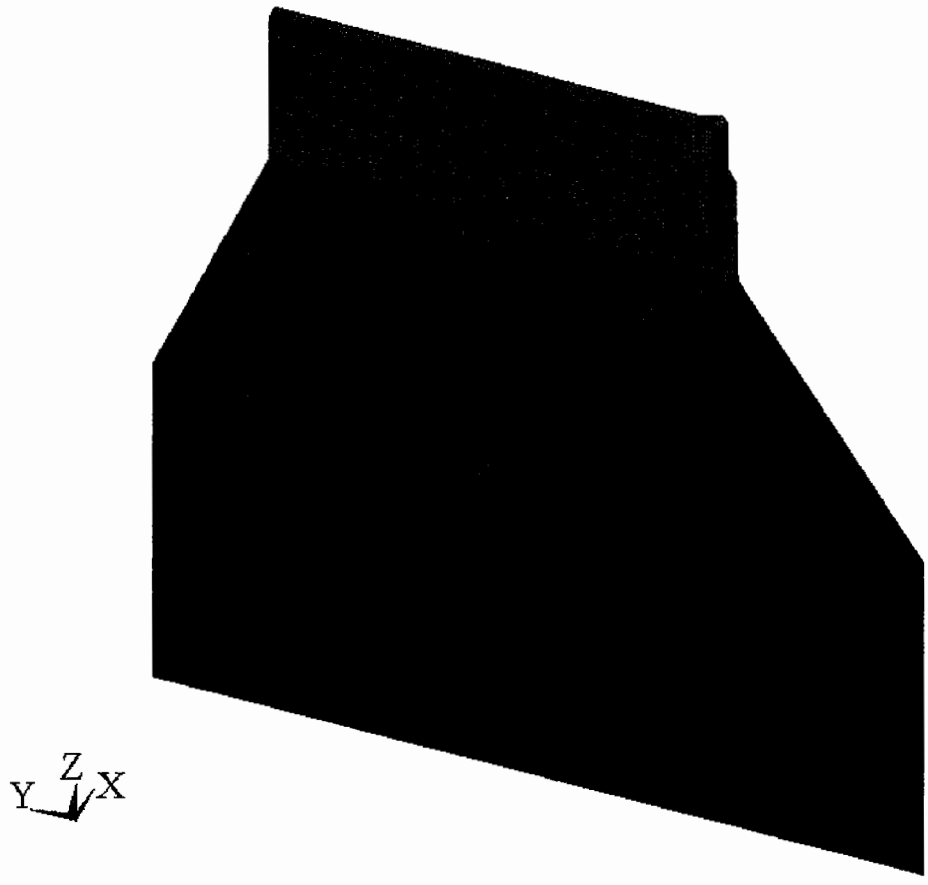

Figure 6.14: Outside view of Model 4. Chieftain 600 x 600 x 150mm deep frame bedded on a 25mm thickness of mortar A with a 20mm thickness of bedding above the flange

6.3 Description of ANSYS

All of the finite element analyses in this research were carried out using the ANSYS computer program. It was first developed in 1971 and has since been revised several times. This research has involved using versions 5.0 and 5.1 which were released in 1993 and 1994 respectively. Version 5.0 was installed on a personal computer and was used to create the prototype test facility model, whereas the other models were created using version 5.1 which was installed on a powerful mainframe computer.

ANSYS is a general purpose program suitable for structural, thermodynamic and magnetic field analyses and is widely used in industry. The program includes the features used in all modern finite element analysis packages. These include the creation of the geometry by combining simple shapes such as cubes and cylinders. This technique is referred to as solid modelling. A mesh generator is then used to fill the solid model with elements. This process is preferred to manually defining each node and element which can be a laborious task and prone to error. However, there was very little control over the ANSYS mesh generator. Only the element size and the shape could be controlled. The density of the mesh could not be easily reduced at the extremities of the model which would have been useful in the two-dimensional analyses presented in Section 4.5, although this facility has been improved in later versions of the program.

6.4 Solution

The educational versions of ANSYS were used to create these models and study the results. Unfortunately, these versions had a limited ability to solve the finite element models that can be created within the program. To overcome this problem, the completed models were sent to Strucom Ltd for solution and the results files were returned.

6.5 Verification

A verification study was carried out before using the results to study the stress distribution and magnitude in these configurations. This study allowed an assessment

of the level of confidence that could be placed on the analyses. The first stage of the verification was to ensure that equilibrium was achieved in the calculations. This was determined by comparing the total calculated reaction loads at the restraints with the applied loads. It was found that there was no difference between the two values in any of the analyses. The second stage was to compare the calculated strains with the values measured in the laboratory experiments. The YZ and XZ planes of the models were parallel and perpendicular to the chamber wall respectively as shown in Figures 6.7 to 6.14. Sections were taken through the models parallel to these planes at positions where the gauges were located. The exact position of each gauge was located on each section and the strain parallel to the gauge alignment at this point was recorded. In some sections, most notably under the cover seating, the calculated value of strain varied over the plotted gauge length. In these circumstances, the average strain over the gauge length was determined by taking the average of the calculated strain magnitudes at the ends of the plotted gauge length. Figure 6.15 illustrates this technique in a section taken through the model with mortar placed above frame flange in the plane where gauge T2-A was located.

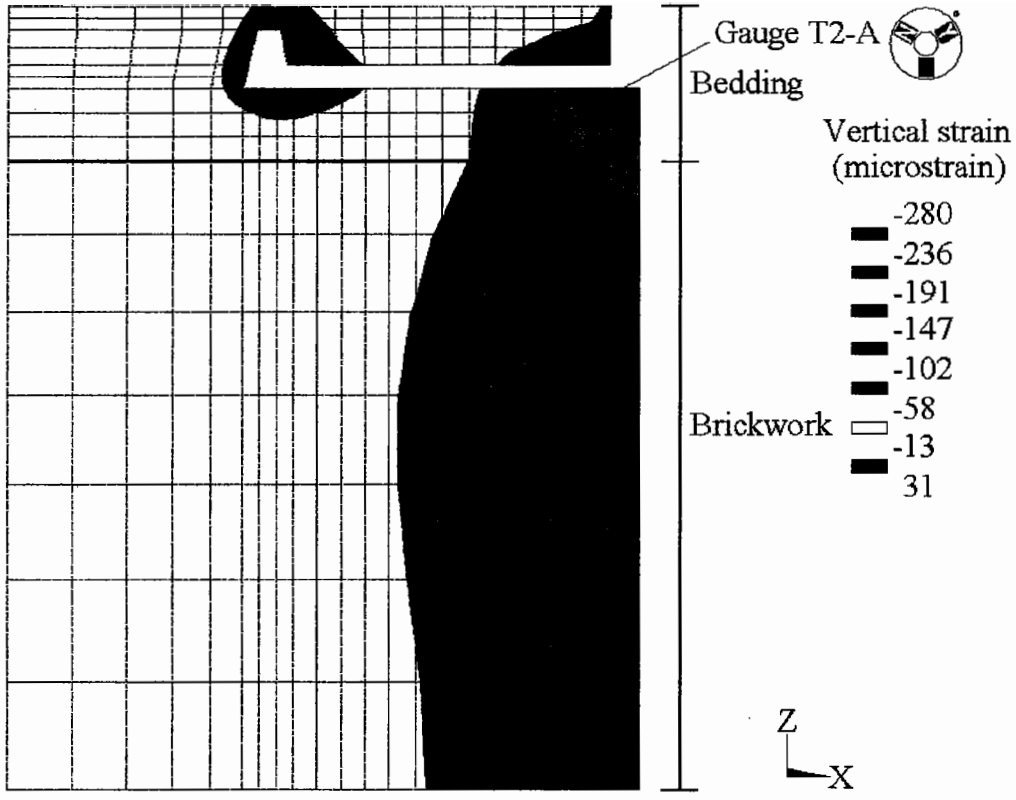

Calculated strain at the top of gauge T2-A = -191 microstrain

Calculated strain at the bottom of gauge T2-A = -147 microstrain

Average strain = -169 microstrain

Figure 6.15: Determination of average strain in a section taken through the model with mortar above the flange

This was repeated for all the gauges placed in the bedding layer in every configuration. The output from some gauges in the bedding layer was not described in Chapter 5 as they largely demonstrated the same effect as seen at other points in the bedding. However, the calculated values were recorded at these points for verification purposes. Table 6.4 provides a comparison of the measured and calculated magnitudes of strain. This data is also presented in a series of graphs illustrated in Figures 6.16 to 6.19. The measured values were determined when the wheel was positioned on the corner of the ironwork cover. The strains calculated in the linear analysis were multiplied by a factor of 0.6 so the applied load was the same between the two sets of results.

The embedment strain gauges used in the laboratory experiments would have recorded an average strain measurement over the entire length of the instrument, rather than at the ends. This would produce a slightly different value of strain compared to the method described above if a non-linear strain distribution existed over the length of the gauge. It is not entirely suitable to quote a single value of strain in the regions where a large variation in the calculated strain magnitude exists over the length of instrument. Error bars have been included on the graphs illustrated in Figures 6.16 to 6.19 to indicate the variability in these results. The extremities of the error bars were the two calculated values of strain used to determine the average.

Proprietary embedment strain gauges are available in several sizes and this research involved using the smallest gauges with overall dimensions of 25 x 5 x 3mm thick. Unfortunately, the analysis results illustrated that the calculated magnitudes of strain varied significantly over the gauge length as shown in Figure 6.15. Local measurements of strain could have been achieved by casting ordinary strain gauges with a gauge length no greater than 5mm within a block of epoxy resin. These instruments could have been installed into the bedding layer by the method described in Section 4.4.2 in the regions where large strain gradients were calculated in the analysis, such as underneath the cover seatings. It is thought this could have provided a suitable method of measuring local strains. Care would have to be taken to avoid too many instruments close together which would be likely to materially affect the readings obtained.

Nevertheless, given the assumptions and approximations in the finite element analysis such as linear material behaviour and mesh discretization, and the repeatability and interpolation issues surrounding the instrumentation discussed in Sections 4.4.2 and previously in this section, the measured and predicted results shown in Figures 6.16 to 6.19 are judged to be very close.

Table 6.4: Comparison of measured and calculated strain values

Model No.	Gauge Orientation and Location	Measured Value (microstrain)	Gauge Ref.	Calculated Value (microstrain)	Difference (microstrain)
1	Horizontal, across the chamber wall underneath cover seating	19	P-A	23	4
1	Horizontal, across the chamber wall underneath cover seating	27	P-B	23	-4
2	Vertical, underneath cover seating	-98	T1-A	-98	0
2	Vertical, in between cover seatings	-35	T1-B	-22	13
2	Horizontal, across the chamber wall and below quarry tile	5	T1-C	5	0
2	Horizontal, across the chamber wall and above quarry tile	26	T1-D	27	1
2	Horizontal, in between cover seatings	3	T1-F	2	1
2	Horizontal, parallel to the chamber wall and underneath seating	10	T1-G	24	14
2	Horizontal, parallel to the chamber wall and in between seatings	-1	T1-H	8	9
3	Vertical, underneath cover seating	-170	T2-A	-167	3
3	Horizontal, across the chamber wall underneath cover seating	53	T2-C	35	-18
3	Horizontal, parallel to the chamber wall and underneath seating	39	T2-D	27	-12
3	Horizontal, parallel to the chamber wall and in between seatings	10	T2-E	14	4
3	Vertical, underneath hole in the frame flange	-30	*	-29	1
3	Horizontal, underneath hole in the frame flange	-15	**	-14	1

Table 6.4 continued: Comparison of measured and calculated strain values

Model No.	Gauge Orientation and Location	Measured Value (microstrain)	Gauge Ref.	Calculated Value (microstrain)	Difference (microstrain)
4	Vertical, underneath cover seating	-178	T2-A	-169	9
4	Horizontal, across the chamber wall underneath cover seating	35	T2-C	29	-6
4	Horizontal, parallel to the chamber wall and underneath seating	15	T2-D	30	15
4	Horizontal, parallel to the chamber wall and in between seatings	5	T2-E	12	7
4	Vertical, underneath hole in the frame flange	-44	*	-34	10
4	Horizontal, underneath hole in the frame flange	-6	**	-6	0

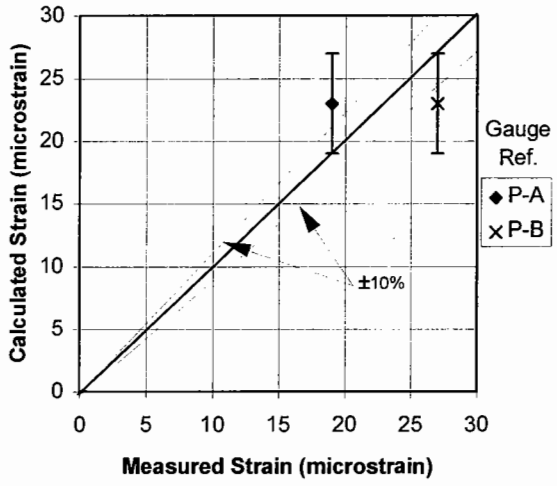

Figure 6.16: Comparison of the measured and calculated values of strain in model 1

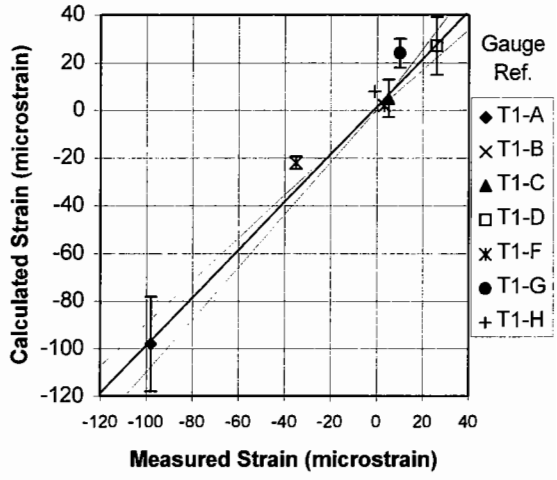

Figure 6.17: Comparison of the measured and calculated values of strain in model 2

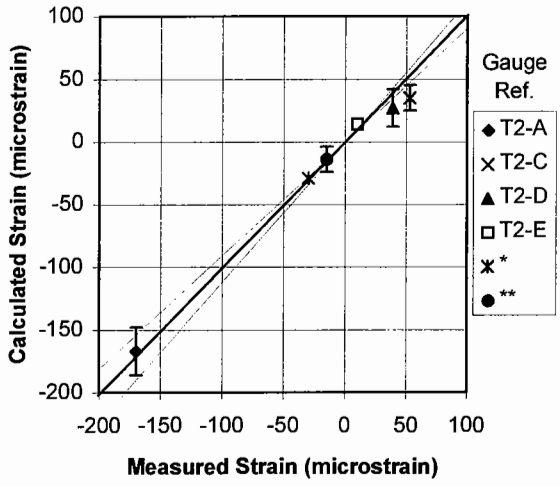

Figure 6.18: Comparison of the measured and calculated values of strain in model 3

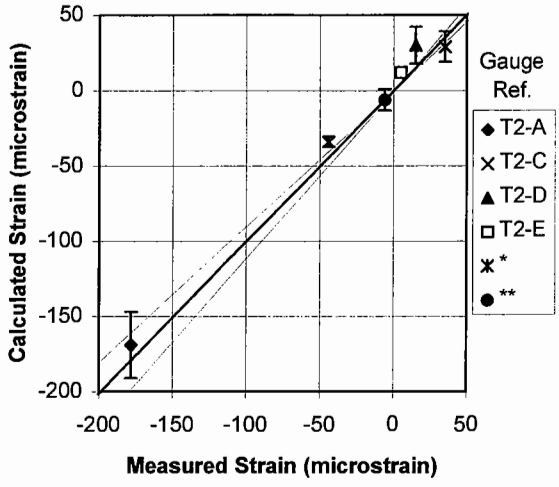

Figure 6.19: Comparison of the measured and calculated values of strain in model 4

The most notable difference was between the strain measured by gauge T2-C in model 3 and the calculated value at this point. However, a comparison with the calculated values at the positions of gauges P-A, P-B, T1-D and T2-C (model 4) illustrate that the calculated values of tensile strain across the width of the bedding are inversely proportional to the thickness of the bedding layer. This was the same trend as identified in the laboratory test facility.

It was assumed in the analyses that the bedding material was homogenous which may explain the differences between the two sets of results. It is likely that pores and voids existed in the laboratory configurations that would have induced large local strains. The same effect would have occurred around the aggregate which is likely to have influenced the measured strains. Such effects cannot be readily incorporated into finite element analyses so only approximate values of calculated strain can be quoted. A principal concern of the laboratory experiments was that the embedment strain gauges may not have been located at the positions of the greatest tensile and compressive strain which may have affected the understanding of the behaviour of road ironwork installations. However, the verification study revealed that the largest strains occurred close to the corners with the peak values developing on the surface of

the bedding directly underneath the cover seatings. Instruments were installed at these positions so it is considered that the results from the laboratory experiments provide a satisfactory description of the bedding layer behaviour.

Overall, the three-dimensional finite element analyses provided a reasonable representation of the strains measured in the laboratory experiments. A further study of the results illustrated that the strain distribution was similar to the stress distribution. Therefore, it is considered that analyses results can be used with some confidence to investigate the stress distribution in these road ironwork configurations.

The validation of the analyses could have been investigated further if sufficient resources were available. It would have been useful to initially create one of the models with a low mesh density. This would have provided an indication of where the stress concentrations and gradients were the greatest and allowed refinement of the mesh at these positions. It would have also provided an indication of the accuracy of the calculated values of stress and strain by comparing magnitudes of stress, strain and displacement at key points in the model with later analyses. This would have indicated whether or not there was any benefit generating further models using a finer mesh. Additionally, the element type could have been varied. The effect of using elements with rotational degrees of freedom could have been studied. These elements provide a better approximation of the displaced shape than elements which only allow translational degrees of freedom. However, the fine mesh density applied in these analyses was considered to mitigate this effect.

These techniques could have also been applied to a small region of the model where large variations in the stress magnitude were present. This section could have be studied in isolation and the effect of varying the mesh density and element type could have been studied. This technique is known as sub-modelling.

It was considered that three-dimensional finite element analysis was required to provide an adequate simulation of the behaviour of road ironwork installations. The laboratory test facility experiments illustrated that bending occurs in two planes which

could not have been simulated in two-dimensional analyses where a plane stress or strain assumption is required. However, the two-dimensional analyses presented in Section 4.5 provided a similar distribution of stresses to the three-dimensional analyses, but there were significant differences in the calculated values of the principal stresses. It is therefore considered that the two-dimensional analyses were only suitable as a sensitivity study.

6.6 Results

6.6.1 Behaviour of the Bedding Layer and Brickwork

The laboratory test facility revealed that tensile strain develops in two planes; parallel and across the width of the chamber wall. The combined effect of the mechanisms producing these strains may produce a larger strain acting in another plane. This could be investigated by studying the principal strains. However, cracking of cementitious material is considered to be related to the stress level [8]. A study of the maximum and minimum principal stresses would indicate the regions of the bedding that are most likely to crack and the magnitudes of the stress at these points. It is considered that an assessment of this quantity would further develop an understanding of the behaviour of road ironwork installations and indicate the greatest compressive and tensile stress magnitudes that the bedding has to withstand.

The largest stresses developed in the ironwork cover seating in all models. This was excluded from studies of the bedding and brickwork to clarify detail in these components. A study of the von Mises stress criterion in the ironwork frame is presented later. Sections were taken though the models at various locations along their length and width. It was found in all cases that the largest maximum and minimum principal stresses in the bedding occurred on the surface. The results have been presented as three-dimensional illustrations showing the calculated values of stress on the surface of the model.

Vertical Load Case

Maximum Principal Stress: The largest peak maximum principal stress of all the analyses was calculated in the model simulating the configuration containing a quarry tile. The magnitude of this stress was 5.8MPa and was located in the top layer of the bedding directly underneath the cover seating. The direction of the stress was aligned at 45° to X-axis in the XY plane. An illustration of the maximum principal stress distribution in this model is shown in Figure 6.20.

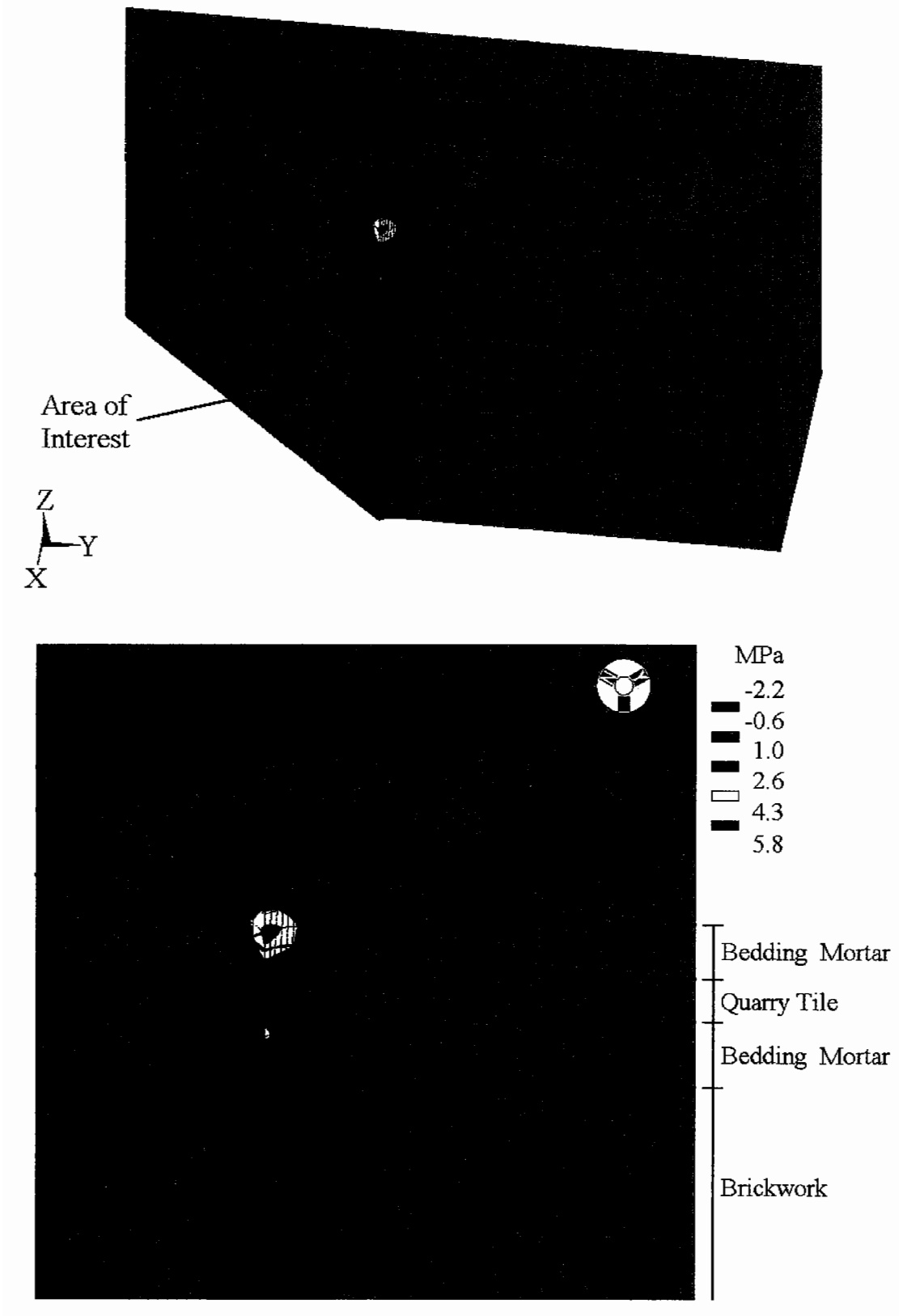

Figure 6.20: Calculated maximum principal stress under a vertical load in the quarry tile configuration model

The quarry tile configuration produced the largest peak maximum principal stress in the top cementitious layer whilst the quarry tile experienced a relatively low stress in comparison. This may explain why the quarry tiles were undamaged when they were removed from the laboratory test facility but the bedding mortar was cracked. The difference in the elastic properties of the materials in the composite bedding layer may be attributable to larger stress that developed in the cementitious component.

A 30kN load was applied during the repeated load test on these installations in the laboratory test facility which would have resulted in a maximum principal stress of approximately 3.0MPa. An investigation of the fatigue behaviour of mortar A described in Section 2.2.1 revealed that a stress of this magnitude resulted in failure after 50,000 cycles. This compares favourably with the laboratory test facility experiment which developed a crack at the position of the calculated peak stress within 150,000 load cycles.

The other models produced similar maximum principal stress distributions; the peak value was located approximately 20mm beneath the cover seating and acting in the same direction as described above. A summary of the results for the vertical load case is given in Table 6.5.

Table 6.5: Summary of the peak maximum principal stress values in the bedding layer calculated in all models

Model	Peak maximum principal stress (MPa)	Location	Extent	Direction
Prototype Test Facility	2.4	Under corner, 40mm beneath seating	10mm along exposed face of bedding	45° to X-axis in XY plane
Quarry tile configuration	5.8	Top layer of bedding, 20mm beneath seating	"	"
25mm bedding layer without mortar above the flange	2.5	Under corner, 20mm beneath seating	"	"
25mm bedding layer with mortar above the flange	3.0	"	"	"

Cracking of cementitious materials generally occurs in a plane perpendicular to the direction of the stress. All the results indicate that vertical cracks are most likely to develop in the bedding directly underneath the cover seating. Such cracks were seen in the field and laboratory experiments which would suggest that the cracking of the bedding layer occurs due to a tensile stress in excess of the tensile strength.

However, in order for a vertical crack to develop in the bedding there would need to be a failure in the horizontal plane at the interface with the ironwork and mortar. An investigation of the shear stress in the XY plane (horizontal) revealed that a small

region of shear stress developed at these interfaces directly above and below the position of the peak maximum principal stress in all the models. The magnitude of this stress was 2.8MPa in the quarry tile configuration model. The analysis assumed that the bond between the bedding and neighbouring materials was rigid, although field and laboratory observations have revealed that this is not the case so the restraint would not be present which would allow the bedding to crack.

Figure 6.20 illustrates that the peak maximum principal stress only exists in a small region. It is considered that due to the magnitude of the tensile stress, and the lack of restraint at the interfaces, localised cracking would occur at this point. This is considered to cause spalling of the bedding material and small pieces may drop into the chamber. This would alter the geometry of the bedding configuration and is considered likely to induce a peak tensile stress at another point in the bedding nearby. It is considered that this would also result in crack development. This process is considered to continue progressively until several cracks develop in the bedding and some fragments directly underneath the seating have fallen into the chamber. Severely crazed bedding with sections missing was seen during some reinstatements and a typical example is illustrated in Figure 3.2. This process was also seen in further laboratory experiments described in Section 7.2 and illustrated in Figure 7.3. The disintegration of the bedding material in this manner would remove the support to the ironwork frame and bituminous material as seen in Figure 1.2. This would allow the frame to move and cause cracking in the asphalt.

The lowest calculated value of maximum principal stress was found in the prototype facility which supported a M-Way ironwork frame. The bearing area of the cover seatings on this frame are approximately twice as large as the Chieftain frames used in the other models. The larger bearing area would have distributed the load over a wider area, hence inducing a lower stress. A similar effect was seen in the strain distribution in the laboratory experiments.

The largest maximum principal stress in the brickwork was calculated to be 1.8MPa. This was present at the interface with the bedding in the configuration containing a

quarry tile as shown in Figure 6.20. The peak values in the other configurations were less than 1.2MPa which may explain the low incidence of failure in this region of a road ironwork installation.

Minimum Principal Stress: The largest minimum principal (compressive) stress was also found in the quarry tile model. The magnitude was 28.2MPa which was located at the surface of the bedding at the interface with the cover seating. The direction of the stress was at 45° to the Z-axis in the XZ plane. This is illustrated in Figure 6.21.

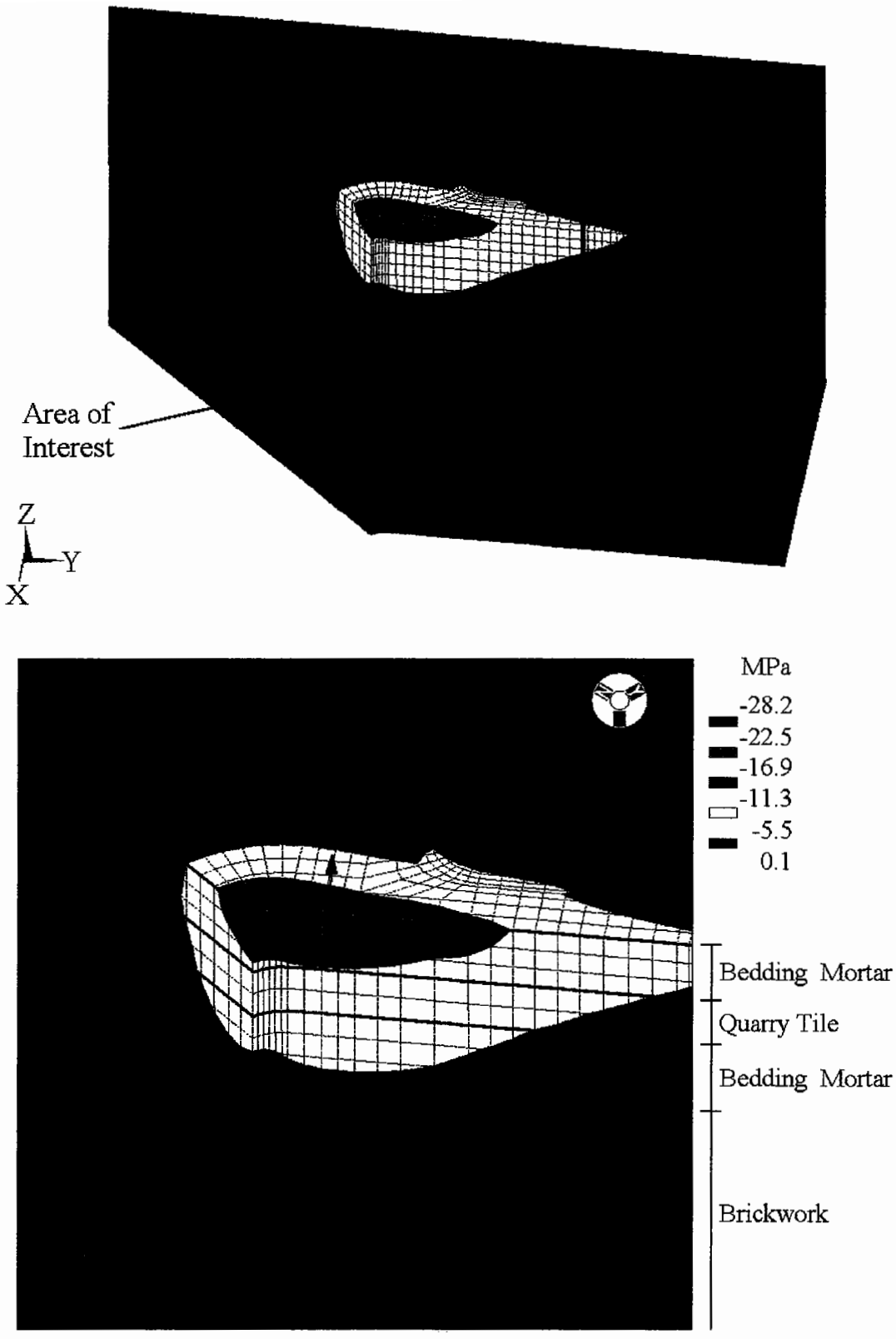

Figure 6.21: Calculated minimum principal stress under a vertical load in the quarry tile configuration model

The peak calculated minimum principal stress was 28.2MPa which is approximately three quarters the mature compressive strength of mortar A. All of the other models produced peak minimum principal stress magnitudes between 8.2 and 16.2MPa at the same position and direction as the model containing a quarry tile in the bedding layer. None of these stress magnitudes are greater than the mature compressive strength of mortar A so these results would suggest that a tensile failure of the bedding is more likely than a compressive failure. A summary of the peak minimum principal stress values calculated in all the models under the vertical load case is given in Table 6.6.

Table 6.6: Summary of the peak minimum principal stress values in the bedding layer calculated in all models

Model	Peak minimum principal stress (MPa)	Location	Extent	Direction
Prototype Test Facility	12.4	Directly underneath cover seating along top edge of bedding	Entire edge of bedding underneath cover seating	45° to the Z-axis in the XZ plane
Quarry tile configuration	28.2	"	"	"
25mm bedding layer without mortar above the flange	8.2	"	"	"
25mm bedding layer with mortar above the flange	16.2	"	"	"

Further calculations were carried out with the prototype test facility model. The static modulus and Poisson's ratio of the bedding were changed to 6.7GPa and 0.07 respectively to represent bedding mortar A at an age of 3 hours. This analysis gave an indication of the stress magnitude and distribution in a newly completed reinstatement. It was found that the location and direction of the maximum and minimum principal stresses were virtually the same as seen in the previous calculations but the peak values were 1.1 and 5.4MPa respectively. These stresses were below the strength of the material at this age so it would appear likely that a reinstatement would be more likely to fail when the bedding mortar had developed its mature properties. This compares well to field observations as reinstatements generally do not fail immediately after re-opening to traffic.

Angled Load Case

Maximum Principal Stress: Further analyses were carried out with the load applied at 25° to the vertical as described previously. This load case was applied to all the models except the configuration without mortar above the flange. The resulting peak maximum principal stress values were found to be either virtually the same or marginally lower in all models except the configuration with mortar above the flange where the peak magnitude was 3.5MPa. The distribution and direction of the maximum principal stress in all models was virtually identical to the vertical load cases. A summary of the largest maximum principal stress magnitudes for both load cases is given in Table 6.7.

Table 6.7: Summary of the calculated peak values of maximum principal stress from the two load cases

Model	Calculated maximum principal stress (MPa)	
	Loading Angle = 0°	Loading Angle = 25°
1	2.4	2.2
2	5.8	5.5
4	3.0	3.5

The calculated values of stress in the mortar in and around the holes in the frame flange in the model with mortar above the flange were also studied. This model is illustrated in Figure 6.12. It is considered by some highway engineers that a horizontal component of force may induce a large tensile stress at this point in the bedding. The results illustrated that this effect did occur when the calculated values of stress at these points were compared to the vertical load case. However, the peak maximum principal stress magnitude in the mortar in the hole was calculated to be 1.6MPa which was considerably lower than the peak value underneath the cover seating. It is considered that the bedding layer would be most likely to crack underneath the cover seating rather than around the holes in the frame flange.

The magnitude of the peak maximum principal stress in the brickwork was slightly larger in the angled load case. The largest value was 1.9MPa in the quarry tile configuration and approximately 1.4MPa in the other models. These stresses occurred at the surface of brickwork at the interface with the bedding as seen in the vertical load case. It is considered that an angled load case would have been applied on the north manhole at the Sandy test site. The larger magnitude of stress in the brickwork may have been attributable to its failure as described in visit No. 5.

Minimum Principal Stress: All of the peak minimum principal stress values were found to be lower in the angled load case, but the distribution and directions were found to be same as the vertical load case. A summary of the peak minimum principal stress values for both load cases is given in Table 6.8.

Table 6.8: Summary of the calculated peak values of minimum principal stress from the two load cases

Model	Calculated minimum principal stress (MPa)	
	Loading Angle = 0°	Loading Angle = 25°
1	12.4	7.0
2	28.2	25.6
4	16.2	15.4

6.6.2 Behaviour of the Ironwork

The ironwork covers and frame are considered to be made from a ductile material. The von Mises stress distribution was studied in this component in isolation as this quantity is often applied as the failure criterion in ductile materials. This theory of elastic failure proposes that failure will occur when the shear or distortion strain energy in the material reaches the equivalent value at yielding in simple tension [45]. The derivation of this criterion results in the expression: [45]

$$(\sigma_1 - \sigma_2)^2 + (\sigma_2 - \sigma_3)^2 + (\sigma_3 - \sigma_1)^2 = 2\sigma_Y^2 \qquad (6.1)$$

where

σ_1, σ_2 and σ_3 = principal stresses

σ_Y = von Mises or equivalent stress

It was found that the peak von Mises stress was 112MPa in all the vertically loaded cases and approximately 162MPa in the angled load cases. These were located at the connection between the cover seating and the frame web. The yield strength of ductile iron measured by Stanton plc was found to be 275MPa so the calculations indicate that the ironwork frames have sufficient strength. Additionally, all of the frames modelled in these analyses comply with EN124 and are rated as class D400 [20]. Their ability to withstand a 400kN test load without cracking gives further confidence in the calculations.

The analyses allowed a study of the distribution of load applied onto the bedding by the frame. An illustration of the reaction force at each node on the surface of the bedding is shown in Figure 6.22.

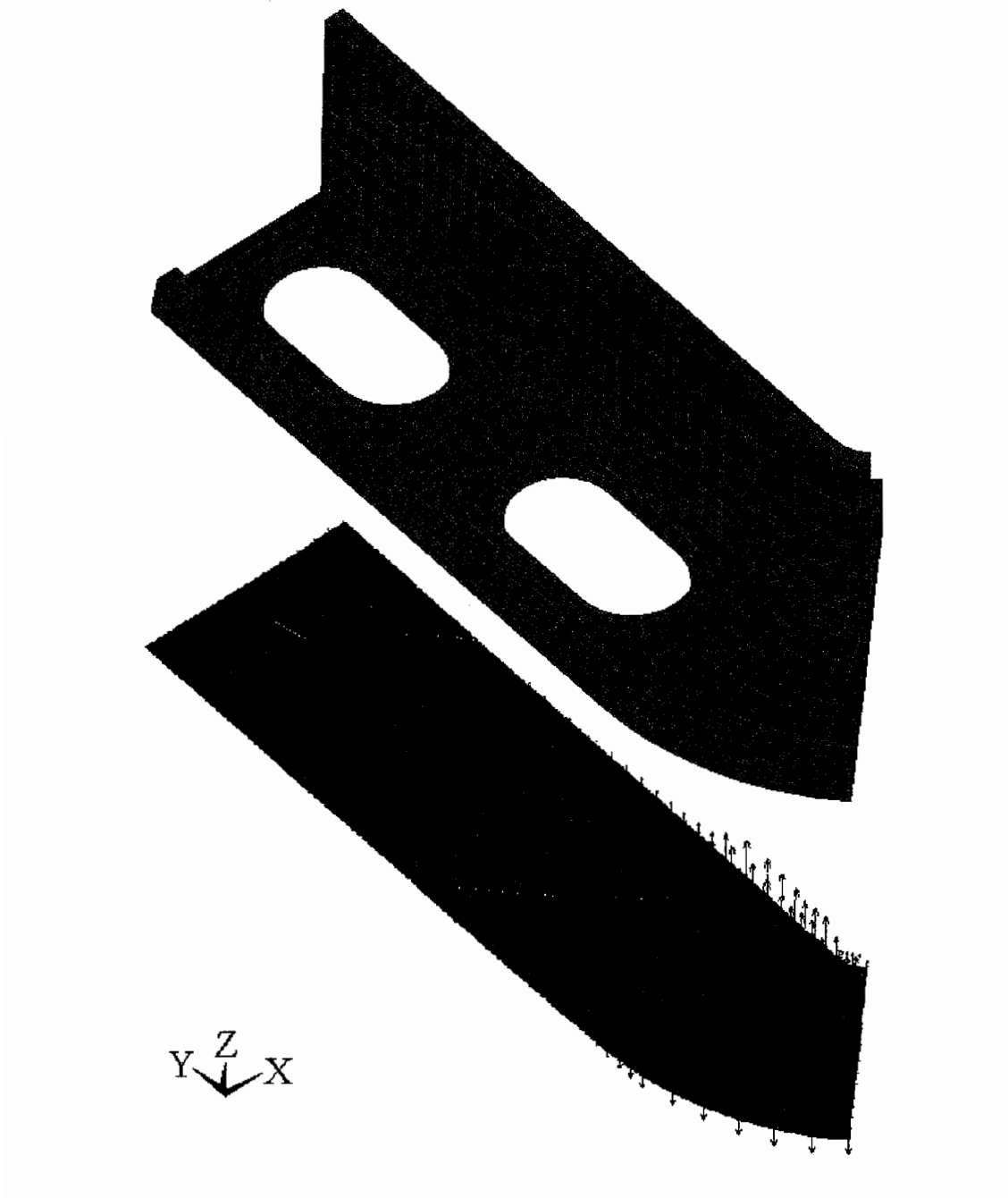

Figure 6.22: Calculated reaction forces at the surface of the bedding in the configuration containing a quarry tile under the angled load case

The size of the arrows are proportional to the magnitude of the reaction force. It can be seen that the greatest concentration of load is immediately adjacent to the cover seating. However, the magnitude of the reaction force rapidly diminishes with distance from the cover seating. This would indicate that the load is concentrated on a very small area underneath this region. Additionally, the hole located in the frame

flange is immediately behind the cover seating in all the configurations as shown in Figures 6.7 and 6.14. The load is transmitted onto the bedding next to this hole by the thin strip of ironwork beneath the web. This causes a high concentration of load to develop at the surface of the bedding in this region. The surface of the bedding at all other regions on the surface generally experiences little or no applied force. It would appear that the frame flange has little purpose in these areas. This result provides further confidence that the load distribution around this seating would not have any effect on the load distribution around an adjacent seating. The simplification of the analyses using four planes of symmetry appears to have a negligible effect.

Figure 6.22 also illustrates that the bedding underneath the outside edge of the flange near the corner experiences a downward reaction force implying that the frame flange moves upwards at this point. This motion was identified in the laboratory test facility and was considered to damage the reinstated bituminous material. This observation was most evident in the angled load cases. However, it was not seen in the configuration with mortar above the flange. It is thought that the additional layer of bedding may have restrained this movement.

A 100mm deep Chieftain frame is compared with its calculated distorted shape in Figure 6.23. It can be seen that the frame appears to twist as considered in the laboratory experiments which was also thought to damage the bituminous material. This distortion may be reduced by installing web stiffeners close to the seating. It would appear that the web stiffener at the current position does very little to prevent this motion or to facilitate an even distribution of load onto the bedding. The 150mm deep Chieftain frame had a stiffener located behind the cover seating. It was noted that the twisting motion was reduced in this model. These observations are considered in discussing refinements to the design of the ironwork frame in Section 7.4.

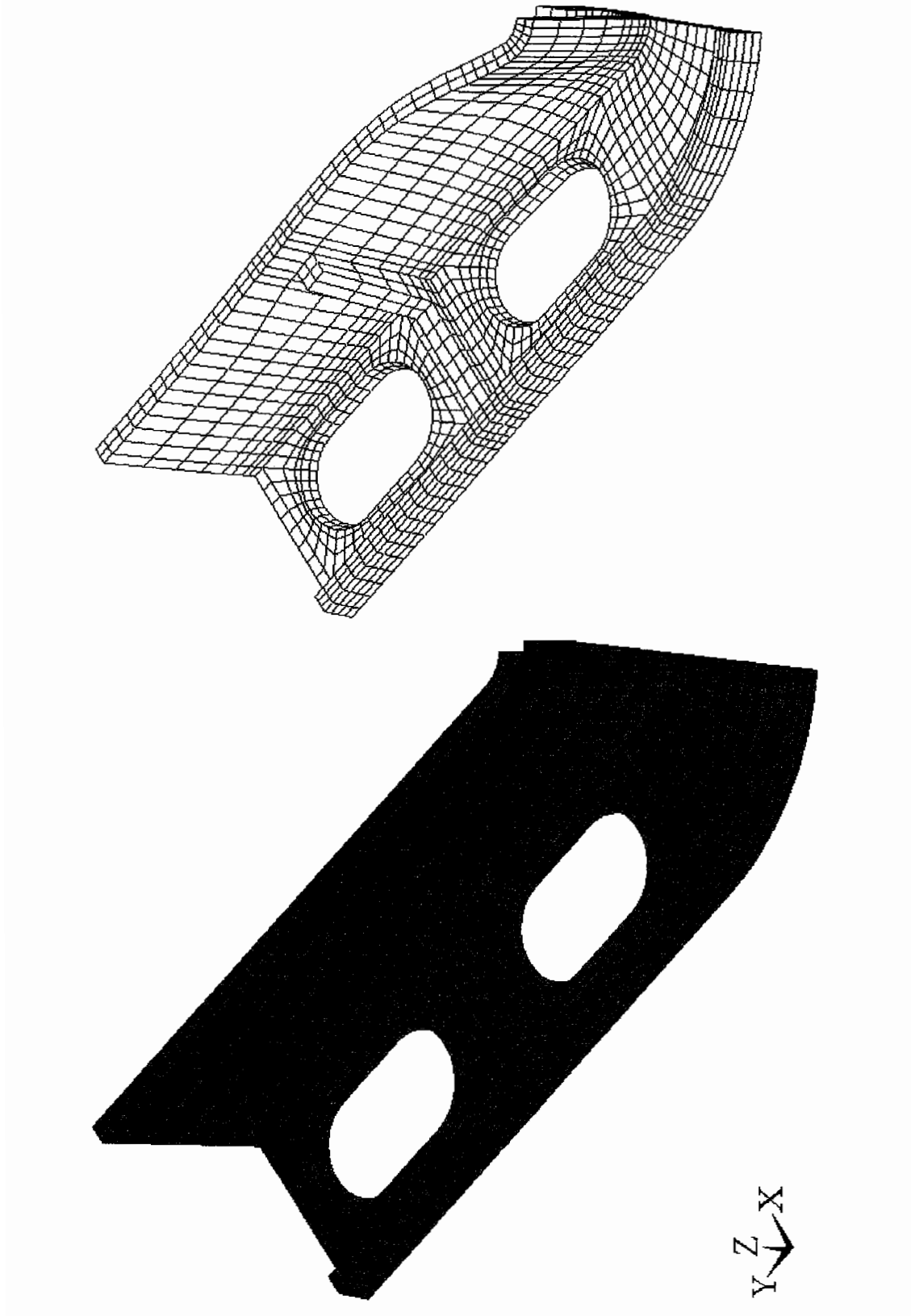

Figure 6.23: Calculated distorted and undistorted shape of a 100mm deep Chieftain frame under the angled load case (not to scale)

6.7 Summary

The calculated values of strain compared well with the values measured in the laboratory experiments. Additionally, the strain distribution was similar to the stress distribution which provided confidence in the calculated values of stress which allowed a study of the maximum and minimum principal stresses in the bedding. The results have illustrated that a tensile stress develops in the bedding material underneath the cover seating. The direction of this stress is in the horizontal plane which would result in vertical cracks if the magnitude was greater than the strength of the bedding. This appeared in all the configurations and the peak values varied between 2.4 and 5.8MPa. Cementitious bedding materials generally have a tensile strength no greater than 3.5MPa, but may experience a fatigue failure at lower stress magnitudes as discussed in Section 2.2.1.

The ironwork frame is considered to have ample strength to withstand the applied forces. However, the design of the frame only distributes an applied load over a very small area which may be related to the tensile stress that develops in the bedding beneath this point. In addition, the distorted shape shows that the frame twists, which is considered to damage the bituminous backfill. Changes could be made to the design of the frame that would improve the conditions the surrounding materials have to withstand.

7. Development of Improved Road Ironwork Installations

7.1 Introduction

The principal objective of this research was to achieve a lower incidence of failure of road ironwork installations. The finite element analyses and the laboratory experiments indicated the magnitudes of the peak stresses and strains that develop within common road ironwork installations. Some of the measurements indicated that bedding mortar A was being overstressed relative to its strength. Experiments to assess the effects of shrinkage also revealed that several cracks developed in the bedding layer of configurations bedded with mortar A without the application of any load. Additionally, good quality workmanship is difficult to achieve with mortar A due to the short workable life and the progressive hardening throughout this period. It would appear that this mortar has inadequate properties for its application as a bedding material.

This chapter contains a further investigation and discussion of these aspects which were used to develop a specification for an improved bedding material. The desired properties of the material are considered to be sufficient to withstand the worst loading condition. Trial specimens of an improved bedding material were developed and its performance was compared to the specification. The in-situ behaviour of this material was later studied in the laboratory test facility and field experiments.

The research has also revealed several shortcomings in the design of the ironwork frame which cause deterioration of the bituminous material around manholes and poor distribution of load onto the bedding. Refinements were made to the design of a standard Chieftain 600 x 600 x 100mm deep frame with the intention of mitigating these effects. Samples of this design were cast and used in subsequent testing in combination with the trial mortar samples.

The research also illustrated that the bedding configuration can mitigate some of the failure mechanisms identified. These aspects were used to develop an improved

reinstatement procedure. This section also contains a discussion of the failure criteria. A description of these developments is given below.

7.2 Crushing Tests

The three-dimensional finite element analyses illustrated that a tensile stress develops in the bedding in the horizontal plane underneath the cover seating. The analysis also indicated that the stress and strain distributions were similar in these road ironwork installations and the laboratory experiments demonstrated that the largest tensile strains developed beneath the corners. The magnitude of the calculated stress was above the critical threshold determined in a fatigue test of mortar A described in Section 2.2.1. Inspections were made at the end of repeated load tests and of field installations which revealed that vertical cracks had developed at these positions. However, the stress magnitudes were calculated by a theoretical approach and the cracks in both instances were observed during regular inspections, so it was not entirely evident that the cracks developed at the exact moment when the load was applied. Experiments to assess the effects of shrinkage revealed that this effect alone can result in cracks appearing at these positions as illustrated in Figure 2.10. The duration of the repeated load tests in the laboratory were approximately 7 days so it was feasible that the cracks may have developed due to shrinkage. Further evidence was required to confirm whether the development of cracks was at least partially attributable to a load induced tensile stress or was solely due to shrinkage. Experiments were carried out to study the development of cracks in standard road ironwork configurations under an applied load. The load producing a crack in these specimens was used to determine the magnitude of the peak tensile stress from the linear three-dimensional finite element analysis. This would provide some indication of whether an excessive tensile stress was a cause of cracking. It was thought that this would be a useful study before committing the findings of this research to the development of an improved bedding material.

7.2.1 Description

Four standard Chieftain 600 x 600 x 100mm frames were bedded onto 18mm thick plywood boards with a variety of bedding configurations using mortar A. Another

four specimens with the same configurations were prepared using mortar B. A summary of these configurations is given in Figure 7.1.

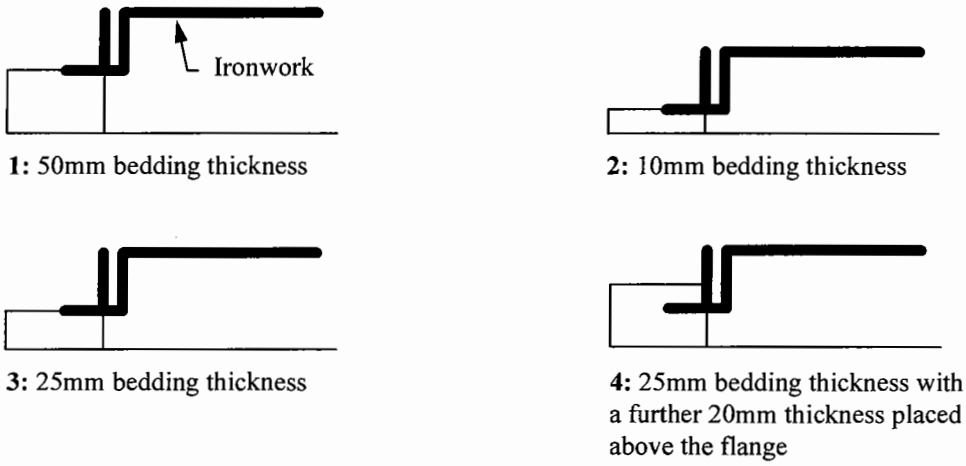

Figure 7.1: Sections through the bedding configurations prepared for crushing tests

The ironwork covers were placed within each frame and a 300mm diameter loading platen was placed on the cover above the seating with the smallest bearing area. Each specimen was placed in a hydraulic test machine at the Stanton laboratory which was capable of gradually applying a compressive force up to a maximum of 400kN. The bedding layer was constantly observed during the load application to monitor the development of cracks. All of the specimens were tested within 48 hours after mixing and placing the mortar. This allowed the effects of shrinkage to be reduced although the mortar A specimen with a 10mm bedding thickness had developed cracks during this curing period around one corner. The specimen was oriented in the test machine so that this corner was not loaded.

Samples of mortars A and B were cast into cubes during the preparation of the test specimens. The cubes were used to determine the compressive strength at 48 hours [11] which was found to be 32 and 28MPa respectively. These values were similar to those measured at this age during a study of the development of compressive stress summarised in Figure 2.2. A comparison between Figures 2.2, 2.7 and 2.8 indicates that the static modulus and Poisson's ratio develop at a similar rate to the compressive

strength and there were only minor differences between the elastic properties measured at 48 hours and 28 days. It is considered that the elastic properties of bedding mortar A used in the crushing tests were approximately the same as the 28 day values which were used in the three-dimensional finite element analysis.

7.2.2 Results

All of the specimens developed a crack in the bedding material underneath the loaded seating at an applied load between 35 and 110kN. All of the cracks were aligned vertically and spread across the full width of the bedding layer. The cracks were either perpendicular to the width of the bedding or aligned at an angle of approximately 45° to the frame webs. This is illustrated in Figure 7.2. The cracks developed suddenly so it was difficult to determine whether cracks propagated from the inside edge of the bedding layer. A summary of the applied load when the first cracks appeared in each configuration is given in Table 7.1. This load magnitude was used to calculated the value of stress in the bedding underneath the seating in the configurations modelled in the linear three-dimensional finite element analysis. This figure is also included, where applicable, in Table 7.1.

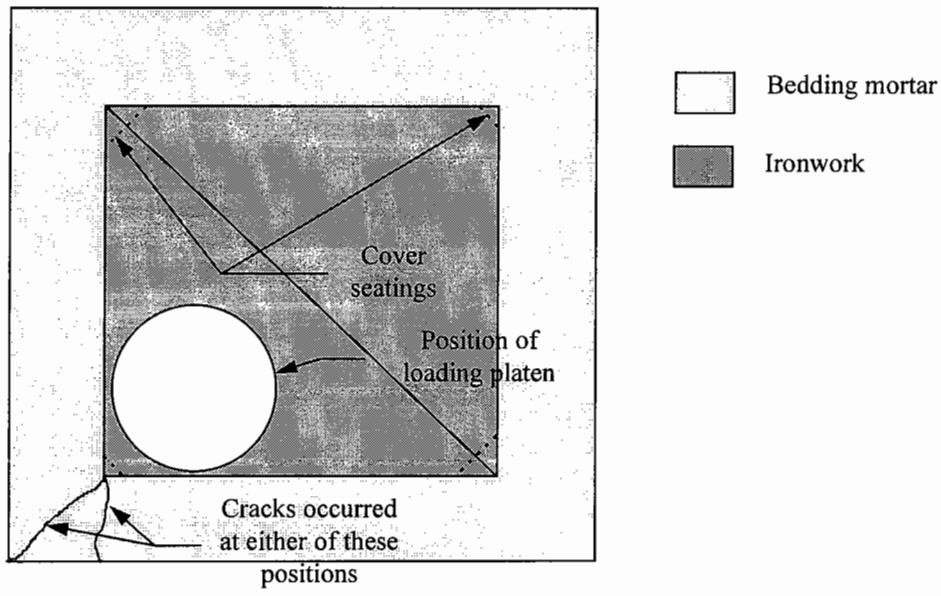

Figure 7.2: Plan view of the initial crack pattern

Table 7.1: Summary of the applied load when the initial cracks appeared and a comparison to the three-dimensional finite element analysis results

Configuration number (see Figure 7.1) and bedding mortar	Load required to produce a crack (kN)	Estimated peak tensile stress in the bedding at the load when a crack was first observed (MPa)
1-A	75	3.2
2-A	35	-
3-A	70	3.1
4-A	55	2.9
1-B	110	-
2-B	40	-
3-B	85	-
4-B	75	-

The direct tensile and splitting strength of mortar A were measured in previous laboratory experiments described in Section 2.2.1. These were found to be 2.8 and 3.6MPa respectively at 48 hours. The crushing tests indicated that the first cracks appeared when the calculated peak tensile stress was between these two values. Additionally, the two-dimensional finite element analysis presented in Section 4.5 indicated that the largest tensile stress developed in the section with a 10mm thick bedding layer when compared to other sections under the same magnitude of applied load. This configuration developed a crack at the lowest applied load during the crushing experiments. The results also illustrated that the comparable mortar B samples required a greater load before a crack developed. This material has a greater tensile strength than mortar A as illustrated by a comparison of Figures 2.3 and 2.4.

Some of the configurations developed further cracks at higher loads. These cracks occurred when the load was greater than 250kN. The secondary cracks radiated from the inside edge of the bedding beneath the loaded corner. These cracks also propagated across the full width of the bedding. A typical final crack pattern on completion of test is shown in Figure 7.3.

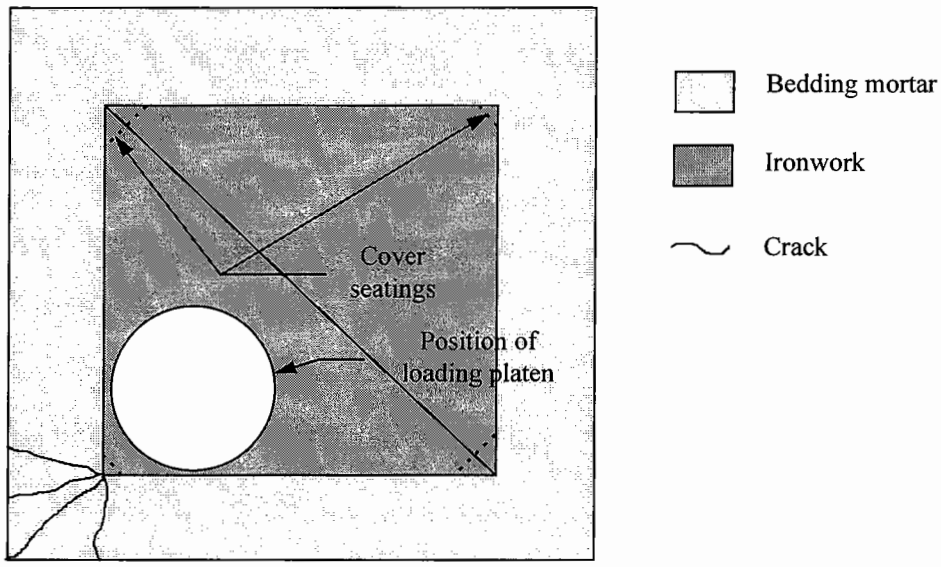

Figure 7.3: Plan view of a typical final crack pattern

A visible distortion of the frame web occurred close to the loaded corner when the applied load was greater than 300kN. This resulted in twisting of the frame web and the appearance of a small gap between the frame flange and the surface of the bedding in the configurations without mortar above the flange. The size of the gap was approximately 1.6mm at a load of 400kN. This distortion of the ironwork frame was observed in the three-dimensional finite element analysis and was considered to have a detrimental effect on the surrounding bituminous material. This laboratory observation provides further confidence in the analysis results.

7.2.3 Summary of Crushing Tests

A comparison of the loads required to produce a crack in the mortar A specimens and the calculated peak tensile stress in these configurations at this load indicated that all the cracks developed when the stress was equivalent to the tensile strength of the material. These results strongly suggest that the bedding cracks were due to a tensile stress in excess of the tensile strength. The initial cracks were in the same position and direction as observed in the field and the laboratory test facility. The majority of the cracks did not appear until the monotonic load was greater than the largest load that is considered to be applied in the field. This was discussed in Section 3.6 and

was estimated to be 57.5kN. However, the fatigue behaviour of mortar A was investigated as described in Section 2.2.1 and it was found that a lower tensile stress magnitude can result in failure after several loading cycles. It is considered that this effect, in addition to shrinkage, is the principal failure mechanism for road ironwork installations when mortar A is used to form the bedding layer.

7.3 Required Bedding Material Properties

7.3.1 Type of Material

Field observations and discussions with highway engineers revealed that cementitious mortars are the most commonly used materials to form the bedding layer. During a review of the BT specification [25] of the reinstatement of road ironwork, it was considered that a proprietary cementitious material should be adopted as the majority of contractors and DLO personnel are familiar with its behaviour. It is thought that an improved bedding material should be of a cementitious composition for this reason. However, certain varieties of polymer resin based products that do not produce strong fumes may also be suitable. HDPE spacers are not considered to be a practical bedding material due to the very narrow range of bedding thicknesses that can be used to form a reliable installation as discussed in Section 5.5. Furthermore, steps in the surface profile of the brickwork provide uneven support for the spacers unless a thin layer of mortar is applied on the brickwork. Highway engineers consider this to be an unnecessary complication for a reinstatement procedure. Proprietary cementitious products are usually supplied in 25kg bags or containers. This was found to be a sufficient quantity to produce a 25mm bedding layer and an improved material should be supplied in multiples of this quantity. By adopting a cementitious material, the desired workable and hardened properties need to be specified. These are discussed below.

7.3.2 Workable Properties

Typical proprietary cementitious mortars possess a very short workable life which varies between 8 and 15 minutes as discussed in Section 2.2.1. Such materials are difficult to mix and place before hardening. Additionally, these materials stiffen throughout their workable life. These factors are thought to be the cause of the low

quality of workmanship found in some reinstatements. It is considered that a workable life of at least 15 minutes and a constant workability in this time should make the material easier to use resulting in a better quality of workmanship. Cementitious mortar A possessed a slump of 50mm immediately after mixing. This material was found to be easy to manipulate at this stage in its workable life so this slump was adopted as the desirable workability.

7.3.3 Hardened Properties

Tensile Strength

This research has indicated that cementitious mortar A has an inadequate tensile strength and this is a principal cause of cracking in the bedding layer. The largest tensile stress calculated in the three-dimensional finite element analysis was 5.8MPa under an applied load of 57.5kN acting over the whole seating. This developed in the configuration containing a quarry tile. The required tensile strength was determined by applying a notional factor of safety of 1.4 to the largest calculated stress. This resulted in a required tensile strength of 8MPa. The factor of safety was considered to be large enough to accommodate any underestimation of the stress magnitude calculated in the finite element analysis due to its approximate nature. This is also the smallest factor of safety applied in the limit state design of structural steel and concrete [41,49]. It was thought that a larger factor would not be necessary as the stress magnitude was based on the worst loading case and a tensile strength greater than 8MPa may be difficult to achieve in a cementitious material. The bedding layer would be required to withstand this stress immediately after re-opening so this strength should be achieved within three hours. Discussions with highway engineers revealed that it would not be possible to extend the duration of a road closure due to the inconvenience it causes to traffic.

Compressive Strength

The finite element analysis calculated that the largest compressive stress was 28.2MPa and this figure was used to determine the required compressive strength. A factor of safety of 1.4 was also applied to the calculated maximum stress resulting in a

required compressive strength of 40MPa. This strength was also required to develop within three hours of mixing.

Static Modulus and Poisson's Ratio

The desirable strengths were based on the finite element analyses using the elastic properties of cementitious mortar A which were verified with the results from the laboratory experiments. The two-dimensional finite element analysis presented in Section 4.5 illustrated that the stress magnitude in the bedding was proportional to the static modulus. This trend was also seen in further calculations with the three-dimensional analysis when the static modulus of the bedding was reduced which resulted in a reduction of the calculated peak tensile and compressive stresses. If the static modulus of an improved bedding material was significantly greater than that of mortar A then larger stresses are likely to be induced by an applied load so the desired strengths of the material may be insufficient. The desirable values of the static modulus and Poisson's ratio of the improved material were chosen as 21GPa and 0.14 respectively which are the mature elastic properties of mortar A. However, small variations in these quantities should not increase the peak tensile and compressive stresses beyond the strengths of the improved material.

Shrinkage

Shrinkage of the bedding material can also result in cracking as described in Section 2.2.1. Cracks developed regardless of the bedding configuration without the application of any load. An improved bedding would be required to resist cracking due to this effect. A large tensile strength would increase its resistance to shrinkage cracking but low shrinkage characteristics were considered to be necessary to reduce the likelihood of this source of cracking. Cementitious mortar A developed cracks within 24 hours in some of the configurations monitored. Further experiments to quantify the shrinkage of this material revealed that samples of the bedding reduced in length by an average of 3.5 microns over a length of 50.8mm during the first 24 hours after mixing. This would result in a tensile strain of 69 microstrain if the bedding layer was fully restrained. It was considered that an improved bedding material should not induce a larger strain by shrinkage within 28 days.

A sample of cementitious mortar A was sieved and the maximum aggregate size was found to be greater than 2.36mm but less than 6mm as described in Section 2.2.1. Bedding layers used in practice are usually greater than 10mm thick so the maximum aggregate size could be as large as 6mm. An improved aggregate structure could be used to enhance the compressive strength [50] and reduce the cement content which would contribute to the reduction of shrinkage [51].

Durability

A bedding material with the improved characteristics described above should increase the lifespan of a reinstatement. During this time, it would be required to be resistant to the environmental conditions found within a highway. An improved mortar would be required to be resistant to the action of frost and not produce other compounds by a chemical reaction with de-icing salts which have a detrimental effect. It should also have a low permeability to prevent chloride ingress which would damage the ironwork.

Specification

All of these criteria were used to prepare a specification for an improved bedding material. A summary of all the required properties is given in Table 7.2. The specification was supplied to Pozzoment Ltd who offered to develop trial samples. This company specialises in the development of cementitious materials for the mining and civil engineering industries. Experiments were carried out with this material to compare its performance with the specification and to study its behaviour in road ironwork installations. These are described in Sections 7.5 and 7.6 respectively.

Table 7.2: Required properties of an improved bedding material

Material Composition:	
Sample sizes	25kg bags
Maximum aggregate size	6mm
Workable Properties:	
Workable life	15 to 30 minutes
Desired workability	50mm slump
Hardened Properties:	
Compressive strength at 3hrs	> 40MPa
Tensile strength at 3hrs	> 8MPa
Static Modulus	≈ 21GPa
Poisson's Ratio	≈ 0.14
Shrinkage	Producing a strain < 69 microstrain over 28 days
Durability Aspects:	
	Mortar should be resistant to sulphate attack, chloride ingress and the action of frost.

7.4 Ironwork Frame Design Improvements

The ironwork units studied in this research complied with EN124 and were rated as class D400 [20]. These units have demonstrated adequate strength but the laboratory experiments and finite element analyses have indicted that there is an uneven distribution of load onto the bedding. This was attributed to the small bearing area of the seatings and the presence of holes in the frame flange located at the corners. The concentration of load under the seatings was considered to be related to the magnitude of tensile stress in the bedding beneath this point. Additionally, the crushing tests described earlier and the three-dimensional finite element analyses revealed that the frame twists under an applied load which causes an uplift of the outside edge of the frame flange. Such motion was considered to be a likely cause of damage to the bituminous material placed above the flange and result in cracks developing parallel to the frame web as seen in the field.

Refinements were made to the design of the existing Chieftain 600 x 600 x 100mm deep unit to provide a better distribution of the load. This involved increasing the bearing areas on the frame and covers. The resulting bearing areas were approximately three times as large as the original unit. Additionally, the holes in the frame flange behind the seatings were filled. Both of these features were considered to distribute the load onto the bedding over a wider area.

The locations of the web stiffeners were also revised to increased the torsional rigidity of the frame which would reduce the twisting motion under an applied load. Stiffeners located in between seatings were removed as they did not appear to have any effect and others were located around the seatings where the twisting motion was the greatest. These revisions increased the volume of iron required to form the frame and, hence, the cost of production. Despite the anticipated better load distribution around the corners, it was still thought that the frame flange between the seatings would not carry any load. The volume of iron required was reduced by narrowing the width of the flange at this point which resulted in a net reduction of iron required when compared to the unmodified frame. Figures 7.4 and 7.5 illustrate the original and revised designs of the ironwork frame.

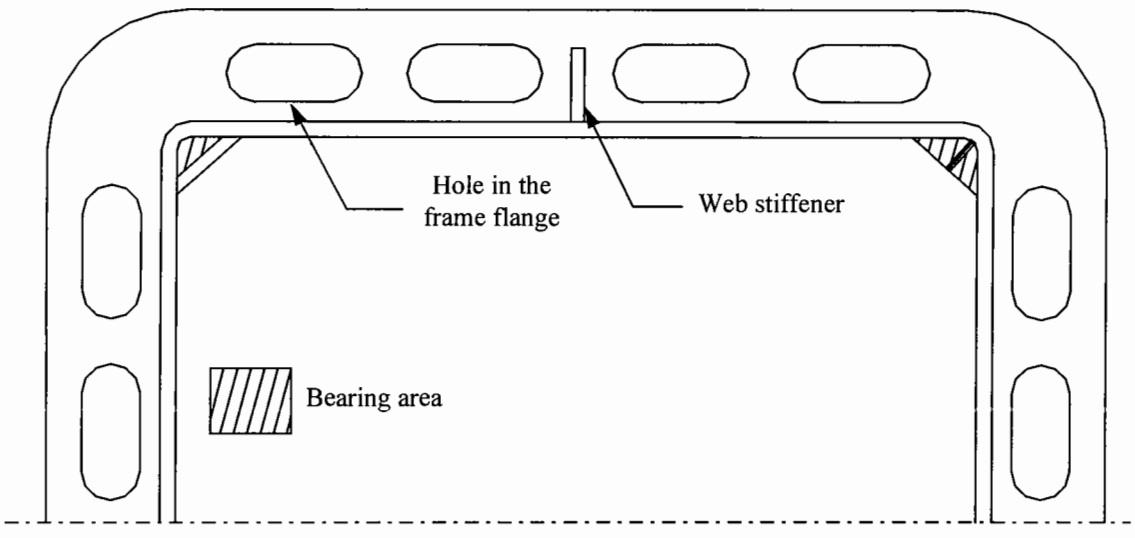

Figure 7.4: Plan view of the original Chieftain 600 x 600 x 100mm deep frame design

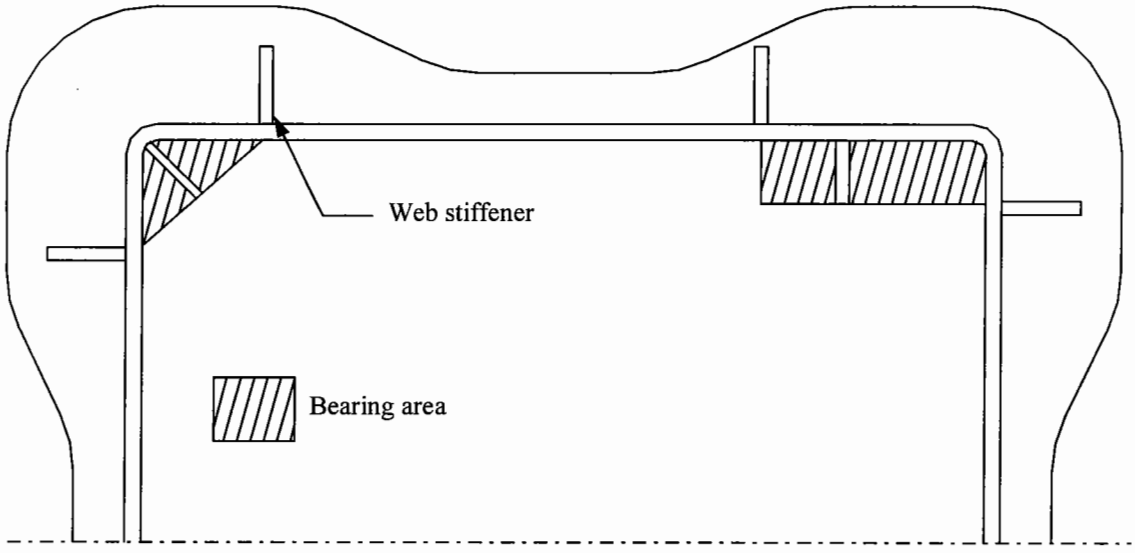

Figure 7.5: Plan view of the revised Chieftain 600 x 600 x 100mm deep frame design

7.5 Material Assessment

7.5.1 Description

A magnesia-phosphate cement (MPC) was developed by Pozzoment Ltd to satisfy the criteria summarised in Table 7.2. This material develops strength through a chemical reaction with water which forms several complex compounds that are the main strength bearing components. The reaction with water is almost instantaneous and curing periods of less than 48 hours are required to develop full strength. A retarder was added to this mixture to increase the workable life and 20mm long fibre glass strands were included to increase the tensile strength. A continuously graded aggregate was blended with the mortar which had a maximum stone size of 6mm. The dry blended material was supplied in 25kg sealed containers. The manufacturer stated that such containers would provide a shelf life of at least 3 months, although samples of the material were mixed within two weeks of supply. MPC mortars are often used in other highway repairs such as filling potholes [52]. It is considered to be particularly suitable due to the rapid development of strength [53].

Polymer resin based products exist that exceed the requirements of the specification given in Table 7.2. Such products have been used by some highway engineers with

favourable results. However, these materials are approximately five times as expensive as proprietary cementitious mortars. It is considered by Pozzoment that the MPC mortar could be produced for a significantly lower cost than the polymer resin based products. An assessment of the performance of the material is described below.

7.5.2 Workable Properties

A superplasticizer was also included in the mixture to aid workability. This was considered to be useful as the mortars previously used containing fibre glass strands produced a very stiff paste at the manufacturer's recommended water content and were consequently difficult to manipulate. The recommended water content was 10% which is lower than other mortars, but produced a slump of 50mm. The slump remained at this value throughout its workable life before undergoing a flash set. The set time was found to be between 12 and 15 minutes at temperatures varying between 18 and 21°C. This is slightly quicker than the specified value, but later discussions with the manufacturer revealed that it had to be reduced to allow sufficient time for strength development. The mixture produced ammonia during mixing so it was necessary to ensure adequate ventilation in the laboratory, although these conditions readily occur in the field. The hydration reaction was highly exothermic after setting. This is a common characteristic of MPC mortars and temperatures of 63°C have been recorded [52]. This would allow the material to be used at temperatures close to freezing which would be useful for reinstatements carried out in winter.

7.5.3 Hardened Properties

Tensile Strength

The direct tensile and splitting strengths of the MPC mortar were measured by the same methods used to determine these properties of mortars A and B. A description of the method and an illustration of the apparatus used to determine the direct tensile strength is shown in Figure A.1 in Appendix A. The tensile stress at failure from both test methods is illustrated in Figure 7.6 and the tensile strain at failure measured during the direct tensile test is shown in Figure 7.7.

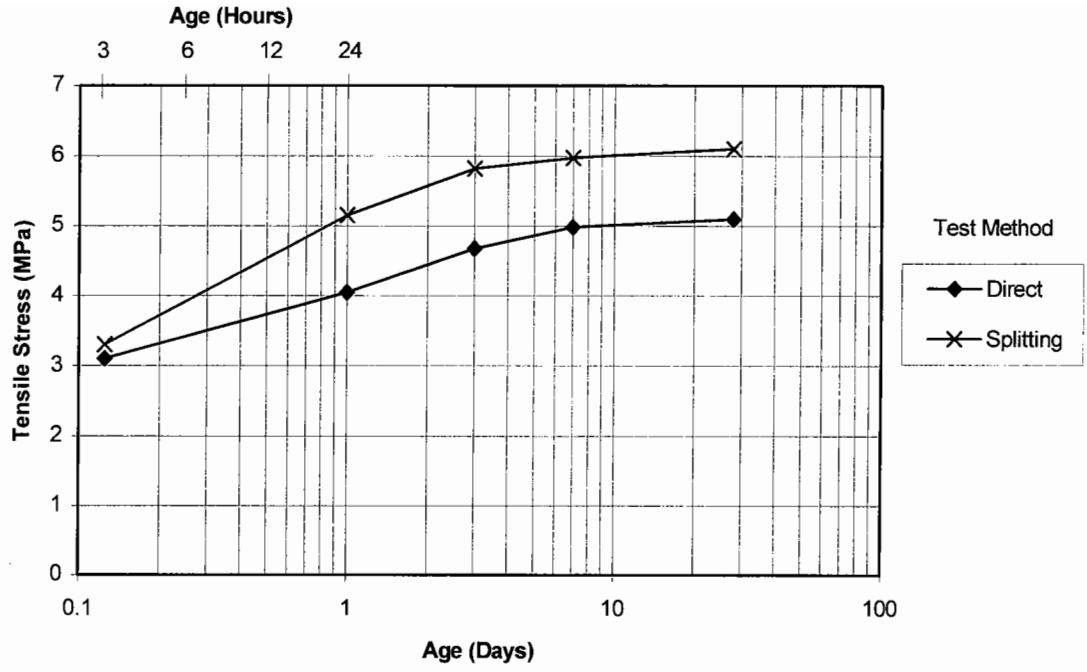

Figure 7.6: Development of tensile strength of the MPC mortar expressed as a limiting stress

Figure 7.7: Development of tensile strength of the MPC mortar expressed as a limiting strain

The results illustrate that the tensile strength expressed as a limiting stress measured by both methods is greater than mortars A and B as illustrated in Figures 2.3 and 2.4

but is below the specified value, even at an age of 28 days. The required strength was determined from the three-dimensional finite element analysis of the bedding configuration containing a quarry tile under the worst loading case. Significantly smaller stresses were calculated in the other configurations so it is considered that the MPC mortar has sufficient strength for use in these circumstances. Additionally, the values of quoted in Figures 7.6 and 7.7 represent the stress and strain in the material when the cement paste cracked. The fibre glass strands did not break immediately so load remained to be carried across the crack, although the magnitude was approximately 25% of the load producing the initial crack. This material was the first attempt by the manufacturer to develop a product that matched this specification. It is claimed that variations could be made to the mixture which could improve the tensile strength and increase the setting time.

Compressive Strength

Samples of the MPC mortar were cast into 100mm cubes and crushed in accordance with BS1881: Part 116: 1983 [11] at various ages. An illustration of the development of compressive strength with age is shown in Figure 7.8. The results illustrate that the MPC mortar achieved a compressive strength of 41MPa after 3 hours which satisfies this criterion. Additionally, this material developed a compressive strength of 65MPa at an age of 28 days.

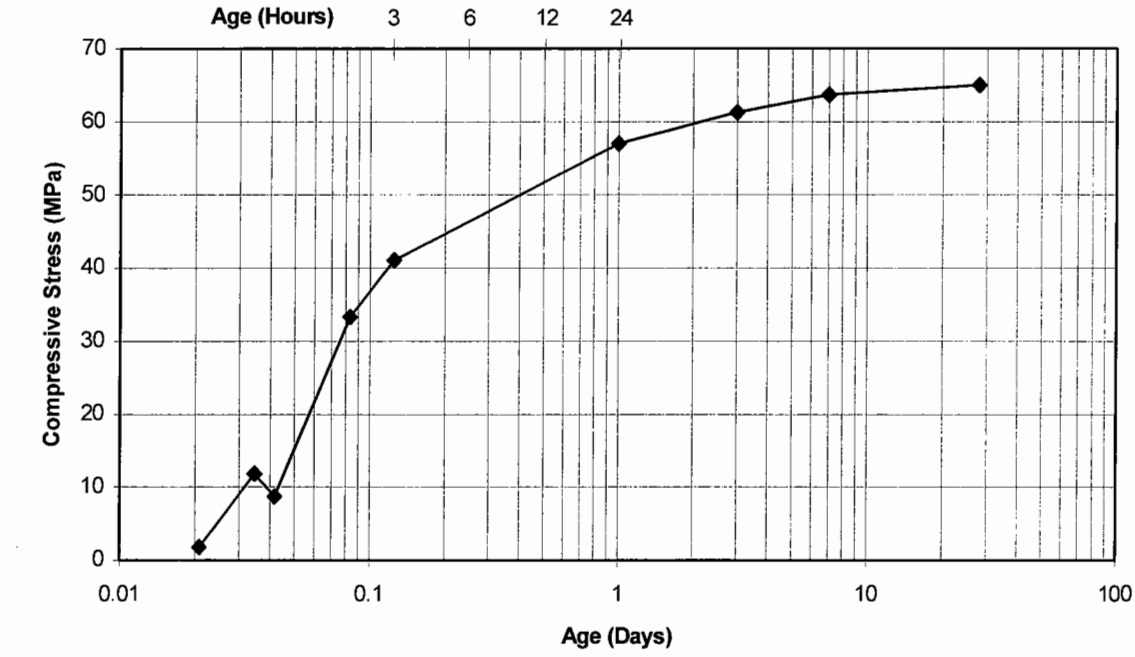

Figure 7.8: Development of compressive strength of the MPC mortar

Static Modulus and Poisson's Ratio

The static modulus and Poisson's ratio were determined by the same method used to measure the elastic properties of mortars A and B. A description of this test method and an illustration of the apparatus is given in Appendix A.3. The development of the static modulus and Poisson's ratio with age is shown in Figures 7.9 and 7.10 respectively.

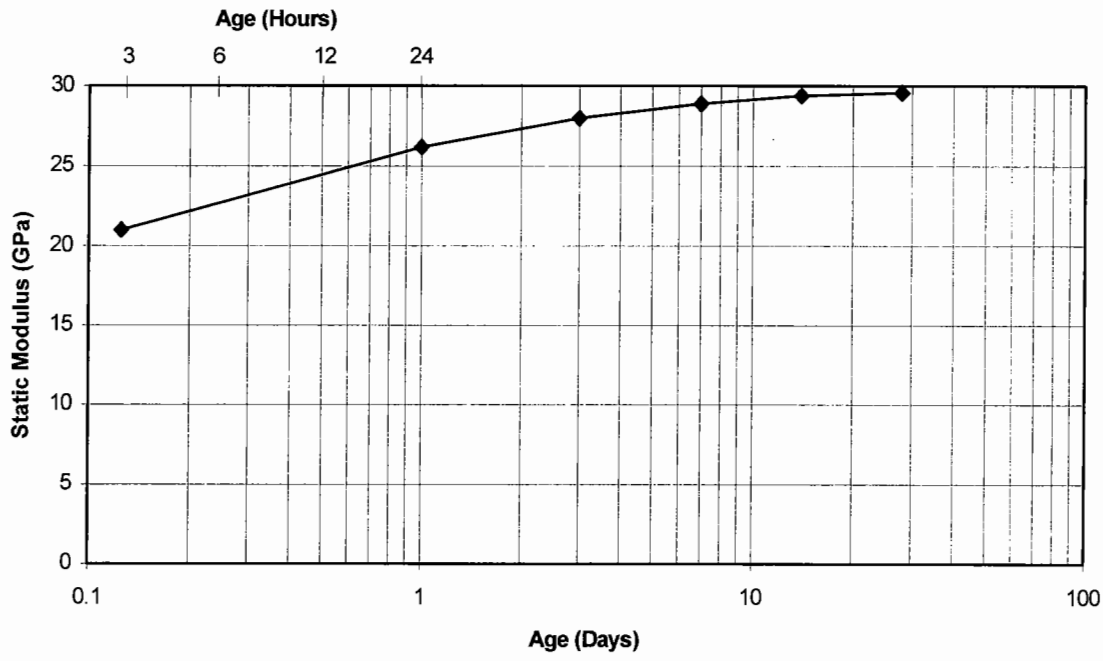

Figure 7.9: Development of the static modulus of the MPC mortar

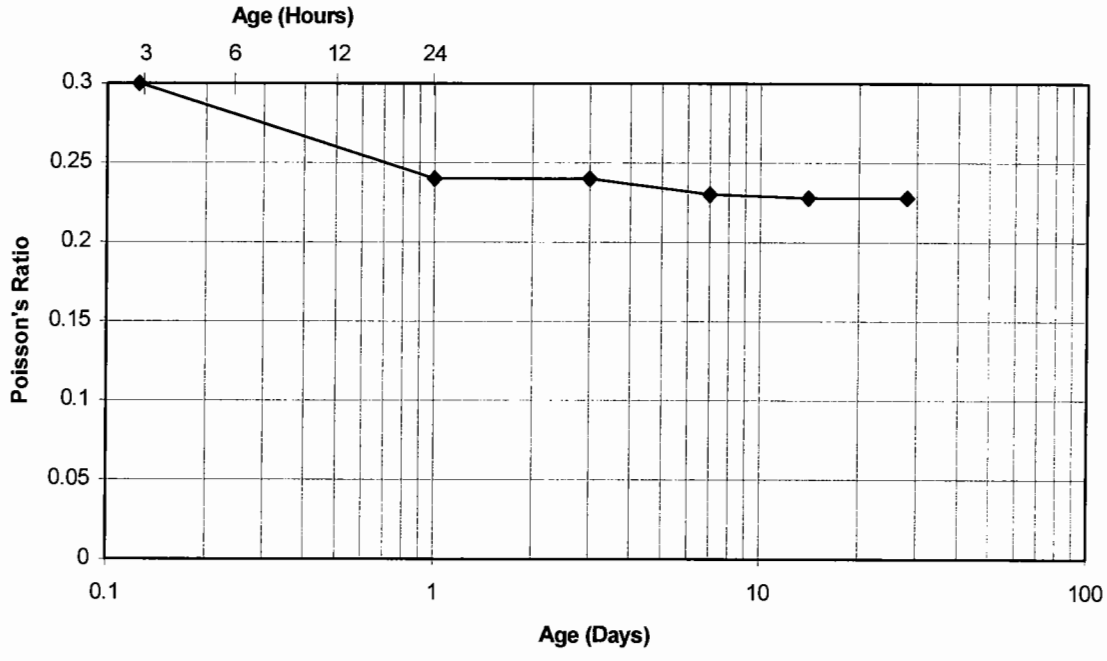

Figure 7.10: Development of the Poisson's ratio of the MPC mortar

A comparison between Figures 7.8 and 7.9 reveals that the compressive strength and the static modulus develop at approximately the same rate. However, the static modulus at an age of 3 hours was found to be 21.6GPa which increased to 29.5GPa after 28 days. These values are greater than the elastic properties of mortar A so it

expected that the stress that develops in the MPC mortar in a road ironwork installation would be larger than previously considered. This was discussed in Section 7.3.3.

Shrinkage

Samples of the MPC mortar were cast into prisms and stored at a constant temperature of 20°C to monitor the shrinkage as previously carried out with mortars A and B described in Section 2.2.1. The strain induced by shrinkage over time is shown in Figure 7.11. These results illustrate that there was very little shrinkage and the strain induced at an age of 28 days was 23 microstrain which satisfies this criterion.

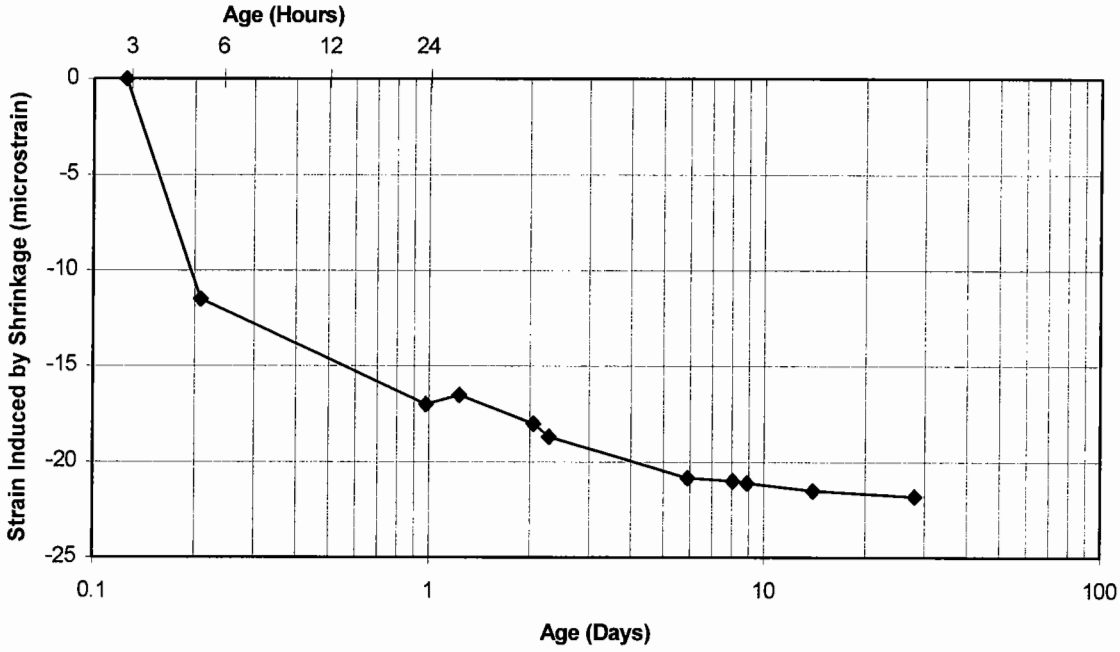

Figure 7.11: Average shrinkage measurement of MPC mortar

Durability

No experiments were carried out to assess the resistance of the MPC mortar to environmental conditions. However, other research into the performance of this material has revealed that the strength was virtually unaffected by a series of 30 freeze/thaw cycles [52]. Additionally, there was little evidence of damage to samples

immersed in a sulphate solution [52] so it could be inferred that the MPC mortar is able to withstand the environmental conditions present within a highway.

7.6 Laboratory Test Facility Experiments

Two configurations were installed in the laboratory test facility involving use of the revised design of ironwork and the MPC bedding material. These experiments allowed a study of the in-situ strains in the bedding layer and the surface displacements that are induced by an applied load. This data was compared to previous bedding configurations to assess any improvements.

The depth of the revised design of ironwork frame was 100mm so an additional course of brickwork was added to each chamber to allow 10mm and 25mm bedding thicknesses to be placed on the installations with stiff and soft foundations respectively. The 25mm bedding thickness was achieved by cutting 15mm from the bricks before laying. The two-dimensional finite element analysis indicated that a 10mm layer of bedding experiences a larger tensile stress than a 50mm thick layer so it would be more likely to crack. A laboratory investigation of the peak strain magnitudes in a 10mm layer would indicate the likelihood of this occurrence. The 25mm bedding layer provided a comparison to the previous configurations. Embedment strain gauges were installed in the bedding and ordinary strain gauges were attached to the surface of the mortar. The same instrument configuration was used in both installations and a plan view is illustrated in Figure 7.12. The response of both installations was studied under the rolling wheel and stationary platen as used previously. A description of these test methods is given in Section 4.6 and an illustration of the wheel positions is shown in Figure 4.24.

The MPC mortar was found to be easy to manipulate by virtue of its constant workability. Bedding mortars used in previous reinstatements stiffened considerably during their workable life so a large compactive effort was required to tamp the frame down to the appropriate level. However, it was found that the 25mm thickness of the MPC mortar began to flow into the chamber before hardening. It was thought that a lower slump value would have prevented this occurrence. Later discussions with the

manufacturer revealed that a lower slump value could be achieved by reducing the water content in the mixture and it was claimed that this would also increase the tensile strength.

The ironwork frame was installed within nine minutes of adding the water to the mixture. It hardened approximately three minutes after completing each reinstatement so the duration of the workable life was sufficient, although this may not be so if the material was manually mixed.

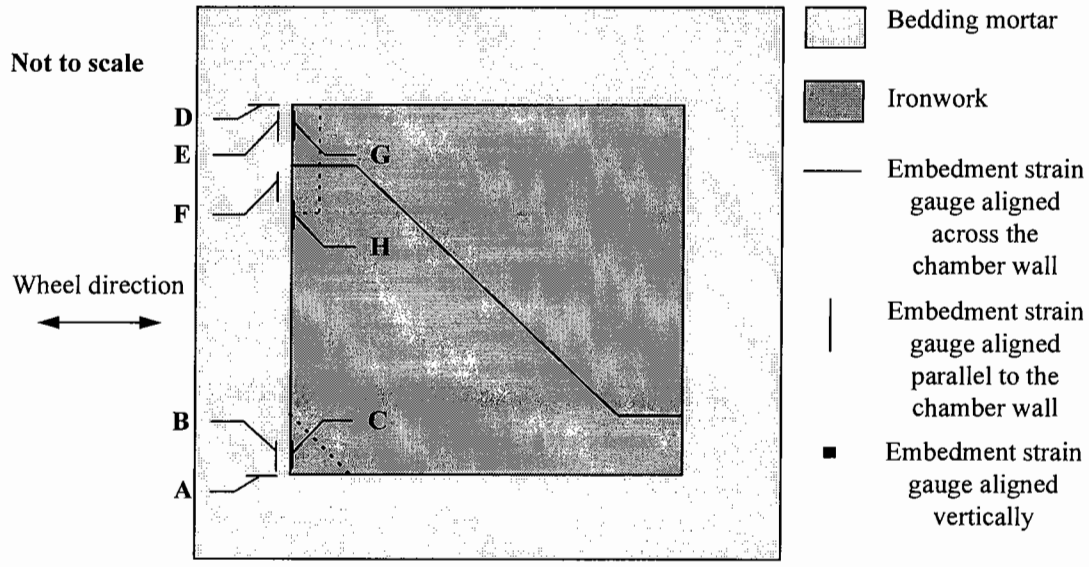

These instrument labels will be prefixed by T5 to denote Test 5.

Figure 7.12: Plan view embedment strain gauge layout used for the revised ironwork design and MPC mortar configurations (Installations 9 & 10, Table 4.4)

7.6.1 Rolling Wheel Test Results

Bedding Material

The strain measured by gauge T5-A when the wheel was positioned in Track 4 is illustrated in Figure 7.13. These measurements are comparable with gauge T2-C which was installed in the 25mm bedding thickness used in Test 2 (Figure 5.19).

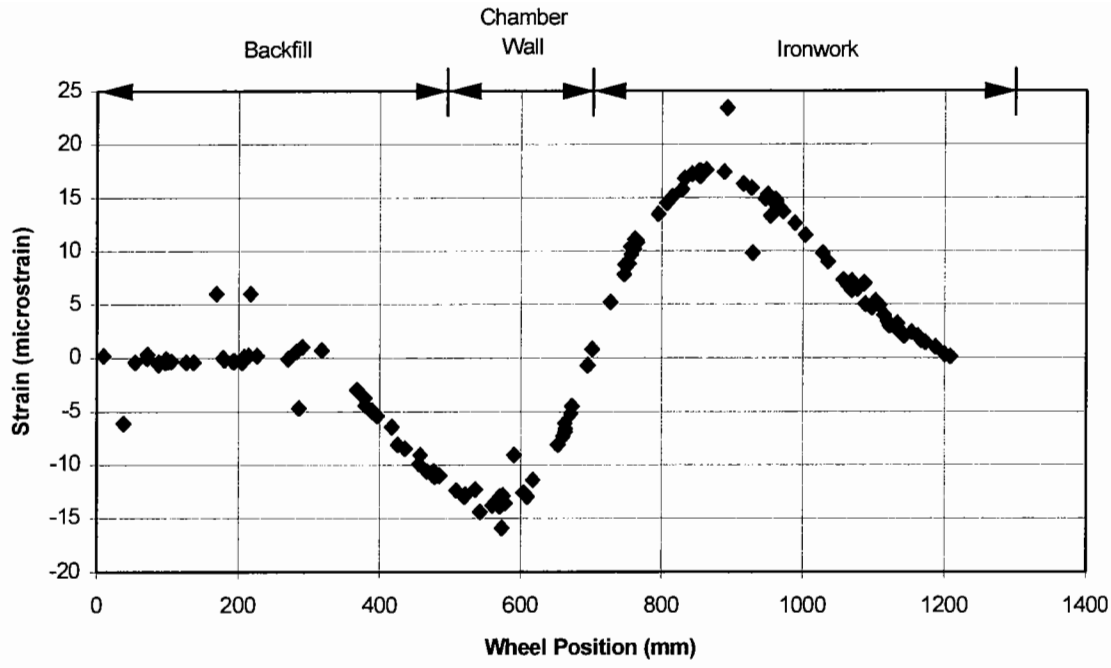

Figure 7.13: Horizontal strain measured by gauge T5-A in the configuration with a 25mm thick bedding layer (No. 10) when loaded in wheel Track 4

The results illustrate a slightly different trend to the strain recorded by gauge T2-C. Compressive strains were measured by gauge T5-A as the wheel passed over the chamber wall before measuring tensile strains as the wheel moved onto the ironwork cover. The largest tensile strain measured by gauge T5-A was 17 microstrain which occurred when the wheel was located on the corner of the ironwork cover above this instrument. The strain measured at this position in Test 2 was 53 microstrain although a lower magnitude of strain was calculated at this point in the three-dimensional finite element analysis.

Embedment strain gauge T5-B and gauge T5-C mounted on the surface of the bedding material were aligned to measure strain parallel to the chamber wall. These instruments were mounted underneath the bottom left hand seating as indicated in Figure 7.12. The output recorded from these instruments is shown in Figure 7.14.

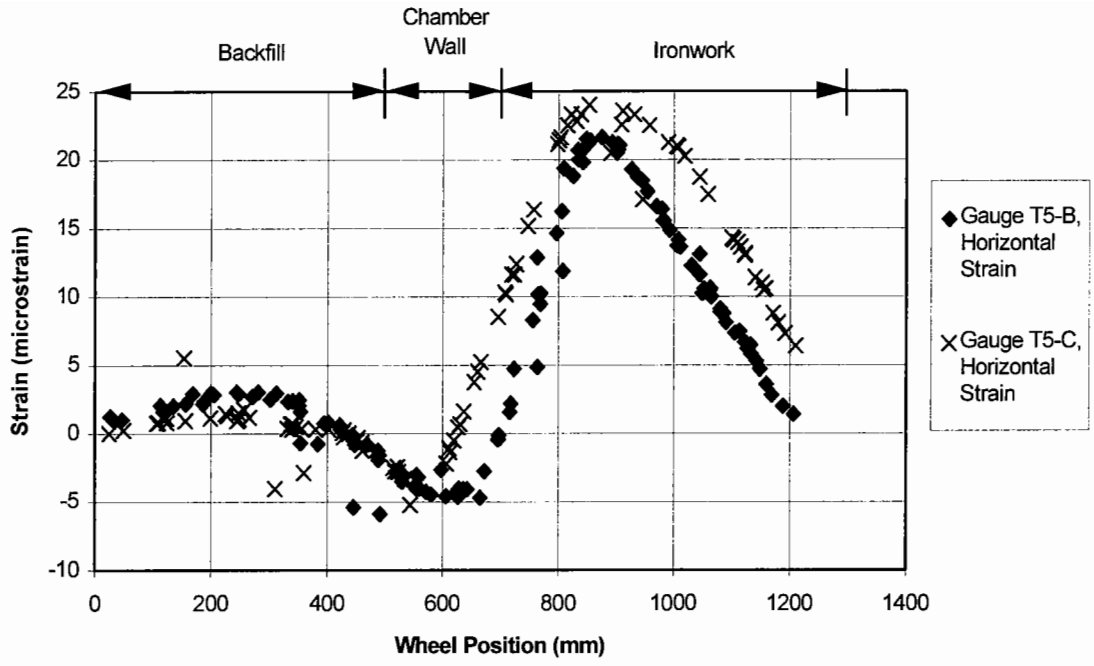

Figure 7.14: Horizontal strain measured by gauges T5-B and T5-C in the configuration with a 25mm thick bedding layer (No. 10) when loaded in wheel Track 4

The results indicate that the peak strain measured by both instruments is approximately 22 microstrain. The same configuration used in Test 3 (No. 6, Figure 5.31) illustrated that the strain on the surface of the bedding was significantly greater than at a distance of 20mm behind the surface. These results suggest that the revised design of ironwork provides a better distribution of the load onto the bedding around this seating. Gauge T5-B also recorded a lower strain than gauges T2-D and T3-D in the previous experiments with 25mm thick bedding layers in the laboratory test facility. However, this is partially attributable to the larger static modulus of the MPC mortar.

Embedment gauge T5-D was placed under the top left hand corner as shown in Figure 7.12. This instrument recorded a peak strain of 12 microstrain when the wheel was positioned in Track 2. The bearing area of the seating above this instrument was larger than the seating above embedment strain gauge T5-A which is thought to be attributed to the lower peak strain measurement as considered during the description

of the Test 1 results. Additionally, instruments T5-E, F, G and H mounted in the bedding and on the surface which were aligned to measure strain parallel to the chamber wall under the larger seating also recorded lower peak magnitudes of strain when compared to gauge T5-B.

The instruments at the same positions in the 10mm thick bedding layer all recorded their peak strains at the same wheel positions as the 25mm thick bedding layer. However, the magnitude of these strains was consistently lower than those recorded in the 25mm thick bedding layer. The experimental results presented in Chapter 5 and the three-dimensional finite element analyses indicated that the bedding layer bends under an applied load resulting in tensile strains. It is thought that the MPC mortar may have formed a stronger bond with the iron and brickwork and hence increased the friction at these interfaces. The boundary effect may have influenced the behaviour of the entire bedding layer. This would be most noticeable in thin layers as the top and bottom faces of the layer are closer together than thicker layers. The restraint at the boundaries is therefore considered to have reduced the tensile strains at the centre of the layer, which is where the embedment gauges were located.

Backfill Material

The gauges at the bottom of the DBM layer recorded a similar trend as seen in the previous experiments (Figure 5.22). The revised design of ironwork and bedding mortar had no effect on reducing the strain in this layer close to the manhole. Surface deflection measurements of both installations were recorded at the positions illustrated in Figure 5.24. The resulting deflection profile was similar to those previously seen in configurations with cementitious bedding layers (Figure 5.25).

A heave of 0.01mm was recorded above the centre of the chamber wall when the wheel was positioned on the cover. Additionally, a peak horizontal movement of 0.015mm of the frame web was also recorded. The frame web moved closer to the centre of the manhole. Both of these results illustrated the same pattern as seen previously as shown in Figures 5.26 and 5.27. The stronger bond between the MPC mortar and the other materials, which was greater than seen with mortars A and B

may have also restrained the frame from twisting. Although these movements were lower than previously measured it is still considered that it may cause damage to the backfill material. It appears that the alterations to the design of the ironwork were not entirely successful.

7.6.2 Repeated Load Test Results

Repeated load plate tests were carried out on each installation with the platen placed above the bottom left hand corner (Figure 7.12). The applied load was oscillated between 0 and 45kN for 1 million cycles and readings were taken from the instruments every 100,000 cycles. It was considered that a slightly larger load than previously applied would have a greater damaging effect on the installations. However, there was no change in the magnitudes of strain measured by the instruments during these tests and an inspection of the bedding layers at end of each test revealed no evidence of cracking.

7.6.3 Summary of Laboratory Test Facility Experiments

Overall, the magnitudes of the tensile strains recorded during the rolling wheel tests were lower in the MPC mortar when compared to the experiments where the bedding layer was formed with mortars A and B. This may be due to the revised design of ironwork providing a better load distribution although the static modulus of the MPC mortar was greater than the other mortars which would have resulted in smaller strains. Nevertheless, the mature MPC mortar demonstrated that it can withstand a tensile strain of over 200 microstrain before cracking as illustrated in Figure 7.7 and the largest in-situ measurement was 22 microstrain. This indicates that the MPC mortar has a greater resistance to cracking under the loads applied in the laboratory test facility than the other materials. This material should result in a lower incidence of failure of road ironwork installations.

7.7 Field Experiments

7.7.1 Description

The laboratory test facility was designed to provide a close simulation of field conditions. A discussion of the simulative features included in the apparatus was described in Section 4.2.3. However, it was thought that the pit walls may have influenced the behaviour of the backfill and possibly the bedding layer due to their proximity. Further experiments were carried out to study the behaviour of the bedding layer in two installations built in the field. This provided a comparison to the laboratory data so an assessment of the simulative properties could be made. Two chambers were built 10m apart on a private road at the Stanton foundry near Ilkeston. They were constructed from pre-cast concrete sections founded on an in-situ concrete slab. Both chambers complied with Nottinghamshire County Council specifications [32]. An illustration of the chambers is shown in Figure 7.15.

All dimensions in mm

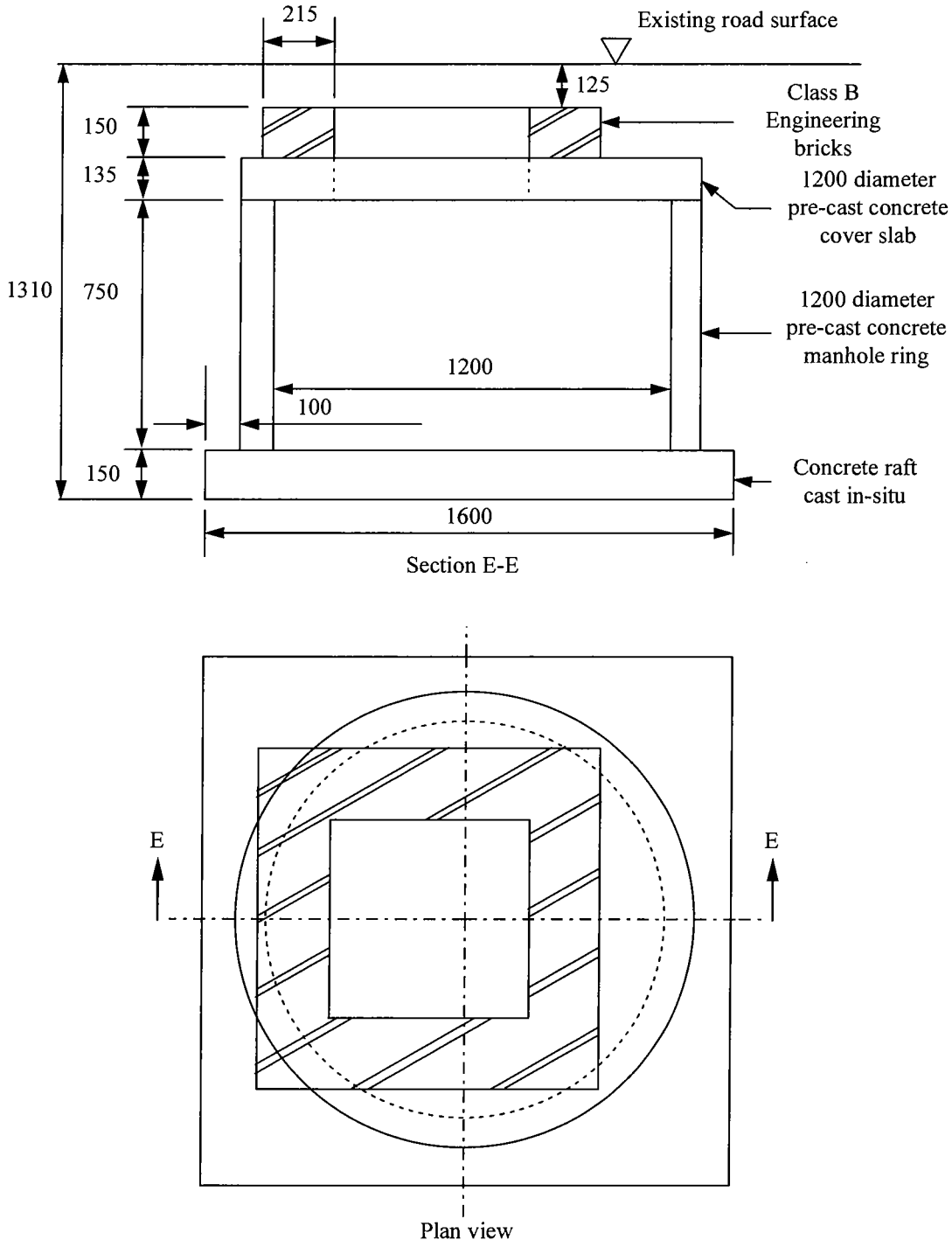

Figure 7.15: Illustrations of the manhole chambers built for the field experiments

Two road ironwork configurations as tested in the laboratory were installed on top of the chambers. These were a standard Chieftain 600 x 600 x 100m deep frame bedded

on a 25mm thickness of mortar A, and the revised design of ironwork bedded on a 25mm thickness of the MPC mortar. Each chamber was backfilled with Type 1 sub-base and surfaced with a 150mm thickness of 30/14 HRA. Discussions with highway engineers revealed that these backfill materials and thicknesses are often used around manholes in public highways. Unfortunately, the configuration installed with bedding mortar A was damaged during the compaction of the bituminous material which produced several cracks in the bedding layer. It was thought that the vibrating roller used to compact the HRA accidentally struck the external face of the bedding and ironwork web. The MPC bedding layer was found to be undamaged during an inspection before testing. Embedment strain gauges were placed in the bedding layer at some of the locations used in the laboratory experiments. An illustration of these positions is shown in Figure 7.16. The arrangement was identical for both installations.

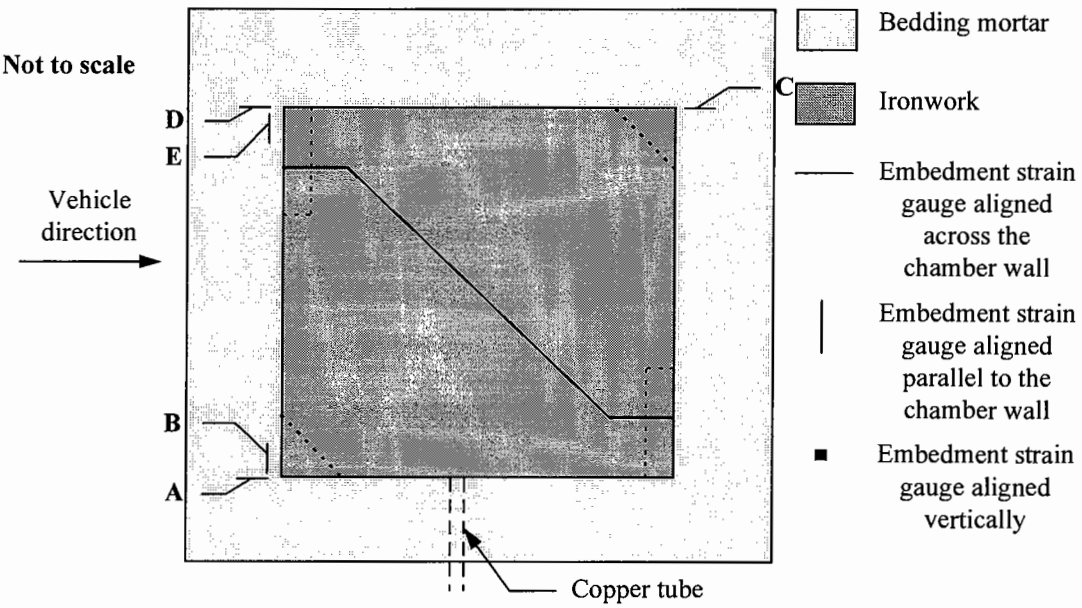

These instrument labels will be prefixed by F to denote field test.

Figure 7.16: Plan view of the embedment strain gauge layout used in the field installations

A length of copper tube was also installed in the bedding layer in between seatings. This allowed the wires from the instruments inside the manhole to be connected to a

data acquisition system at the roadside. This was the same system as used in the repeated plate load tests in the laboratory test facility.

7.7.2 Results

The chambers were initially loaded by a light goods vehicle. The first experiment involved positioning the offside rear wheel of the vehicle on the corner of the cover above gauges F-A and F-B. The weight carried by the rear axle was extracted from the vehicle handbook and was found to be 790kg. The vehicle was moved off the ironwork and the strains measured by the instruments were recorded. The output recorded by gauges F-A and F-B in the installation bedded with the MPC mortar is shown in Figure 7.17.

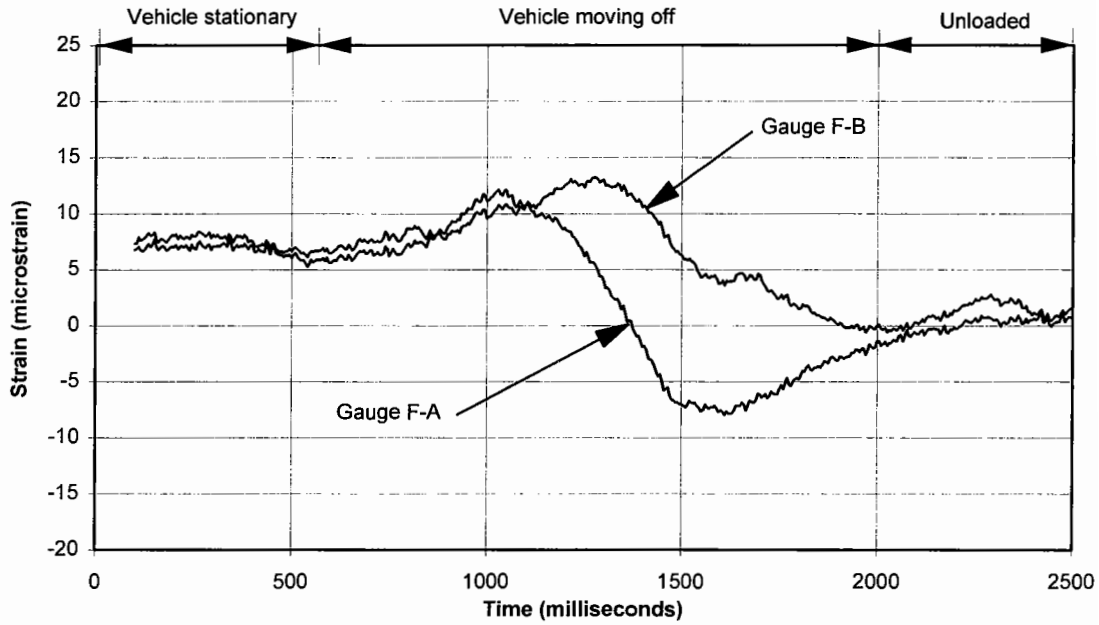

Figure 7.17: Horizontal strain measured by gauges F-A and F-B

The results illustrate that a tensile strain of 7 and 8 microstrain was recorded by gauges F-A and F-B respectively when the vehicle wheel was stationary on the cover. These strain measurements increased as the vehicle moved off the cover before diminishing when the cover was unloaded. It is considered that vehicle load may have redistributed over the rear axle when the vehicle accelerated which induced the slightly higher strain. The magnitudes of the strain were small but the difference in

the measurements between gauges F-A and F-B was relative to those measured in the laboratory test facility.

The experiment was repeated on the installation bedded with mortar A but the tensile strain magnitudes were greater than 200 microstrain. It was thought that the cracks in this bedding layer significantly affected its behaviour so the results could not be compared to the laboratory experiments.

Subsequent field experiments involved loading the manhole with an articulated heavy goods vehicle with five axles. The vehicle was loaded with iron pipes which resulted in a total weight of 35.8 tonnes. The combined weight of the front two axles and rear three axles was measured separately. These weights were found to be 12.2 and 23.6 tonnes respectively. The width of the trailer tyres were 300mm whereas the tyre used in the laboratory test facility was 215mm wide. It is thought that the trailer tyres would not produce the same concentration of load as experienced in the laboratory test facility and may account for discrepancies between the two sets of results.

The vehicle was driven over the installation so that the edge of each tyre ran over half of the cover and above gauges F-A and F-B. This was equivalent to wheel Track 4 as used in the laboratory test facility (Figure 4.24). Further experiments involved loading the other half of the cover which induced the greatest strain in the bedding at the location of gauges F-C, F-D and F-E which was equivalent to wheel Track 2 (Figure 4.24). These experiments were repeated at speeds of approximately 2, 5, 20 and 30mph. The vehicle was travelling at an approximately constant speed during all of these experiments. A study of the results revealed that the trailer wheels induced the largest strains. The strains measured by gauge F-A when the trailer wheels passed over the cover at 5mph directly above this instrument are shown in Figure 7.18.

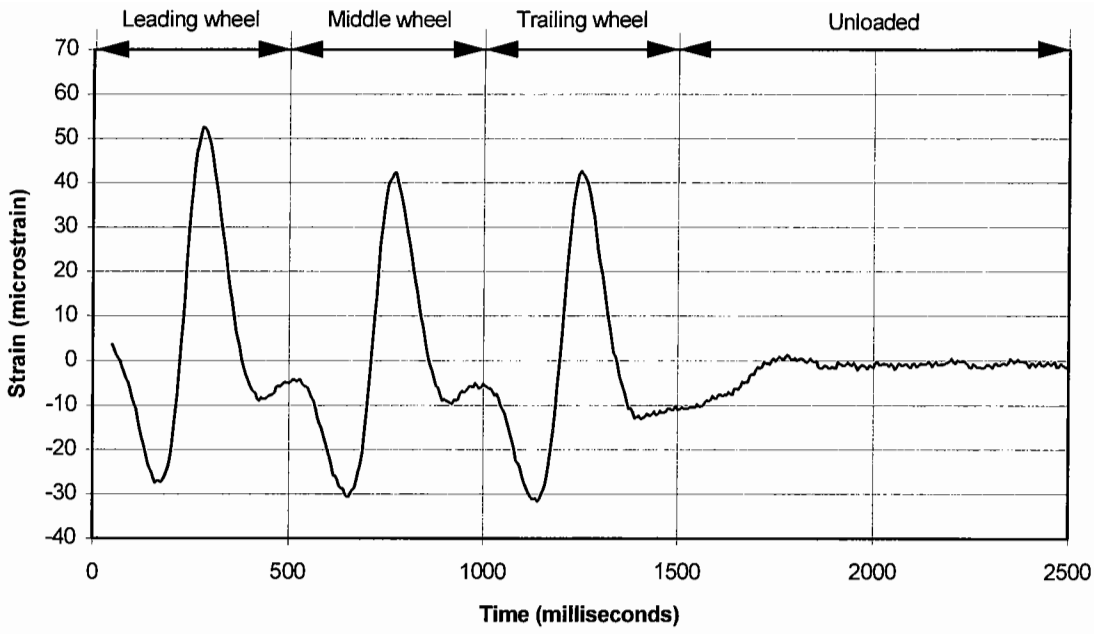

Figure 7.18: Horizontal strain measured by gauge F-A when the vehicle was travelling at 5mph

The largest peak tensile strain measured by gauge F-A was induced by the leading trailer wheel. This instrument recorded a compressive strain followed by a tensile strain as each wheel passed over the cover. The peak value of these strains were 53 and 31 microstrain respectively. These were the largest magnitudes of tensile strain measured in this installation. A similar trend was recorded by this instrument in the laboratory test facility experiments with this configuration as shown in Figure 7.13. The strain measured by gauge F-B during this test is shown in Figure 7.19.

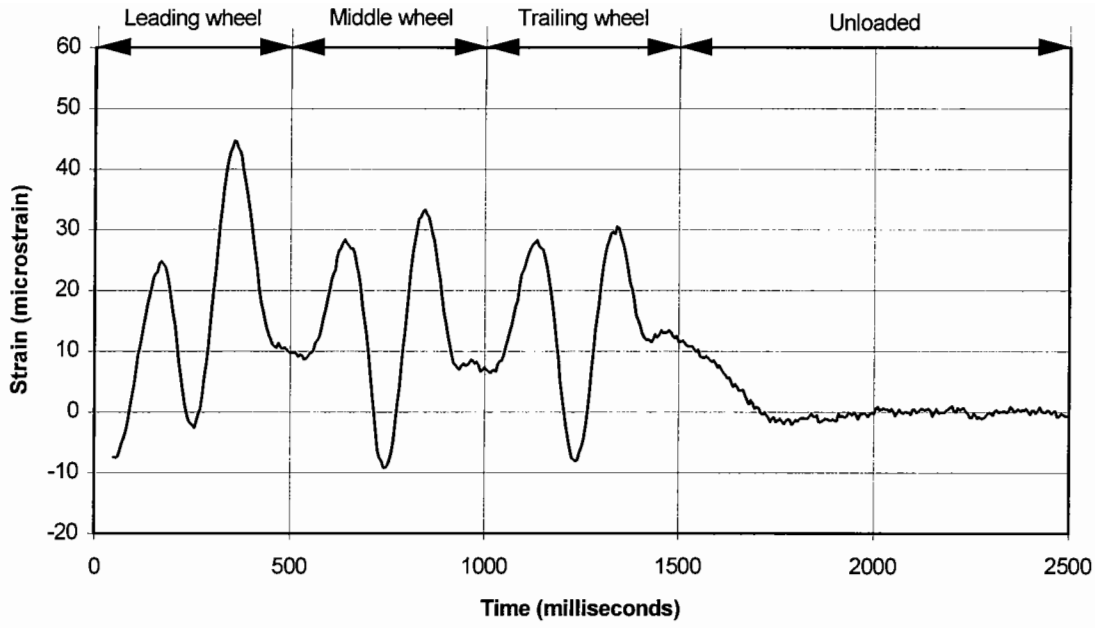

Figure 7.19: Horizontal strain measured by gauge F-B when the vehicle was travelling at 5mph

The largest tensile strain measured gauge F-B also occurred when the installation was loaded by the leading trailer wheel which was 44 microstrain. The pattern of the results illustrates that each wheel produced two peak tensile strains separated by a small compressive strain. The laboratory test facility results illustrated that a peak tensile strain rapidly developed as the wheel moved onto the cover before diminishing as the wheel moved away from the leading edge as shown in Figure 7.14. However, the wheel did not travel over the full width of the ironwork cover so the second tensile strain peak was not observed.

Gauge F-C was located under the top right hand corner as shown in Figure 7.16. The cover seating in this corner was of the same design as the seating above gauges F-A and F-B. The strain measured by gauge F-C when the trailer wheels moved over this corner at 5mph is shown in Figure 7.20.

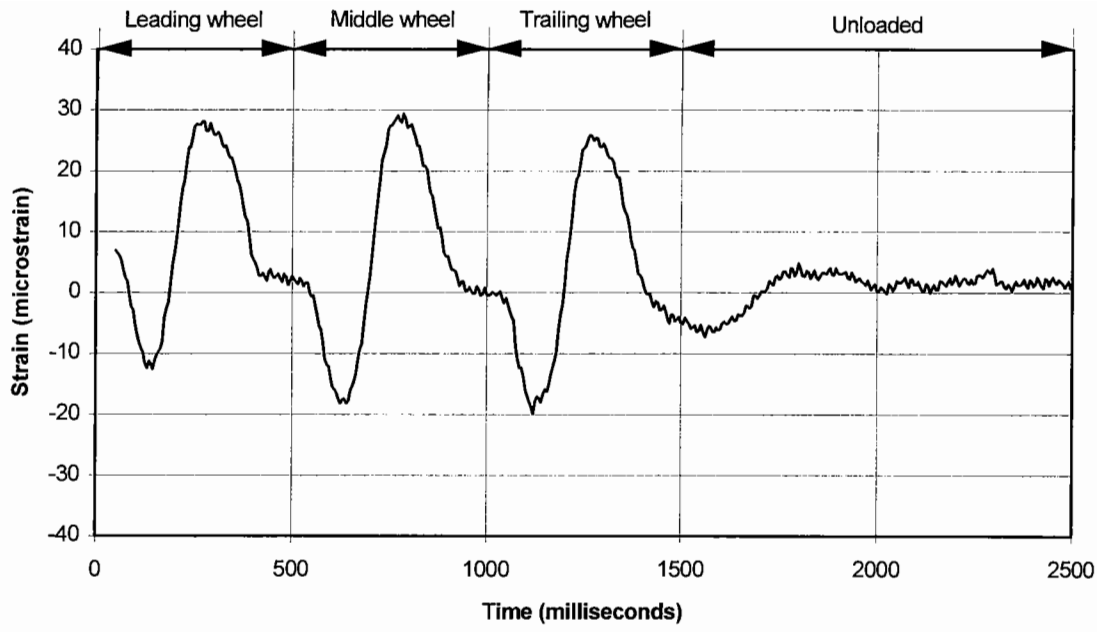

Figure 7.20: Horizontal strain measured by gauge F-E when the vehicle was travelling at 5mph

The results broadly illustrate the same pattern as recorded by gauge F-A but the magnitudes were lower. The field observations of failed installations has revealed that the leading edge of the bedding exhibits more damage than the trailing edge. A comparison between the peak tensile strains measured by the gauges F-A and F-C indicates that this would be a likely occurrence in this installation.

Gauges F-D and F-E were located underneath the seating with the largest bearing area. These instruments recorded a similar pattern of results as gauges F-A and F-B but the peak magnitudes were lower. This was the trend observed in the laboratory where the peak tensile strain measurement was inversely proportional to the bearing area of the seating.

The peak magnitudes of the strain generally remained constant at all vehicle speeds. Video footage was recorded as the vehicle passed over the ironwork. This was later studied and it was found that the vehicle wheels did not lift off the cover at the higher speeds.

7.7.3 Summary of the Field Experiments

The pattern of the strain measurements in the field installation generally reflects the trends seen in the laboratory test facility so it is considered that the apparatus provided a close simulation to field conditions and the results can be quoted with confidence. However, there were discrepancies in the magnitudes between the two sets of results. This may be attributed to a difference in the load magnitude which was considered to be greater in the field and a difference in the size of the tyres used in the two experiments. This would have spread the vehicle load over a larger area and reduced the concentration of load onto a single seating.

7.8 Improvements in Reinstatement Procedure

A review of the relevant literature revealed that a failure threshold was not clearly defined. It is considered that expressing failure purely as a settlement of the ironwork does not adequately describe the failure characteristics as described in Section 1.2 and observed on the A1 at Sandy. It is considered that road ironwork installations should be reinstated when they present a severe impairment to the riding quality. This occurs when the bedding material deteriorates allowing the ironwork to settle and move, and the surrounding bituminous material is heavily cracked. The settlement threshold was defined as 20mm in Preferred Method 7 [1]. This was chosen by judgement but, nevertheless, it was subjectively considered to be the extreme limit of riding quality and should be included in a revised failure criteria. The deterioration of the bituminous material is difficult to quantify but the disintegration of this layer around a manhole also affects the riding quality and should also constitute as a failure criterion. Movement of the ironwork generates a distinctive noise when loaded by vehicles. Any noise associated with a road ironwork installation is considered as another failure criterion. It is thought that failure should be defined when any of these characteristics is evident.

The research has indicated failure mechanisms in the bedding and bituminous materials. Some of these have been mitigated in moderate conditions by the development of an improved bedding material and ironwork design. However, the laboratory and theoretical results have illustrated that some configurations yield lower

stress and strain magnitudes in the bedding and the backfill than others. These observations could be included into a method of reinstatement.

The laboratory test facility and three-dimensional finite element analysis indicated that the smallest stress and strain magnitudes developed in the 50mm bedding layer. Unfortunately, the required bedding thickness is chosen so that the ironwork is installed at the same level as the surrounding carriageway so it would be impractical to specify this bedding thickness for all installations.

A vertical heave of the backfill above the centre of the chamber wall was still observed during the laboratory test facility experiments with the MPC mortar and revised ironwork design. This was thought to be related to the frame twisting under an applied load which was considered to damage the bituminous backfill material. Negligible heave of the backfill and only a small horizontal movement of the frame web were measured in the configurations with an additional layer of bedding mortar placed above the frame flange. This addition could easily be incorporated into reinstatement practice. However, the finite element analysis indicated that the inclusion of mortar above the flange increased the peak tensile stress magnitude on the surface of the bedding beneath the flange. Although the MPC did not exhibit sufficient strength to resist cracking in a combination of the worst bedding configuration and load case it is considered that it could withstand moderate conditions, so a layer of mortar above the flange could be included provided that this material was used.

Field experiments revealed a difference in the effective in-situ stiffness between a manhole wall and the surrounding pavement which was considered to be another source of cracking in the bituminous layer. This was also identified in the laboratory test facility and was thought to be partially attributable to the large strain in the bituminous backfill close to the manhole. Investigations were made into providing a better compatibility of stiffness by using proprietary HDPE spacers to form the bedding layer but this approach was unsuccessful as described in Section 5.5. The most effective method of reducing the difference in the overall stiffness was by

cutting through the bituminous layer above the outside edge of the chamber. This allowed the bituminous layer of the backfill and that above the chamber to displace independently. Unfortunately, this approach still resulted in a difference in the strains measured by the two instruments in the backfill but did have a beneficial effect. It is considered that placing a cut in the bituminous material at this position and filling with a flexible sealant is the most practical method of reducing the large tensile strains that develop in this material around manholes and could also be applied in reinstatement practice.

These observations and other examples of good working practice either developed in the laboratory or seen in the field have been used to develop a method of reinstatement. This is presented in Appendix D.

7.9 Summary

A specification for an improved bedding material and revised ironwork design were developed from the results of the previous research. An MPC mortar was developed to satisfy the suggested criteria but it was found that the workable life was too short and the tensile strength was too low. However, experiments in the laboratory test facility indicated that the in-situ behaviour was an improvement on the other products studied in this research so it is considered to be better suited for use as a bedding material. Additionally, the manufacturer claimed that this material could be further developed to improve its performance.

Refinements were made to the ironwork frame with the objective of providing a better distribution of load onto the bedding material and increasing the torsional rigidity to restrain the frame from twisting. Twisting was considered to have a detrimental effect on the bituminous backfill. Laboratory experiments demonstrated that a better load distribution was achieved but twisting of the frame still occurred although this could be mitigated by placing a layer of bedding mortar above the flange.

Further experiments were carried out to study the behaviour of a MPC bedding layer in field conditions. The measurements were compared to those from the laboratory

test facility to assess the simulative accuracy of the apparatus. It was found that the strains measured in the laboratory followed the same trend as those measured in the field. Discrepancies in the magnitudes were considered to be attributable to the difference in the load regimes but it was considered that the laboratory test facility provided a reasonable simulation of field conditions.

Overall, the experimental evidence has indicated that a combination of the MPC mortar and the revised design of ironwork can withstand moderate loading conditions so should provide a longer lasting reinstatement, although it is doubtful whether it would resist cracking in a combination of the worst bedding configuration and load case.

8. Discussion, Conclusions and Recommendations for Future Research

8.1 Laboratory Test Facility

This research involved the construction of a major laboratory test facility for studying the response of typical road ironwork installations under simulated traffic loading. An understanding of the resilient behaviour was derived from measurements of strain and displacement in the bedding and bituminous materials within and around each installation. These findings were used to identify likely failure mechanisms. It was important to ensure that the laboratory test facility was simulative of field conditions. Field experiments were carried out to study the behaviour of installations in public highways and these characteristics were included in the design of the apparatus. Later experiments involved constructing two manhole chambers on a private road at the Stanton foundry near Ilkeston and installing identical bedding configurations to those tested in the laboratory. Unfortunately, one of the installations was damaged during the compaction of the backfill material. The undamaged installation was loaded by a heavy goods vehicle and the response of the bedding material was recorded. It was found that there was a reasonable comparison between the two sets of results so it is considered that the laboratory test facility provided an adequate simulation of field conditions.

8.2 Finite Element Analysis

The laboratory test facility only provided measurements of strain at discreet positions within each installation. It was possible that the gauges may not have been located at the positions where the largest resilient strains developed. This was investigated by three-dimensional finite element analysis. Models were created using the same geometry as installed in the laboratory test facility. These analyses provided calculated values of strain at all points and it was found that some of the embedment strain gauges used in the laboratory had been installed at the positions of the peak strain. Additionally, the measured and calculated values of strain provided a close comparison so confidence could be placed on these results.

The majority of bedding materials are cementitious and it is generally considered that such materials fail at a limiting stress [8]. The analyses allowed an investigation of the principal stresses in the bedding layer. These data were used to support the findings of the laboratory experiments in the identification of failure mechanisms and provide an estimation of the stress magnitudes that the bedding material has to withstand. Several causes of failure were identified in the bituminous surround and bedding materials. These mechanisms compared favourably with field observations carried out during this research and are described below.

8.3 Mechanisms of Failure in the Bedding Material

Typical materials are two-component mortars that have to be mixed before use and have a short workable life which is often less than 15 minutes. Additionally, cementitious bedding materials progressively stiffen throughout this period. These bedding materials may often harden before the ironwork frame has been set at the desired level, so uniform support to the frame flange is not reliably achieved. It is difficult to mix and place a material with these characteristics so good quality workmanship is rare. This was considered to be the cause of the high incidence of failure of road ironwork installations in practice. However, reinstatements that were installed to a high quality of workmanship on the A1 Trunk road at Sandy still failed after a relatively short period so poor workmanship is not the sole cause of failure.

The laboratory experiments and finite element analyses revealed that a region of tensile strain and stress developed in the horizontal plane in the bedding material immediately underneath the cover seatings. Vertical cracks developed at these locations in some of the repeated plate load tests carried out in the laboratory test facility. Cracks at similar positions were noticed in field studies including those on the A1 Trunk Road at Sandy. These instances occurred when the ironwork was bedded with cementitious mortar A. Later experiments at the Stanton laboratory revealed that the cracks developed when the calculated value of stress at this position was equivalent to the tensile strength of the material. Laboratory experiments indicated that it was possible for this material to suffer failure after several load cycles

at the calculated magnitude of tensile stress in the bedding layer that is likely to be induced by passing vehicles.

Other laboratory experiments were carried out to study the effects of shrinkage on cementitious bedding layers. These experiments revealed that all the configurations bedded with mortar A developed cracks within 7 days, whereas a configuration using mortar B, which contained fibre glass strands, did not develop any cracks after 3 months. Load was not applied to these specimens during the monitoring period. Some of the cracks caused by shrinkage appeared in between the cover seatings of the ironwork frame. Cracks of this nature were also noted in field observations. The shrinkage of both cementitious materials was later quantified and it was found that mortar A had a far greater ability to shrink than mortar B.

The laboratory and three-dimensional finite element analyses results indicated that a high concentration of load developed underneath the cover seatings of the ironwork frame. This was considered to cause the region of high tensile stress and strain at this point. Ironwork units with large cover seatings resulted in a lower magnitude of tensile strain in laboratory experiments.

The following conclusions can be drawn about the behaviour of the bedding material:

1. Materials with a short workable life and progressive hardening are difficult to mix and place before setting so good quality workmanship is difficult to achieve.

2. The magnitude of tensile stress induced by an applied load in the bedding underneath the ironwork cover seating is sufficient to cause a tensile failure.

3. Cracks can form in the bedding layer due to shrinkage in addition to the load associated mechanism.

4. The magnitude of the tensile stress is inversely proportional to the area of the cover seating on the ironwork frame.

8.4 Mechanisms of Failure in the Bituminous Material

Severe cracking of the bedding material was observed in some field installations. In these instances, sections of the bedding had completely disintegrated which removed the support for the bituminous surfacing. Subsequent loading of the bituminous surfacing was considered to have induced cracks in this layer.

Field measurements revealed that the in-situ effective stiffness of a pavement is greater around a manhole than at some distance away. This effect was also seen in the laboratory test facility. Instruments were installed 25mm from the bottom of the DBM layer in the laboratory test facility. Readings from these instruments indicated that the strain closer to the manhole was far greater than at some distance away. This was thought to be partially attributable to the difference in in-situ effective stiffness causing flexure of the DBM. These results indicated that fatigue cracking of a bituminous layer was likely to develop around a manhole. Experiments were carried out in the laboratory test facility using proprietary HDPE spacers to form the bedding layer. This product has a significantly lower modulus of elasticity than cementitious mortars so it was considered that it would reduce the difference in the in-situ effective stiffness between the installation and the pavement. However, the spacers only covered half the width of the chamber wall and did not reduce the large tensile strain in the DBM layer. The most effective method of ameliorating this effect was to cut through the bituminous surfacing above the outside edge of the chamber. This allowed the bituminous surfacing above the chamber to displace independently from the rest of the backfill. However, only a slight reduction in the strain measurement was recorded by the instrument in the bottom of the DBM layer close to the manhole.

The field and laboratory experiments also revealed that the strength of the bond between the ironwork and bituminous material is weak. This would allow the bituminous layer to rotate at this boundary under an applied load. A rotation at one end of a beam on an elastic foundation would increase the tensile strain at the bottom of the beam. Such instances occurred immediately adjacent to a manhole which would also account for the large strain measurement at this point and increase the likelihood of cracking.

The laboratory experiments and the three-dimensional analysis revealed that the ironwork frame twists when a load is applied on the cover. This can lead to uplift of the frame flange which is also considered as another cause of damage to the bituminous backfill.

The following conclusions can be drawn on the behaviour of the bituminous material:

1. Disintegration of the bedding material removes the support to the bituminous material which can lead to damage of this layer.

2. Cracking can occur in the bituminous material around a road ironwork installation due to a difference in the in-situ effective stiffness between a manhole and the pavement.

3. A poor bond between the ironwork and bituminous material induces large strain in the bottom of the asphalt layer near the manhole which can cause cracking.

4. The current design of ironwork frame twists under an applied load and is reacted against by the bituminous backfill which can also lead to damage in this layer.

8.5 Development of Improved Road Ironwork Installations

These findings were used to develop a specification for an improved bedding material. The principal criteria were a workable life of at least 15 minutes, low shrinkage characteristics and a tensile and compressive strength of at least 8 and 40MPa respectively at three hours after mixing. The strength values were based on a cementitious material possessing a static modulus and Poisson's ratio of 21GPa and 0.14 respectively. It was considered that a bedding material with these properties could be installed in the most highly stressed bedding configuration and withstand the worst loading conditions. The design of the ironwork frame was also revised to provide a better distribution of the load on to the bedding material and increased torsional rigidity to prevent an uplift of the frame flange.

These components were installed into the laboratory test facility and provided satisfactory performance, although an assessment of the bedding material properties revealed that the mature tensile strength was no greater than 6.1MPa. It is thought that the bedding material should be able to be installed in configurations that develop moderate tensile stresses but would not be able to withstand the most extreme conditions.

Surface heave of the backfill material, thought to be induced by an uplift of the frame flange, was not mitigated with the revised design of ironwork. Previous experiments revealed that the presence of a layer of mortar above the flange was effective in restraining this movement. It is considered that the frame flange should be completely encapsulated within the bedding mortar during a reinstatement.

The following conclusions can be made on the development of improved road ironwork installations:

1. The tensile strength of the improved bedding material was too low, but is considered capable of withstanding moderate loading conditions.

2. The workable life of this material was too short, although it did remain at a constant workability during this time.

3. The material satisfied the other specified criteria which included requirements for compressive strength after three hours and shrinkage.

4. The improved design of the ironwork frame was not entirely successful, although rotations of the frame flange may be mitigated by encapsulating the frame flange within the bedding mortar.

5. The combination of improved bedding mortar and revised design of ironwork should provide improved performance and reduce the incidence of failure in road ironwork installations.

8.6 Recommendations for Future Research

The results from the experiments to assess the properties of the improved bedding material revealed some shortcomings. The most notable of these were the inadequate workable life and low tensile strength. Further developments could result in improvement of the properties of this bedding mortar so that it satisfied the criteria described in Table 7.2.

Attempts were made to reduce the magnitude of the strain that developed in the bottom of the bituminous layer and next to the chamber in the laboratory test facility. Several sources of this high strain were identified but none of the remedies were particularly successful. Further experiments could be carried out to measure the effective in-situ stiffness of a pavement around a manhole and to assess the influence of various types of bedding material. Investigations could be carried out to study the effect of HDPE spacers or other materials with a lower modulus of elasticity than cementitious mortars covering the full width of the chamber wall. This research could be carried out using the laboratory test facility without any modification.

This project has highlighted other areas of research considered worthy of investigation. Evidence from field observations and discussions with highway engineers has revealed that there is a higher incidence of failure of road ironwork installations located next to junctions and on roundabouts. This was also seen at the north manhole on the A1 trunk road at Sandy. This may be due to a larger magnitude of applied loads in these regions compared to straight sections of road and/or dynamic behaviour of manhole structures. The finite element analyses revealed that a lateral component of load did not significantly increase the peak tensile stress magnitude in the bedding. A manhole may be considered as a series of vertically mounted springs, each spring representing the various components. Each spring would have a resonant frequency. It may be conceivable that vehicles travelling at a certain speed may apply

loads at a frequency that would cause resonance. It may be speculated that this frequency may be equivalent to slow moving traffic as seen at junctions and on roundabouts. The increased movement of the manhole structure is likely to inflict some damage which may manifest itself in the bedding layer. Experiments could be carried out to study whether this effect occurs.

References

1. Various, "Preferred Method 7, Adjustment of Street Ironwork", Cornwall County Council, 1985.
2. Anon, "New Roads and Streetworks Act 1991 - Specification for the Reinstatement of Openings in Highways," HMSO, 1992.
3. British Standards Institution, "Soils for Civil Engineering Purposes," BS1377: Part 2: 1990.
4. Whiteoak, C.D. "The Shell Bitumen Handbook," Shell Bitumen U.K., 1990.
5. Neville, A.M. "Properties of Concrete," 3rd Edition, Longman Scientific & Technical, Harlow, Essex, 1991.
6. Czernin, W. "Cement Chemistry and Physics for Civil Engineers," Crosby Lockwood, London, 1962.
7. Neville, A.M. & Brooks J.J., "Concrete Technology," Revised 1st Edition, Longman Scientific & Technical, Harlow, Essex, 1991.
8. Mindess, S. & Diamond, S. "The Cracking and Fracture of Mortar," Proceedings of a session sponsored by the Committee on Properties of Materials of the ASCE Engineering Materials Division, Hollywood, Florida, 1980.
9. Griffith, A.A. "The Phenomena of Rupture and Flow in Solids," Royal Society, Philosophical Transactions, Series A, 1920, pp. 163-98.
10. Hannant, D.J. "Fibre Cements and Fibre Concretes," 1st Edition, John Wiley & Sons, Chichester, 1978, pp 3-8.
11. British Standards Institution, "Method for Determination of Compressive Strength of Concrete Cubes," BS 1881: Part 116: 1983.
12. American Society for Testing and Materials, "Test for Flexural Strength of Concrete (Using Simple Beam with Third-Point Loading)," ASTM C 78-84.
13. American Society for Testing and Materials, "Test for Splitting Tensile Strength of Cylindrical Concrete Specimens," ASTM C 496-71.
14. British Standards Institution, "Method for Determination of Tensile Splitting Strength," BS 1881: Part 117: 1983.
15. British Standards Institution, "Method for Determination of Static Modulus of Elasticity in Compression," BS 1881: Part 121: 1983.

16. British Standards Institution, "Testing of Resin Compositions for use in the Construction Industry," BS 6319: Part 2: 1983.
17. Ekerfors, L. & Dejus, R. "Testing of Manhole Spacer Rings," Summary report, Swedish National Testing Institute, 1988.
18. British Standards Institution, "Ceramic Floor and Wall Tiles", BS 6431: Part 2: 1984.
19. British Standards Institution, "Hot Rolled Asphalt for Roads and Other Paved Areas," BS 594: Part 1: 1992.
20. European Committee for Standardisation, "Gully Tops and Manhole Tops for Vehicular and Pedestrian Areas - Design Requirements, Type Testing, Marking, Quality Control," EN 124: 1994.
21. British Standards Institution, "Manhole Covers, Road Gully Gratings and Frames for Drainage Purposes," BS 497: Part 1: 1976.
22. British Standards Institution, "Pre-cast Concrete Pipes & Ancillary Concrete Products," BS 5911: Part 1: 1981.
23. British Standards Institution, "Clay Bricks," BS3921: 1985.
24. Anon, "Manual Handling, Guidance of Regulations," Health and Safety Executive Publication, 1992.
25. Anon, "Frames and Covers, Carriageway, Installation, Renewal and Relevelling," British Telecommunications plc Specification A2 G0071, 1982.
26. Anon, "Specification for Resin Bedding," British Telecommunications plc Specification LN M330, 1993.
27. Anon, "Re-levelling of frames and covers in the carriageway," Mercury Communications Ltd Specification C8 0138, 1995.
28 Anon, "Manual of Contract Documents for Highway Works," Department of Transport Publication, HMSO, December 1991.
29. Anon, "Trunk Road Maintenance Manual, Volume 2: Routine and Winter Maintenance Code," Highways Agency Publication, Version No.2, February 1996, pp1.5-1.
30. Anon, "Traffic Signs Manual, Chapter 8: Traffic Safety Measures and Signs for Road Works and Temporary Situations," Department of Transport Publication, 1st Edition, HMSO, 1991.

31. Tam, W.S. "Pavement Evaluation and Overlay Design," PhD Thesis, University of Nottingham, Department of Civil Engineering, October 1987. pp57-124.
32. Anon, "Standard Detail for Inspection Chambers," Nottinghamshire County Council Specification, 1980.
33. De Beer, M. "Pavement Response Measuring System," Paper intended for the 2nd International Symposium on Pavement Response Monitoring Systems for Roads and Airfields, September 1991, Hanover, USA.
34. Craig, R.F. "Soil Mechanics," 4th Edition, Van Nostrand Reinhold (International) Co. Ltd, 1987.
35. G. Ahlborn, "ELSYM5, Computer Program for Determining Stresses and Deformations in Five Layer Elastic System", University of California, Berkerley, 1972.
36. Cebon, D. "Interaction Between Heavy Vehicles and Roads," Proceedings of the 39th L. Ray Buckendale Lecture, Society of Automotive Engineers, Inc. 1993, pp 33-34.
37. Brown, S.F. & Dawson, A.R. "The Effects of Groundwater on Pavement Foundations," Proceedings of the 9th European Conference on Soil Mechanics and Foundation Engineering, Vol.2, 1987, pp. 657-660.
38. Rowe, G.M., Brown, S.F., Pell, P.S. & Armitage, R.J. "Fatigue Wheel Tracking - Validation Studies," SWK Pavement Engineering Ltd Client Report, P156, January ,1993.
39. British Standards Institution, "British Standard Method of Test for Flexible Cellular Materials," BS4443: Part 3: Method 8: Determination of creep: 1988.
40. British Standards Institution, "Soils for Civil Engineering Purposes," BS1377: Test 16: 1975.
41. British Standards Institution, "Design in Simple and Continuous Construction: Hot Rolled Sections," BS5950: Part 1: 1990(Amendment 1).
42. Brown, S.F. & Brodrick, B.V. "Instrumentation for the Nottingham Pavement Test Facility," Transportation Research Record, No. 810, pp 73-79.

43. Brown, S.F. & Brodrick, B.V. "The Performance of Stress and Strain Transducers for use in Pavement Research," Science Research Council Report, Department of Civil Engineering, University of Nottingham, June, 1973.

44. Bergman, W., Clemett, H.R., & Sheth, N.J. "Tire Traction Measurement on the Road and in the Laboratory," SAE Transactions, Society of Automotive Engineers Inc, Paper No. 710630, 1971.

45. Megson, T.H.G. "Strength of Materials," 2nd Edition, Edward Arnold, London, 1987.

46. Young, W.C. "Roark's Formulas for Stress and Strain," 6th Edition, McGraw-Hill Book Co., 1989, pp. 136-155.

47. Hendry, A.W. "Structural Brickwork," 1st Edition, The Macmillan Press Ltd, London, 1981, pp. 43-45.

48. Anon, "ANSYS User Manual," Volume 1, Swanson Analysis Systems, Inc. 1992.

49. British Standards Institution, "Structural Use of Concrete: Code of Practice for Design and Construction," BS8110: Part 1: 1985.

50. Discussion of paper by Gilkey, H.J. "Water/Cement Ratio versus Strength - Another Look," American Concrete Institute, December 1961, pp 1851-78.

51. Pickett, J. "Effect of Aggregate on Shrinkage of Concrete and Hypothesis Concerning Shrinkage," American Concrete Institute, January 1956, pp 581-90.

52. Seehra, S.S., Gupta, S. & Kumar, S. "Rapid Setting Magnesium Phosphate Cement for Quick Repair of Concrete Pavements - Characterisation and Durability Aspects," Cement and Concrete Research, Vol. 23. pp 254-266, 1993.

53. Macadam, D., Smith, K., Fowler, D.W. & Meyer, A.H. "Evaluation of Rapid Setting Concretes," Transportation Research Record 1003, pp 19-28.

54. Read, J.M. "Fatigue Cracking of Bituminous Paving Mixtures," PhD Thesis, University of Nottingham, Department of Civil Engineering, May 1996.

Appendix A: Test Methods used to Measure Bedding Material Properties

A number of tests methods were used to measure the strength and elastic properties of bedding materials. A description of these methods are given below.

A.1 Determination of the Tensile Strength of Cementitious Bedding Materials in Direct Tension

Laboratory experiments were carried out to measure the limiting stress and strain at failure of specimens tested in direct uniaxial tension. Specimens of mortar were cast with dimensions of 75 x 20 x 300mm long and cured at 20°C before placing in the Zwick test machine. These were the largest cross sectional dimensions that could be fitted into the jaws of the machine. This machine is electrically powered and applies load through a screw driven crosshead with feedback control. It can apply tensile loads to a tolerance of ±10N. This allows the limiting tensile stress to be calculated accurately. A load was applied at a constant rate of stress of 0.03MPa per second and the value at failure was recorded. Care was taken to ensure the samples were evenly gripped at the ends. Two linear variable differential transformers (LVDT's) were mounted on opposite sides of the specimen as illustrated in Figure A.1. The readings from these instruments provided an indication of the eccentricity of the load. It was found that there was a difference no greater than 5% in the measured values. These readings also provided data to calculate the strain in the sample.

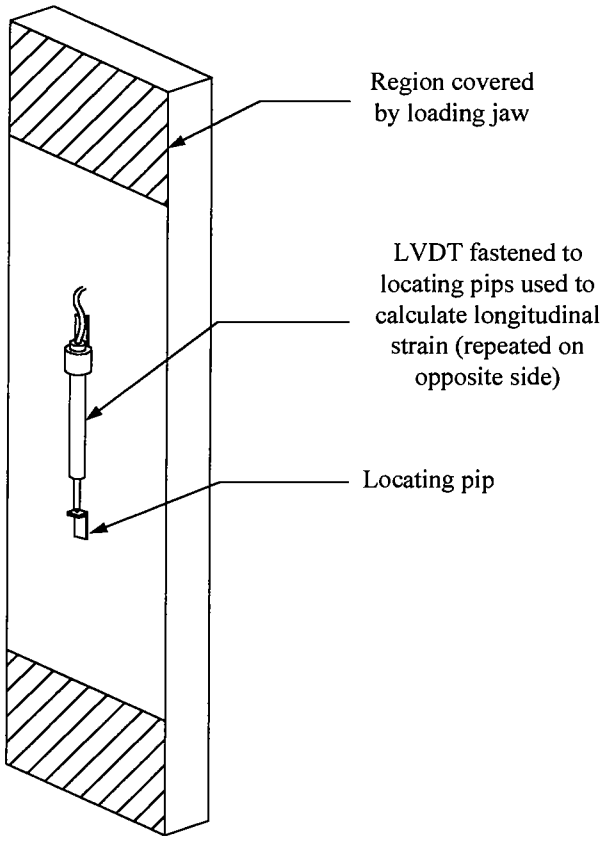

Figure A.1: Illustration of a specimen used to measure the direct tensile strength of bedding mortars

A.2 Determination of the Fatigue Strength of Cementitious Mortar

The fatigue strength of cementitious materials has previously been determined by others either in uniaxial tension or compression [7]. It is considered that samples prepared for testing in uniaxial tension would have been cast so that a neck was formed at the centre of the sample. This would have concentrated the highest stress at this point and would have mitigated the localised high stresses that are considered to develop around the clamps of a test machine. However, due to the high shrinkage of mortar A it was thought that such samples would crack whilst initially curing in the mould.

The force required to produce an adequate stress level in a test specimen in uniaxial compression would require a large test machine. Such machines cannot be operated at high frequencies so it was thought that it would take several weeks to determine the fatigue strength of mortar A by this method.

An indirect tensile fatigue test (ITFT) [54] was chosen as the method to determine the number of cycles to cause failure at various stress levels in mortar A as the apparatus already existed and did not require modification. Cylindrical samples with a diameter of 100mm were prepared and allowed to cure at a constant temperature of 20°C for 28 days before testing. It was considered that the duration of the test would take approximately seven days so the samples may still have been developing strength if they had not been sufficiently cured. The cylinders were cut into 30mm thick slices and placed in the test machine. This thickness was chosen so that an adequate tensile stress would develop in the sample without overloading the test machine which had been designed for use with asphalt mixtures of a lower stiffness. A total of 10 specimens were tested and the number of cycles required to produce failure at a constant amplitude of stress oscillating at 2Hz was recorded. An illustration of the ITFT apparatus is shown in Figure A.2.

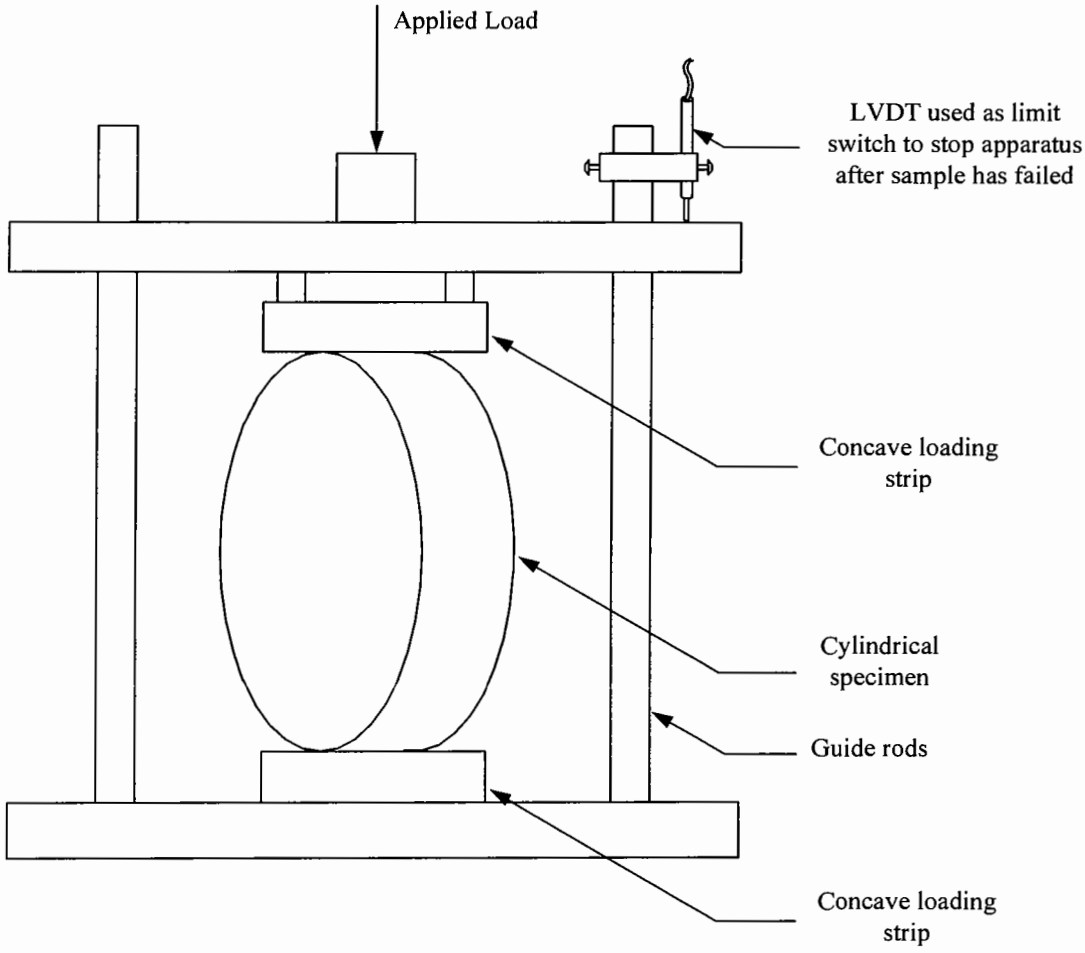

Figure A.2: Illustration of the ITFT apparatus

A.3 Determination of the Static Modulus and Poisson's Ratio of Cementitious and Polymer Resin Based Bedding Materials

Bedding materials were acquired and cast into cylinders with a diameter of 150mm and a height of 300mm and cured at 20°C. Cylindrical specimens were chosen as this is the method recommended to measure the static modulus in BS 1881: Part 121: 1983 [15]. Additionally, the apparatus already existed for measuring lateral strain used in calculating the Poisson's ratio. The previous experiments had been carried out with apparent success.

Each cylinder was loaded in the Instron servo-hydraulic test machine that can apply tensile and compressive loads of 100kN but only compressive loads were applied in these experiments. Repeated or cyclic loading can be applied. The pattern of load application can be controlled by various waveforms, a sinusoidal waveform being selected for these experiments. A frequency of 0.3Hz was used as the output from the LVDT's was recorded on a chart plotter which would not have been able to react quick enough at faster rates of loading. Further readings were taken at 0.01Hz and it was found that there was no difference in the magnitude of the measurements.

Two LVDT's were mounted vertically on each specimen and the output was used to calculate the vertical strain and static modulus. The diametrical strain was calculated from the output of the LVDT placed in the hoop surrounding the cylinder. The readings of strain in the two mutually perpendicular directions were used to calculate the Poisson's ratio. An illustration of this instrumentation is shown in Figure A.3. The cylinders were subjected to cyclic loading varying from 0.1 to 3.5MPa. This produced a peak stress in the sample less than one-third of the compressive strength.

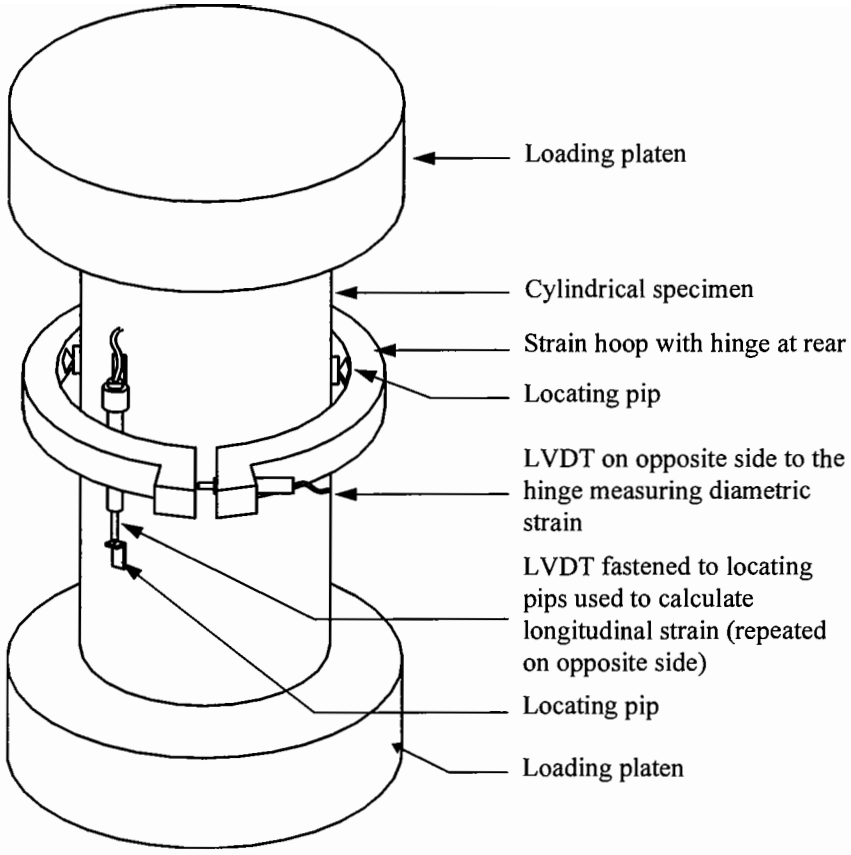

Figure A.3: Apparatus used to measure the static modulus and Poisson's ratio of bedding mortars

A.4 Determination of the Modulus and Strain Ratio of HDPE Spacers

The method used to determine the modulus and strain ratio of HDPE spacers involved cutting a single spacer into strips 300mm long. Five strips were placed in a stack on the bottom loading platen of the Instron test machine. Another loading platen with an even surface was placed on top of the stack of spacers and the load was applied at its centre. Two LVDT's were placed on the surface of the platen, aligned to measure vertical deflection. Another LVDT was placed at the centre of the stack of spacers, mounted to measure horizontal deflection. All the deflections were measured relative to a stable datum. An illustration of the apparatus is shown in Figure A.4.

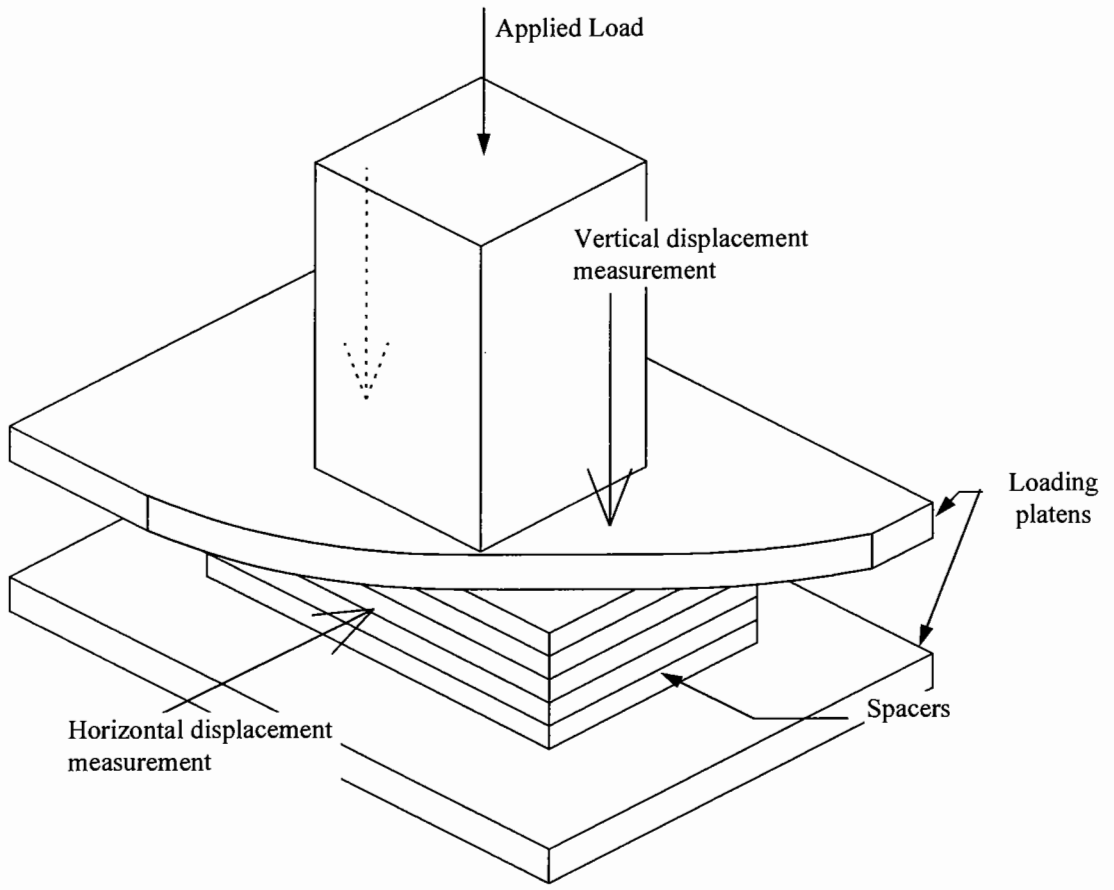

Figure A.4: Apparatus used to measure the elastic properties of HDPE spacers

A cyclic load inducing a compressive stress varying from 0.1MPa to 1.67MPa was applied at a rate of 0.3Hz and the LVDT measurements were recorded on chart plotters. These data were used to calculate values for the modulus and strain ratio.

Appendix B: Summary of Surface Displacements of Pavements and Manholes Determined by Theoretical Calculations

Load applied in calculations = 57.5kN

Load applied over a radius = 168mm

Table B.1: Range of pavement surface displacements

Constants:

Poisson's ratio

Asphalt = 0.35

Granular material = 0.3

Subgrade = 0.4

Subgrade assumed to extend to a semi-infinite depth

Reference Number	Asphalt Stiffness (MPa)	Asphalt Thickness (mm)	Granular Stiffness (MPa)	Granular Thickness (mm)	Subgrade Stiffness (MPa)	Vertical Deflection (mm)
1	2000	100	50	100	20	3.086
2	8000	100	50	100	20	2.114
3	2000	150	50	100	20	2.226
4	8000	150	50	100	20	1.445
5	2000	250	50	100	20	1.414
6	8000	250	50	100	20	0.933
7	2000	100	200	100	20	2.670
8	8000	100	200	100	20	1.977
9	2000	150	200	100	20	2.025
10	8000	150	200	100	20	1.392
11	2000	250	200	100	20	1.346
12	8000	250	200	100	20	0.919
13	2000	100	50	400	20	2.518
14	8000	100	50	400	20	1.842
15	2000	150	50	400	20	1.915
16	8000	150	50	400	20	1.332
17	2000	250	50	400	20	1.303
18	8000	250	50	400	20	0.897
19	2000	100	200	400	20	1.577
20	8000	100	200	400	20	1.322
21	2000	150	200	400	20	1.344
22	8000	150	200	400	20	1.082
23	2000	250	200	400	20	1.059
24	8000	250	200	400	20	0.814
25	2000	100	50	100	70	1.409

Table B.1 continued: Range of pavement surface displacements

Reference Number	Asphalt Stiffness (MPa)	Asphalt Thickness (mm)	Granular Stiffness (MPa)	Granular Thickness (mm)	Subgrade Stiffness (MPa)	Vertical Deflection (mm)
26	8000	100	50	100	70	0.949
27	2000	150	50	100	70	1.019
28	8000	150	50	100	70	0.656
29	2000	250	50	100	70	0.664
30	8000	250	50	100	70	0.401
31	2000	100	200	100	70	1.143
32	8000	100	200	100	70	0.844
33	2000	150	200	100	70	0.883
34	8000	150	200	100	70	0.608
35	2000	250	200	100	70	0.610
36	8000	250	200	100	70	0.385
37	2000	100	50	400	70	1.536
38	8000	100	50	400	70	1.020
39	2000	150	50	400	70	1.095
40	8000	150	50	400	70	0.694
41	2000	250	50	400	70	0.699
42	8000	250	50	400	70	0.416
43	2000	100	200	400	70	0.862
44	8000	100	200	400	70	0.671
45	2000	150	200	400	70	0.701
46	8000	150	200	400	70	0.514
47	2000	250	200	400	70	0.521
48	8000	250	200	400	70	0.353
49	2000	100	50	4000	20	1.782
50	2000	100	50	2000	20	1.939
51	2000	100	50	1000	20	2.132
52	8000	100	50	4000	20	1.233
53	8000	100	50	2000	20	1.384
54	8000	100	50	1000	20	1.564
55	2000	150	50	4000	20	1.310
56	2000	150	50	2000	20	1.461
57	2000	150	50	1000	20	1.637
58	8000	150	50	4000	20	0.873
59	8000	150	50	2000	20	1.017
60	8000	150	50	1000	20	1.171
61	2000	250	50	4000	20	0.870
62	2000	250	50	2000	20	1.011
63	2000	250	50	1000	20	1.157
64	8000	250	50	4000	20	0.559
65	8000	250	50	2000	20	0.689
66	8000	250	50	1000	20	0.814
67	2000	100	200	4000	20	0.645
68	2000	100	200	2000	20	0.824
69	2000	100	200	1000	20	1.110

Table B.1 continued: Range of pavement surface displacements

Reference Number	Asphalt Stiffness (MPa)	Asphalt Thickness (mm)	Granular Stiffness (MPa)	Granular Thickness (mm)	Subgrade Stiffness (MPa)	Vertical Deflection (mm)
70	8000	100	200	4000	20	0.472
71	8000	100	200	2000	20	0.622
72	8000	100	200	1000	20	0.902
73	2000	150	200	4000	20	0.512
74	2000	150	200	2000	20	0.677
75	2000	150	200	1000	20	0.951
76	8000	150	200	4000	20	0.352
77	8000	150	200	2000	20	0.493
78	8000	150	200	1000	20	0.755
79	2000	250	200	4000	20	0.375
80	2000	250	200	2000	20	0.520
81	2000	250	200	1000	20	0.769
82	8000	250	200	4000	20	0.240
83	8000	250	200	2000	20	0.365
84	8000	250	200	1000	20	0.592
85	2000	100	50	4000	70	1.687
86	2000	100	50	2000	70	1.657
87	2000	100	50	1000	70	1.619
88	8000	100	50	4000	70	1.145
89	8000	100	50	2000	70	1.117
90	8000	100	50	1000	70	1.083
91	2000	150	50	4000	70	1.219
92	2000	150	50	2000	70	1.191
93	2000	150	50	1000	70	1.158
94	8000	150	50	4000	70	0.788
95	8000	150	50	2000	70	0.761
96	8000	150	50	1000	70	0.734
97	2000	250	50	4000	70	0.787
98	2000	250	50	2000	70	0.760
99	2000	250	50	1000	70	0.734
100	8000	250	50	4000	70	0.482
101	8000	250	50	2000	70	0.457
102	8000	250	50	1000	70	0.435
103	2000	100	200	4000	70	0.615
104	2000	100	200	2000	70	0.667
105	2000	100	200	1000	70	0.726
106	8000	100	200	4000	70	0.449
107	8000	100	200	2000	70	0.496
108	8000	100	200	1000	70	0.555
109	2000	150	200	4000	70	0.485
110	2000	150	200	2000	70	0.535
111	2000	150	200	1000	70	0.591
112	8000	150	200	4000	70	0.330
113	8000	150	200	2000	70	0.376

Table B.1 continued: Range of pavement surface displacements

Reference Number	Asphalt Stiffness (MPa)	Asphalt Thickness (mm)	Granular Stiffness (MPa)	Granular Thickness (mm)	Subgrade Stiffness (MPa)	Vertical Deflection (mm)
114	8000	150	200	1000	70	0.430
115	2000	250	200	4000	70	0.352
116	2000	250	200	2000	70	0.398
117	2000	250	200	1000	70	0.448
118	8000	250	200	4000	70	0.220
119	8000	250	200	2000	70	0.262
120	8000	250	200	1000	70	0.308
					Average	**0.975**

Table B.2: Range of manhole surface displacements

Constants:

Young's/Static modulus

Bedding = 21GPa

Brickwork = 14GPa

Ironwork = 165GPa

Poisson's ratio

Bedding material = 0.18

Brickwork = 0.2

Ironwork = 0.275

Subgrade = 0.4

Subgrade assumed to extend to a semi-infinite depth

Reference Number	Bedding Thickness (mm)	Ironwork Frame Depth (mm)	Chamber Depth (mm)	Subgrade Stiffness (MPa)	Vertical Deflection (mm)
1	10	100	4000	20	0.009
2	10	100	2000	20	0.015
3	10	100	1000	20	0.045
4	25	100	4000	20	0.009
5	25	100	2000	20	0.015
6	25	100	1000	20	0.044
7	50	100	4000	20	0.009
8	50	100	2000	20	0.014
9	50	100	1000	20	0.041
10	10	150	4000	20	0.007
11	10	150	2000	20	0.012
12	10	150	1000	20	0.038

Table B.2 continued: Range of manhole surface displacements

Reference Number	Bedding Thickness (mm)	Ironwork Frame Depth (mm)	Chamber Depth (mm)	Subgrade Stiffness (MPa)	Vertical Deflection (mm)
13	25	150	4000	20	0.007
14	25	150	2000	20	0.012
15	25	150	1000	20	0.036
16	50	150	4000	20	0.007
17	50	150	2000	20	0.012
18	50	150	1000	20	0.035
19	10	100	4000	70	0.009
20	10	100	2000	70	0.015
21	10	100	1000	70	0.040
22	25	100	4000	70	0.009
23	25	100	2000	70	0.014
24	25	100	1000	70	0.039
25	50	100	4000	70	0.009
26	50	100	2000	70	0.014
27	50	100	1000	70	0.037
28	10	150	4000	70	0.007
29	10	150	2000	70	0.012
30	10	150	1000	70	0.034
31	25	150	4000	70	0.007
32	25	150	2000	70	0.012
33	25	150	1000	70	0.033
34	50	150	4000	70	0.007
35	50	150	2000	70	0.012
36	50	150	1000	70	0.032
				Average	**0.020**

Appendix C: Photographs of the Laboratory Test Facility under Construction

These photographs were taken during the construction of the laboratory test facility. The construction started in December, 1994 and the apparatus was completed and commissioned in March, 1995.

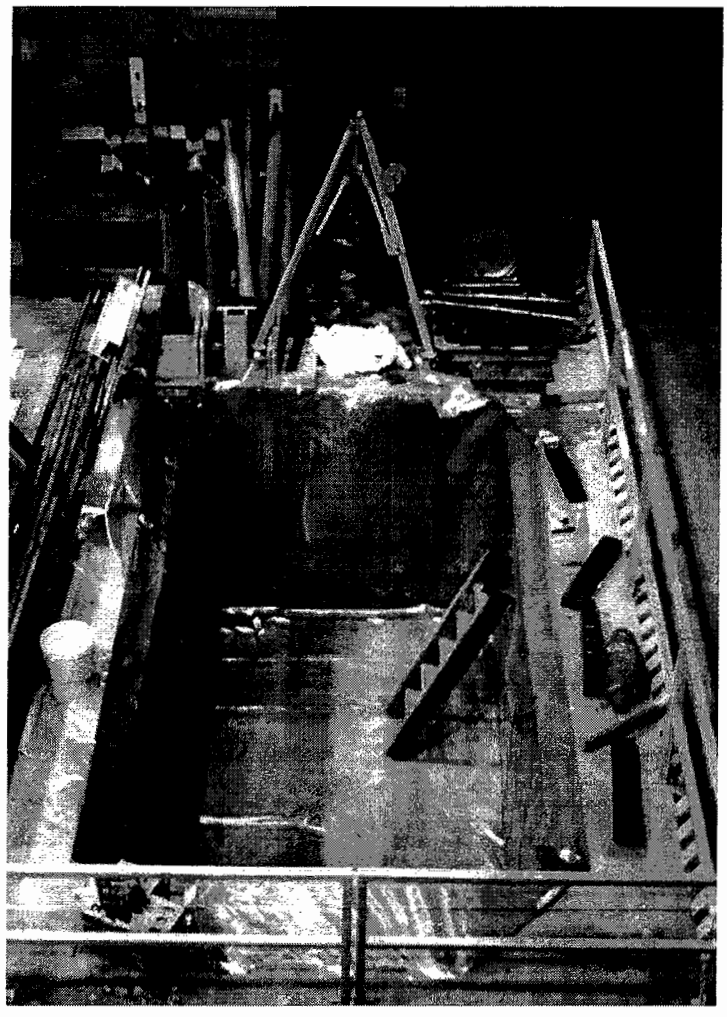

Figure C.1: View of the empty pit lined with plastic

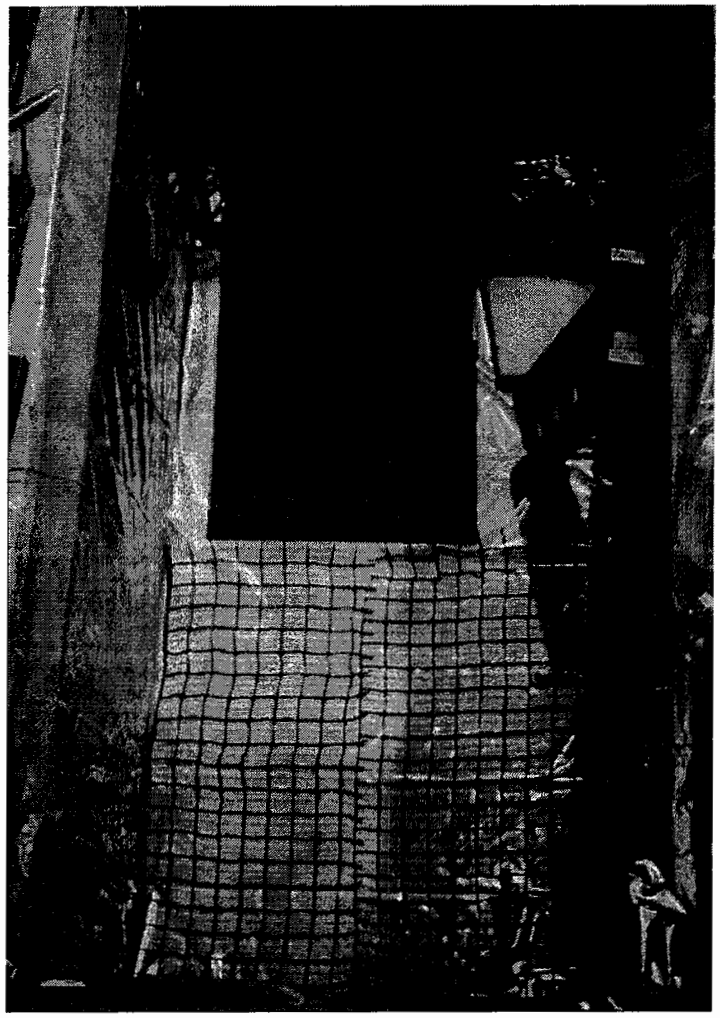

Figure C.2: Installation of the rubber layers later covered with wisaform boards

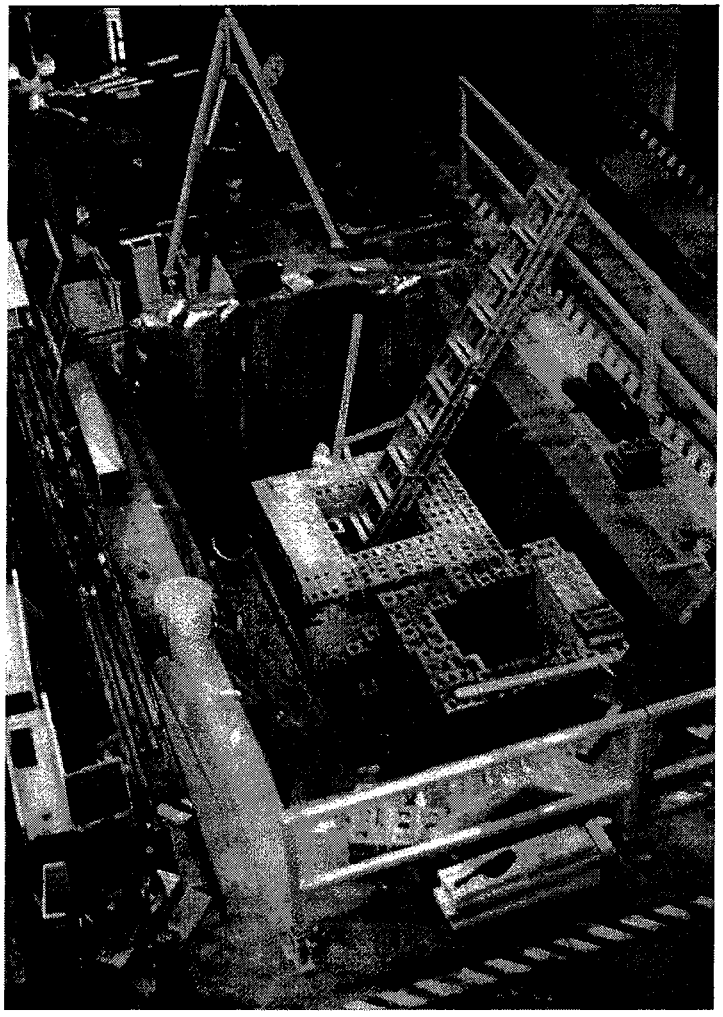

Figure C.3: Construction of the manhole chambers supported by concrete slabs

Figure C.4: Completed manhole chambers. Pipes later used as access conduit for instrument wires

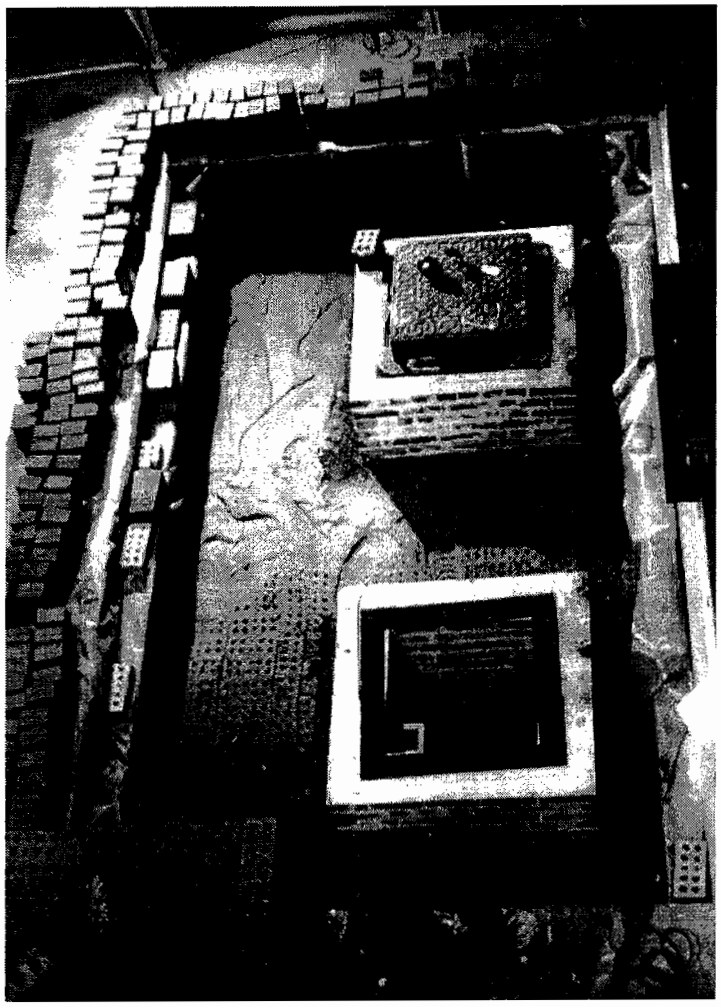

Figure C.5: Partially compacted clay layer

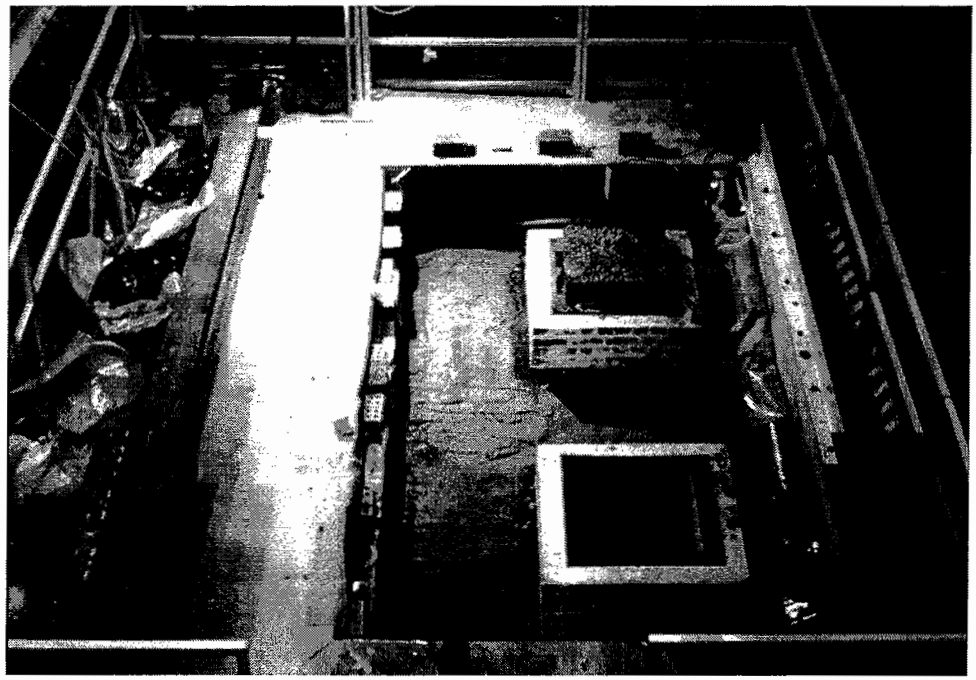

Figure C.6: Completed clay layer (1350mm deep)

Figure C.7: Installation of quarry tile configuration. Wires connected to instruments in the bedding

Figure C.8: Installation of bedding layer on top of quarry tiles and frame prior to tamping

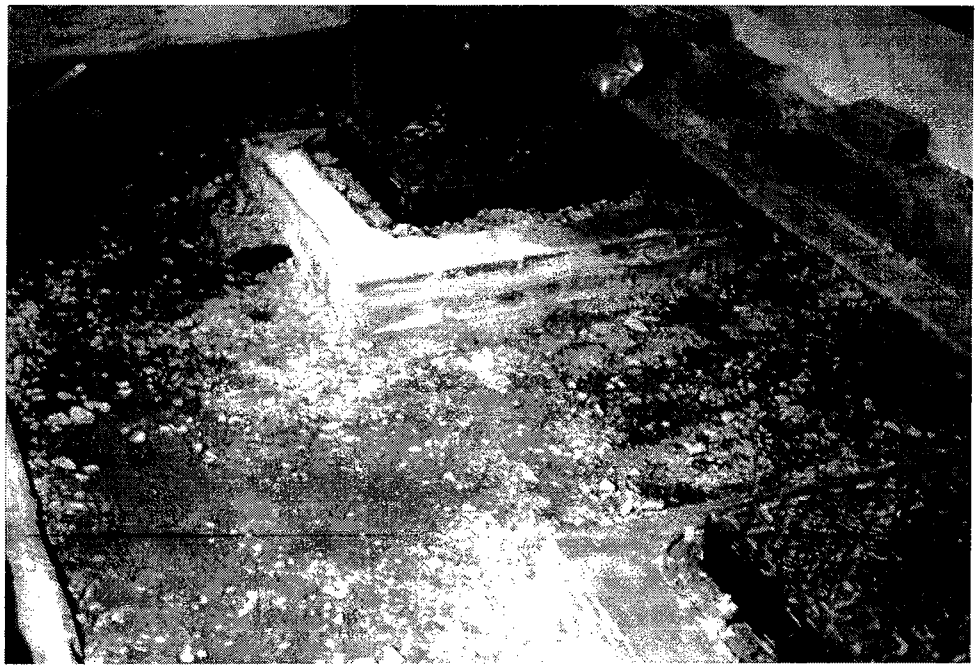

Figure C.9: Completed installations and sub-base (300mm deep)

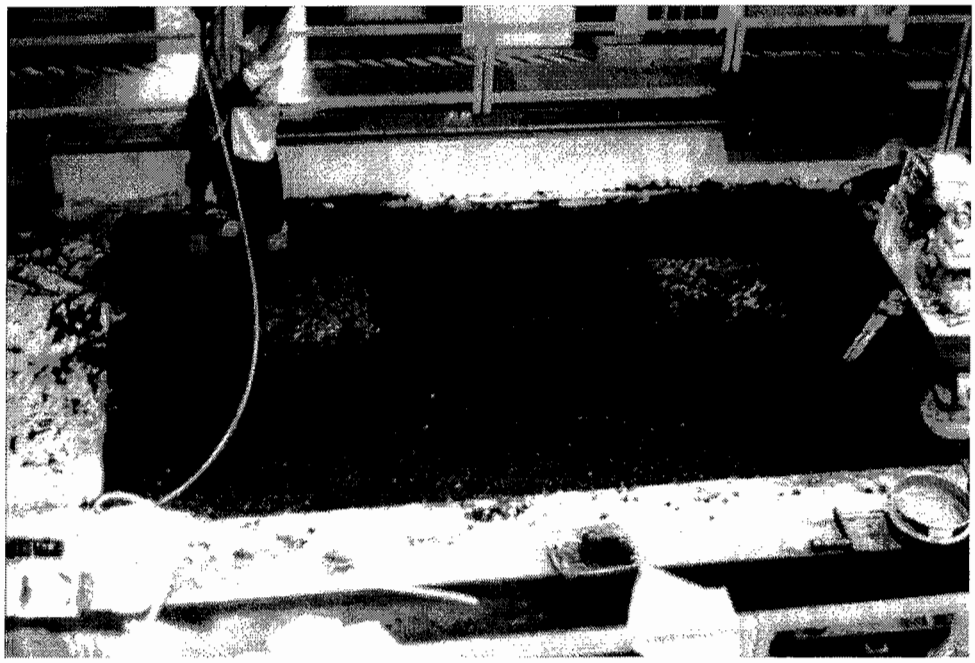

Figure C.10: Compaction of the DBM. Care was taken not to place the vibrating roller on the ironwork

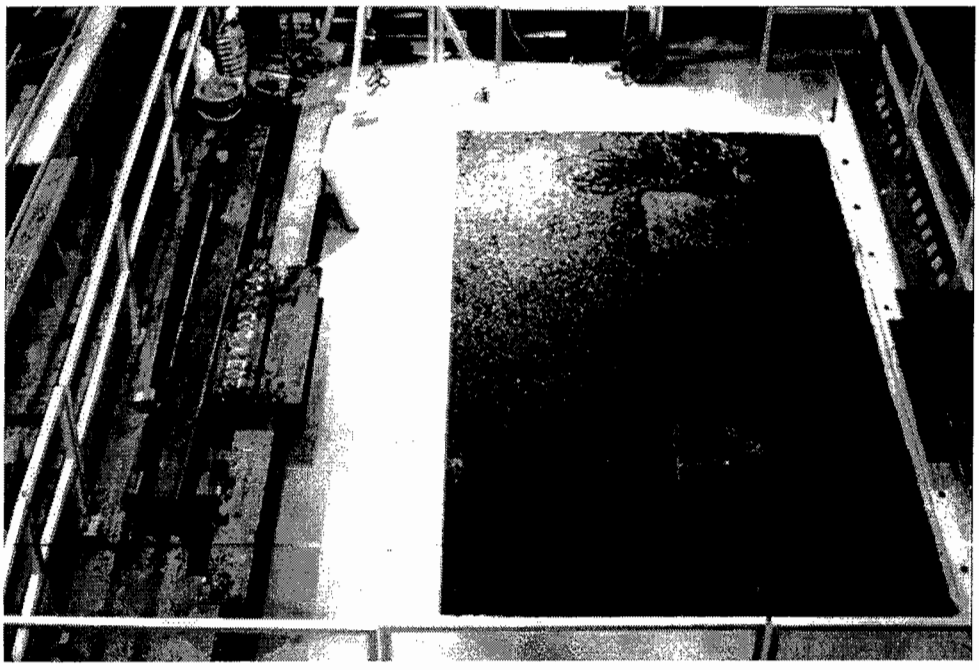

Figure C.11: Completed DBM layer (240mm deep). Pit topped out

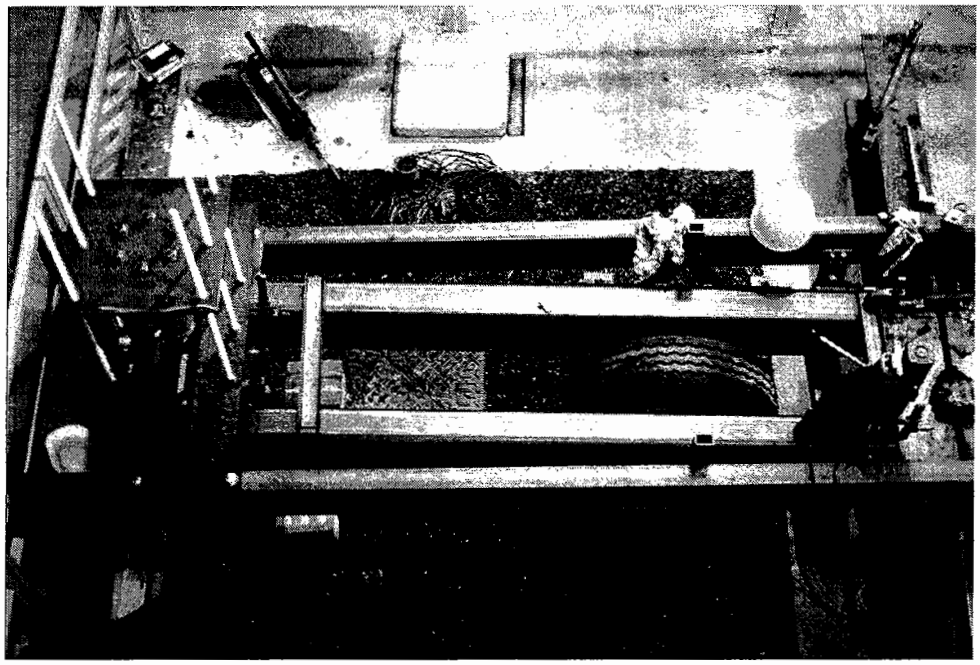

Figure C.12: Construction of the steel loading frame

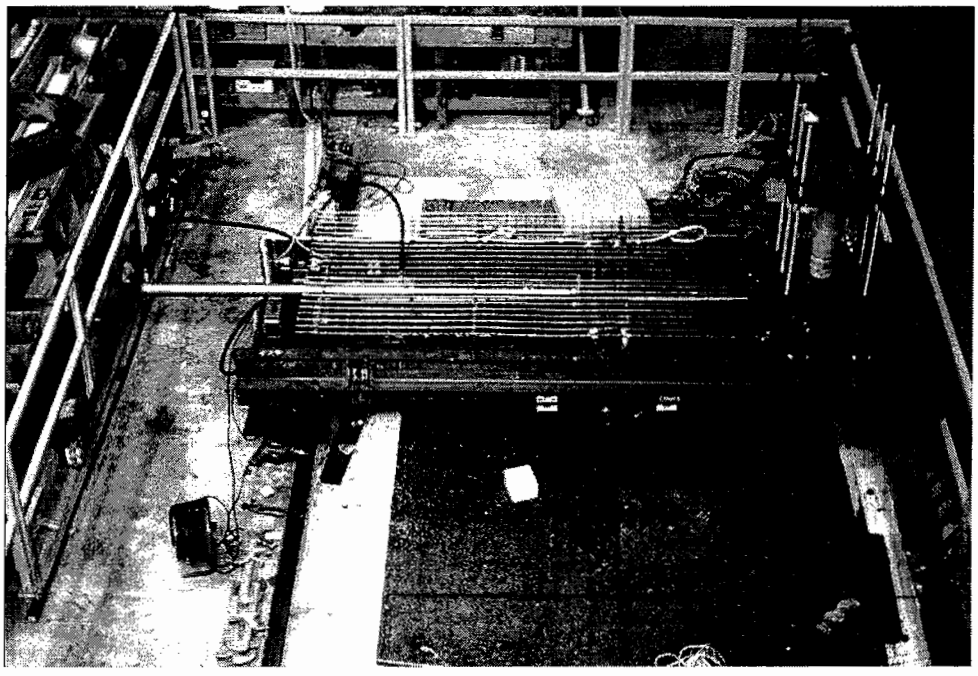

Figure C.13: Completed laboratory test facility

Appendix D: Recommended Method of Reinstatement

This method of reinstatement was developed from this research and other examples of good working practice. Some of these procedures were included in previous reinstatement specifications [1,25,27]. It is considered that the method described below is practical and should provide a high quality of workmanship.

1. Failure Criterion

An installation is considered to have failed when any of the following characteristics is evident:

(a) The difference in level of the ironwork with the surrounding carriageway is greater than 20mm [1].

(b) Sections of the bituminous material immediately surrounding a road ironwork unit are missing leaving a hole large enough to allow an impairment of riding quality.

(c) Movement of the ironwork unit produces a loud noise when load is applied by passing vehicles.

2. Site Closure

Access may be gained to an installation at times least likely to cause disruption to traffic. Such times include night-time or Sundays or between 10am and 3pm during weekdays. Traffic management in accordance with Chapter 8: Traffic Management and Road Signs [30] must be applied in all circumstances.

3. Removal of Failed Installation

(a) Cut through the full depth of the bound layers of the pavement around the ironwork with a circular saw or similar apparatus. The position of the cut should be located 200mm away from the outside edge of ironwork frame. If the surfacing is cracked beyond this distance around the installation, then the cut must be located 50mm beyond the extent of cracking. This is illustrated in Figure D.1.

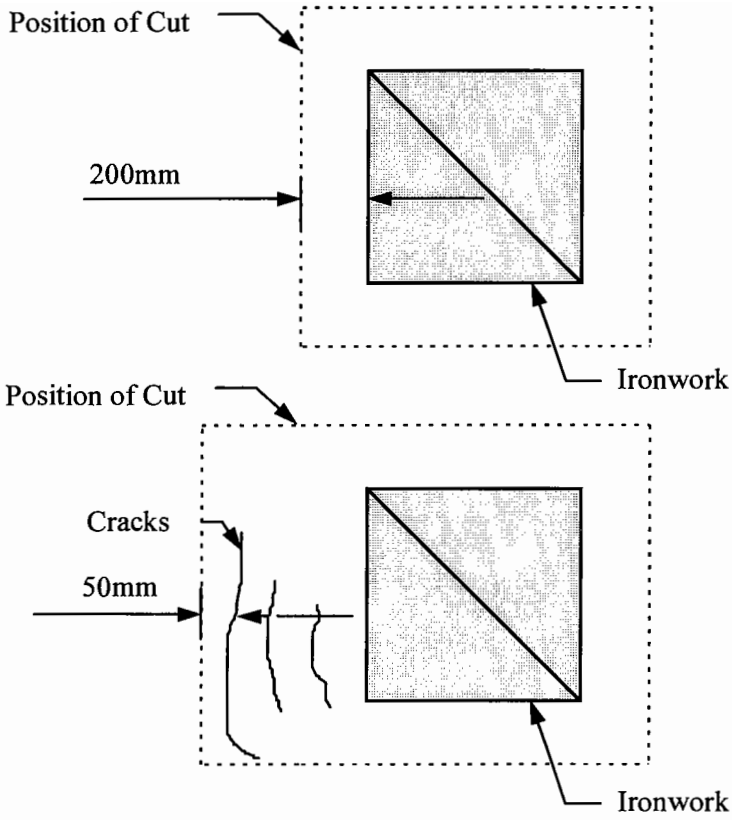

Figure D.1: Position of cut in the bituminous surfacing

(b) Remove the pavement surfacing between the position of the cut and the ironwork to reveal the frame and the full width of the chamber wall along all edges.

(c) Extract the ironwork covers using lifting keys with a long shank. The handle of such keys should be approximately at waist height. The use of keys with short shanks are not recommended as the risk of injury is increased.

(d) Lift the ironwork frame to reveal the bedding layer underneath. Lifting of the frame should involve at least two people [24].

(e) Remove all bedding materials so that the surface of the brickwork chamber is revealed.

4. Inspect Chamber Condition

(a) Inspect the brickwork for any signs of deterioration.

(b) All damaged brickwork should be removed and the exposed surfaces cleared of any debris.

(c) The chamber should be reconstructed with Class B Engineering bricks. A proprietary cementitious mortar that develops a compressive strength of at least 10MPa in 24 hours and has a workable life greater than 1 hour but less than 2 hours must be used in circumstances when a reinstatement is to be re-opened to traffic immediately after completion.

(d) Bricks without holes or frogs must be used in corbels.

5. Determine Required Bedding Thickness and Mortar Type

(a) The finished surface of the brickwork on all chambers should allow a bedding thickness between 10 and 75mm.

(b) Bedding layers greater than 50mm thick should be laid in two stages. The first layer should not exceed a thickness of 40mm and must be covered with quarry tiles that have a low moisture absorption rate or proprietary packing materials whilst the mortar is workable. Uniform contact between the materials is essential in a composite bedding layer. Such materials should be tamped down to ensure even contact with the bedding.

(c) Cementitious or polymer resin based mortars with the properties given in Table D.1 must be used to form the bedding layer when a reinstatement is to be re-opened to traffic on completion. Materials that develop these strengths over longer periods may be used if an adequate curing period can be ensured.

Table D.1: Required properties of the bedding material

Workable Properties:	
Workable life	15 to 30 minutes
Desired workability	50mm slump
Hardened Properties:	
Compressive strength at 3hrs	> 40MPa
Tensile strength at 3hrs	> 8MPa
Shrinkage	Low shrinkage or shrinkage compensated (Bedding material should produce a strain < 69 microstrain over 28 days)
Durability Aspects:	
	Mortar should be resistant to sulphate attack, chloride ingress and the action of frost.

6. Mixing and Placing the Bedding Layer

(a) Mechanical mixing of the materials is preferred, although manual mixing is permitted. The maximum quantity to be mixed by each method should not exceed 50kg and 25kg respectively. Additionally, the manufacturer's recommended water content must be accurately measured if the material is of a cementitious nature. Subjective judgement of the required workability may adversely affect the hardened properties of the bedding material.

(b) The bedding material must be placed on the chamber immediately after mixing. It should be placed at a depth approximately 5mm greater than the required bedding thickness and spread across the full width of the chamber wall. Deep trowel marks in the bedding should be filled and the surface of the bedding floated to an approximately even finish.

7. Placing the Ironwork

(a) The ironwork frame may be lowered on the bedding using a lifting device or by a two man lift.

(b) The ironwork must be placed on the bedding so that the webs of the frame are supported on all sides of the chamber. This is illustrated in Figure D.2.

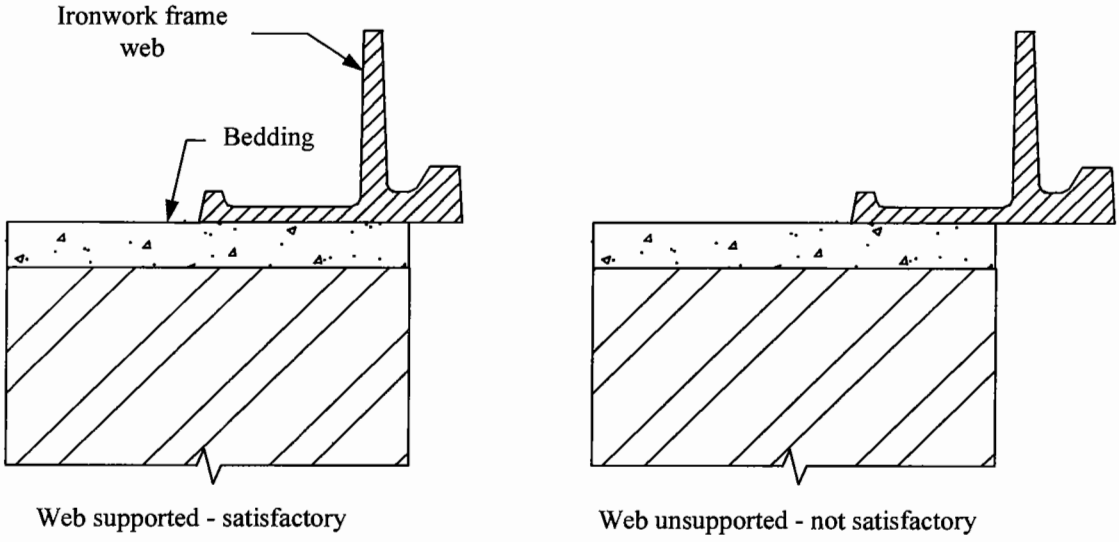

Figure D.2: Recommended support conditions for the ironwork frame webs

(c) Tamp the frame down with a large hammer to required level and slope. This can be indicated by placing a straight edge over the frame webs and surrounding carriageway. The level should be checked above all frame webs.

(d) Place an additional thickness of mortar in the frame holes and above the flange. This thickness should be greater than 10mm. Float the exposed surface of the bedding around the outside of the frame to fill any voids and remove any loose fragments.

(e) The exposed surface of the bedding material inside the chamber should be pointed to a smooth finish. Any voids on the surface should be filled, especially under the cover seatings. This operation must be completed before the bedding material hardens.

(f) Allow bedding to cure for at least 30 minutes before laying the backfill material. A tack coat may be applied to the vertically exposed surfaces of the existing

carriageway and the ironwork covers may be carefully inserted into the frame during this time.

8. Reinstate Carriageway

(a) The surrounding backfill material must be the same as used to form the wearing course of the adjacent pavement [2]. This is usually 30/14 HRA. Bitumen emulsion products may be used as a temporary measure but should be replaced within 10 days. A vibrating roller or plate should be used to compact this layer. Care must be taken to avoid contact between the compaction device and the ironwork cover to avoid damaging the bedding layer.

(b) Layers not exceeding a 150mm thickness should be placed in a single layer and thoroughly compacted on the surface. Placing the bituminous material in thinner layer leaves the ironwork frame web exposed. Contact between the web and the compaction device could easily occur and would crack the bedding material.

(c) Layers greater than 150mm thick should be placed in two layers. The level of the first layer should be below the top of the chamber surface to minimise the risk of cracking the bedding material. The second layer should be placed in a single operation as described above.

(d) Seal the joint in the carriageway between the reinstated and existing materials with a flexible bituminous material.

9. Completion

(a) Remove any debris from the surface around the reinstatement.

(b) Lift the covers of the ironwork and inspect the bedding layer for any signs of cracks before re-opening the site to traffic. If cracks have appeared then repeat operation.

(c) If no cracks are visible then re-open site to traffic.